

Curriculum Vitae of Ralf Cuntze

comprising Career, Scientific Findings & some Personal Pictures

Prof. Dr.-Ing. habil. Ralf Cuntze VDI, Ralf_Cuntze@t-online.de

Retired from industry, MAN-Technologie, Augsburg, Germany



Engineer and hobby scientist:

application-oriented with a touch for material modelling and with the hope to be some bridge-builder between mechanical and civil engineering (construction).

Hobbies: exploring the world, nature photography, gardening, mountaineering, cyclamen breeding, ...



- 1939 born Sept 8 in Erfurt. Survived bombing and a machine gun fire from a U.S. tank, March 31, 1945
- 1964: Dipl.-Ing. Civil Engineering CE (construction, **TU Hannover**). 1968: Dr.-Ing. in Structural Dynamics (CE). 1978: Dr.-Ing. habil. Venia Legendi in Mechanics of Lightweight Structures (TU-M)
- 1980-1983: Lecturer at Universität der Bundeswehr München: on ‘Fracture Mechanics’ in the construction faculty and 1990-2002 on ‘Composite Lightweight Design’ in aerospace faculty
- 1987: Full professorship ‘Lightweight Construction’, *not started in favor of industry*
- 1998: Honorary professorship at Universität der Bundeswehr München
- 1968-1970: FEA-programming (**DLR**-Essen/Mühlheim)
- 1970-2004: MAN-Technologie (München and Augsburg). Headed the Main Department ‘Structural and Thermal Analysis’. 50 years of life with fibers CF, AF, GF, BF, BsF.
- *Theoretical fields of work: structural dynamics, finite element analysis, rotor dynamics, structural reliability, partial/deterministic safety concepts, material modeling and model validation, fatigue, fracture mechanics, design development ‘philosophy’ & design verification
- *Mechanical Engineering applications at **MAN**: ARIANE 1-5 launcher family (design of different parts of the launcher stages, inclusively Booster) Cryogenic Tanks, High Pressure Vessels, Heat Exchanger in Solar Towers (GAST Almeria) and Solar Field, Wind Energy Rotors (GROWIAN Ø103 m, WKA 60, AEROMAN. Probably the first world-wide wind energy conferences organized in 1979, 1980 with Dr. Windheim), Space Antennas, Automated Transfer Vehicle (Jules Verne, supplying the space station ISS), Crew Rescue Vehicle (CMC application) for ISS, Carbon and Steel Gas-Ultra-Centrifuges for Uranium enrichment. Filament Winding theory. Material Databank etc.
- *Civil Engineering applications: Supermarket statics, armoring plans, pile foundation, 5th German climbing garden (1980 designed, concreted and natural stone-bricked)
- 1971-2010: Co-author of **ESA/ESTEC**-Structural Materials Handbook, Co-author and first convener of the ESA-Buckling Handbook and co-author in Working Groups WGs for ESA-

Standards ‘Structural Analysis’, ‘High Pressure Vessels’ (metals and composites) and ‘Safety Factors’

1972–2015, **IASB**: Luftfahrt-Technisches Handbuch HSB ‘Fundamentals and Methods for Aeronautical Design and Analyses’. Author and Co-author of numerous HSB sheets and about 2006-2008 co-transfer with co-translation of the HSB aerospace structural handbook into its present English version.

1980-2011: **Surveyor/Advisor** for German BMFT (MATFO, MATEC), BMBF (LuFo), DFG

1980-2006: **VDI Guideline 2014**, co-author of Parts 1 and 2, Beuth Verlag ‘*Development of Fiber-reinforced Plastic Components*’; Part 3 ‘*Analysis*’, editor/convener/co-author

1986 and 1889: One week lecture on composite design in Pretoria, SA

2019: ***GLOSSAR**. ”Fachbegriffe für Kompositbauteile - *technical terms for composite parts*“. Springer 2019. Edited at the suggestion of carbon concrete colleagues to help to better understand each other

2000-2013: World-Wide-Failure-Exercises WWFE on UD materials’ strength: WWFE-I (2D stress states) non-funded winner against institutes of the world, WWFE-II (3D states) top-ranked

2009-2021 linked to **Carbon Composites e.V.** at Augsburg, later **Composites United CU e.V.** and to TUDALIT Dresden. Since 2011 working on the light weight material Fiber-reinforced (polymer) Carbon Concrete. **Founded and headed the working groups**: (1) 2009: ‘Engineering’ linked to the WG Non-Destructive Testing and the WG Connection Technologies, mechanical engineering. (2) 2010: ‘Composite Fatigue’. In 2010 the author held an event that was excellently attended by international speakers. (3) 2011: ‘Design Dimensioning (*Auslegung, Bemessung*) and Design Verification (*Nachweis*)’ mainly for carbon concrete. This working group was the foundation stone for the later specialist network **CU Construction**, aiming at “*Fiber-based lightweight construction*”. (4) 2017: ‘Automated fabrication in construction including serial production’ (3D-Print). (5) 2020, 2021: Forum ‘Carbon concrete for practice’ at ‘Ulm Concrete Days’.

2022: *** Life-Work Cuntze - a compilation from the author’s papers, presentations, published and non-published design sheets and project works in industry** (850 Pages)

2023: *** Design of Composites using Failure-Mode-Concept-based tools - from Failure Model Validation to Design Verification**. Mechanics of Composite Materials, Vol. 59, No. 2, May, 2023, pp. 263-282.

*** Minimum Test Effort-based Derivation of Constant-Fatigue-Life curves, displayed for the brittle UD composite materials**. Mechanics of Composite Materials, Springer, Advanced Structured Materials, Vol.199, 107–146, draft. ***Comparative Characterization of Four Significant UD Strength Failure Criteria (SFC)**, 54 pages. *** Cuntze R and Kappel E: Benefits, applying Tsai’s Ideas ‘Trace’, ‘Double-Double’ and ‘Omni Failure Envelope’ to Multiply UD-ply composed Laminates?**

Preprints, drafts downloadable from

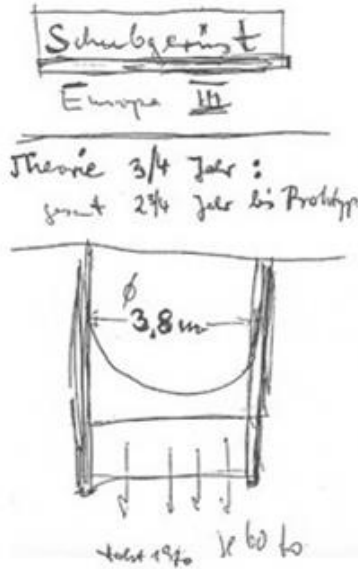
*** <https://www.carbon-connected.de/Group/Prof.Ralf.Cuntze> or from Research Gate**

The presented novel ideas invite for discussion.

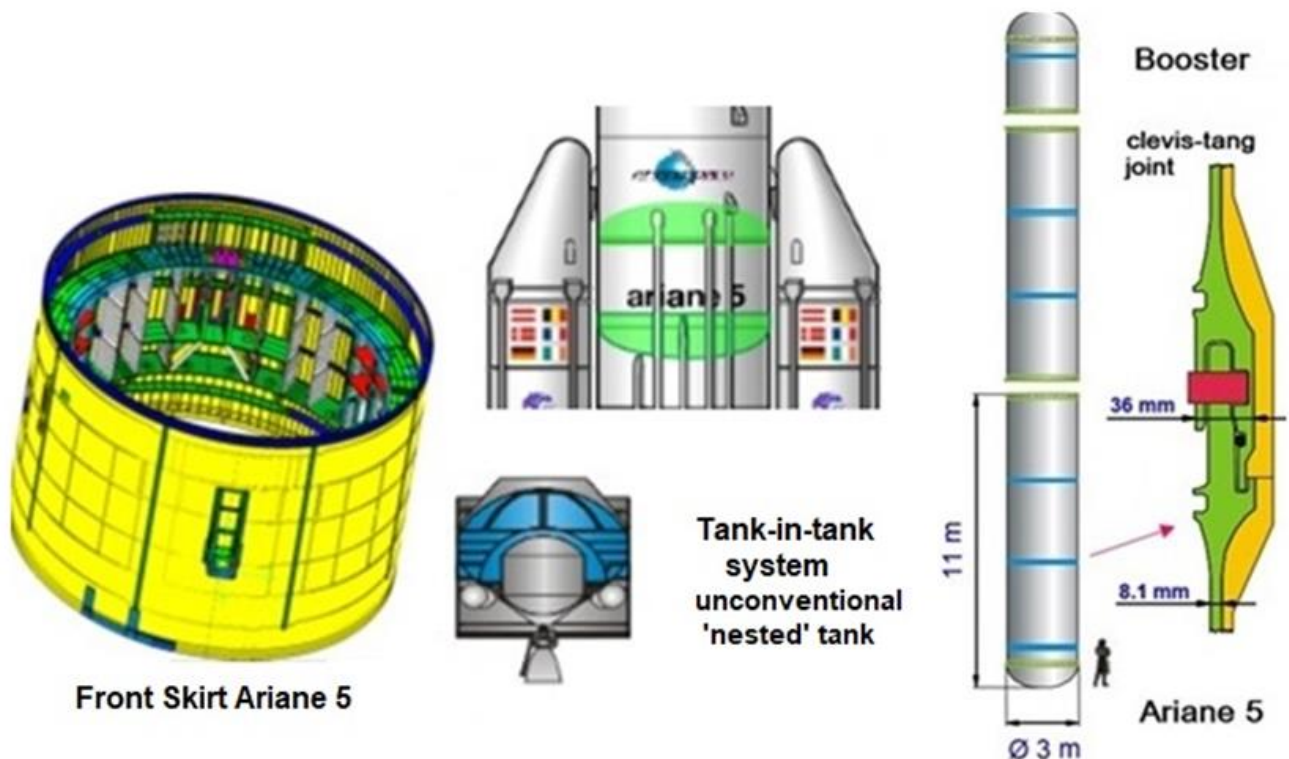
1	Creation of the ‘Failure Mode Concept’ (FMC, about 1996).....	9
2	<i>Interaction of Stresses</i> using FMC-based Strength Failure Criteria	10
3	Material Symmetry and ‘Generic’ Number	11
4	Direct use of a Friction Value μ in the SFCs.....	12
5	Material stressing effort Eff (Werkstoffanstrengung)	15
6	<i>Interaction of Failure Modes</i> and a Multi-fold (fracture) Failure Mode	16
7	So-called ‘Global’ SFCs and (failure mode-linked) ‘Modal’ SFCs	17
8	Validity Limits of UD SFC Application → Finite Fracture Mechanics (FFM)	19
9	‘Curiosities’ regarding Classical Material Mechanics.....	21
10	Automated Generation of Constant Fatigue Life curves considering Mean Stress Effect.....	24
11	Evidence 120°-symmetrical Failure Body of Brittle and also Ductile Isotropic Materials	30
12	Completion of the Strength Mechanics Building	37
13	Safety Concept in Structural Engineering Disciplines	38
14	Non-linear Stress-Strain relationships, Beltrami Theory with Change of Poisson’s Ratio	44
15	A measurable parameters-based ‘Extended-Mises’ Model instead of a ‘Gurson’ Model?.....	55
16	Note on Continuum (micro-)Damage Mechanics (CDM).....	69
17	Multi-scale Structural modelling with Material Modelling and its Analyzing	77
18	Some Lessons Learned from Testing and Evaluation of Test Results.....	83
19	Determination of 2D ‘Omni principal FPF strain failure envelopes and Reserve Factor.....	87
20	Note on Fiber Micro-Fragments and Dusts of CFRP/CFRConcrete	92
21	A novel Determination of the Residual Strength R_{res} , non-cracked, Fatigue Phase 2	97
22	Technical Terms, Glossar.....	102
23	Miscellaneous	108
24	References since 2000	120
25	Hobbies: Globetrotter, Hiking, photography, house & garden with alpine-cyclamen breeding.....	121

Some Project Activities

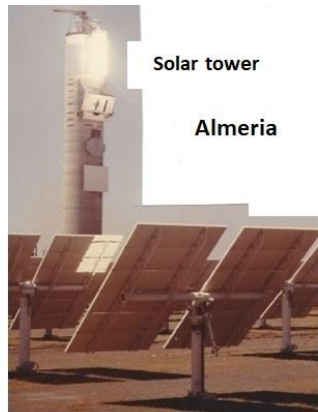
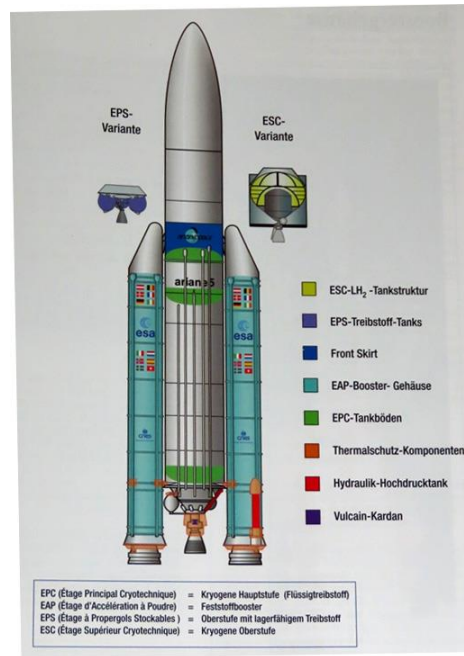
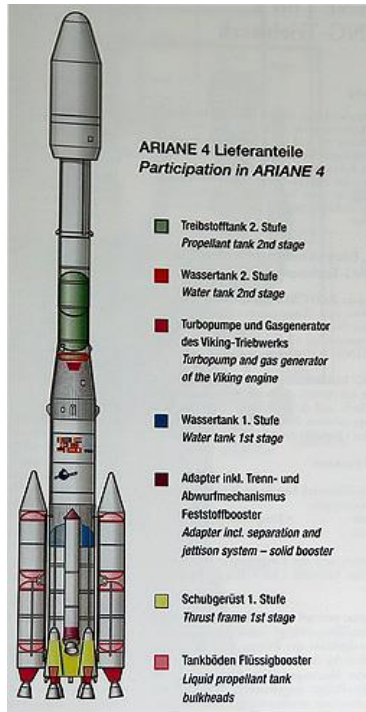
The slip of paper below was the start of my work at MAN-Neue Technologie in 1970 regarding the development of the **Ariane launcher family**:
"Make a design proposal for an offer, please" (Thrust structure).



*Offer for Europe III as the Forerunner of Ariane I and following Family
 (nearly all structural parts had to be designed)*



Ariane Launcher 1-5



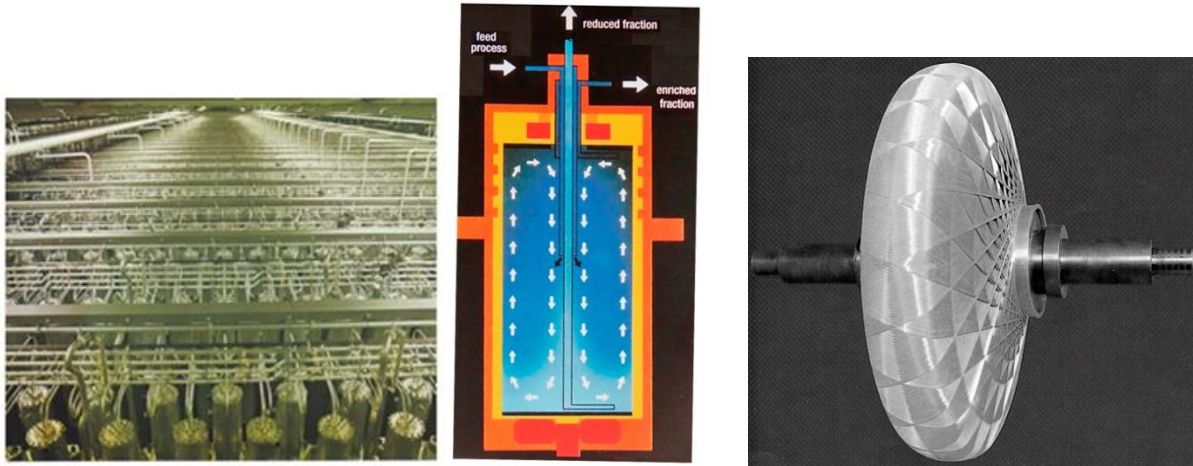
Solar field



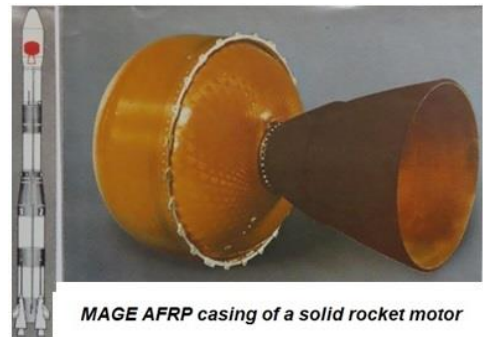
Solar Farm Plant with tower.



Wind Energy Rotor (GROWIAN, 1980, 51 m blade, GFRP shell) with wind speed measurement facility



Uranium enrichment Centrifuges, Process. Composite brake energy storage flywheel for a bus



MAGE AFRP casing of a solid rocket motor

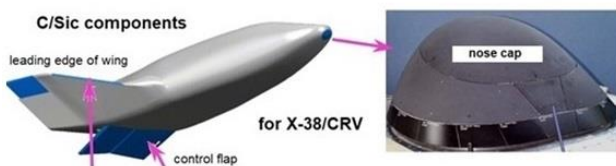
Airbus A330/340 drinking water tanks. High Pressure Vessels. Apogee Kevlar Motor Case



NIESYTO design, S. Guisard,



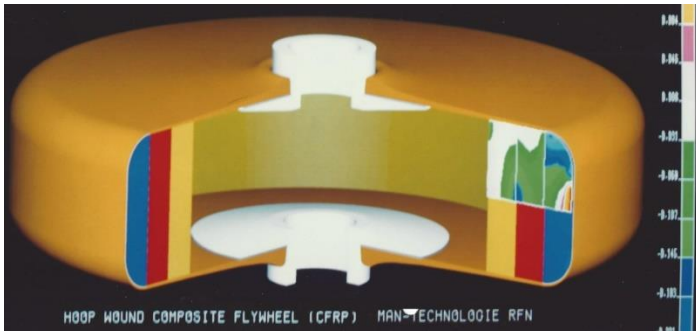
Automated Transfer Vehicle for supply of the ISS



SOFIA telescope, ISS-linked structures



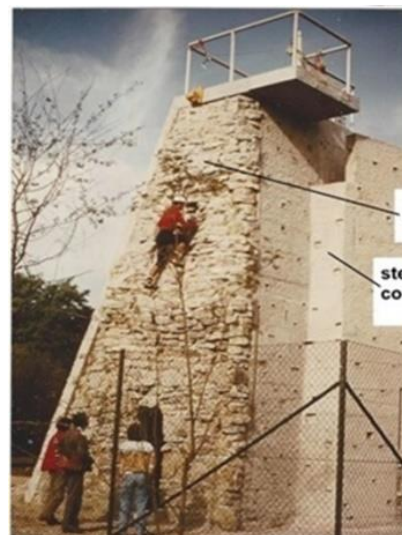
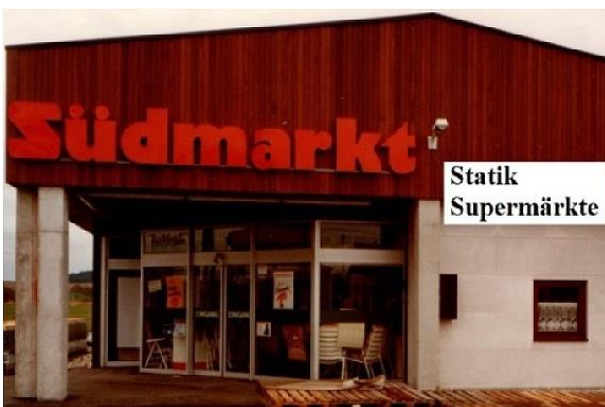
Small wind energy rotors 1980



(left) FEA of a delamination-less energy storing fly wheel. (right) Development of a braided CFRP hip

Working in Civil Engineer Applications

Structural engineering, armoring plans, pile foundation



5th German
'climbing garden'

rock material

steel reinforced
concrete

Designed,
concrete casted,
one side masoned with
rock stones from the alps
by the author

Findings of the author during his long-lasting non-funded Research Activities

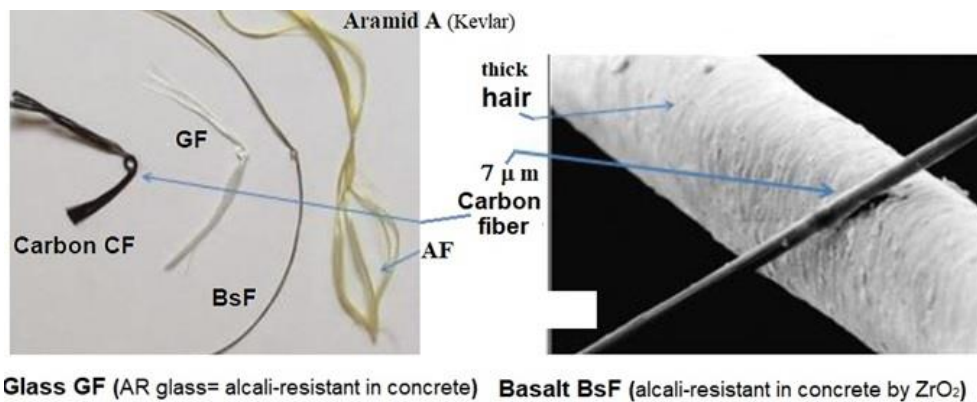
Novel simulation-driven product development shifts the role of physical testing to virtual testing, to simulation, respectively. This requires High Fidelity and therefore the use of reliable material models. (*Simulation means: imitation of the operation of a real-world process and model adaption due to test information by performing many analyses.*)

Basic desire of the macro-scopically working structural engineer is a material model linked to an ideally homogeneous material which might be isotropic or anisotropic. Connecting desire is to be provided with a clear Strength Mechanics Building in order to get a cost-saving basis due to only analyze and test what is really physically necessary.

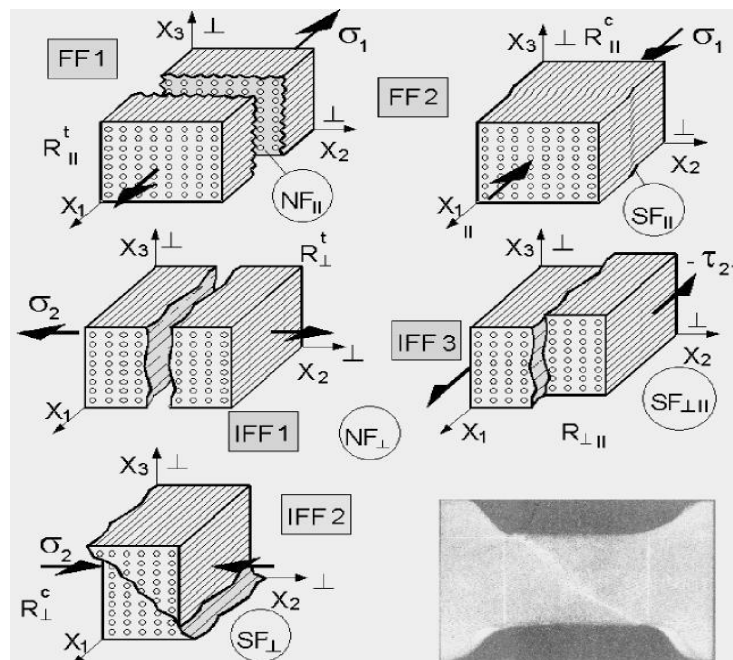
For the 3D-Demonstration of Strength are required - nowadays practically a must regarding the usual 3D FEA stress output - so-called 3D Strength Failure Criteria (SFC) rendered by 3D failure bodies to firstly perform Design Dimensioning and to finally achieve Design Verification.

All this is targeted in the following elaboration.

The following figure displays some of the different strengthening fibers applied in construction, and a comparison of a standard Carbon Fiber with a human hair.



And the next figure shall provide for the applied stringent failure mode thinking the observed 5 failure modes faced with Uni-directional fiber-reinforced materials.



1 Creation of the ‘Failure Mode Concept’ (FMC, about 1996)

Aim: Creation of a Static & Cyclic Strength Mechanics Building as basis for all materials.

Being since 1970 in the industrial composite business the author tried to sort out applicable SFC for UD materials in regular discussions with Alfred Puck. Puck developed his Hashin-based Action-plane SFC which was included in 2006 into the VDI 2014 guideline, sheet 3 (editor Cuntze). Working with practically all material types the author was encouraged to find a Concept for all the material families isotropic, UD and orthotropic ones including dense with porous materials.

The finally developed so-called Failure-Mode-Concept (FMC) incorporates a rigorous thinking in failure modes and can be briefly described by the features: *Failure mode-wise mapping, *Stress invariant-based formulation, *Equivalent stress generation, *Each neat failure mode is governed by just one strength R^{mode} , witnessed for ductile and brittle materials, and *All SFC model parameters are measurable entities! Each SFC represents a failure surface, therefore for the originator the FMC will be the foundation upon which he physically based SFCs generated.

In the case of brittle materials this failure surface is the surface of a fracture failure body. Such a surface is determined by the peaks or ends of all failure stress vectors. It is mathematically defined by a Failure function F which becomes 1 at ‘Onset-of-Failure’. $F = 1$ is the formulation of the SFC (mathematically, we write a condition). *Fig.1-1* presents the pioneers in the isotropic SFC field.

Model parameters are just the measurable technical strengths R and the friction values μ , and on top the Weibull statistics-based interaction exponent m . The value of μ comes from mapping the compression stress-shear stress domain and of m by mapping the transition zone between the modes. A good guess is $m = 2.6$ for all mode transition domains and all material families.



Fig.1-1: Some pioneers which set up strength failure hypotheses (ductile, brittle)

The author’s idea was to create physically-based SFCs and to note his Lessons Learned LL during the elaboration. The FMC was originally derived for UD materials because there was the big demand at that time.

LL: *Similarly behaving materials possess the same shape of a fracture body using the same SFC!*

Note, please: Strength notations

R means strength (resistance) in general and further Strength Design Allowable used for Design Verification. \bar{R} means average strength used for modelling.

2 Interaction of Stresses using FMC-based Strength Failure Criteria

Aim: Provision of a failure mode-based stress-interaction ('Modal') and not a mathematical one.

The derivation of the FMC-based SFCs builds up on the hypotheses of Beltrami, Hencky-Mises-Huber (HMH) and Mohr-Coulomb. Therefore the depicted SFC approaches consider - following Beltrami and Mohr-Coulomb – that the solid material element may experience, generated from different energy portions, a shape change (HMH), a volume change and friction. FMC-based SFCs will be given for a large variety of isotropic brittle structural materials such as porous Concrete Stone, Normal Concrete, UHPC sandstone, monolithic ceramics and for the transversely-isotropic fiber-reinforced polymers Lamina (ply, lamella) and finally orthotropic fabrics inclusively fabric ceramics, see [CUN22, Cun23a,24b].

Since two decades the author believes in a macroscopically-phenomenological 'complete classification' system, where all strength failure types are included, see the figure below. In his assumed system several relationships may be recognized: (1) Shear stress yielding SY, followed by Shear fracture SF considering 'dense' materials. For porous materials under compression, the SF for dense materials is replaced by Crushing Fracture CrF. (2) In order to complete a mechanical system beside SY also NY should exist. This could be demonstrated by PMMA (plexiglass) with its chain-based texture showing NY due to crazing failure under tension and SY in the compression domain, [see subsection 9.1 or CUN22,§4.1]. The right side of the scheme outlines that a full similarity of the 'simpler' isotropic materials with the transversely-isotropic UD materials exists.

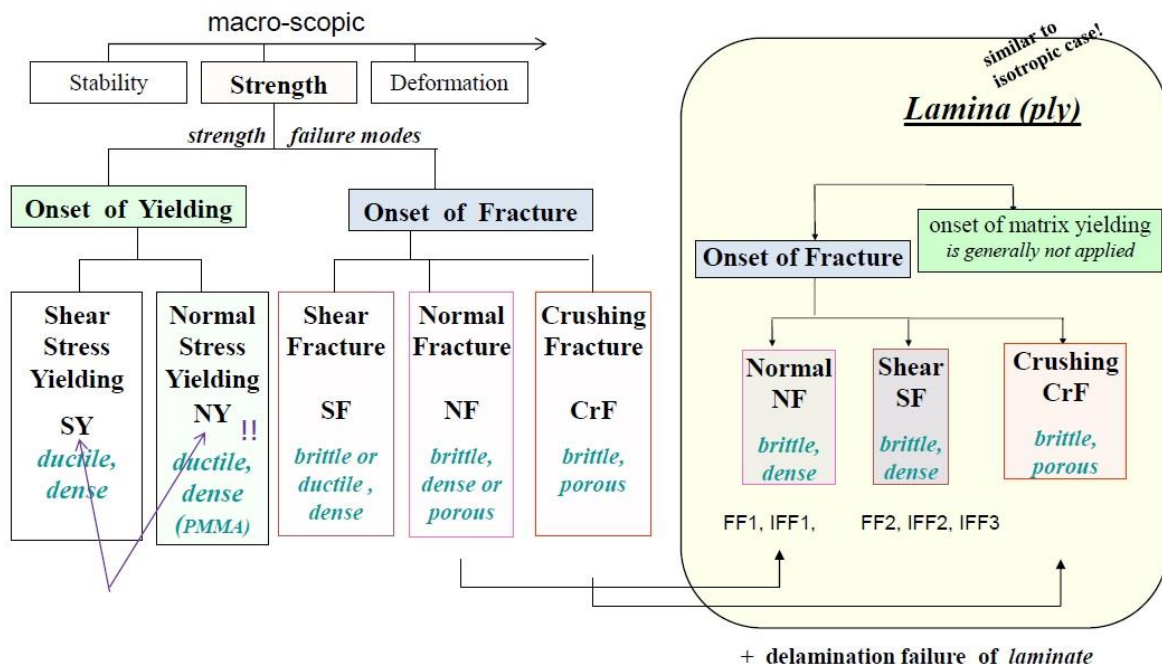


Fig.2-1.: Scheme of macro-scopic strength failure types and modes of isotropic materials and transversely-isotropic UD-materials (Cuntze1998)

LL:

* Failure behavior of Fiber-Reinforced materials is similar to isotropic ones

* Principally, instead of stress-based SFC, strain-based SFC might be applied if the full stress-strain history is accurately considered. However, just limit strain conditions are used in pre-dimensioning (§22), because the certification process is stress-based.

3 Material Symmetry and ‘Generic’ Number

Aim: Consideration of the available material knowledge.

During the derivation of the FMC a closer look at material symmetry facts was taken whereby the question arose: “Does a material symmetry–linked Generic Number exist with a number 2 for isotropic and 5 for UD materials?”

Under the design-simplifying presumption “Homogeneity is a permitted assessment for the material concerned”, and regarding the respective material tensors, it follows from material symmetry that the number of strengths equals the number of elasticity properties!

Fracture morphology gives further evidence: Each strength property corresponds to a distinct strength failure mode and to a distinct strength failure type, to Normal Fracture (NF) or to Shear Fracture (SF). This means, a characteristic number of quantities is fixed: 2 for isotropic material and 5 for the transversely-isotropic UD lamina (\equiv lamellas in civil engineering). Hence, the applicability of material symmetry involves that in general just a minimum number of properties needs to be measured (benefits:& test cost + time) which is helpful when setting up strength test programs. \Rightarrow Witnessed material symmetry knowledge seems to tell: “There might exist a ‘generic’ (term was chosen by the author) material inherent number for”:

Isotropic Material: of **2**

- 2 elastic ‘constants’, 2 strengths, 2 strength failure modes fracture (NF with SF) and 2 fracture mechanics modes (defined as modes, where crack planes do not turn)
- 1 physical parameter (such as the coefficient of thermal expansion CTE, the coefficient of moisture expansion CME, and the friction value μ , etc.)

Transversely-Isotropic Material: of **5** for the these basically brittle materials

- 5 elastic ‘constants’, 5 strengths, 5 strength failure modes fracture (NFs with SFs)
- 2 physical parameters (CTE, CME, $\mu_{\perp\perp}$, $\mu_{\parallel\parallel}$ etc.).

Orthotropic Material: of **9** (6).

This looks to be proven by the investigation of Normal Yielding NY of plexiglass and (theoretically) by a compressive fracture toughness K_{IIcr}^c for a brittle material with an ideally homogeneous state at the crack tip [see section 9 or CUN22, §4].

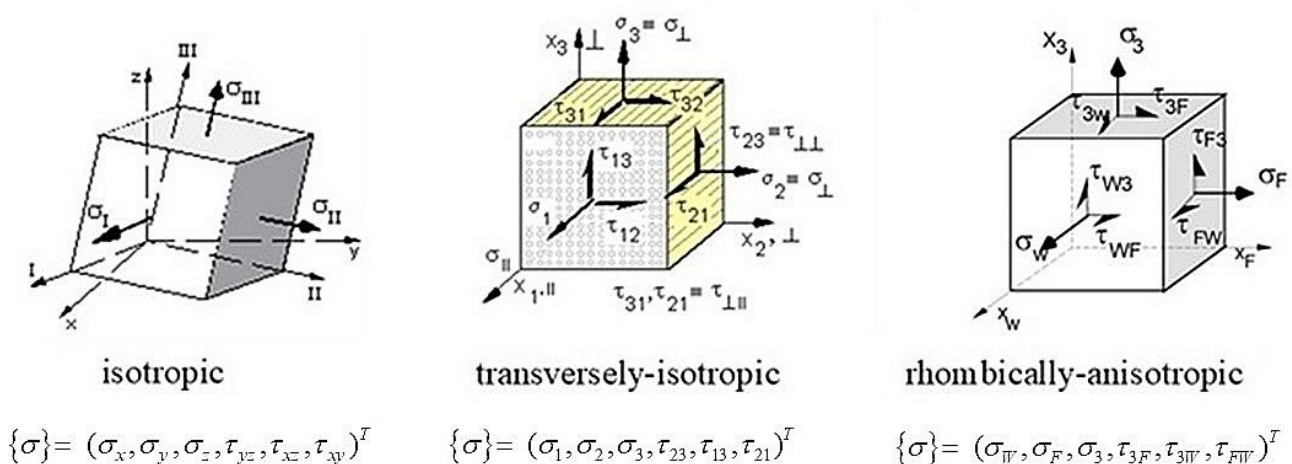


Fig.3-1: Presentation of the stresses faced with the envisaged three material families

LL: A ‘generic’ number seems to be inherent for the different material families.

4 Direct use of a Friction Value μ in the SFCs

Aim: Direct use of the measurable μ instead of applying a μ -hiding friction model parameter.

Mohr-Coulomb acts. Therefore, in the case of compressed brittle materials the effect of friction is to capture, which usually is performed by ‘fictitious’ friction-linked model parameters. Such a model parameter for friction, here the a or the b in the SFC, can be replaced by the measured μ .

In order to achieve this, the very challenging task to transform an SFC in structural stresses into a SFC in Mohr stresses had to be successfully to be performed [Cun23c, Annex2]. Ultimately, an engineer prefers the application of a measurable and physically understandable value μ , especially, because it does not scatter that much, which is essential in design.

Exemplarily for UD material this is executed within the full SFC set in the Table 4-1:

Table 4-1, UD materials: 3D SFC formulations for FF1, FF2 and IFF1, IFF2, IFF3 and 2D

<p>FF1: $Eff^{\parallel\sigma} = \check{\sigma}_1 / \bar{R}_{\parallel}^t = \sigma_{eq}^{\parallel\sigma} / \bar{R}_{\parallel}^t$ with $\check{\sigma}_1 \cong \varepsilon_1^t \cdot E_{\parallel}$ (matrix neglected)</p> <p>FF2: $Eff^{\parallel\tau} = -\check{\sigma}_1 / \bar{R}_{\parallel}^c = +\sigma_{eq}^{\parallel\tau} / \bar{R}_{\parallel}^c$ with $\check{\sigma}_1 \cong \varepsilon_1^c \cdot E_{\parallel}$</p> <p>IFF1: $Eff^{\perp\sigma} = [(\sigma_2 + \sigma_3) + \sqrt{\sigma_2^2 - 2\sigma_2 \cdot \sigma_3 + \sigma_3^2 + 4\tau_{23}^2}] / 2\bar{R}_{\perp}^t = \sigma_{eq}^{\perp\sigma} / \bar{R}_{\perp}^t$</p> <p>IFF2: $Eff^{\perp\tau} = [a_{\perp\perp} \cdot (\sigma_2 + \sigma_3) + b_{\perp\perp} \sqrt{\sigma_2^2 - 2\sigma_2 \sigma_3 + \sigma_3^2 + 4\tau_{23}^2}] / \bar{R}_{\perp}^c = \sigma_{eq}^{\perp\tau} / \bar{R}_{\perp}^c$</p> <p>IFF3: $Eff^{\perp\parallel} = \{ [b_{\perp\parallel} \cdot I_{23-5} + (\sqrt{b_{\perp\parallel}^2 \cdot I_{23-5}^2 + 4 \cdot \bar{R}_{\perp\parallel}^2 \cdot (\tau_{31}^2 + \tau_{21}^2)^2})] / (2 \cdot \bar{R}_{\perp\parallel}^3) \}^{0.5} = \sigma_{eq}^{\perp\parallel} / \bar{R}_{\perp\parallel}$</p> <p>$\{ \sigma_{eq}^{mode} \} = (\sigma_{eq}^{\parallel\sigma}, \sigma_{eq}^{\parallel\tau}, \sigma_{eq}^{\perp\sigma}, \sigma_{eq}^{\perp\tau}, \sigma_{eq}^{\perp\parallel})^T$, $I_{23-5} = 2\sigma_2 \cdot \tau_{21}^2 + 2\sigma_3 \cdot \tau_{31}^2 + 4\tau_{23}\tau_{31}\tau_{21}$</p> <p>Inserting the compressive strength point $(0, -\bar{R}_{\perp}^c) \rightarrow a_{\perp\perp} \cong \mu_{\perp\perp} / (1 - \mu_{\perp\perp})$, $b_{\perp\perp} = a_{\perp\perp} + 1$ from a measured fracture angle $\rightarrow \mu_{\perp\perp} = \cos(2 \cdot \theta_{fp}^c \cdot \pi / 180)$, for $50^\circ \rightarrow \mu = 0.174$.</p> <p>$b_{\perp\parallel} = 2 \cdot \mu_{\perp\parallel}$. Typical friction value ranges: $0 < \mu_{\perp\parallel} < 0.25$, $0 < \mu_{\perp\perp} < 0.2$.</p>

And additionally for the 2D-case, using a simplified friction modelling ($Eff^?$. See Fig.13-4):

$$Eff^m = [(Eff^{\parallel\sigma})^m + (Eff^{\parallel\tau})^m + (Eff^{\perp\sigma})^m + (Eff^{\perp\tau})^m + (Eff^{\perp\parallel})^m]$$

with the mode portions inserted, 2D,

$$Eff = [(\frac{(\sigma_1 + |\sigma_1|)}{2 \cdot \bar{R}_{\parallel}^t})^m + (\frac{(-\sigma_1 + |\sigma_1|)}{2 \cdot \bar{R}_{\parallel}^c})^m + (\frac{(\sigma_2 + |\sigma_2|)}{2 \cdot \bar{R}_{\perp}^t})^m + (\frac{(-\sigma_2 + |\sigma_2|)}{2 \cdot \bar{R}_{\perp}^c})^m + (\frac{|\tau_{21}|}{\bar{R}_{\perp\parallel} + 0.5 \cdot \mu_{\perp\parallel} \cdot (-\sigma_2 + |\sigma_2|)}})^m]^{1/m}$$

Table 4-2, Isotropic materials:

<p>Assumption: Fracture failure body is rotationally symmetric like Mises yield body.</p> <p>$I_1 = (\sigma_I + \sigma_{II} + 0) = f(\sigma)$, $6J_2 = (\sigma_I - \sigma_{II})^2 + (\sigma_{II} - 0)^2 + (0 - \sigma_I)^2 = f(\tau)$</p> <p>* Normal Fracture NF, $I_1 > 0$ \leftrightarrow * Shear Fracture SF, $I_1 < 0$</p> <p>Strength Failure Criterion (SFC), mode interaction exponent $m = 2.7$, $\mu = 0.2$</p> $Eff^{NF} = \frac{\sqrt{4J_2 - I_1^2 / 3} + I_1}{2 \cdot R^t} = \frac{\sigma_{eq}^{NF}}{\bar{R}^t} \leftrightarrow Eff^{SF} = \frac{c_2^{SF} \cdot I_1 + \sqrt{(c_2^{SF} \cdot I_1)^2 + 12 \cdot c_1^{SF} \cdot 3J_2}}{2 \cdot R^c} = \frac{\sigma_{eq}^{SF}}{\bar{R}^c}$ <p>$c_1^{SF} = 1 + c_2^{SF}$, $c_2^{SF} = (1 + 3 \cdot \mu) / (1 - 3 \cdot \mu)$ from $\mu = \cos(2 \cdot \theta_{fp}^c \cdot \pi / 180)$.</p> $Eff = [(Eff^{NF})^m + (Eff^{SF})^m]^{m^{-1}} \rightarrow f_{RF} = 1 / Eff$
--

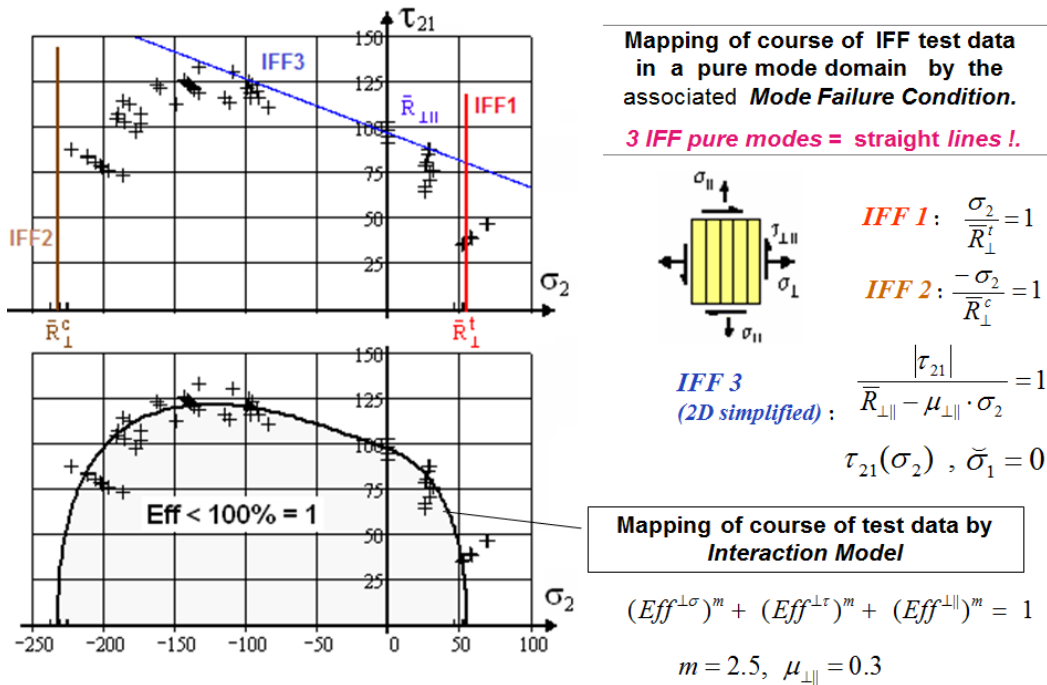


Fig.4-1: Exemplary visualization of the IFF interaction of a UD-material [Cun06]

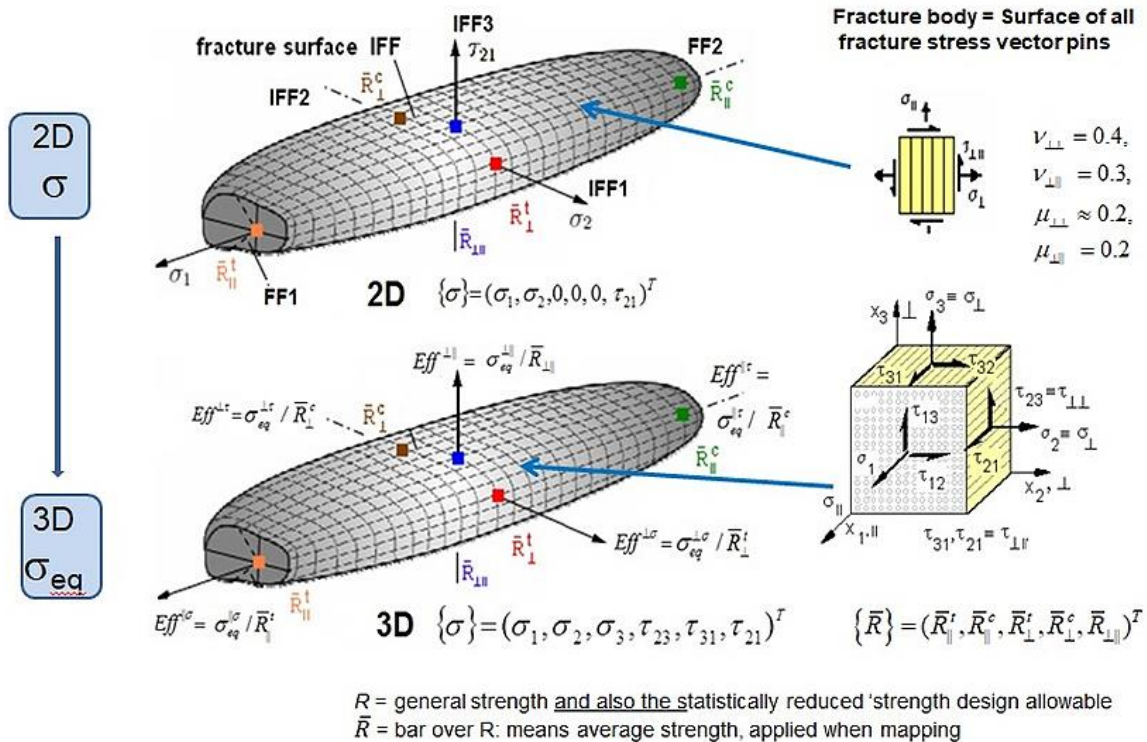


Fig.4-2: From a 2D failure body to a 3D failure body by replacing stresses by equivalent stresses

The upper figure displays the UD failure body as the visualization of the associated SFC set. The lower figure documents that if moving from the ply stresses to the mode-linked equivalent ply stresses one keeps the same UD failure body, usable now as 3D failure body!

Often, SFCs employ just strengths and no friction value. This is physically not accurate and the undesired consequence in Design Verification is: *The Reserve Factor may be not on the safe side.*

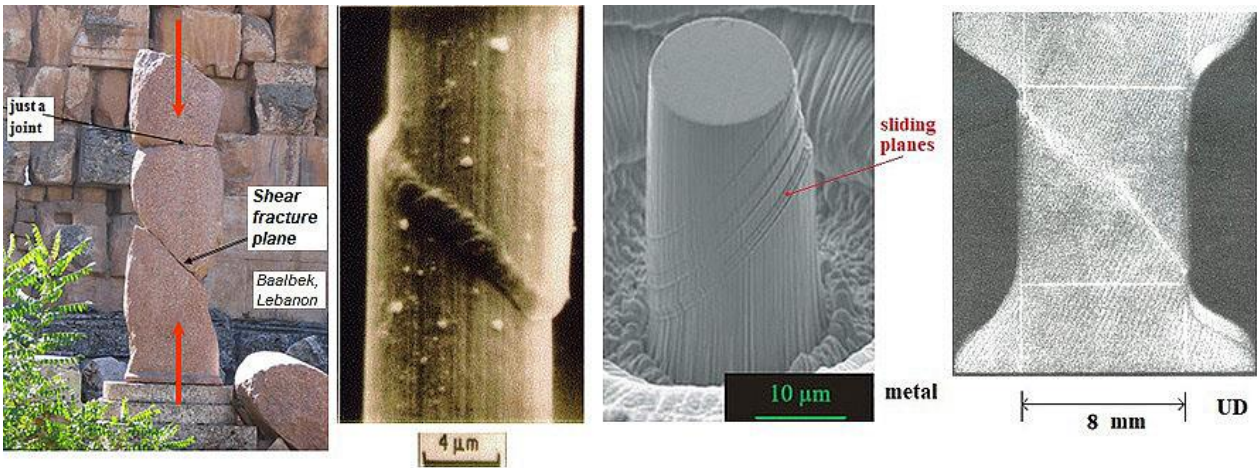


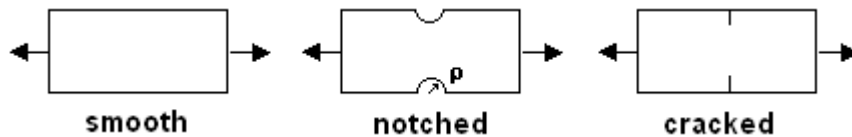
Fig.4-3,Friction driven shear fracture planes at extreme length scales : Fracture angles of the brittle materials Rock material, Carbon fiber [K. Schulte, TU Hamburg-Harburg], Ductile metal compression cut from a single crystal (deformed pillar after compression testing. Monnet, G. & Pouchon, M. A. (2013), Determination of the so-called critical resolved shear stress and the friction stress in austenitic stainless steels by compression of pillars extracted from single grains', Mater. Letters 98, 128-130) and laterally compressed UD-CFRP

LL:

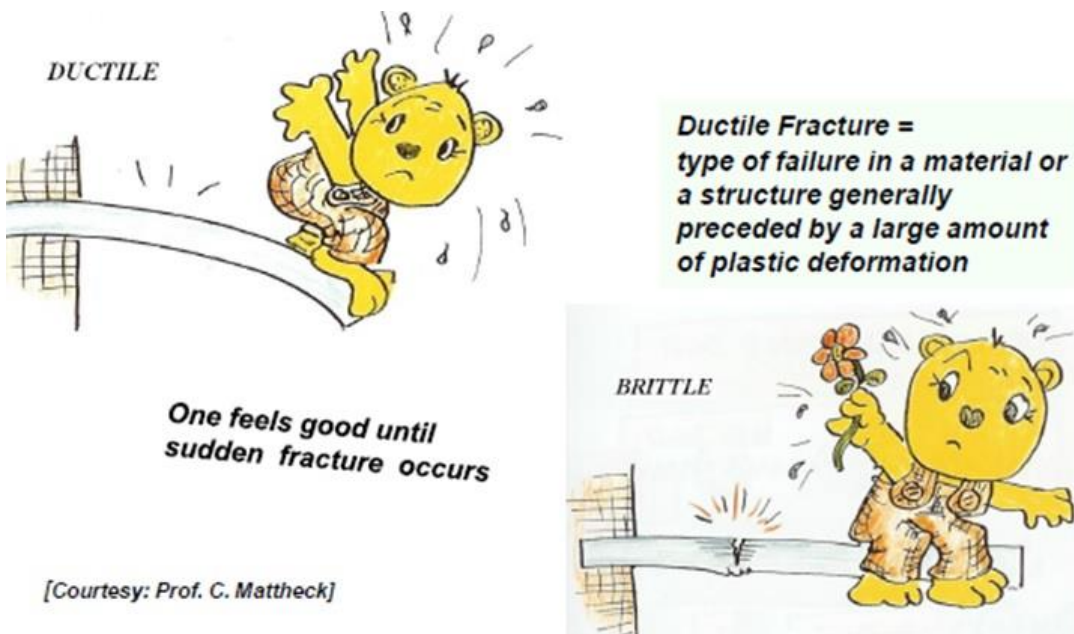
- * In contrast to the 'doing': Friction must and can now be directly considered by the measured μ
- * Friction occurs similarly over the scales.

In the above context:

Two basic features are faced by the structure-designing engineers, three types of surfaces



and the behavior of the material, whether it is brittle (about $R^c > \approx 3 \cdot R^t$) or ductile.



5 Material stressing effort Eff (Werkstoffanstrengung)

Aim: Generation of a physical basis for the interaction of failure modes and for an excellent understanding of a failure body (Eff = 100%) with multi-axial strength (capacity) values.

If several failure modes are activated by the stress state then the application of the so-called *material stressing effort Eff* (in German: *Werkstoffanstrengung*. This artificial name had to be created in the World Wide Failure Exercise on UD-SFCs, together with the UK-organizers, because an equivalent term to the excellent German term is not known in English) is very helpful because the full *Eff* consists of all mode portions Eff^{mode} . It works analogous to ‘Mises’

$$Eff^{\text{yield mode}} = \sigma_{eq}^{\text{Mises}} / R_{0.2} \rightarrow Eff^{\text{fracture mode}} = \sigma_{eq}^{\text{fracture mode}} / R .$$

The contribution of each single Eff^{mode} informs the designing engineer about the importance of the single portions in the SFC and thereby about the critical failure driving mode and thereby outlining the design-driving mode.

Whereas the structural engineer is more familiar with the equivalent stress the material engineer prefers above ‘material stressing effort’ *Eff*. The terms are linked by $\sigma_{eq}^{\text{mode}} = Eff^{\text{mode}} \cdot R^{\text{mode}}$.

The use of *Eff* supports ‘Understanding the multi-axial strength capacity of materials’ (Fig.13-4): For instance, 3D-compression stress states have a higher bearing capacity, but the value of *Eff* nevertheless stays at 100%. Consequently, this has nothing to do with an increase of a (*uniaxial*) technical strength *R* which is a fixed result of a Standard!

The following fracture test result of a brittle concrete impressively shows how a slight hydrostatic pressure of 6 MPa increases the strength capacity in the longitudinal axis from 160 MPa up to 230 MPa - 6 MPa = 224 MPa. Thereby, the benefit of 3D-SFCs–application could be proven as the fracture stress states below depict:

$$\sigma_{fr} = (\sigma_I, \sigma_{II}, \sigma_{III})_{fr}^T = (-160, 0, 0)^T \text{ MPa} \Leftrightarrow (-224 - 6, -6, -6)^T \text{ MPa}$$

Because both the *Eff*s are 100% for $(-160, 0, 0)^T$ and for $(-224 - 6, -6, -6)^T$ [CUN,§5.5]!

This can be transferred to the quasi-isotropic plane of the transversely-isotropic UD-materials, $\sigma_2 - \sigma_3$, see [Cun23c], and to the orthotropic CMC fabric, when beside shear τ_{WF} the compressive stress σ_W^c acts together with σ_F^c and both activate friction on the sides [Cun24b].

LL: The physically clear-based quantity Eff gives an impressive interpretation of what 100% strength capacity in 3D stress states physically really means.

6 Interaction of Failure Modes and a Multi-fold (fracture) Failure Mode

Aim: Displaying the general effect of a failure mode interaction

If two neighboring modes are activated at the same time then this combined action (= *interaction*) reduces the strength capacity, the natural frequency and the stability loading, being quantities in three different fields. The combined action of strength failure modes can be captured by the material stressing effort Eff . Due to this two effects can be simply treated by the use of Eff in contrast to the traditional SFCs, where the effects cannot be directly considered.

Mixed Strength fracture Failure (mode interaction),

Different failure modes may be activated by the acting stress state. The interaction of both the activated fracture mode types Normal Fracture NF (tension) with Shear Fracture SF (under compression) increases the danger to fail! Hence, the associated fracture test data is a so-called joint-probabilistic results of two acting modes!

Multi-fold fracture Failure Mode:

An acting in-plane stress state with maximally equal orthogonal stresses activates the same mode two-fold. Hence, the associated fracture test data is a so-called joint-probabilistic result of a two-fold acting mode!

Lessons Learned:

* A usual SFC just describes a 1-fold occurring failure mode or mechanism! A multi-fold occurrence of the same failure mode (*as given for $\sigma_1 = \sigma_{II}$ or for $\sigma_2 = \sigma_3$*) with its joint probabilistic failure effect is in addition to be considered in each formulated modal SFC. The effect is to map by an additional term in Eff ,

Two-fold failure danger in the σ_2 - σ_3 -domain stands for a failure surface closing, modelled by

$$Eff^m = (Eff^{\parallel\tau})^m + (Eff^{\parallel\sigma})^m + (Eff^{\perp\sigma})^m + (Eff^{\perp\tau})^m + (Eff^{\perp\parallel})^m + (Eff_{\perp}^{MfFd})^m = 1$$

with $Eff_{\perp}^{MfFd} = (\sigma_2^t + \sigma_3^t) / 2\bar{R}_{\perp}^t$, and $\bar{R}_{\perp}^t \approx \bar{R}_{\perp}^c / \sqrt{2}$ after [Awa78]

considering $\sigma_2^t = \sigma_3^t$ and $\sigma_2^c = \sigma_3^c$; $\bar{R}_{\perp}^t \leq \bar{R}_{\perp}^c$, $\bar{R}_{\perp}^{cc} \leq \bar{R}_{\perp}^c$ if porous.

* Traditional SFCs may not capture this effect and thus violate for instance in the case of isotropic materials the isotropy-inherent 120°-symmetry of the failure body.

[Awa78] Awaji H and Sato S: A Statistical Theory for the Fracture of Brittle Solids under Multiaxial Stresses. Int. J. of Fracture 14 (1978), R 13-16

LL:

* *Unfortunately, the two effects Mixed Strength fracture Failure (=mode interaction) and facing a Multi-fold fracture Failure Mode are not taught, but are very essential to understand strength mechanics.*

* *There is no difference between utilizing a strength criterion or a limit strain criterion if both are accurately applied considering the behavior. (However, who does this?).
Stress states are the usual basis for a design engineer to assess a design's strength because stresses destroy the material. Limit strain conditions are helpful in pre-dimensioning.*

7 So-called ‘Global’ SFCs and (failure mode-linked) ‘Modal’ SFCs

Aim: Shortly explaining the difference of ‘Global’ and ‘Modal’ SFCs.

There are a lot of possibilities to generate SFCs. *Fig.7-1* presents a survey:

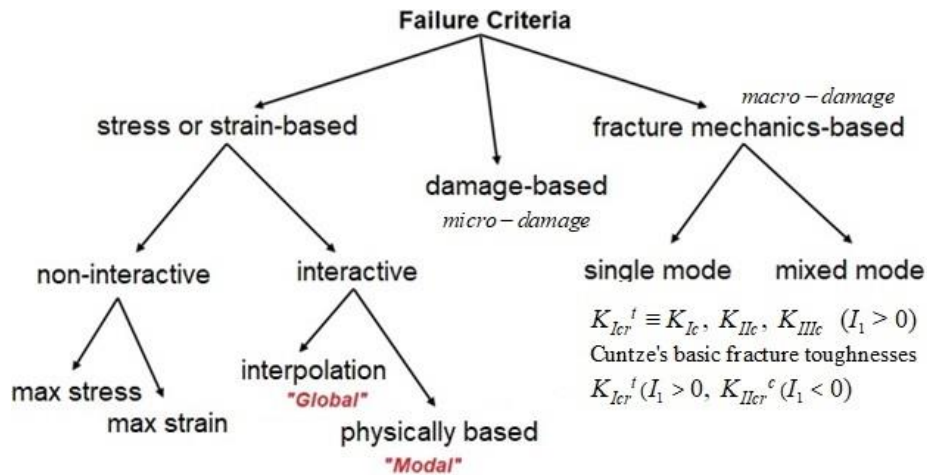


Fig.7-1: Possibilities to generate SFCs when following Klaus Rohwer [Rohwer K.: Predicting Fiber Composite Damage and Failure. Journal of Composite Materials, published online 26 Sept. 2014 (online version of this article can be found at: <http://jcm.sagepub.com/content/early/2014/09/26/0021998314553885>)

Above depicted interactive SFCs can be discriminated. To do that the author choose the term “global“ as a ‘play on words’ to “modal” hoping both the terms are self-explaining. Here, global and modal have a similar level of abstraction, as in the case of stability the terms ‘global’ and ‘local’ have.

In the case of ‘modal’ SFCs (such as the FMC-based ones) equivalent stresses can be computed, not only for isotropic materials like for ‘Mises’, such as $\{\sigma_{eq}^{mode}\} = (\sigma_{eq}^{\parallel\sigma}, \sigma_{eq}^{\parallel\tau}, \sigma_{eq}^{\perp\sigma}, \sigma_{eq}^{\perp\tau}, \sigma_{eq}^{\parallel\perp})^T$, and this is advantageous for design decisions. Within a ‘global’ SFC formulation all modes are mathematically married. This has a very bad impact: Each change, coming from a new test information for any pure mode, has an effect on all other independent failure modes and might include some redesign, see the full change of the ZTL-curve in *Fig.7-2*. Such a bad impact is never faced using a ‘modal’ formulation, like the FMC one.

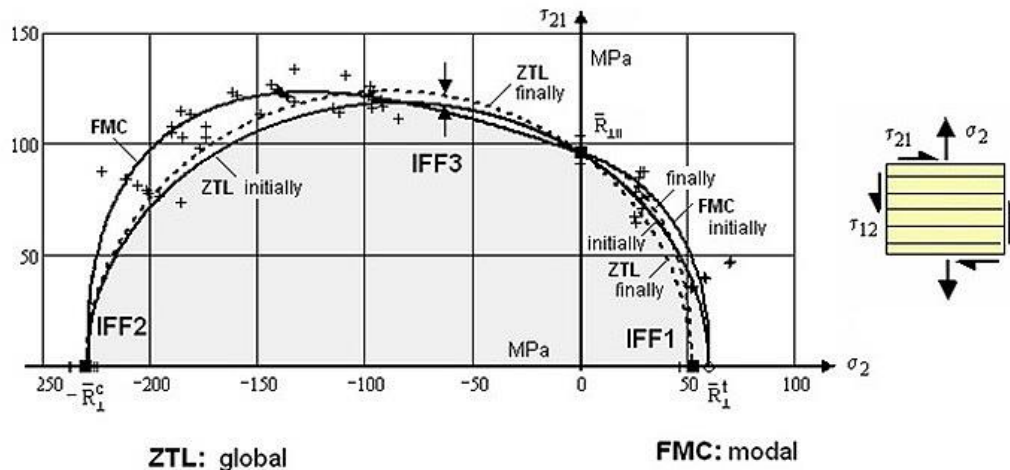
Of course, as still cited, a modal FMC-approach requires an interaction in all the mode transition zones This is performed by a probabilistic approach, using a ‘series failure system’ in the transition zone of adjacent modes NF with SF, reading:

$$Eff = \sqrt[m]{(Eff^{mode\ 1})^m + (Eff^{mode\ 2})^m + \dots} = 1 = 100\% \quad \text{for Onset-of-Failure}$$

and applying a mode interaction exponent m , also termed rounding-off exponent, the size of which is high in case of low scatter and vice versa. The value of m is obtained by curve fitting of test data in the transition zone of the interacting modes. Experience delivered that $2.5 < m < 2.9$.

With the FMC-based SFCs for the three ‘material families’ available multi-axial fracture test data were mapped to validate the SFCs being the mathematical descriptions of the envisaged fracture failure models. For a large variety of materials the associated fracture bodies were displayed with

distinct cross-sections of them, for instance for the isotropic applications: Principal stress plane, octahedral stress plane and tensile and meridian planes. Various links or interrelationships between the materials could be outlined.



$$\frac{\sigma_2^2}{\bar{R}_\perp^t \cdot \bar{R}_\perp^c} + \sigma_2 \cdot \left(\frac{1}{\bar{R}_\perp^t} - \frac{1}{\bar{R}_\perp^c} \right) + \frac{\tau_{21}^2}{\bar{R}_{\perp\parallel}} = 1 \quad \left(\frac{\sigma_2}{\bar{R}_\perp^t} \right)^m + \left(\frac{-\sigma_2}{\bar{R}_\perp^c} \right)^m + \left(\frac{|\tau_{21}|}{\bar{R}_{\perp\parallel} - \mu_{\perp\parallel} \cdot \sigma_2} \right)^m = 1$$

Fig.7-2: Modelling example, impact of a novel test information in the mode IFF1 considering a global (ZTL-SFC, still used in the HSB) and a modal SFC,

Considering the shortcomings of ‘global’ UD SFCs, my friend John Hart-Smith cited:

“It is scientifically incorrect to employ polynomial interaction failure models (the ‘global’ ones), if the mechanism of failure changes”!

Drucker-Prager, Ottosen, Willam-Warnke, Tsai –Wu, Altenbach/Bolchun/Kolupaev, Yu, etc.

1 Global strength failure condition : $F(\{\sigma\}, \{R\}) = 1$ (usual formulation)
Set of Modal strength failure conditions: $F(\{\sigma\}, R^{mode}) = 1$ (addressed in FMC)

Mises, Puck, Cuntze

... and more precisely, considering Mohr-Coulomb for brittle materials under compression

$$F(\{\sigma\}, (R^{mode}, \mu^{mode})) = 1$$

UD: $\{\sigma\} = (\sigma_1, \sigma_2, \sigma_3, \tau_{23}, \tau_{31}, \tau_{21})^T$, $\{R\} = (\bar{R}_\parallel^t, \bar{R}_\parallel^c, \bar{R}_\perp^t, \bar{R}_\perp^c, \mu_{\perp\parallel}, \bar{R}_{\perp\parallel}, \mu_{\perp\parallel})^T$
 vector of 6 stresses (general) vector of 5 strengths with 2 friction values

Isotrop: $\{\sigma\} = (\sigma_x, \sigma_y, \sigma_z, \tau_{yz}, \tau_{zx}, \tau_{xy})^T = (\sigma_I, \sigma_{II}, \sigma_{III})^T$, $\{R\} = (\bar{R}^t, \bar{R}^c, \mu)^T$

Test data mapping : \bar{R} average strength value (statistical mean)
 Design Verification : R strength design allowable

Fig. 7-3: Scheme for displaying ‘global’ and ‘modal’ SFCs

LL: So-called ‘Global’ SFCs couple physically different failure modes whereas the Modal SFCs describe each single failure mode and therefore will better map the course of test data and not lead to a wrong Reserve Factor.

8 Validity Limits of UD SFC Application → Finite Fracture Mechanics (FFM)

Aim: Giving the SFC user a warning by information on the validity limits.

There are three approaches available to deal with the occurring stress situations: Strength criteria (SFC), Continuum (micro-)Damage mechanics (CDM) criteria and Fracture Mechanics (FM) which employ macro-crack growth models.

A SFC is a necessary condition but might not be a sufficient condition for the prediction of ‘initiation of cracking’ (Onset-of-Failure). This is known for a long time from the so-called ‘thin layer effect’: Due to being strain-controlled, the material flaws in a thin lamina cannot grow freely up to micro-crack size in the thickness direction, because the neighboring laminas act as micro-crack-stoppers. Considering fracture mechanics, the strain energy release rate, responsible for the development of damage energy in the 90° plies - from flaws into micro-cracks and larger -, increases with increasing ply thickness. Therefore, the actual absolute thickness of a lamina in a laminate is a driving parameter for initiation or onset of micro-cracks, i.e. [Fla82].

In the case of plain structural parts crack initiation (*according to FF, IFF of the ply and delamination of the laminate*) in brittle and semi-brittle materials cannot be fully captured by the SFCs, because both a critical energy and a critical stress state must be fulfilled.

Further known is, in the case of discontinuities such as notch singularities with steep stress decays only a *toughness + characteristic length-based energy balance condition* may form a sufficient set of two fracture conditions.

When applying SFCs usually ideal solids are viewed which are assumed to be free of essential micro-voids or microcrack-like flaws. When applying Fracture Mechanics the solid is considered to contain macro-voids or macro-cracks. Since about 20 years Finite Fracture Mechanics (FFM) fills a gap between Continuum Mechanics (CM) strength criteria and classical FM. FFM is an approach to offer a criterion to predict the crack initiation in brittle isotropic and UD materials. This is the the bridge had to be built from strength failure to fracture mechanics failure. Attempts to link SFC-described ‘onset of fracture’ prediction methods and FM prediction methods for structural components have been performed. Best known is the Hypothesis of Leguillon [Leg02]:

“A crack is critical when and only when both the released energy and the local stress reach critical values along an assumed finite crack”.

Within FFM assumed cracks of finite length are considered. In his finite fracture mechanics Leguillon assumes a crack as one more unknown but one can solve the equation system by one more equation from FM.

His coupled criterion does not refer to microscopic mechanisms to predict crack nucleation.

[Leg02] Leguillon D: *Strength or Toughness? –A criterion for crack onset at a notch*. Europ. J. of Mechanics A/Solids 21 (2002), 61 – 72 end. Ist. D. sci. Lett., Cl. Mat. Nat.18, 705-714 (1885)

[Fla82] Flagg D L and Kural M H: *Experimental Determination of the In Situ Transverse Lamina Strength in Graphite Epoxy Laminates*. J. Comp. Mat. Vol 16 (1982), S. 103-116

LL:

** SFCs are ‘just’ necessary but not sufficient for the prediction of strength failure. Basically, due to internal flaws, also an energy criterion is to apply. The novel approach ‘Finite Fracture Mechanics (FFM)’ offers a hybrid criterion to more realistically predict the stress-based crack initiation in brittle isotropic and UD materials.*

- * The coupled criterion SFC-FM can be used with some confidence to predict the crack initiation in brittle materials in new design situations as never could be done before.*
- * When applying test data from 'isolated lamina' test specimens (like tensile coupons) to an embedded lamina of a laminate one should consider that coupon test deliver tests results of 'weakest link' type. An embedded or even an only one-sided constrained lamina, however, possesses redundant behavior*
- * It is to regard thereby, when considering the formulations to be applied: Short cracks behave differently to Large Cracks*
- * For usual 'strength problems' FFM is not applicable.*
- * It is advantageous for the analysis of notched structural parts and captures applications usually performed by the well-known Neuber theory.*

9 ‘Curiosities’ regarding Classical Material Mechanics

Aim: Filling two rooms in the material mechanics building by proving the assumed ‘generic’ number.

Regarding a material ‘generic’ number of 2 to be valid for isotropic materials there are two ‘empty rooms’ in the author-assumed ‘Mechanics Building’ of Isotropic Materials namely Normal Yielding NY and a counterpart of the tensile fracture toughness $K_{Icr}^{(I)}$ in the compressive domain.

9.1 Normal Yielding NY: [CUN22, §4]

Glassy, amorphous polymers like polystyrene (PS), polycarbonate (PC) and PolyMethylMethacrylate (PMMA = plexiglass) are often used structural materials. They experience two different yield failure types, namely crazing under tension (*Fig.9-1*)

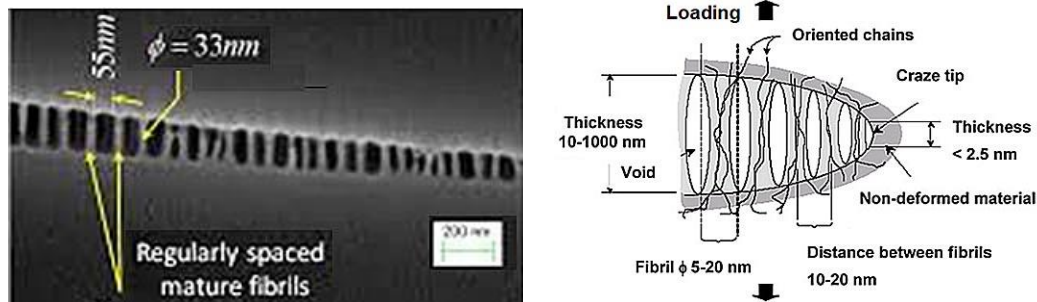


Fig. 9-1: PMMA, SEM image of a craze in Polystyrene Image (created by Y. Arunkumar)

and under compression a shear stress yielding that is often termed shear-banding.

. Crazing can be linked to Normal Yielding (NY) which precedes the crazing-following tensile fracture. Crazing occurs with an increase in volume through the formation of fibrils bridging built micro-cracks and shear banding does not (keeps volume). Therefore, due to the FMC ‘rules’ the dilatational I_I^2 is to employ in the SFC-approach for tension $I_I > 0$. Under compression, brittle amorphous polymers classically shear-band (SY) and experience friction. Therefore, I_I must be em-

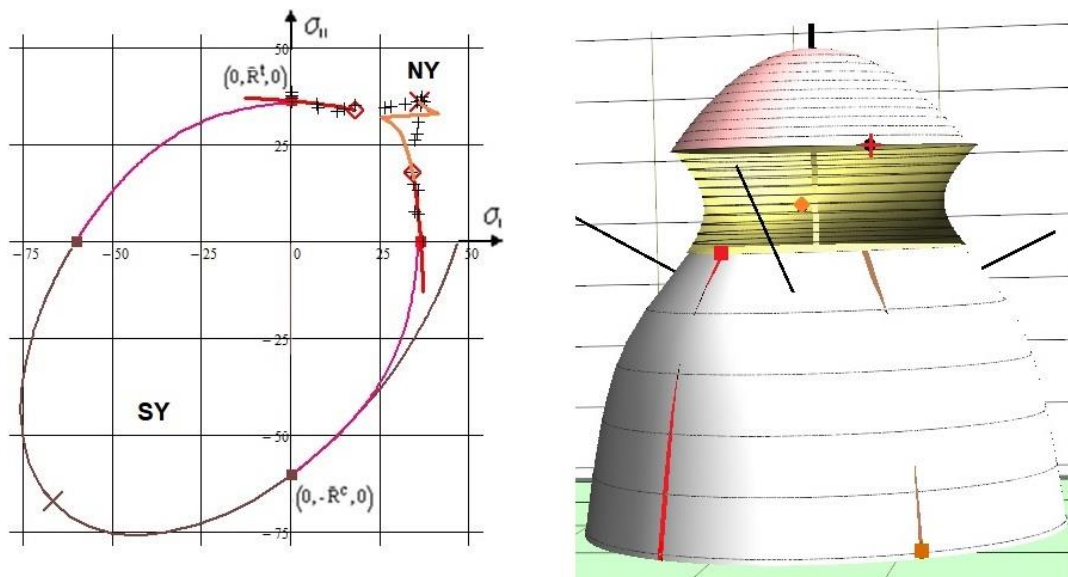


Fig. 9-2, PMMA: (left) Mapping of test data in tension and compression principal stress domain with and without interaction; (right) depiction of the fracture body shape with some representative points. For the validation of the FMC-based SFC for PMMA two data sets were available, one NY-2D-data set from Sternstein-Myers and a SY-3D-data set from Matsushige

[Ste73] Sternstein S S and Myers F A: *Yielding of glassy polymers in the second quadrant of principal stress space*. J. Macromol. Sci, Phys. B 8 (1973), 539-571

[Mat75] Matsushige K, Radcliffe S V and Baer E: *The mechanical behavior of polystyrene under pressure*. J. of Material Science 10 (1975), 833-845.

ployed in the approach for $I_1 < 0$ in order to consider material internal friction. ‘Mises’ means frictionless yielding and therefore it forms a cylinder.

For obtaining the complete yield failure body (*Fig.9-2*) its parts NY and SY are to interact in the transition zone. Doing this the used Mathcad 15 code had no problems to generate the **3D**-failure body, however the **2D**-visualization of the NY failure surface using Mathcad 15 code (*a 35 DIN A4-pages application*) was too challenging for the solver which had to face a concave 2D principal stress plane situation instead of a usual convex one.

LL: *The failure type crazing shows a ‘curiosity’ under tensile stress states: A non-convex shape exists for Onset-of-Crazing (\bar{R}_{NY}^t). This violates the convexity stability postulate of Drucker, meaning “If the stress-strain curve has a negative slope then the material is not Drucker-stable”.*

9.2 Compressive (shear) Fracture Toughness $K_{IIcr}^{(c)}$, [CUN22,§4.2]

Some reasons caused the author to search a compressive fracture toughness:

- An early citation of A. Carpinteri, that approximately reads: “*With homogeneous isotropic brittle materials there are 2 real energy release rates G_{Icr} , G_{IIcr} , one in tension and one in compression*”
- The number of the (basic) fracture toughness quantities may be *theoretically at least* also 2, namely $K_{Icr}^t \equiv K_{Ic}$ together with K_{IIcr}^c (*Fig.9-3*) and
- The novel approach Finite Fracture Mechanics (FFM) that offers a hybrid criterion to more realistically predict the crack initiation in brittle isotropic and UD materials.

A stringent postulate for the author was crack path stability which can be explained “*Only an angle-stable, self-similar crack growth plane-associated critical Stress Intensity Factor (fracture toughness) is a ‘basic’ property*”. This requires as presumption an *ideally* homogeneous isotropic material in front of the crack-tip. Therefore, the investigation is only for an ideal structural mechanics building of importance, because in practice, there are usually no ideal homogeneous conditions at the crack-tip.

Practically, fracture mechanics is presently only tensile driven performed using $K_{Ic} = K_{Icr}^t$ as a clear critical fracture intensity (the index cr is necessarily to be taken in this document in order to separate tension ^t from compression ^c), where the crack plane does not change. K_{IIc} and K_{IIIc} are ‘just’ very helpful model parameters driving the crack plane in direction of a finally K_{Ic} -failure mode. Why shouldn’t there not be a quantity K_{IIcr}^c that fits as compliment to K_{Icr}^t and where, in an ideal case of no flaws in front of the crack tip, the crack plane grows further along the generated shear fracture angle under a compressive fracture load?

The Fracture Mechanics Mode I delivers a real, ‘basic’ fracture resistance property generated under a tensile stress. Both the Modes II K_{IIc} , and III K_{IIIc} do not show a stable crack plane situation but are nevertheless essential FM model parameters to capture ‘mixed mode loading’ for performing a multi-axial assessment of the far-field stress state. $\rightarrow \bar{R}^t$ and \bar{K}_{Icr}^t correspond!

With the Mode-II compressive fracture toughness K_{IIcr}^c it is like with strength. One says compressive failure, but actually shear (stress) failure is meant, compressive stress is ‘only’ the descriptive term. Therefore the shear index _{II} is to apply. One has to keep in mind: In mechanical

engineering the structural tasks are usually lie in the tension domain (*index ^t is skipped*), whereas oppositely in civil engineering the compression domain is faced (*index ^c is skipped*):

*Tension domain: One knows from K_{Icr}^t (tension), that – viewing the transversal angle - it corresponds to R^t .

*Compression domain: The not generally known second basic SIF K_{IIcr}^c seems to exist under ideal conditions. It corresponds to shear fracture SF happening under compressive stress R^c and leading to the angle Θ_{fp}^c . The crack surfaces are closed for K_{IIcr}^c , friction sliding occurs.

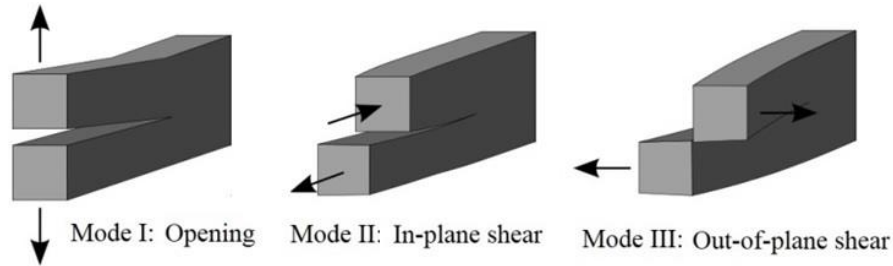


Fig.9-3: Classical Fracture Mechanics modes

Some proof of the author’s postulate could be: There exists a minimum value of the compressive loading at a certain fracture angle. This means that the K_{IIcr}^c becomes a minimum, too. Liu et al performed in [Liu14] tests using a cement mortar material, (Fig.9-4).

► From the measured results, by now, it seems to theoretically at least that the ‘generic’ number 2 is met.

Note on $K_{IIcr}^{(c)}$ as a design entity:

Of theoretical and not of practical value due to the faced not ideal homogeneous isotropic materials.

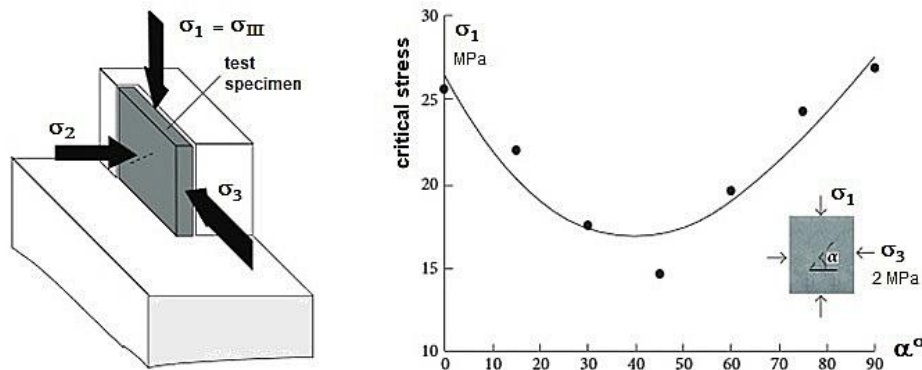


Fig.9-4.: Scheme of the test set-up and of the test points obtained for cement mortar [Liu14], σ_1 represents the mathematical stress σ_{III} (largest compressive stress value).

[Liu J, Zhu Z and Wang B: The fracture characteristic of three collinear cracks under true tri-axial compression. The scientific World Journal, V 2014, article ID459025]

For the transversely-isotropic UD lamina materials it seems directly to match:

► 5 fracture toughness properties correspond to the 5 strength properties, the ‘generic’ number postulate would be fulfilled.

LL: Fracture Mechanics seems to follow material symmetry ‘rules’ and to possess a ‘generic’ number, too.

10 Automated Generation of Constant Fatigue Life curves considering Mean Stress Effect

Aim: Automated derivation of the Constant Life Curve with discussion of the Mean Stress Correction

Generally, in Design Verification (DV) it is to demonstrate that “No relevant limit failure state is met considering all Dimensioning Load Cases (DLCs)”. This involves cyclic DLCs, focusing lifetime with non-cracked and cracked structural parts (*the latter would require Damage Tolerance tools*).

Methods for the prediction of durability, regarding the lifespan of the structural material and thereby of the structural part, involves long time static loading which is linked to ‘static fatigue’ and in particular to ‘cyclic fatigue’. Fatigue failure requires a procedure for the Fatigue Life Estimation necessary to meet above cyclic DV.

Domains of Fatigue Scenarios and Analyses are:

LCF: high stressing and straining

HCF: intermediate stressing $10.000 < n < 2.000.000$ cycles (*rotor tubes, bridges, towers, off-shore structures, planes, etc.*)

VHCF: low stress and low strain amplitudes (*see SPPI466 Very High Cycle Fatigue > 10^7 cycles (in centrifuges, wind energy rotor blades, etc.)*).

Principally, in order to avoid either to be too conservative or too un-conservative, a separation is required of the always needed ‘analysis of the average structural behaviour’ in Design Dimensioning (*using average properties and average stress-strain curves*) in order to obtain best information (= 50% expectation value) from the mandatory single DV-analysis of the final design, where statistically minimum values for strength and minimum, or mean and maximum values for other task-demanded properties are applied as Design Values.

10.1 Fatigue Micro-Damage Drivers of Ductile and Brittle behaving Materials, see [Cun23b]

There are strain-life (*plastic deformation decisive, plastic strain-based $\epsilon_p(N)$*) and stress-life models (*SN*) used. For ductile materials, strain-life models are applied because a single yield mechanism dominates and the alternating stress amplitude counts. For brittle materials, the elastic strain amplitude becomes dominant and stress-life models are applied. With brittle materials inelastic micro-damage mechanisms drive fatigue failure and several fracture mechanisms may come to act. This asks for a modal approach that captures all failure modes which are now fracture modes.

Above two models can be depicted in a Goodman diagram and in a Haigh diagram. The Haigh diagram (σ_a, σ_m) will be applied here because the often used Goodman employs just one quantity σ_a or $\Delta\sigma = 2 \cdot \sigma_a$ or σ_{\max} is not sufficient. A Haigh Diagram represents all available SN curve information by its ‘Constant Fatigue Life (CFL) curves, being the focus here and using the two quantities σ_a, R .

Basic differences between ductile and brittle materials are the following ones,:

- Ductile Material Behavior, isotropic materials: mild steel
 - 1 *micro-damage* mechanism acts \equiv “*slip band shear yielding*“ and drives micro-damage under tensile, compressive, shear and torsional cyclic stresses: *This single mechanism is primarily described by 1 SFC, yield failure condition (HMH, ‘Mises’)*!

- Brittle Material Behavior, isotropic materials: concrete, grey cast iron, etc.
2 micro-damage driving mechanisms act \equiv 2 fracture failure modes Normal Fracture failure (NF) and Shear Fracture failure (SF) under compression described by 2 fracture conditions, the 2 SFCs for NF and SF, where porosity is always to consider
- Brittle Material Behavior, transversely-isotropic UD-materials:
5 micro-damage driving fracture failure mechanisms act \equiv 5 fracture failure modes described by 5 SFCs or strength fracture failure conditions.

A very essential topic is the so-called ‘Mean stress sensitivity’: Within [Cun23b] the author attempts to redirect the ‘Thinking, resulting from ductile material behavior using ‘Mean stress influence correction factors’, which in reality means ‘Walking on crutches’, into a direct ‘Thinking with fracture modes facing brittle material behavior’.

Not fully ductile isotropic materials show an influence of the mean stress on the fatigue strength depending on the (static) tensile strength and the material type. Mean stresses in the tensile range, $\sigma_m > 0$ MPa, lead to a lower permanently sustainable amplitude, whereas compressive mean stresses $\sigma_m < 0$ MPa increase the permanently sustainable amplitude or in other words: A tensile mean stress lowers the fatigue strength and a compressive mean stress increases the fatigue strength.

LL:

- * *A tensile mean stress lowers the fatigue strength and a compressive mean stress increases the fatigue strength*
- * *If it is a pretty ductile material one has one mode ‘yielding’ and if pretty brittle then many modes ‘fracture modes’ are to consider*
- * *Brittle materials like the transversely-isotropic UD material with its five fracture failure modes possess strong mean stress sensitivity, a brittle steel material just 2 modes*
- * *Whether a material has an endurance fatigue limit is usually open regarding the lack of VHCF tests. The strength at $2 \cdot 10^6$ cycles might be only termed apparent fatigue strength (scheinbare Dauerfestigkeit). However, e.g. CFRP could possess a high fatigue limit.*
- * *Whether the material’s micro-damage driver remains the same from LCF until VHCF is questionable and must be verified in each given design case (continuum micro-damage mechanics is asked)*
- * *The ductile material behavior thinking in ‘Mean stress influence’ is to redirect for brittle materials into a thinking in fracture modes.*

10.2 Mapping Challenge of the decisive Transition Zone in the Haigh diagram [Cun23b]

The course of the test data in the transition zone determines the grade of the mean stress sensitivity, which shall be redirect here to a fracture mode-application thinking.

In *Fig.10-1* at first all essential quantities are illustrated. Further, two Constant Fatigue Life (CFL)-curves of a brittle material are displayed, for the envelopes $N = 1$ and $N = 10^7$. The pure mode domains are colored and the so-called transition zone is separated by R_{trans} into two influence parts. The course of the R-value in the Haigh diagram is represented by the bold dark blue lines. The CFL curve $N = 1$ is curved at top because 2 modes act in the case of brittle materials. This is in contrast to uniaxial static loading, depicted by the straight static envelopes, $N \neq N_f$: One micro-damage cycle results from the sum of 2 micro-damage portions, one comes from uploading and one from unloading! For fully ductile materials practically no transition zone between 2 modes exists,

because just one single mode reigns, namely ‘shear yielding’. Therefore, it is no mean stress effect to correct in this case!

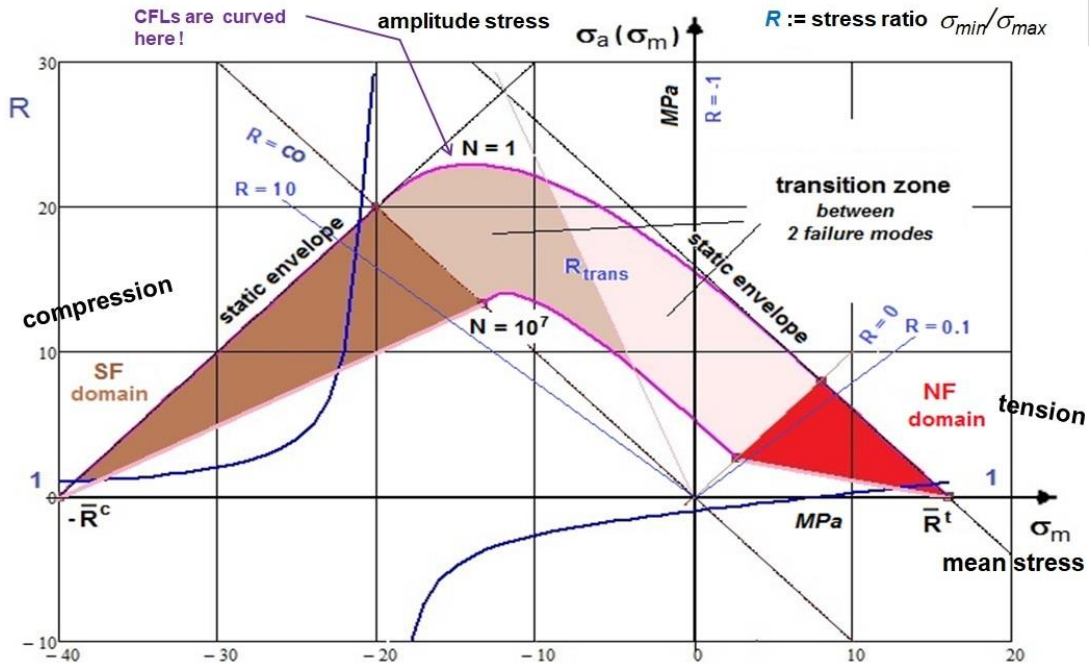


Fig.10-1, Haigh Diagrams: Scheme of pure mode domains, course of R and transition zone parts .
 ($a :=$ amplitude, $m :=$ mean, $N :=$ number of fracture cycles, $\bar{R} :=$ strength and $R := \sigma_{min}/\sigma_{max}$)

The quality of mapping the course of data in the transition zone is practically checked by “How good is the more or less steep course along the stress ratio R_{trans} -line mapped?” This is performed by following the physical reality, that the pure SF-domain is fully decoupled from the NF-domain, and employing oppositely running decay functions f_d , see Fig. 10-2.

$$Eff = [(Eff^{NF})^m + (Eff^{SF})^m]^{m^{-1}} = 100\% \text{ or}$$

$$\left(\frac{-(\sigma_{2m} - \sigma_{2a}) + |\sigma_{2m} - \sigma_{2a}|}{2 \cdot \bar{R}_\perp^c \cdot f_d} \right)^m + \left(\frac{\sigma_{2m} + \sigma_{2a} + |\sigma_{2m} + \sigma_{2a}|}{2 \cdot \bar{R}_\perp^t \cdot f_d} \right)^m = 1$$

$$\rightarrow f_d = 1 / [1 + \exp(\frac{c_1 + \sigma_m}{c_2})]$$

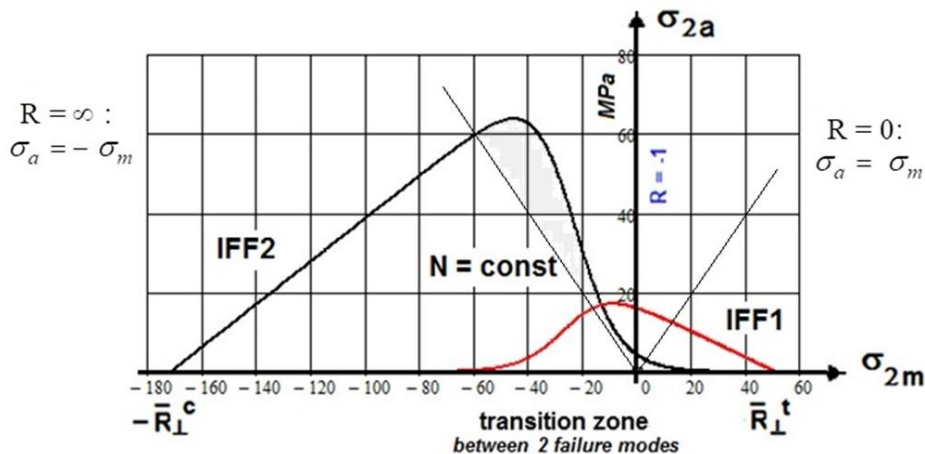


Fig.10-2, example UD material: Course of the decay functions in the transition zone $-\infty < R < 0$

Fig.10-2 illustrates the course of the mode decay functions f_d for the tension and the compression domain. The straight lines in the figure present the extreme SN curve beams, $R = \infty$ for the SF domain and $R = 0$ for the NF domain. In between, the envisaged slightly colored transition zone ($-\infty < R < 0$) is located. Mean stress sensitivity of brittle materials is demonstrated very impressively if the so-called ‘strength ratio’ = compressive strength / tensile strength is high. The two plots in Fig.10-3 will clearly document this.

LL:

- * A large strength ratio R^c/R^t stands for a large mean stress sensitivity
- * A steep decay cannot be captured by a ‘mean stress correction factor’ as can be usually still performed with not fully ductile materials

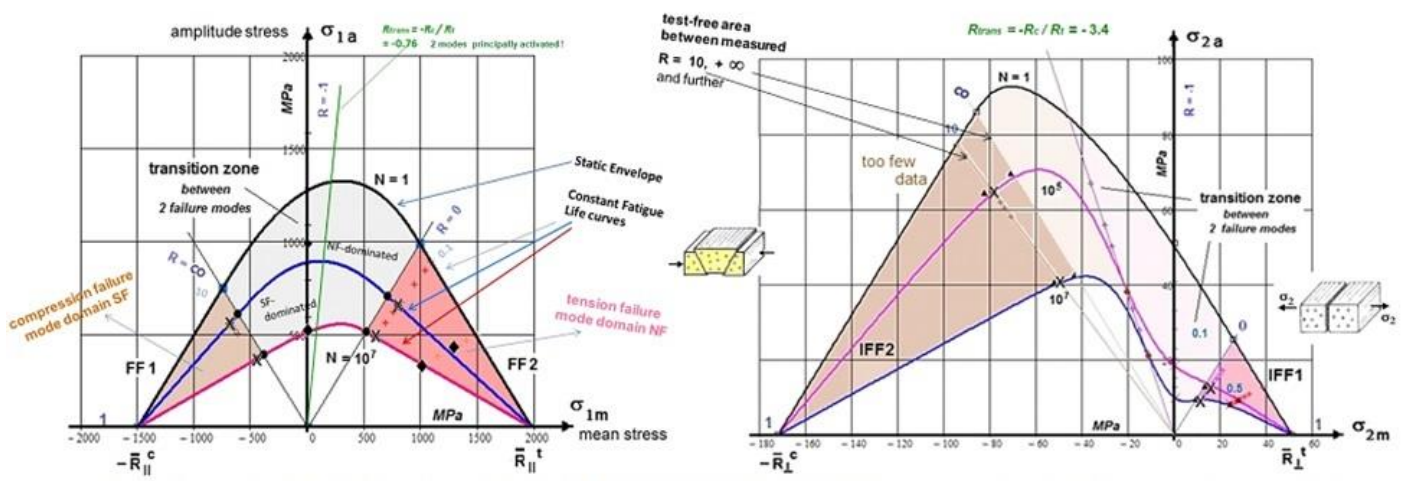
30.3 Estimation of the cyclic Micro-damage Portions of Brittle Materials

A very essential question in the estimation of the lifetime of brittle materials is a means to assess the micro-damage portions occurring under cycling. Here, for brittle behavior the response from practice is: It is permitted to apply validated static SFCs due to the experienced fact:

“If the failure mechanism of a mode cyclically remains the same as in the static case, then the fatigue micro-damage-driving failure parameters are the same and the applicability of static SFCs is allowed for quantifying micro-damage portions”. This is supported because FMC-based static SFCs apply equivalent stresses of a mode SF or NF. See again Fig.10-2 above.

10.4 Automatic Establishment of Constant Fatigue Life Curves (for details , see [Cun23b])

For a decade the author’s intensive concern was to automatically generate Constant Fatigue Life curves on basis of just a few tested Master SN curves coupled to an appropriate physically based model. Such a model the author obtained when M. Kawai gave a presentation during the author’s conference on composite fatigue in 2010 at Augsburg. Kawai’s so-called ‘Modified fatigue strength ratio’ Ψ - model was the fruitful tool found. Kawai’s procedure was a novelty and is applicable to brittle materials such like UD plies (depicted later in Fig.10-4) and isotropic concrete as well.



Rigorous Interpretation of the Haigh diagram for the UD-example FF1-FF2 IFF1- IFF2 UD Haigh diagram (similar for UD, lamella and concrete) displaying the failure mode domains, transition zone

CFRP/EP, $\bar{R}_1^c = 1980$, $\bar{R}_1^t = 1500$, $\bar{R}_1^c = 51$, $\bar{R}_1^t = 172$, $\bar{R}_{1c} = 71$ [MPa].

Fig.10-3: Haigh Diagrams for a UD material: (left) low strength ratio as with ductile materials, (right) high strength ratio as with brittle materials (test data CF/EP, courtesy Clemens Hahne, Audi)

Fig.10-3 (left) displays the differently-colored failure mode domains FF1-FF2 in a UD FF Haigh diagram and (right) IFF1-IFF2 in a UD IFF Haigh diagram. The available test data set along R_{trans} in the transition zone is represented by the crosses.

The decay model quality in Fig.10-3(right) proves the efficiency of the decay functions in the transition zone. For proving this the author is very thankful because this was only possible because he got access to the test results of C. Hahne, AUDI.

In Fig.10-4 the course of the cyclic failure test data can be well mapped by the 4-parameter Weibull formula $R = \text{constant}$: $\sigma_{max}(R, N) = c_1 + (c_2 - c_1) / \exp(\log N / c_3)^{c_4}$.

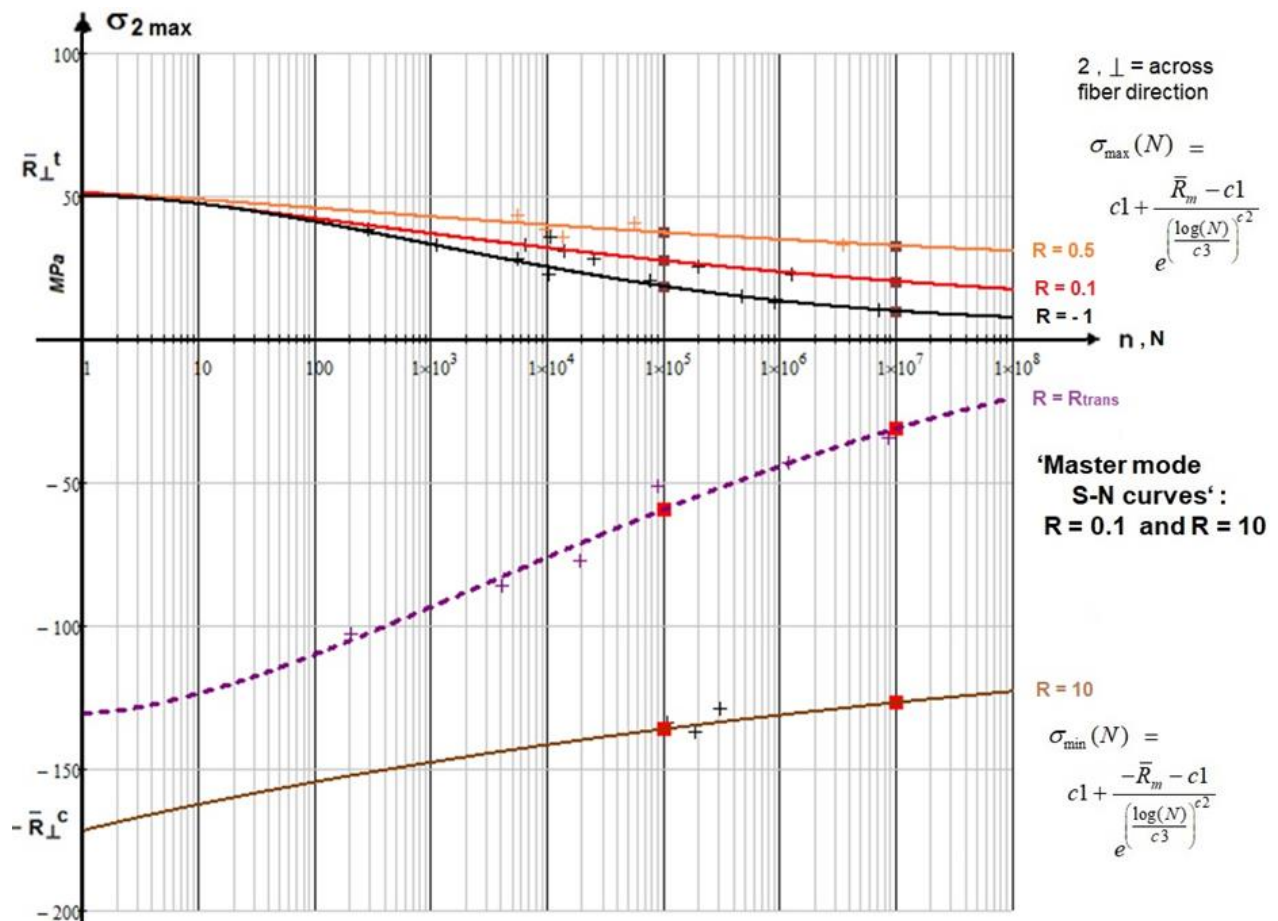


Fig.10-4: SN-curve, lin-log displayed IFF1-IFF2-linked SN curves [test data, courtesy C. Hahne, AUDI] [Kawai M: A phenomenological model for off-axis fatigue behavior of uni-directional polymer matrix composites under different stress ratios. Composites Part A 35 (2004), 955-963]

10.4 Lifetime Estimation

The so-called Palmgren-Miner rule is applied for summing up the cyclic micro-damage portions. HSB-linked statistical analyses have shown that the fatigue life estimation using the linear accumulation method of Palmgren-Miner tends to be too optimistic. However a satisfactory reason could not yet found. One explanation is the 'Right use of the right SFC: Mises not anymore applicable?' A more severe explanation is the loss of the loading sequence, an effect which is

different for ductile and brittle materials. This inaccuracy is practically considered in design by the application of the so-called Relative Miner with defining a $D_{feasible}$ and which must be $< 100\%$.

In the case of variable amplitude loading several SN curves are needed. An example for the computation of the lifetime estimation is displayed by *Fig.10-5*.

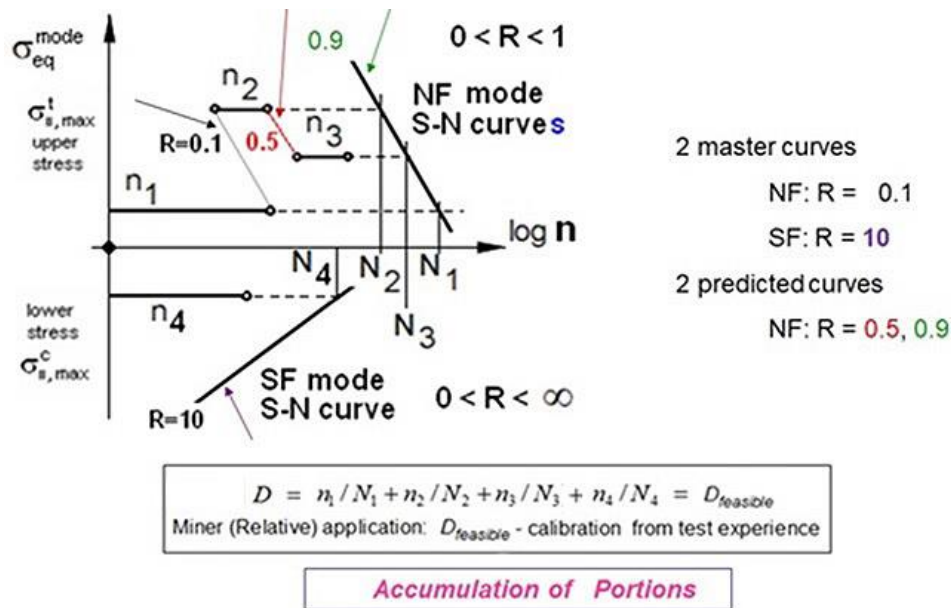


Fig.10-5: Lifetime Prediction (estimation) Method .Summing up of micro-damage portions by the Palmgren-Miner rule. Schematic application of a simple example, 4 blocks. $D_{feasible}$ from test experience

LL:

- * A 'closed CFL-procedure' - as a coupled method - could be found to design-optimally generate mandatory test data-based Constant Life Fatigue curves by using a Master SN curve plus the supporting model to determine other required SN-curves employing Kawai's Ψ -model
 - * The challenging decay along $R_{trans} = -R^c / R^t$ could be modelled
 - * Test data along R_{trans} are more helpful than for $R = -1$, which is the same for ductile behavior
 - * Right use of the right SFC. One cannot blame 'Mises' if yielding is not anymore decisive for the creation of the micro-damage portions
 - * The Palmgren-Miner rule cannot account for loading sequence effects, residual stresses, and for stresses below the fatigue limit (life $\rightarrow \infty$?)
 - * Viewing brittle materials, all the SN curves have their origin in the strength points.
- The author feels that he must redirect the traditional 'Thinking, resulting from ductile material behavior regarding Mean stress correction' into a 'Thinking with fracture modes' in the case of the usually not fully ductile structural materials.

11 Evidence 120°-symmetrical Failure Body of Brittle and also Ductile Isotropic Materials

Aim: Structural Materials Building, Proof that ‘All isotropic materials possess 120° rotational symmetry’ with presentation of 3D-SFCs for isotropic, transversely isotropic UD-materials and orthotropic ones.

11.1 General

From experiments is known, that brittle isotropic materials possess a so-called 120°-axially symmetric fracture failure body in the compressive domain. The question arises: Should ductile materials in the tensile domain not also possess a 120°-axially symmetric yield loci envelope instead of having just the rotationally symmetric ‘Mises cylinder’?

According to the French saying ” Les extrêmes se touchent” and based on his FMC-thinking the author assumed that there is a large similarity in the description of the behavior of very ductile and very brittle materials. Also with ductile materials a 120°-rotational symmetry should be found. In order to prove the 120°-rotational symmetry, test results from bi-axially measuring test specimens are necessary, such as a cruciform or a cylinder.

Searched is the description of a complete failure body. This requires that the SFC captures both the positive and the negative I_1 -domain. Further, the 120°- rotational symmetry should be mapped by the SFC approach (*use of J_3*), too.

Thereby, brittle and ductile material behaviors are to discriminate:

Brittle: In order to show the difference of brittle to ductile materials *Fig. 11-1* outlines the brittle material with its features $\bar{R}^{tt} < \bar{R}^t$ and $\bar{R}^{cc} > \bar{R}^c$. (*Probably not considering the natural flaws in concrete, in [Lem08] was published $\bar{R}^{tt} > \bar{R}^t$ which is physically not explainable and might be the consequence of the difficult measurement*).

Ductile: Deformation measurements prove that for the same strain value of the growing yield surface it holds that equi-biaxial stress $\bar{\sigma}^{tt}(2D) > \bar{\sigma}^t(1D)$. This is similar to brittle concrete in the compressive domain where $\bar{R}^{cc} > \bar{R}^c$ and demonstrates the validity of the 120°-axial symmetry here, too.

Note:

Brittle: bi-axial tension = ‘weakest link failure behavior’ (schwächstes Glied‘-Versagen)
 Brittle: bi-axial compression = redundant (benign) failure behavior (Stützwirkung)
 Ductile: bi-axial compression = redundant (benign) failure behavior (Stützwirkung).

11.2 Brittle Isotropic Materials (Metals, Glass, Ceramics, Concrete, Soil, ..)

2 modes → 2 SFCs, which is in line with the ‘generic’ number 2 according to the FMC.

3D-SFCs of Isotropic Dense Materials

<p>* Normal Fracture NF for $I_1 > 0$ \Leftarrow SFCs \Rightarrow Shear Fracture SF for $I_1 < 0$</p> $F^{NF} = c_{\Theta}^{NF} \cdot \frac{\sqrt{4J_2 \cdot \Theta^{NF} - I_1^2 / 3 + I_1}}{2 \cdot \bar{R}^t} = 1 \quad \leftrightarrow \quad F^{SF} = c_{\Theta}^{SF} \cdot \frac{\sqrt{4J_2 \cdot \Theta^{SF} - I_1^2 / 3 + I_1}}{2 \cdot \bar{R}^c} = 1$ <p style="text-align: center;">after inserting $\sigma = R \cdot Eff$ and dissolving for Eff follows</p> $Eff^{NF} = c_{\Theta}^{NF} \cdot \frac{\sqrt{4J_2 \cdot \Theta^{NF} - I_1^2 / 3 + I_1}}{2 \cdot \bar{R}^t} = \frac{\sigma_{eq}^{NF}}{\bar{R}^t} \quad \leftrightarrow \quad Eff^{SF} = c_{\Theta}^{SF} \cdot \frac{\sqrt{4J_2 \cdot \Theta^{SF} - I_1^2 / 3 + I_1}}{2 \cdot \bar{R}^c} = \frac{\sigma_{eq}^{SF}}{\bar{R}^c}$
--

The formulation of F^{NF} generates a straight line in the principal stress plane!

3D-SFCs of Isotropic Porous Materials with model parameter determination

* **Normal Fracture NF** for $I_1 > 0$ \Leftrightarrow SFCs \Rightarrow **Crushing Fracture CrF** for $I_1 < 0$

$$F^{NF} = c_{\Theta}^{NF} \cdot \frac{\sqrt{4J_2 \cdot \Theta^{NF} - I_1^2 / 3} + I_1}{2 \cdot \bar{R}^t} = 1 \quad \Leftrightarrow \quad F^{CrF} = c_{\Theta}^{CrF} \cdot \frac{\sqrt{4J_2 \cdot \Theta^{CrF} - I_1^2 / 3} + I_1}{2 \cdot \bar{R}^c} = 1$$

after inserting $\sigma = R \cdot Eff$ and dissolving for Eff follows

$$Eff^{NF} = c_{\Theta}^{NF} \cdot \frac{\sqrt{4J_2 \cdot \Theta^{NF} - I_1^2 / 3} + I_1}{2 \cdot \bar{R}^t} = \frac{\sigma_{eq}^{NF}}{\bar{R}^t} \quad \Leftrightarrow \quad Eff^{CrF} = c_{\Theta}^{CrF} \cdot \frac{\sqrt{4J_2 \cdot \Theta^{CrF} - I_1^2 / 3} + I_1}{2 \cdot \bar{R}^c} = \frac{\sigma_{eq}^{CrF}}{\bar{R}^c}$$

with $I_1 = (\sigma_I + \sigma_{II} + \sigma_{III}) = f(\sigma)$, $6J_2 = (\sigma_I - \sigma_{II})^2 + (\sigma_{II} - \sigma_{III})^2 + (\sigma_{III} - \sigma_I)^2 = f(\tau)$

$$27J_3 = (2\sigma_I - \sigma_{II} - \sigma_{III}) \cdot (2\sigma_{II} - \sigma_I - \sigma_{III}) \cdot (2\sigma_{III} - \sigma_I - \sigma_{II})$$

If a failure body is rotationally symmetric, then $\Theta = 1$ like for the neutral or shear meridian, respectively.

A 2-fold acting mode makes the rotationally symmetric fracture body 120°-symmetric and is modelled by using the invariant J_3 and Θ as non-circularity function with d as non-circularity parameter

$$\Theta^{NF} = \sqrt[3]{1 + d^{NF} \cdot \sin(3\vartheta)} = \sqrt[3]{1 + d^{NF} \cdot 1.5 \cdot \sqrt{3} \cdot J_3 \cdot J_2^{-1.5}} \quad \Leftrightarrow \quad \Theta^{CrF} = \sqrt[3]{1 + d^{CrF} \cdot 1.5 \cdot \sqrt{3} \cdot J_3 \cdot J_2^{-1.5}}$$

Lode angle ϑ , here set as $\sin(3 \cdot \vartheta)$ with 'neutral' (shear meridian) angle $\vartheta = 0^\circ$ ($\rightarrow \Theta = 1, d = 0$);

tensile meridian angle $30^\circ \rightarrow \Theta^{NF} = \sqrt[3]{1 + d^{NF} \cdot (+1)}$; compr. mer. angle $-30^\circ \rightarrow \Theta^{CrF} = \sqrt[3]{1 + d^{CrF} \cdot (-1)}$.

Mode interaction \rightarrow Equation of the fracture body: $Eff = [(Eff^{NF})^m + (Eff^{CrF})^m]^{m^{-1}} = 1 = 100\%$

$$Eff = \sqrt[m]{\left(c_{1\Theta}^{NF} \cdot \frac{\sqrt{4J_2 \cdot \Theta^{NF} - I_1^2 / 3} + I_1}{2 \cdot \bar{R}^t}\right)^m + \left(c_{\Theta}^{CrF} \cdot \frac{\sqrt{4J_2 \cdot \Theta^{CrF} - I_1^2 / 3} + I_1}{2 \cdot \bar{R}^c}\right)^m} = 1$$

* 120°-rotat. symmetric $\Theta \neq 1$:

$$c_{\Theta}^{NF} \rightarrow c^{NF} = 1 \quad (\Theta^{NF} = 1 \text{ in practice chosen}).$$

c_{Θ}^{NF}, d^{NF} from the 2 points $(\bar{R}^t, 0, 0) \rightarrow c_{\Theta}^{NF}$ and $(\bar{R}^{II}, \bar{R}^{II}, 0) \rightarrow d^{NF}$ or min.error fit of data course

$c_{\Theta}^{CrF}, d^{CrF}$ from the 2 points $(-\bar{R}^c, 0, 0) \rightarrow c_{\Theta}^{CrF}$ and $(-\bar{R}^{cc}, -\bar{R}^{cc}, 0) \rightarrow d^{CrF}$.

The failure surface is closed at both the ends! A paraboloid serves as closing cap and bottom

$$\frac{I_1}{\sqrt{3} \cdot \bar{R}^t} = s^{cap} \cdot \left(\frac{\sqrt{2J_2 \cdot \Theta^{NF}}}{\bar{R}^t}\right)^2 + \frac{\max I_1}{\sqrt{3} \cdot \bar{R}^t}, \quad \frac{I_1}{\sqrt{3} \cdot \bar{R}^t} = s^{bot} \cdot \left(\frac{\sqrt{2J_2 \cdot \Theta^{CrF}}}{\bar{R}^t}\right)^2 + \frac{\min I_1}{\sqrt{3} \cdot \bar{R}^t}$$

Slope parameters s are determined connecting the respective hydrostatic strength point with the associated point on the tensile and compressive meridian, $\max I_1$ must be assessed whereas $\min I_1$ can be measured. \bar{R}^t works as normalization strength. [CUN22, §5].

[Lem08] Lemnitzer L, Eckfeld L, Lindorf A and Curbach M (IfM TU Dresden): *Bi-axial tensile strength of concrete – Answers from statistics*. In: Walraven, J. C.; Stoelhorst, D. (Hrsg.): *Tailor made concrete structures. New solutions for our society*. Amsterdam, The Netherlands: CRC Press / Balkema, 2008, S. 1101-1102

In order to illustrate the various SFCs a 3D-concrete Fracture Body is presented: (more pictures of such fracture bodies are found in [CUN22]).

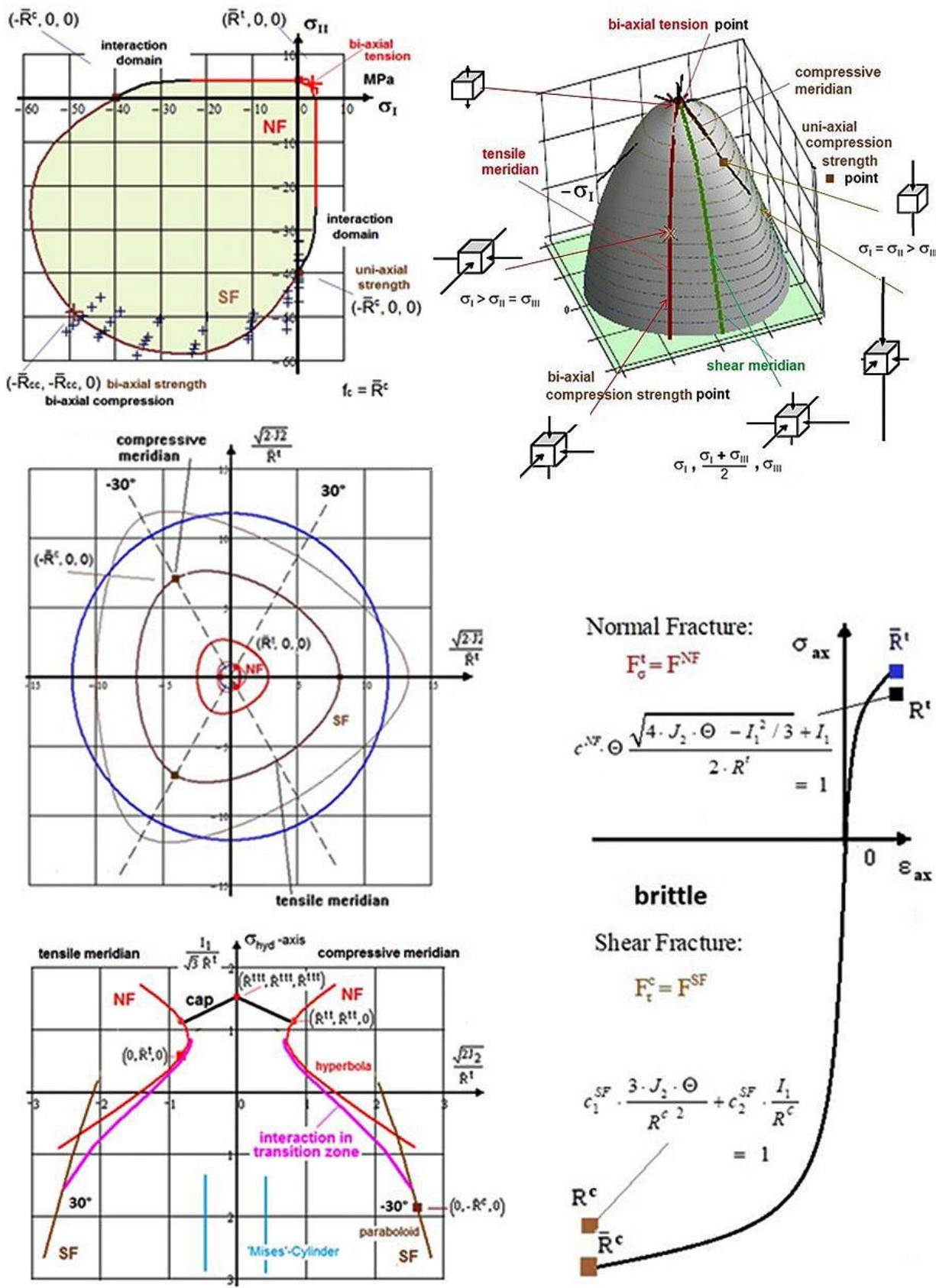


Fig.11-1: Visualization of the behavior of a brittle material (Normal Concrete) considering 1D stress-strain curve with 2D- and 3D-fracture failure curves and fracture body (surface). 120°-rotationally-symmetric

11.3 3D-SFCs of (quasi-)Brittle UD Materials

5 modes → 5 SFCs is in line with ‘generic’ number according to the FMC.

IFF1 generates a straight line in the stress plane!

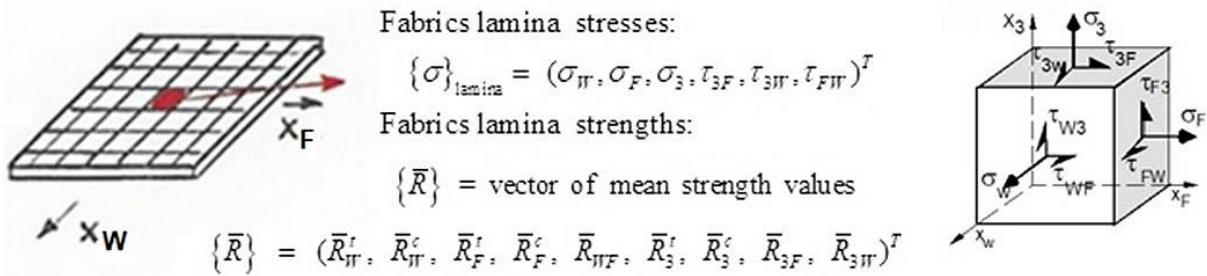
$$\begin{aligned}
 \text{FF1: } Eff^{\parallel\sigma} &= \sigma_1 / \bar{R}_{\parallel}^t = \sigma_{eq}^{\parallel\sigma} / \bar{R}_{\parallel}^t \\
 \text{FF2: } Eff^{\parallel\tau} &= -\sigma_1 / \bar{R}_{\parallel}^c = +\sigma_{eq}^{\parallel\tau} / \bar{R}_{\parallel}^c \\
 \text{IFF1: } Eff^{\perp\sigma} &= 0.5 \cdot [(\sigma_2 + \sigma_3) + \sqrt{\sigma_2^2 - 2\sigma_2 \cdot \sigma_3 + \sigma_3^2 + 4\tau_{23}^2}] / \bar{R}_{\perp}^t = \sigma_{eq}^{\perp\sigma} / \bar{R}_{\perp}^t \\
 \text{IFF2: } F^{SF} &= 0.5 \cdot \sqrt{a_{\perp\perp por}^2 \cdot I_2^2 + b_{\perp\perp por}^2 \cdot I_4 - a_{\perp\perp por} \cdot I_2} / \bar{R}_{\perp}^c = 1 \\
 \text{IFF2: } F_{porous}^{SF} &= 0.5 \cdot \sqrt{a_{\perp\perp por}^2 \cdot I_2^2 + b_{\perp\perp por}^2 \cdot I_4 - a_{\perp\perp por} \cdot I_2} / \bar{R}_{\perp}^c = 1 \\
 \text{FF3: } Eff^{\perp\parallel} &= \{0.5 \cdot [b_{\perp\parallel} \cdot I_{23-5} + (\sqrt{b_{\perp\parallel}^2 \cdot I_{23-5}^2 + 4 \cdot \bar{R}_{\perp\parallel}^2 \cdot (\tau_{31}^2 + \tau_{21}^2)})] / \bar{R}_{\perp\parallel}^3\}^{0.5} . \\
 \left\{ \sigma_{eq}^{\text{mode}} \right\} &= \left(\sigma_{eq}^{\parallel\sigma}, \sigma_{eq}^{\parallel\tau}, \sigma_{eq}^{\perp\sigma}, \sigma_{eq}^{\perp\tau}, \sigma_{eq}^{\perp\parallel} \right)^T, I_{23-5} = 2\sigma_2 \cdot \tau_{21}^2 + 2\sigma_3 \cdot \tau_{31}^2 + 4\tau_{23}\tau_{31}\tau_{21}. \\
 \text{Insertion: Compressive strength point } &(0, -\bar{R}_{\perp}^c) + \text{bi-axial fracture stress } \bar{R}_{\perp}^{\prime\prime} \text{ (porosity effect)} \\
 &\text{delivers } a_{\perp\perp por} \cong \mu_{\perp\perp} / (1 - \mu_{\perp\perp}), b_{\perp\perp por} = a_{\perp\perp por} + 1 = 1 / (1 - \mu_{\perp\perp}), b_{\perp\parallel} \cong 2 \cdot \mu_{\perp\parallel}. \\
 &\text{From mapping experience obtained typical FRP-ranges: } 0 < \mu_{\perp\parallel} < 0.3, 0 < \mu_{\perp\perp} < 0.2. \\
 &\text{From the few CMC test results, due to Fig.15, it is recommended } \mu_{\perp\parallel} < 0.3. \\
 \text{Failure Surface (failure body) = interaction equation:} \\
 Eff^m &= (Eff^{\parallel\tau})^m + (Eff^{\parallel\sigma})^m + (Eff^{\perp\sigma})^m + (Eff^{\perp\tau})^m + (Eff^{\perp\parallel})^m = 100\% \text{ if failure} \\
 \text{Two-fold failure danger in the } \sigma_2 - \sigma_3 \text{-domain stands for a failure surface closing, modelled by} \\
 Eff^m &= (Eff^{\parallel\tau})^m + (Eff^{\parallel\sigma})^m + (Eff^{\perp\sigma})^m + (Eff^{\perp\tau})^m + (Eff^{\perp\parallel})^m + (Eff_{\perp}^{\text{MffFd}})^m = 1 \\
 \text{with } Eff_{\perp}^{\text{MffFd}} &= (\sigma_2^t + \sigma_3^t) / 2\bar{R}_{\perp}^{\prime\prime}, \text{ and } \bar{R}_{\perp}^{\prime\prime} \approx \bar{R}_{\perp}^t / \sqrt[3]{2} \text{ after [Awa78]} \\
 \text{considering } \sigma_2^t = \sigma_3^t \text{ and } \sigma_2^c = \sigma_3^c; &\bar{R}_{\perp}^{\prime\prime} \leq \bar{R}_{\perp}^t, \bar{R}_{\perp}^{\text{cc}} \leq \bar{R}_{\perp}^c \text{ if porous.} \\
 \text{From mapping experience obtained typical range of interaction exponent } &2.5 < m < 2.9.
 \end{aligned}$$

Modelling of laminates may be lamina-based (basic layers are UD layers), sub-lamina-based (semi-finished non-crimp orthotropic fabrics) or even laminate-based. Thereby, modelling complexity grows from UD, via non-crimp fabrics (NCF) through plain weave and finally to the spatial 3D-textile materials.

11.4 3D-SFCs of the Orthotropic Fabrics, (see [Cun24b])

9 modes → 9 SFCs. This is in line with Cuntze’s ‘generic’ number 9 according to the FMC.

In this context, my thanks to Roman (Prof. Dr. Keppeler, UniBw; formerly Siemens AG).



The following table includes the FMC-based SFCs for the **porous orthotropic** (rhombic-anisotropic) 2D-woven fabric **materials**

$$Eff = \left(\frac{\sigma_w + |\sigma_w|}{2 \cdot \bar{R}_w^t} \right)^m + \left(\frac{-\sigma_w + |\sigma_w|}{2 \cdot \bar{R}_w^c} \right)^m + \left(\frac{\sigma_f + |\sigma_f|}{2 \cdot \bar{R}_f^t} \right)^m + \left(\frac{-\sigma_f + |\sigma_f|}{2 \cdot \bar{R}_f^c} \right)^m + \left(\frac{|\tau_{wf}|}{\bar{R}_{wf} - \mu_{wf} \cdot (\sigma_w + \sigma_f)} \right)^m$$

$$+ \left(\frac{\sigma_3 + |\sigma_3|}{2 \cdot \bar{R}_3^t} \right)^m + \left(\frac{-\sigma_3 + |\sigma_3|}{2 \cdot \bar{R}_3^c} \right)^m + \left(\frac{|\tau_{3w}|}{\bar{R}_{3w} - \mu_{3w} \sigma_3^c} \right)^m + \left(\frac{|\tau_{3f}|}{\bar{R}_{3f} - \mu_{3f} \sigma_3^c} \right)^m = 1 = 100\% .$$

For a cross-ply fabric with Warp = Fill $\rightarrow \bar{R}_w^t = \bar{R}_f^t, \bar{R}_w^c = \bar{R}_f^c$, the inter-laminar *Effs*, suffix ₃, vanish and just the in-plane (intra-laminar) *Effs* remain.

The range of parameters is for the interaction-exponent $2.5 < m < 2.9$, and since the strong porosity-dependency very different \rightarrow recommendation: $\mu_{wf} < 0.2, \mu_3 < 0.2$.

11.5 Ductile Materials, Metal

In Fig.11-2(left), the failure body is presented with its meridians as axial lines. The center figure fully **proves** the general isotropic 120° material symmetry which is supported by the Mises **ellipse** being the *inclined cross-section of the Mises cylinder failure body* is added. The right octahedral figure shows the inner green curve with the Mises circle at the ‘**Onset-of-yielding**’ and the **outer one** at tensile strength R^t .

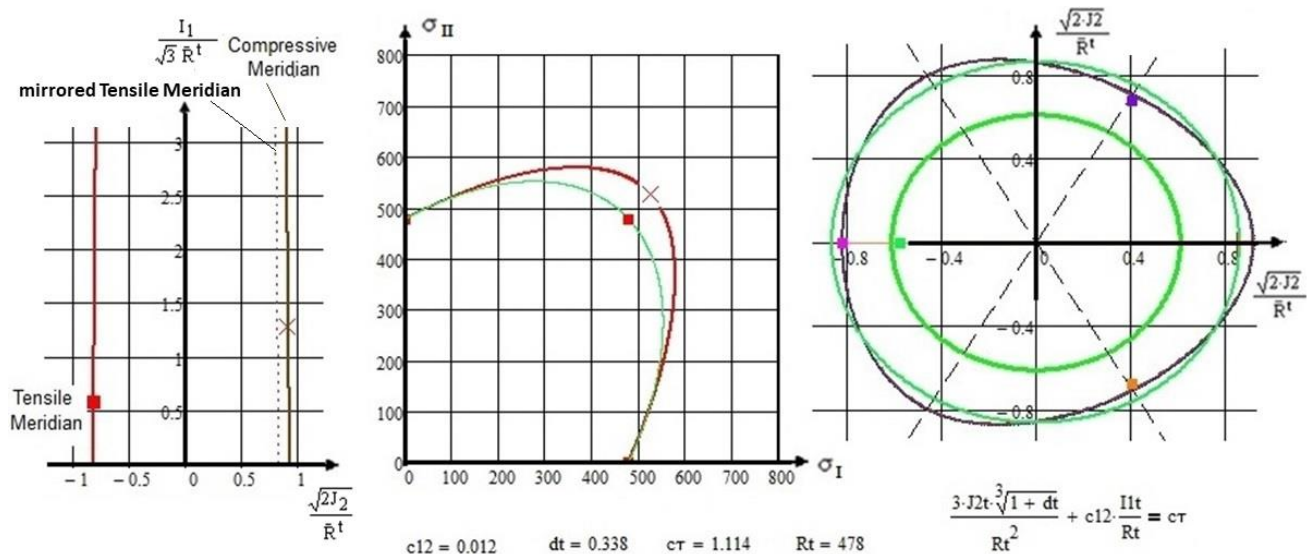


Fig.11-2, isotropic steel AA5182-0: Visualization of the behavior of a ductile material. (left) Yield body in Haigh-Lode-Wintergaard coordinates; (center) 120°-symmetry, visualized in the principal stress plane; (right) 120°-symmetry, visualized in the octahedral stress plane

The 120°-rotational symmetry can be best displayed in the octahedral stress plane which is a ‘horizontal’ cross-section of the failure body at a distinct I_1 , Fig.11-2(right). The points and curves on the spatial body (*left figure*) are projected onto the octahedral plane (*right figure*). Since they depend on I_1 , they have different cross-section heights I_1 , such as the uniaxial tensile strength point which is located higher than the equi-biaxial strength point x .

In the center figure, Mises is the green curve; red square: the tensile strength point; cross: the equi-biaxial tensile strength point ductile ($trueR^t$, $trueR^t$, 0), i. e. the cross x . In the case of ductile metals it can be assumed $R^t \cong 1.1 \cdot R^t$.

An elaboration of four materials with the Mathcad calculation program leads to the Fig.11-3 below: Fig.11-3(left) presents curves through the uniaxial tensile strength points and the equi-biaxial strength R^t . The curves are inclined cross-sections of the failure body. Fig.11-3(right), for completion, displays the Beltrami potential surface (egg shaped), the ‘Mises’ cylinder and the three principal axes.

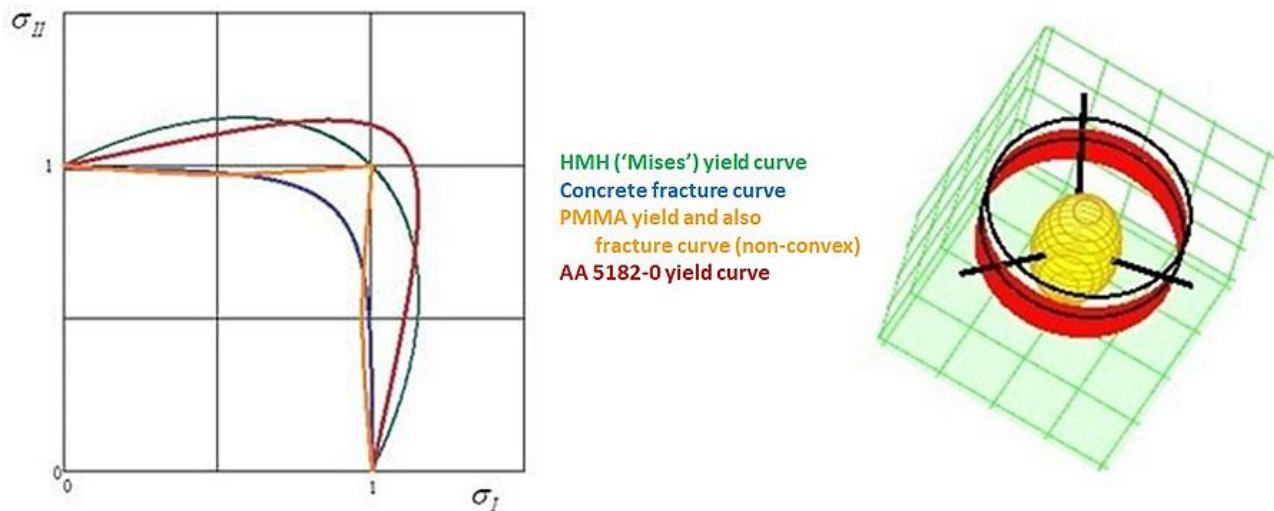


Fig.11-3: (left) Normalized principal stress plane failure curves of a set of fully different isotropic materials. (right) Failure body surface

The figure above shows extreme curve examples at $trueR^t$ level in the positive principal stress range. The red curve is occupied by the data of Kuwabara given below in the table, shown within Fig.11-4. The metal test data AA 5182-0 are from [Kuw98] T. Kuwabara et al: *Journal of Materials Processing Technology* 80–81 (1998) 517–523. Gotoh's biquadratic yield criterion (not given here) was used to map the test data of the cold-rolled low-carbon steel AA 5182-0 sheets.

Fig.11-4 depicts several failure cross-sections of an isotropic ductile steel demonstrating 120°-rotational symmetry like the brittle isotropic materials such as concrete in the compression domain and other ductile ones in the tensile domain.

The author was able to map the course of all the corresponding courses of test data points with his isotropic SFC models.

For the generation of *Fig.11-4* biaxial tensile tests of cold-rolled low-carbon steel sheet were carried out using flat cruciform specimens with the biaxial loads maintained in fixed proportion. Contours of plastic work (of flow potential) were determined in stress space under the shown strain range.

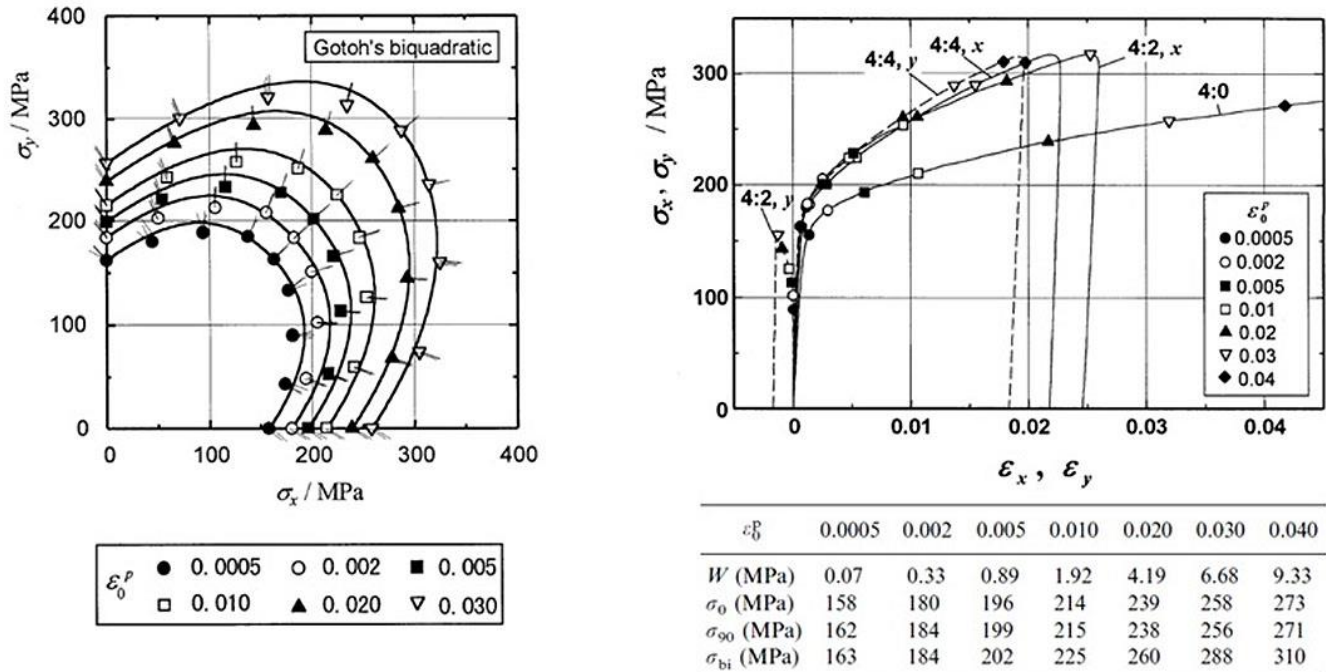


Fig.11-4: (left) Test points as function of the experienced plastic straining ϵ_0^p ; mapping by using Gotoh's bi-quadratic criterion. (right) True stress–true strain curves for different biaxial loadings = different stress ratios. Measured values using r_0, r_{45}, r_{90} . $T = 1\text{mm}$, flat cruciform

LL:

- * Also for the ductile materials, the 120°-rotational symmetry was demonstrated, see further [CUN22, §5.8].
- * The 120°-rotational symmetry of isotropic materials is nothing else than a 'double mode effect'.
- * This effect is faced with all isotropic materials independent whether they are ductile or brittle.

Reminder to illustrate elastic and plastic behavior:

- * Elastic deformation of crystalline structures occurs on the atomic scale: The bonds of the atoms in the crystal lattice are stretched. When de-loading, the energy stored within these bonds can be reversed. The material behaves elastic.
- * Plastic deformation or sliding occurs along gliding planes inter-crystalline or intra-crystalline and is permanent (plastic). No volumetric change is faced.

12 Completion of the Strength Mechanics Building

Aim: Completion of a material-‘generic’ number driven Strength Mechanics Building

In the frame of his material symmetry-driven thoughts the author intended to test-proof some ideas that help to complete the Strength Mechanics Building by finding missing links and by providing engineering-practical strength criteria (SFCs), the parameters of which are directly measurable.

All this supports the assumption of a ‘generic’ number for the smeared-modelled materials.

The obtained Strength Mechanics Building matured, became clearer and more complete.

LL:

- ✓ *Beside the standard Shear (band) Yielding SY there also exists Normal Yielding NY analogous to the failure modes Shear Fracture SF and Normal Fracture NF (author assumption proven)*
- ✓ *120°-rotational symmetry is inherent to brittle and ductile isotropic materials (author assumption proven)*
- ✓ *Generic number 2, K_{Icr}^I with $K_{IIcr}^c : K_{IIIcr}^c$ was theoretically proven for the non-real, ideal case of no flaws in front of crack tip*
- ✓ *Also in consequence of above building: Different but similar behaving materials can be basically treated with the same SFC. Examples are: Concrete ↔ foam, different fabrics.*

Material Symmetry seems to tell:

In the case of ideally homogeneous materials a generic number is inherent. This is valid for elastic entities, yield modes and fracture modes, for yield strengths R_{02} and fracture strengths R , fracture toughness entities K_{cr} and for the invariants used to generate strength criteria.

This **generic number** is
2 for isotropic and 5 for transversely–isotropic materials,

One might think:

“Mother Nature gives Strength Mechanics a mathematical order ! ?”



The author
after the yearly
‘pilgrimage’,
26 miles.
To and from
Kloster Indersdorf (home)
↔
Kloster Scheyern

STRENGTH is still his Life !

“Anyone who stops learning is old,
whether at twenty or beyond eighty.
Anyone who keeps learning stays young.
The greatest thing in life is to keep your
mind young”

[Henry Ford]

Application-oriented engineer with a scientific touch for material modelling and with the hope to be some bridge-builder between mechanical and civil engineering (= construction).

This document includes results of the author’s non-funded, non-supported research work.

13 Safety Concept in Structural Engineering Disciplines

Aim: Providing basic knowledge, in order to not forget the required design verification of a component when modeling.

13.1 General with Old safety Concept

A *Safety Concept* means to implement reliability into the structural component by ‘capturing’ the uncertainty of the design parameters! It can just provide an unknown safety distance between load (i.e. ‘stress’ S) and load resistance (‘strength’ R). FoS capture uncertainties, small inaccuracies, and simplifications in analyses w.r.t. manufacturing process, tolerances, loadings, material properties (strength, elasticity, ..), structural analysis, geometry, strength failure conditions. FoS do not capture missing accuracies in modeling, analysis, test data generation and test data evaluation!

In the deterministic concepts or formats, respectively, the worst case scenario is usually applied for loadings considering temperature, moisture, undetected damage. Further, a load is to increase by a ‘Design FoS’ and the resistances are to decrease. For the decrease of the strength, statistical distributions are used. If the loading is also based on a statistical distribution, then one speaks about a semi-probabilistic format.

Design Development was the basic task of the author in industry. This is why at first the Flow Chart below shall remind of the structural analysis tasks. There are basically four blocks, where – after the material Model Validations - the fulfillment of the Design Requirements has to be demonstrated for obtaining Design Verification as precondition of the final Certification Procedure.

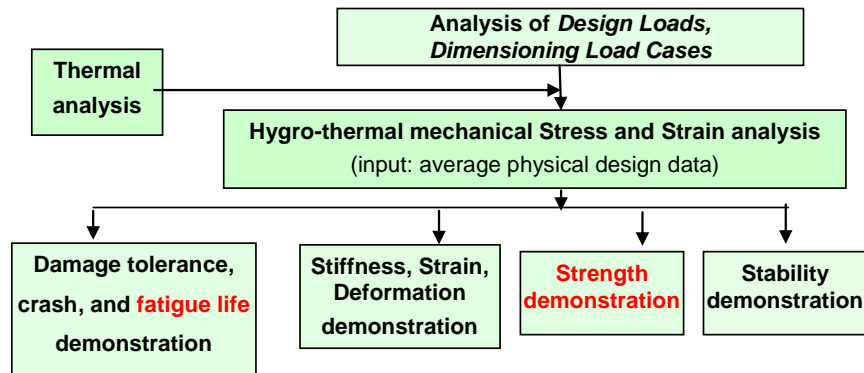


Fig13-1: Structural Design-Analysis Flow Chart

Essential question of engineers in mechanical and in civil engineering is: “How much could one further increase the loading“. Which is the reserve?

Old Safety Concept of Allowable Stresses:

At least, since 1926 the civil engineer M. Mayer questioned above safety concept, where the *resistance was reduced* by a safety factor. This gives no accurate results in the case of non-linear behavior. In construction this was replaced in DIN 1054 by the Partial Safety Factor concept, which applies design safety factors and combination factors for general service loads, live loads, snow, ice loads, and wind loads. Temperature effects are specified in DIN 1055-100.

Material resistance must be generally demonstrated by a positive Margin of Safety MoS or a Reserve Factor $RF = MoS - 1 > 1$ in order to achieve Structural Integrity for the envisaged Design Limit State! A FoS is given and not to calculate (as it is too often to read) like the Margin of Safety MoS or the Reserve Factor $RF = MoS + 1$.

Fig.13-2 visualizes the stress-strength distribution which outline that the crossing over will determine the probability of failure p_f . Its value is the area of the p_f -distribution within the overlapping (gusset) of the stress and the strength distribution tails, see for details [CUN22, §16]

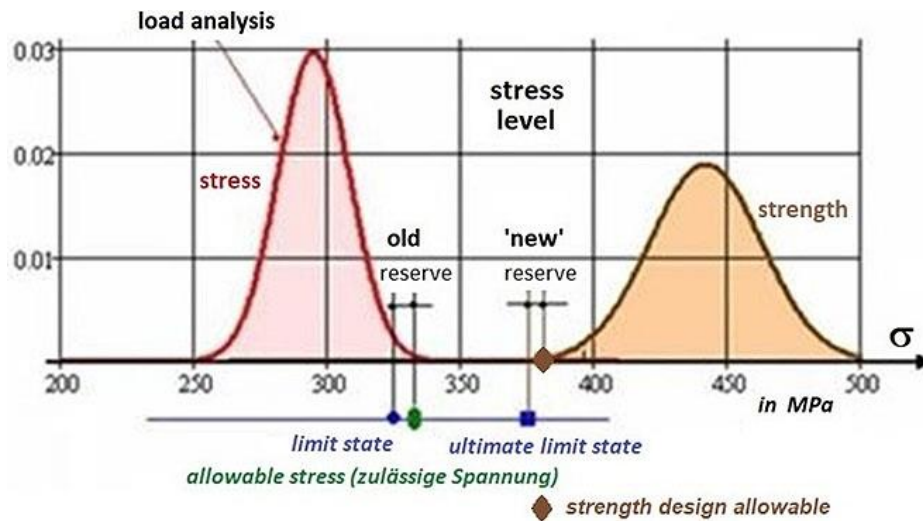


Fig.13-2: Visualization of the present ('new') and the old safety concept

LL:

The citation of the term 'allowable stress' is restricted to the former 'Concept of Allowable Stresses' and shall be not applied within present concepts anymore. Why? The usual application of the abbreviating term 'allowable' instead of 'strength design allowable may not confuse, but 'allowable stress' does confuse because the relation below is valid:

$$j \cdot \text{allowable stress} = \text{strength design allowable} !! \text{ (see again the figure above) !}$$

13.2 Global (lumped) Factor of Safety Concept ('deterministic format') on Loading

Concept, that deterministically accounts for design uncertainties in a lumped (global) manner by enlarging the 'design limit loads' through multiplication with a design Factor of Safety FoS .

As still mentioned, FoS are applied to decrease the chance of failure by capturing the uncertainties of all the given variables outside the control of the designer. In the design process the scatter of individual values and parameters is usually treated by using fixed deterministic FoS , which act as load increasing multiplying factors FoS and should be called, more correctly, *Design FoS* .



Personal Experience:
 "A safety distance pays off".

Comodo waran ≈ 80 kg

Presently, in mechanical engineering the loading is increased by one lumped FoS j , and in civil engineering the procedure was improved by using several partial Design FoS γ for the uncertain stochastic design variables. These chosen FoS are based on long term minimum risk experience

with structural testing. Depending on the risk consequences different classes of *FoS* are applied, e.g. for manned space-crafts higher *FoS* are used than for unmanned space-crafts.

Present spacecraft safety concept is an *improved global deterministic format (intention: semi-probabilistic)* = ‘Simplest’ Partial Safety Factor concept: It discriminates load model uncertainties considering factors (K_{Model} , $K_{Project}$) from design uncertainties which are considered by one global *FoS* j !

The to be applied values j for the *FoS* are risk or task driven. Facts to consider are:

- As mentioned exemplarily: Different application in cases of manned, un-manned spacecraft
- Design verification by ‘Analysis only’ (*by the way the usual case in construction*)
- Different risk acceptance attitude of the various industries.

Example: $DUL = j_{ult} \cdot \text{design limit load } DLL$

Mind: UL represents the real test fracture load. Therefore the virtual design value must be discriminated by writing DUL.

Different loading (action) *FoS* in aircraft and space engineering:

The first task in aerospace industry is load analysis. In any load analysis to establish are all load events the structure is likely to experience in later application. This includes as well the estimation of loadings induced by the hygro-thermal, the mechanical (*static, cyclic and impact*) and the acoustical environment of the structure as further the corresponding lifetime requirements (*duration, number of cycles*), specified by an authority or a standard. Then, the so-called Design Limit Load values are determined, usually derived from mission simulations utilizing the so-called mathematical models of the full structure (*dynamical analyses, at first on basis of the preliminary design*).

When preparing the HSB sheet [Cun12] the author sorted out that there practically is no different risk view between air-craft and space-craft:

- * Spacecraft: using a dynamic load model obtaining a basic load prediction dLL considering a load model uncertainty considering factor $j_{LM} = 1.2$ delivering a Design Limit Load $DLL = 1.2 \cdot dLL$, and from this follows $DUL = dLL \cdot j_{LM} \cdot j_{ult}$, with $1.2 \cdot 1.25 = 1.5$! The DLL level is applied in spacecraft in fatigue life demonstration.
- * Aircraft: Definition of a so-called (design) Limit Load LL delivering $DUL = LL \cdot 1.5$.

LL: *Comparing the ESA/ESTEC aerospace Standards (he had to work on), the author could find that the DUL-value is practically the same value in aircraft and in spacecraft !*

The resistance strength and bearable loads (at joints etc ...):

Dependent on the design requirements the average, the upper or a lower value of the property is used for the various properties. In the case of strength a statistically reduced value R . To achieve a reliable design the so-called Design Allowable has to be applied. It is a value, beyond which at least 99% (“A”-value) or 90% (“B”-value) of the population of values is expected to fall, with a 95% confidence (*on test data achievement*) level, see MIL-HDBK 17. A “B”-value is permitted to use for multi-layered, redundant laminates.

Bearable loads require series tests of the distinctive structural component with statistical evaluation in order to determine the ‘load-resistance design allowables’.

Measurement data sets are the result of a Test Agreement (norm or standard), that serve the desire to make a comparability of different test procedure results possible. The Test Agreement consists of test rig, test specification, test specimen and test data evaluation method and the Test Procedure. Therefore, one can only speak about 'exact test results in the frame of the obtained test quality'. Hence, there are no exact property values.

Test specimens shall be manufactured like the structure ('as-built').

Considering property input: When applying test data from 'isolated lamina' test specimens (*like tensile coupons*) to an embedded lamina of a laminate one should consider that coupon test deliver tests results of 'weakest link' type. An embedded or even an only one-sided constrained lamina, however, possesses redundant behavior → "B"-values permitted.

Reserve Factor RF and Margin of Safety MoS : Formulas:

Linear analysis is sufficient (presumption): $\sigma \sim \text{load} \Rightarrow RF \equiv f_{RF} = 1 / Eff$

$$\text{Material Reserve Factor} \quad f_{RF, ult} = \frac{\text{Strength Design Allowable } R}{\text{Stress at } j_{ult} \cdot \text{Design Limit Load}} > 1,$$

Non-linear analysis required: σ not proportional to load

$$\text{Reserve Factor (load-defined)} \quad RF_{ult} = \frac{\text{Predicted Failure Load at } Eff = 100\%}{j_{ult} \cdot \text{Design Limit Load}} > 1.$$

Fig.13-3 presents a numerical example how the reserve factor RF is to compute.

Assumption: Linear analysis permitted, design FoS $j_{ult} = 1.25$

* Design loading (action): $\{\sigma\}_{design} = \{\sigma\} \cdot j_{ult}$

* 2D-stress state: $\{\sigma\}_{design} = (\sigma_1, \sigma_2, \sigma_3, \tau_{23}, \tau_{31}, \tau_{21})^T \cdot j_{ult} = (0, -76, 0, 0, 0, 52)^T \text{ MPa}$

* Residual stresses: 0 (*effect vanishes with increasing micro-cracking*)

* Strengths (resistance): $\{\bar{R}\} = (1378, 950, 40, 125, 97)^T \text{ MPa}$ average from measurement statistically reduced $\{R\} = (R'_{//}, R''_{//}, R'_{\perp}, R''_{\perp}, R_{\perp//})^T = (1050, 725, 32, 112, 79)^T \text{ MPa}$

* Friction value(s): $\mu_{\perp//} = 0.3, (\mu_{\perp\perp} = 0.35)$, Mode interaction exponent: $m = 2.7$

$$\{Eff^{mode}\} = (Eff^{c//\sigma}, Eff^{//\tau}, Eff^{\perp\sigma}, Eff^{\perp\tau}, Eff^{\perp//})^T = (0.88, 0, 0, 0.21, 0.20)^T$$

$$Eff^m = (Eff^{c//\sigma})^m + (Eff^{//\tau})^m + (Eff^{\perp\sigma})^m + (Eff^{\perp\tau})^m + (Eff^{\perp//})^m = 100\% .$$

The results above deliver the following material reserve factor $f_{RF} = 1 / Eff$

* $Eff^{\perp\sigma} = \frac{\sigma_2 + |\sigma_2|}{2 \cdot \bar{R}'_{\perp}} = 0, \quad Eff^{\perp\tau} = \frac{-\sigma_2 + |\sigma_2|}{2 \cdot \bar{R}'_{\perp}} = 0.60, \quad Eff^{\perp//} = \frac{|\tau_{21}|}{\bar{R}_{\perp//} - \mu_{\perp//} \cdot \sigma_2} = 0.55$

$$Eff = [(Eff^{\perp\sigma})^m + (Eff^{\perp\tau})^m + (Eff^{\perp//})^m]^{1/m} = 0.80.$$

$\Rightarrow f_{RF} = 1 / Eff = 1.25 \rightarrow RF = f_{RF}$ (if linearity permitted) $\rightarrow MoS = RF - 1 = 0.25 > 0 !$

Fig.13-3: Computation of a Reserve Factor RF

LL:

- * A FoS is given and not to calculate such as a Margin of Safety MoS or the Reserve Factor $RF = MoS + 1$.
- * A MoS is usually the result of worst case assumptions that does not take care of the joint actions of the stochastic design parameters and thereby cannot take care of their joint failure action and probability. This failure probability is a 'joint failure probability' because it considers the probability of joint acting

- * A material with a high coefficient of variation CoV disqualifies itself, when computing the statistically-based strength design allowable values. Therefore, one must not penalize it further as performed in some standards in the past in the case of new materials.
- * Both, an increasing mean value and a decreasing standard deviation will lower p_f
- * The MoS value does not outline a failure probability. Failure probability p_f does not dramatically increase if MoS turns slightly negative
- * A local safety measure of $MoS = -1\%$ is no problem in design development if a 'Think (about) Uncertainties' attitude is developed in order to recognize the main driving design parameters and to reduce the scatter (uncertainty) of them
- * Nowadays often non-linear analyses are performed, delivering true quantities, however Design Verification is executed with engineering strength values R . Why do we not use in such a case the true tensile strength, but calculate f_{RF} with four numbers accuracy?
- * Fig.13-4 (left) visualizes strength distribution, Eff versus micro-damage growth and material reserve factor f_{RF}
- * True-in requires True-out and an assessment by $true\bar{R}^t$. The Fig.13-4(right) shows for an aluminum alloy a difference between the mean (material model) strength values $eng\bar{R}^t \rightarrow true\bar{R}^t$ of 8%.

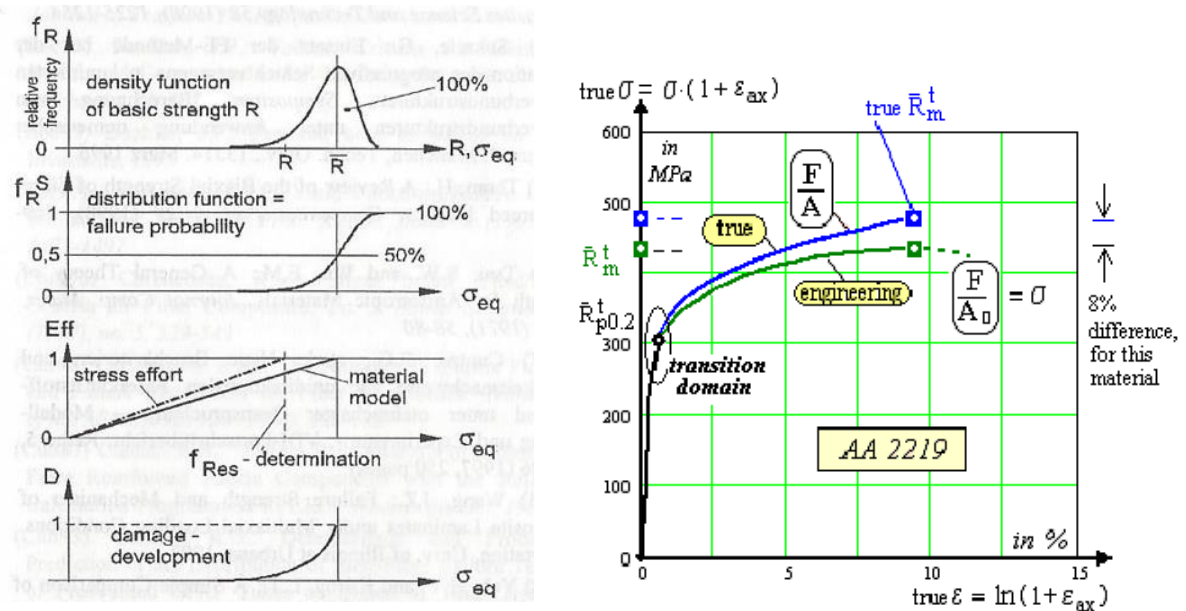


Fig.13-4: Difference engineering and true tensile strength of AA2219.

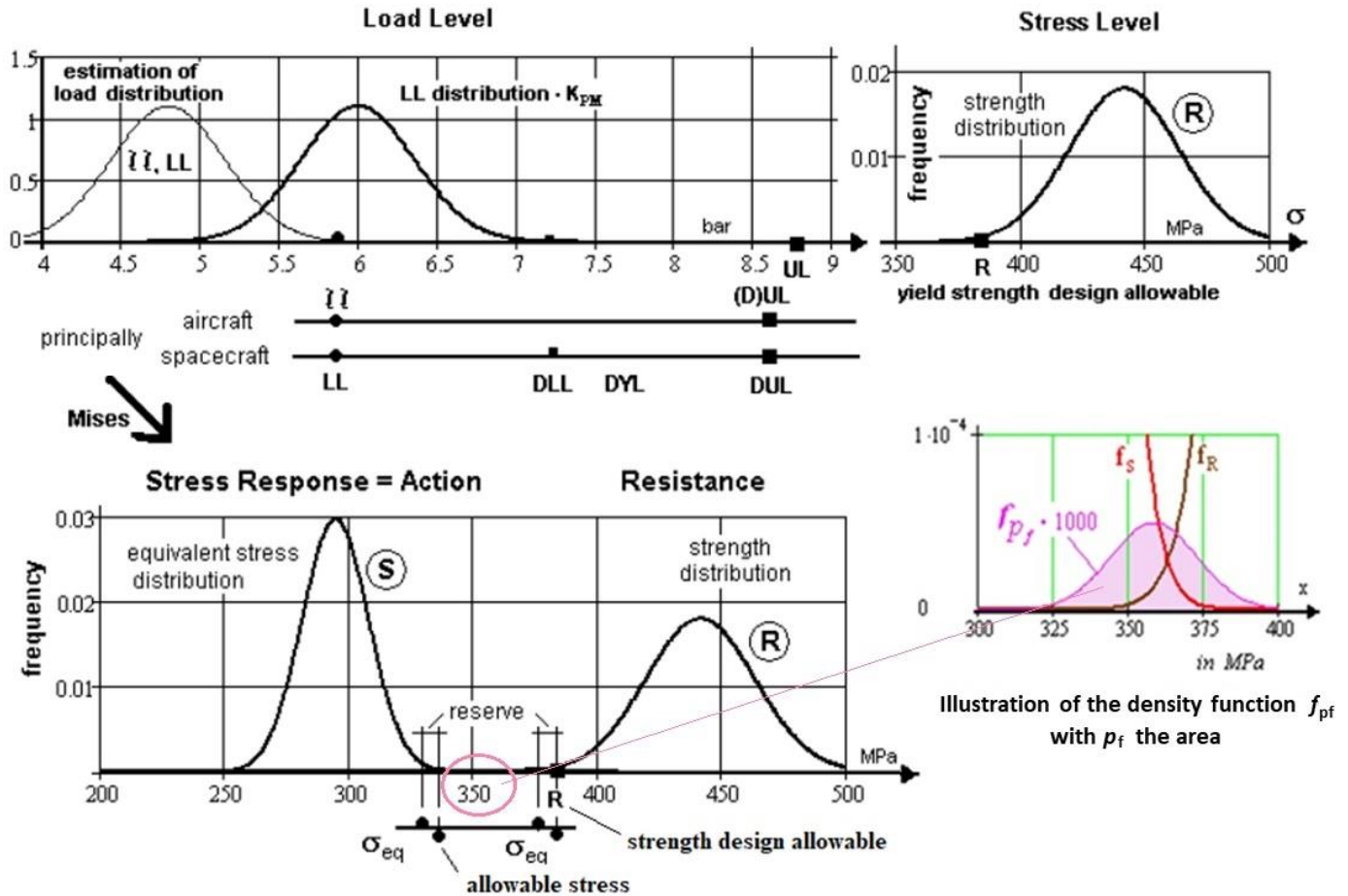
Robust Design Requirements:

The goal of any design engineer should be to end up with a robust design. To achieve this, the main stochastic design parameters have to be used to outline the robustness of the design against the envisaged actual failure mode by firstly computing the sensitivity measures α and then investigating the reduction of the design's sensitivity to changes of X_j while keeping p_f at the prescribed level. This is important for the production tolerances. Probabilistic design may be used as an assessment of the deterministic design or as design method required if a *reliability* target \mathcal{R} or its complement, the probability of failure p_f , is assigned instead of a *FoS*.

A structural reliability analysis in a Hot Spot reveals the influence of each stochastic design parameter on the distinct failure mode by means of the sensitivity measures. Robust designs (*robust to later changes of the design parameters*) are required with identification of the most sensitive design parameters!

For better illustration of the Safety Concepts from [CUN22, §12] the Fig.13-5 is included. It clearly depicts the definition of the failure probability in this two-parameter case.

Fig.13-5: Visualization of the difference of the aerospace load terms used in the Strength Design Allowable Safety Concept and of the 'hopefully forgotten' Allowable Stress Safety Concept



Design advantage with the Ariane Booster, when using a probabilistic tool:

Two advantageous applications of the probabilistic tool shall be shortly demonstrated where probabilistic modelling and computation were successfully applied:

- * A reduced production tolerance width leads to a reduced mass which sequentially reduced further fuel mass savings. Improved production reduced the wall thickness tolerance from 8.2 ± 0.20 mm to 8.2 ± 0.05 mm. Keeping the same given reliability value $\mathcal{R} = 1 - p_f = 1 - 5 \cdot 10^{-6}$ the nominal wall thickness could be set → 8.1 ± 0.05 mm leading to mass and fuel savings. (As early as 1985 for the pre-design of the Ariane 5 launcher target survival probabilities \mathcal{R} were fixed for the several structural parts!)
- * Probabilistic modelling of the geometrical tolerances of bore hole, pin, position (pitch) and strength minimum restrains with minimum residual stresses could be achieved, for the pin connection an optimum number of pins of 130 pins for a simpler assembly process and for reduced mounting stresses.

14 Non-linear Stress-Strain relationships, Beltrami Theory with Change of Poisson's Ratio

Aim: Provision of a Basis to generate an 'Extended Mises' model as a simplified 'Gurson' model.

14.0 General on Stress-Strain curves $\sigma(\epsilon)$, Strengths R and Poisson's Ratio ν

There are two different stress-strain curves existing: the *monotonic* and the *cyclic stress-strain curve*. The first curve is derived by the static tests, whereas the second one is generated by fatigue tests. Strain-controlled hysteresis loops (*Fig.14-1, left down*) are performed on different strain levels with several test specimens. Dependent on hardening and softening behavior of the actual material these two curves may discriminate significantly. Monotonic stress-strain curves have long been used to obtain design parameters for limitation of the stresses in engineering structures subjected to static loading. Similarly, cyclic stress-strain curves are useful for assessing the durability of structures subjected to repeated loading.

Further, in the case of monotonic σ - ϵ -curves there are very different, material-specific stress-strain curves in the elastic-plastic transition domain, see *Fig.14-1, left up and right*. Some show an 'Onset-of-yield' at an upper yield stress level \bar{R}_e^{upper} and others at a lower yield strength \bar{R}_e^{lower} . In this case usually the lower yield point is taken as the yield strength of the metal.

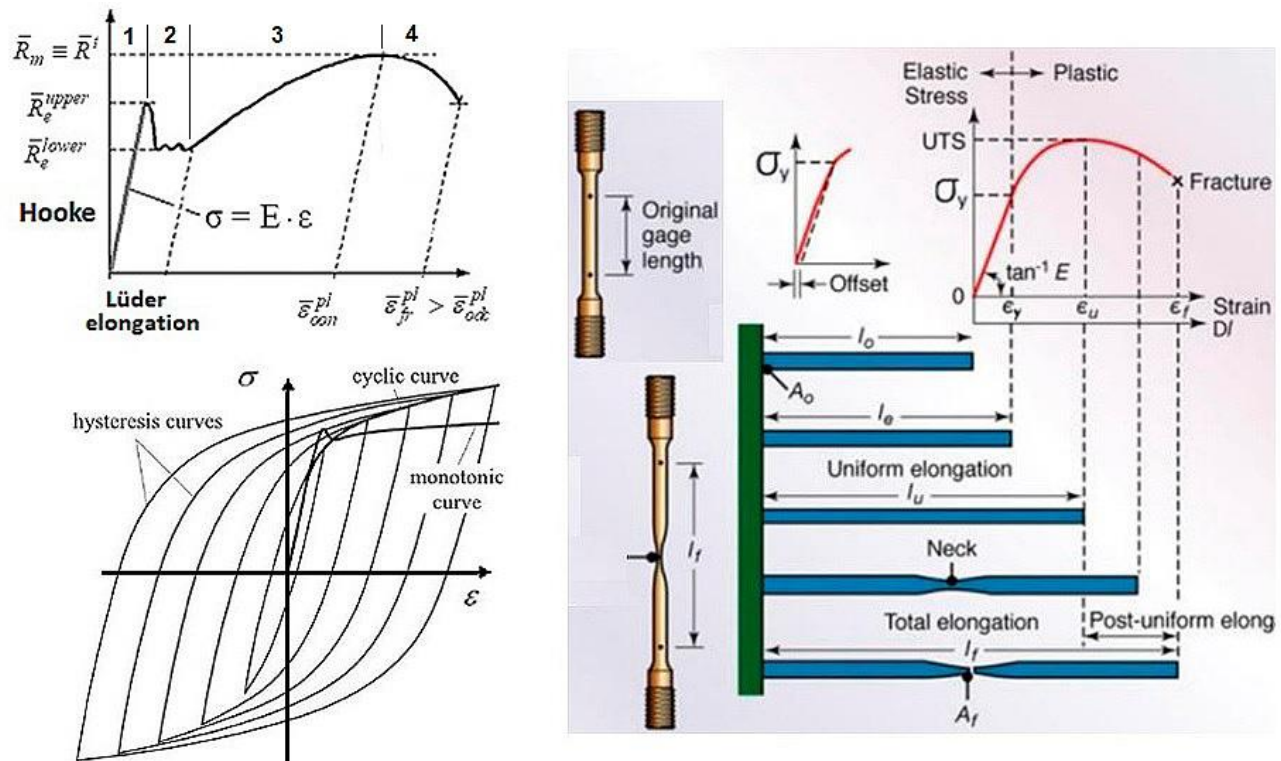


Fig.14-1, engineering quantities. modelling: (left,up) Discontinuous yielding, mean curve for mild steel showing the yield point phenomenon, termed Lüder's elongation effect. (left, down) Cyclic curves. (right) Tensile-test specimen with gage length, elongation before and after testing and finally after rupture (from Kalpakjian S and Schmid S: Evaluation of the Possibility of Estimating Cyclic Stress-strain Para-meters and Curves from Monotonic Properties of Steels. Manufacturing Engineering & Technology. 2013

For the 'left up'- metals in the paper of Hai Qiu and Tadanobu Inoue: *Evolution of Poisson's Ratio in the Tension Process of Low-Carbon Hot-Rolled Steel with Discontinuous Yielding. Metals* **2023**, *13*, 562. <https://doi.org/10.3390/met13030562> four different regimes are distinguished: Phase 1: Uniform elastic elongation, Phase 2: Discontinuous yielding, Phase 3 beyond R_{02} : Uniform elongation in the

hardening regime, Phase 4 beyond \bar{R}^t : Macroscopic plastic-strain localization experiencing radial deformation. Low-alloy iron usually has such an upper yield limit R_e^{upper} (R_{eH} , *Streckgrenze*). If it is stretched during the tensile test, a spontaneous yielding in the crystals-compound takes place under loading. This so-called Lüder's elongation effect of mild metals as a part of plastic stretching disappears until all crystals are finally commonly stretched. Austenitic steels do not have a pronounced yield strength. Essential for an accurate analysis is a stress-strain curve which is derived from a set of test curves, delivering distributions for the *design parameters* $R_{p0.2}$, R_m , ε_{on}^{pl} and ε_{fr}^{pl} .

The yield strength is a material property defined as the stress at which a material begins to deform plastically. If it is not well-defined (*remind Lüder*) on the stress-strain curve, it is difficult to determine a precise onset-of-yield point. In general, discriminating the proportional (tensile) limit R_{prop} and $R_{p0.2}$ ($\equiv R_{0.2}^t$), the offset yield point is taken as the stress at which 0.2% plastic deformation remains (*in English literature $R_{p0.2}$ is termed proof stress*). The mean stress at Onset-of-Yielding, denoted $\bar{R}_{0.2}$, will be applied for ductile modeling. The stress $\sigma(\varepsilon_{pl})$, considering only the plastic deformation or plastic flow of the material, is termed Flow stress σ_F .

By the way, the actual 'Onset-of-yielding at $R_{prop} \equiv \sigma_{prop}$ can be determined by a temperature measurement. If a metallic material is subjected to tensile stress, it first cools down in the area of elastic elongation analogous to an ideal gas (thermo-elastic effect). With onset of plasticization heat is released, which leads to an increase in temperature. This temperature is measurable with glued thermocouples. In other words: The proportionality stress σ_{prop} can be allocated to that applied stress level, where the test specimen experiences a temperature increase due to internal dislocations.

Regarding not only metals - for a conflict-free understanding – it will be denoted $R_{p0.2}$ ($\rightarrow R_{0.2}^t$) and $R_{c0.2}$ ($\rightarrow R_{0.2}^c$) in the body text from now on. At the maximum of the curve, characterized by the so-called 'End-of-uniform elongation' = 'Onset-of-(ductile) necking' in the ductile material case, the tensile strength R_m ($\rightarrow R^t$) is given. For very ductile materials is valid $R_{0.2}^c \equiv R_{0.2}^t$.

Beyond the tensile strength R^t a multiaxial state of stress follows in the tensioned ductile behaving test specimen. Therefore, the index ax holds up to the 'End-of-uniform elongation' (Gleichmaßdehnung) at R^t (*index pl for plastic strain, oon for Onset-of-(ductile) necking, and odc for Onset-of-ductile cracking located before rupture = plastic collapse*). In this respect, any formulations in this domain afford equivalent quantities in order to perform an accurate non-linear analysis with a correct $\sigma(\varepsilon)$ -input.

14.2 Engineering and True Stress and True Strain Quantities

The larger the strains the more the engineering quantities lose their applicability in structural dimensioning. Therefore, logarithmic (*usually termed true*) strains have to be used in an accurate dimensioning process. The derivation of these quantities is collected in [Table 14-1](#).

[Fig.14-2](#) contains a true and an engineering stress-strain curve. The figure presents a general view and uses classical Ramberg-Osgood mapping. Mapping of the course of stress-strain data in the non-linear domain is well performed by applying the Ramberg-Osgood equation for the true stress-true strain curve (*maps the true curve better than the engineering curve*)

$$\text{eng } \varepsilon = \varepsilon = \varepsilon^{\text{el}} + \varepsilon^{\text{pl}} = \frac{\sigma}{E_0} + 0.002 \cdot \left(\frac{\sigma}{\bar{R}_{0.2}} \right)^{\bar{n}} \quad \text{and} \quad \text{true } \varepsilon = \frac{\text{true } \sigma}{E_0} + 0.002 \cdot \left(\frac{\text{true } \sigma}{\text{true } \bar{R}_{0.2}} \right)^{\text{true } \bar{n}}$$

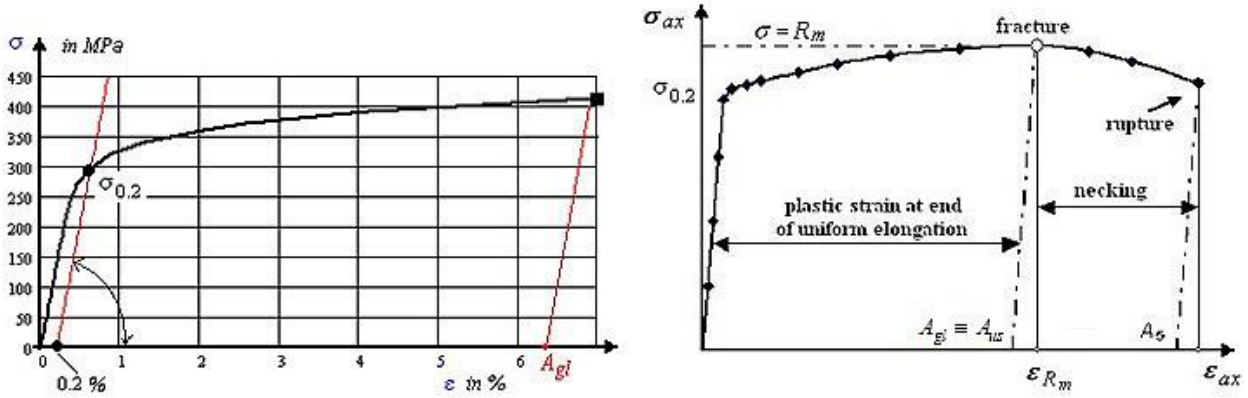


Fig.14-2: R-O mapping of a single engineering measurement test results, $A_{gl} = \min \varepsilon_{oon}^{pl}$.

Typical (mean) engineering stress-strain curve of a distinct ductile metal material. End of uniform elongation (Gleichmassdehnung ε_{gl})

Table 14-1 presents the derivation of true stresses and true strains in the ‘Mises’-validity domain. In Fig.13-4 the difference between the mean strength values $\text{eng } \bar{R}^t \rightarrow \text{true } \bar{R}^t$ was shown to be 8% for AA2219 !

Fig.14-3(left) depicts the linear elastic proportional domain and the hardening domain. Fig.14-3(right) presents stress-strain measurement with Ramberg-Osgood mapping. The course of the area reduction would show in a slight kink beginning at ‘Onset-of-ductile cracking $_{odc}$ ’ (= onset-of-localized necking) according to the deteriorating effect of the void coalescence.

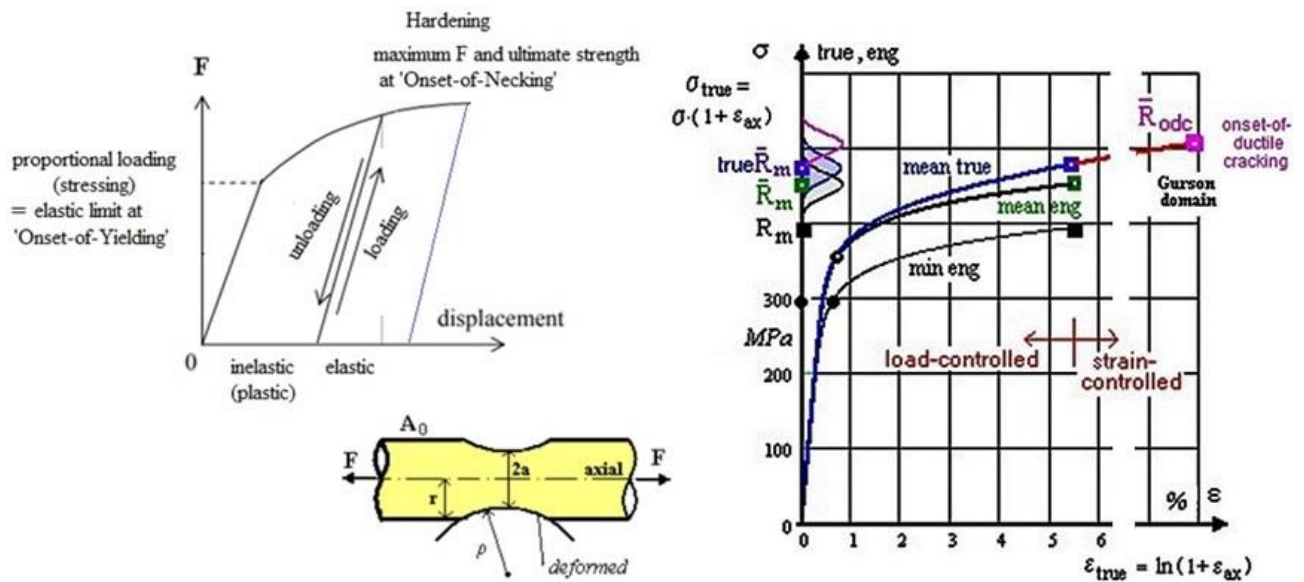


Fig. 14-3, modelling: (left) Display of proportional domain and hardening domain with the tensile rid test specimen. (right) Ramberg-Osgood-mapped true and engineering stress-strain curves of AA2219. F :=Force

F_{ax} , A_0 := original cross-section, A := actual cross section of the necked rod. $\bar{R}^t = \max F / A_0$, $\varepsilon \leq \bar{A}_{gl}$

(permanent strain linked to load-controlled fracture at \bar{R}^t). Necking radius is ρ . A bar over \bar{R} indicates a mean (average) value of a sufficiently large test data set, and no bar over R will generally mean strength and later indicate a ‘strength design allowable’.

Table 14-1: Derivation of true stresses and true strains in the 'Mises'-validity domain

True Strains (logarithmic strains):

The application of engineering strain cannot be correct for larger strains, since it is based on the original gage length ℓ_0 , whereas the length is continuously growing. Ludwik [Lud09] therefore introduced the true strain (logarithmic strain), the increment of which for a given length is defined as

$d(\text{true}\varepsilon) = d\ell / \ell$ and the total true strain, integrated from ℓ_0 to current length ℓ , is

$$\text{true}\varepsilon_{ax} = \int_{\ell_0}^{\ell} d\ell / \ell = \ln(\ell / \ell_0) = \ln(1 + \text{eng}\varepsilon_{ax}).$$

Above equation delivers an accurate value up to 'onset-of-necking' or \bar{R}^t .

The replacement of the logarithmic function by a Taylor series

$$\text{true}\varepsilon_{ax} = \text{eng}\varepsilon_{ax} - \text{eng}\varepsilon_{ax}^2 / 2 + \text{eng}\varepsilon_{ax}^3 / 3 - \dots$$

clearly shows that identity is given for small strains, only. Applying the true strain has a physical and a numerical advantage: The incompressibility equation really becomes zero

$$\sum \text{true}\varepsilon_i = \text{true}\varepsilon_I + \text{true}\varepsilon_{II} + \text{true}\varepsilon_{III} = 0,$$

whereas in terms of engineering strains the correct equation from solid geometry reads

$$(1 + \text{eng}\varepsilon_I) \cdot (1 + \text{eng}\varepsilon_{II}) \cdot (1 + \text{eng}\varepsilon_{III}) - 1 = 0,$$

which reduces to 0 for negligible strains, only.

Once necking starts most of the deformation occurs in the smallest cross section. The longer the gage length used the smaller the percent elongation will be. Therefore, a better procedure is the measurement of the reduction of the cross-section. → Beyond \bar{R}^t , the true σ - ε curve can be more accurately obtained by measuring the radial strain

$$\text{eng}\varepsilon_{radial} = (r - r_0) / r_0 = r / r_0 - 1 \quad \text{and} \quad \text{true}\varepsilon_{radial} = -\ln(1 + \text{eng}\varepsilon_{radial}) = -\ln(r / r_0),$$

provided, the tensile test specimen has a circular cross-section, a rod. In this case $\varepsilon_{radial} = \varepsilon_{hoop}$

$$\text{true}\varepsilon_{ax} + \text{true}\varepsilon_{radial} + \text{true}\varepsilon_{hoop} = 0 \quad \text{and it holds} \quad \text{true}\varepsilon_{ax} = -2\text{true}\varepsilon_{radial} = 2\ln(r / r_0),$$

which delivers an accurate value above 'onset-of-necking'. The equivalent strain in the center reads

$$\begin{aligned} \text{true}\varepsilon_{eq} &= \frac{\sqrt{2}}{3} \cdot \sqrt{(\text{true}\varepsilon_{ax} - \text{true}\varepsilon_{hoop})^2 + 0 + (\text{true}\varepsilon_{hoop} - \text{true}\varepsilon_{ax})^2} \\ &= \frac{\sqrt{2}}{3} \cdot \sqrt{2(2 - (-1))^2} \cdot \text{true}\varepsilon_{radial} = \frac{2}{3} \cdot \sqrt{3^2} \cdot \text{true}\varepsilon_{radial} = 2\ln(r / r_0) \end{aligned}$$

$$\Rightarrow \text{Transferring strain data:} \quad \text{true}\varepsilon = \ln(1 + \text{eng}\varepsilon), \quad \text{eng}\varepsilon = e^{\text{true}\varepsilon} - 1.$$

True Stresses

True σ can be obtained from eng σ , if the small changes in volume at the end of the transition domain are neglected. Then, incompressibility $\sum \varepsilon_i^{pl} = 0$ can be assumed and it follows:

$$\text{eng}\sigma = F / A_0, \quad \text{true}\sigma = F / A \quad \text{with} \quad A \cdot \ell = A_0 \cdot \ell_0, \quad F: = \text{load } F_{ax}$$

wherein ℓ_0 := original gage length, and A, ℓ current values of the necking cross-section.

Introducing the equation $\varepsilon_{ax} = (\ell - \ell_0) / \ell_0$ derived above, the true stress is linked by

$$\text{true}\sigma_{ax} = F / A = (F / A_0) \cdot (\ell / \ell_0) = \text{eng}\sigma \cdot (1 + \text{eng}\varepsilon_{ax}) = \sigma_{ax} \cdot (1 + \varepsilon_{ax}) \quad \text{usually written}$$

$$\Rightarrow \text{Transferring stress data:} \quad \text{true}\sigma = \text{eng}\sigma \cdot (1 + \text{eng}\varepsilon) \quad \text{and} \quad \text{eng}\sigma = \text{true}\sigma / \exp(\text{true}\varepsilon).$$

Fig.14-4 (left) shows an experiment in the elastic-plastic transition region, carried out by O. Mahrenholtz/H. Ismar. The test was a flat compression test of a cube. One side constrained, one free, one compressed \rightarrow Principal stress state ($\sigma_I = \sigma_{\text{action}}, \sigma_{II} = \sigma_I \text{ (re-action)}, \sigma_{III} = 0$) \rightarrow principal strain $\rightarrow \nu$. It turns out that R_{p01} is approximately $\nu = 0.4$. The value at R_{p02} in Lode coordinates is $0.82 = \sqrt{2/3} = \sqrt{2J_2} / R_{02}$, with $J_2 = 2R_{02} / 6$. Poisson's ratio, determined by a coupon measurement, reads $\nu = -\epsilon_{\text{lat}}/\epsilon_{\text{ax}}$ or $\nu = -(\Delta d/d)/(\Delta \ell/\ell)$. Concerning sheet test specimens the measurement problem increases because localized necking will occur at 'onset-of-ductile cracking and this depends on the thickness of the test specimen.

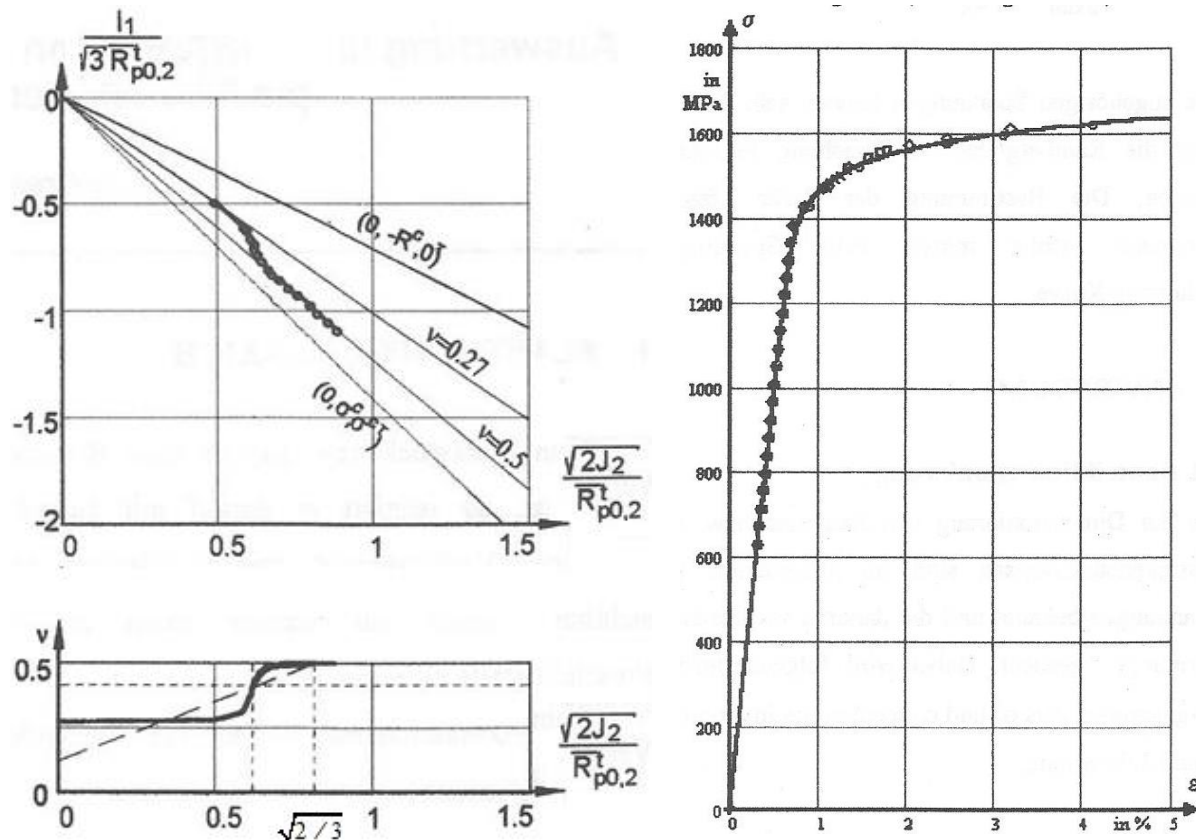


Fig. 14-4: (left) St37 Development of ν in Beltrami's elastic-plastic transition regime, a cube plane compression test. (right) D6AC, Ariane 5 Booster) Stress-strain measurement points with a Ramberg-Osgood engineering stress-strain data mapping curve under axial tension

14.4 Mapping of the measured stress-strain curve by the Ramberg-Osgood Model

At first in the mentioned contract with the institute IWF at Freiburg all model-required properties have been determined. The hopefully material-handbook given plastic strain A_5 and the also given final necking value Z are usually minimum and not average values. $A_{fr} \equiv A_{\text{rupture}}$ comes from measurement of A_5 (type: $L_0 = 5 \cdot d_0$, original length L_0 and initial diameter d_0) as plastic or permanent change in length, measured on the load-controlled broken test specimen and Z the radial plastic necking A-reduction ratio value, in %. (Unfortunately material mechanics also uses the letter A for strain properties).

Table 14-2 lists analysis-relevant quantities (in MPa and %), to be applied in Ramberg-Osgood curve modelling.

Table 14-2: AA2219 material properties and Ramberg-Osgood parameters. Isotropic materials, in MPa and (%), $d = 4.0 \text{ mm}$. Regarding \bar{R}_{odc} , see the following Sub-chapter 14-6.

$\bar{R}_{p0.2}$	\bar{R}_m	A_{gl}	true \bar{R}_m	true A_{gl}	\bar{R}_{odc}	$A_{fr} = A_{rupt}$	true A_{fr}	Z	\bar{n}	true \bar{n}	$R_{p0.2}$	R_m	R_{odc}
352	453	4.9	478	4.8	535	7.7	7.5	20	12.7	10.6	297	417	492
MPa	MPa	%	MPa	%	MPa	%	%	%	-	-	MPa	MPa	MPa
average (mean, typical, characteristic) values for best mapping											Design Allowables		

$$\text{true}\varepsilon = \frac{\text{true}\sigma}{E_0} + 0.002 \cdot \left(\frac{\text{true}\sigma}{\text{true}\bar{R}_{0.2}} \right)^{\text{true}\bar{n}} = \text{true}\varepsilon_{ax}^{el} + \text{true}\varepsilon_{ax}^{pl},$$

$$E_{\text{sec}}^{\text{hard}} = \frac{\sigma}{\varepsilon} = \frac{\sigma}{\frac{\sigma}{E_0} + 0.002 \cdot \left(\frac{\sigma}{\bar{R}_{0.2}} \right)^{\bar{n}}} = \frac{E_0}{1 + 0.002 \cdot \frac{E_0}{\bar{R}_{0.2}} \cdot \left(\frac{\sigma}{\bar{R}_{0.2}} \right)^{\bar{n}-1}}, \quad E_{\text{tan}}^{\text{hard}} = \frac{d\sigma}{d\varepsilon} = \frac{E_0}{1 + 0.002 \cdot \bar{n} \cdot \frac{E_0}{\bar{R}_{0.2}} \cdot \left(\frac{\sigma}{\bar{R}_{0.2}} \right)^{\bar{n}-1}}.$$

14.5 Poisson's ratio

If analytically necessary the value of Poisson's ratio ν , which increases when stresses narrow the plastic regime, can be determined for stability analyses as a function of the stress. The formula, which uses quantities of the R-O-mapped true stress-true strain curve, is derived in [Table 14-3](#).

However, this formula does not fully lead to $\nu = 0.5$ at R_{02} as can be seen in [Fig.14-5](#). A better approximation

$$\nu = 0.5 - (E_{\text{tan}}^{\text{hard}} / E_0) \cdot (0.5 - \nu_0) = \text{true}\nu$$

is usually applied in the elastic-plastic domain in stability analysis employing the tangent modulus function above in order to approximately consider the changing ν in analysis.

Table 14-3: Derivation of a formula for Poisson's ratio

$$\begin{aligned} \text{true}\varepsilon &= \text{true}\varepsilon^{el} + \text{true}\varepsilon^{pl} \text{ with } \text{true}\varepsilon_{ax} = \text{true}\varepsilon_{ax}^{el} + \text{true}\varepsilon_{ax}^{pl}, \text{ true}\varepsilon_{lat} = \text{true}\varepsilon_{lat}^{el} + \text{true}\varepsilon_{lat}^{pl}, \nu_0 = \frac{-\text{true}\varepsilon_{lat}^{el}}{\text{true}\varepsilon_{ax}^{el}} \\ &\text{from incompressibility in the plastic range (}\equiv \text{volume conservation law)} \quad \frac{V}{V_0} = \frac{\ell}{\ell_0} \cdot \frac{A}{A_0} = 1 \\ &\text{follows } \text{true}\varepsilon_{ax}^{pl} + 2 \cdot \text{true}\varepsilon_{lat}^{pl} = 0 \text{ and } \text{true}\varepsilon_{lat}^{el} = -\nu_0 \cdot \text{true}\varepsilon_{ax}^{el}, \text{ which gives after insertion of above relations} \\ \text{true}\nu &= -\frac{\text{true}\varepsilon_{lat}}{\text{true}\varepsilon_{ax}} = -\frac{\text{true}\varepsilon_{lat}^{el} + \text{true}\varepsilon_{lat}^{pl}}{\text{true}\varepsilon_{ax}} = -\frac{\text{true}\varepsilon_{lat}^{el} - 0.5 \cdot \text{true}\varepsilon_{ax}^{pl}}{\text{true}\varepsilon_{ax}} = -\frac{\text{true}\varepsilon_{ax}^{el}}{\text{true}\varepsilon_{ax}} \cdot \left(-\nu_0 - 0.5 \cdot \frac{\text{true}\varepsilon_{ax}^{pl}}{\text{true}\varepsilon_{ax}^{el}} \right) \\ &= -\frac{\text{true}\varepsilon_{lat}^{el} - 0.5 \cdot \text{true}\varepsilon_{ax}^{pl}}{\text{true}\varepsilon_{ax}} = -\frac{-\nu_0 \cdot \text{true}\varepsilon_{ax}^{el} - 0.5 \cdot \text{true}\varepsilon_{ax}^{pl}}{\text{true}\varepsilon_{ax}} = -\frac{-\nu_0 \cdot \text{true}\varepsilon_{ax}^{el} - 0.5 \cdot (-\text{true}\varepsilon_{ax}^{el} + \text{true}\varepsilon_{ax})}{\text{true}\varepsilon_{ax}} \\ &= -\frac{-\nu_0 \cdot \text{true}\varepsilon_{ax}^{el} - 0.5 \cdot (-\text{true}\varepsilon_{ax}^{el} + \text{true}\varepsilon_{ax})}{\text{true}\varepsilon_{ax}} = 0.5 + \frac{-\nu_0 \cdot \text{true}\varepsilon_{ax}^{el} - 0.5 \cdot (-\text{true}\varepsilon_{ax}^{el})}{-\text{true}\varepsilon_{ax}} \\ &= 0.5 - \frac{\text{true}\varepsilon_{ax}^{el}}{\text{true}\varepsilon_{ax}} \cdot (0.5 - \nu_0). \end{aligned}$$

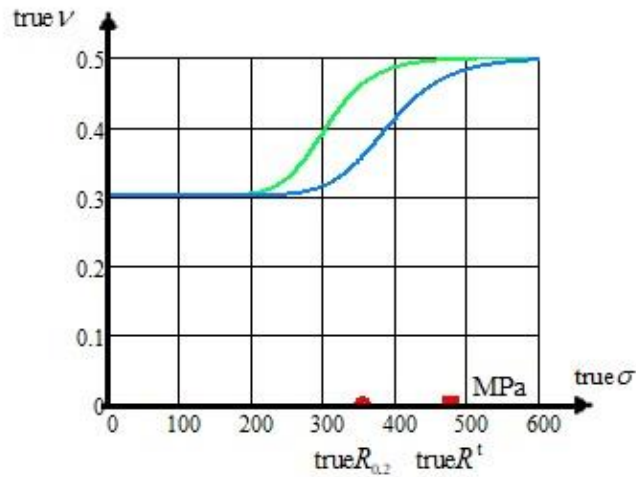


Fig.14-5: Course of Poisson's ratio in the elastic-plastic domain, determined with several formulas

LL:

- * The determination of the properties of a solid material requires a force-elongation curve which is then accurately to transfer into a stress-strain curve that is independent from the specimen type rod, sheet, coupon, cube.
- * Before any performance of a non-linear analysis is executed it is to check whether true or engineering curve quantities are to provide for input and which then represents the FEA output
- * Beyond R^t necking occurs generating a hydrostatic stress σ_{hyd} in the tensile rod, which lowers the stress-strain curve (see Chapter 15) in the high plastic regime
- * Poisson's ratio can only approach the limiting points $0.5 > \nu > (-1, \text{principally})$
- * UD-materials have different ν -values in the directions of anisotropy
- * Mind: So-called auxetic materials possess a negative ν . Being strained, the transverse strain in the material will also be positive
- * True strains can be added while engineering strains can not!

In Fig.14-6 the different growth of the engineering and the true stress-strain curve is displayed up to the tensile strength point at the 'End-of-uniform elongation'. Beyond R^t , in test data evaluation the axial stress has to be replaced by the equivalent stress because necking in the test specimen activates a hydrostatic residual stress state, dependent on the test specimen used.

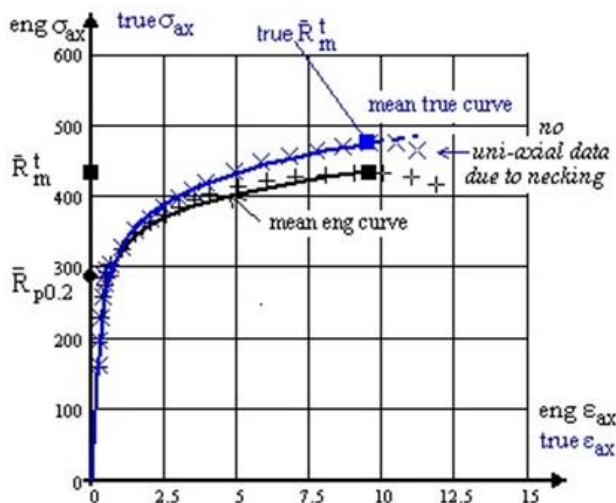


Fig.14-6, AA 2219:

Differences in R-O-mapping of engineering and true stress-strain curve, single measurement.. Bar over R indicates a mean value. F/A_0 at 'End of uniform elongation' = 'Onset-of-(diffuse) Necking'

In *Fig.14-7* the full stress-strain curve is presented and associated significant points including strength design allowables points are depicted. Additionally for ‘Onset-of-yielding’ the Margin of Safety is rendered in order to visualize the size of the fulfillment of the ‘Design Yield’ Limit State.

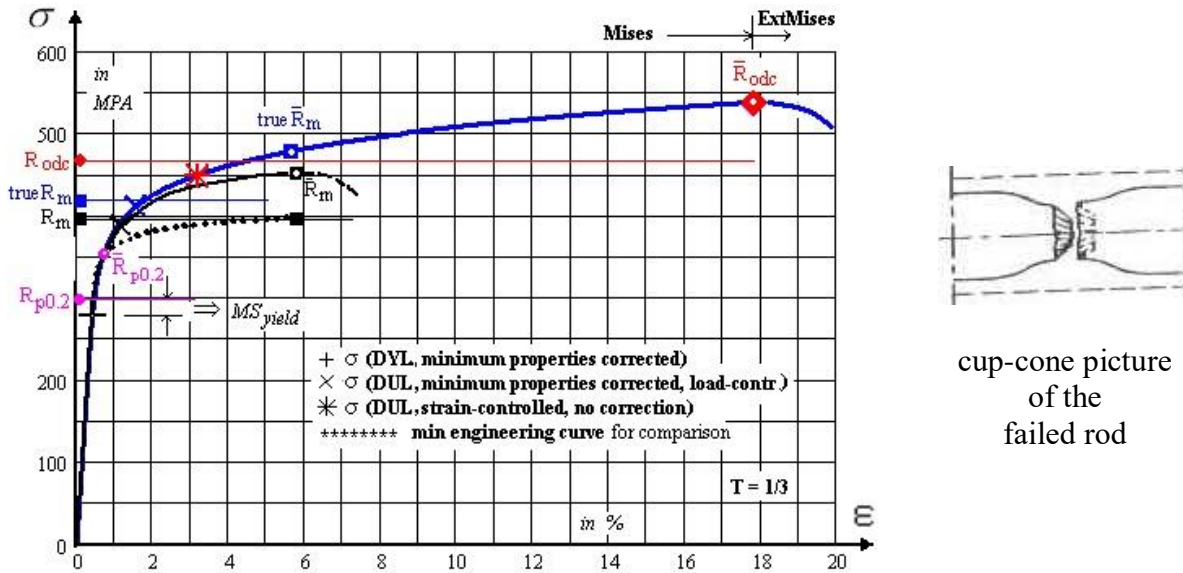


Fig. 14-6: Equivalent true stress-equivalent true strain curve. Proposed local strain-controlled extended stress-strain curve incl. mean fracture points and strength design allowables

The curve ends with reaching the ‘Onset-of-ductile cracking’ point at the associated strength R_{0dc} .

LL:

* *Opposite to some regulations it is to note “In general, it can be not correct to use a minimum engineering curve in order to obtain the desired structural behavior because structures are usually statically indeterminate”.*

* *The elliptical shape of the ‘Beltrami egg’ and its surface potential description can be used in the ‘Gurson domain’ too.*

14.6 Estimation of the Strength \bar{R}_{0dc}

Beyond ‘Onset-of-diffuse necking’ the axial strain measurement becomes senseless, only representative is the rod radius-decrease measurement to investigate in this full plastic domain the influence of the hydrostatic stress. From the measured plastic cross-section reduction the plastic portion ϵ_{0dc}^{pl} can be estimated and the ‘plastic’ curve point \bar{R}_{0dc} computed if the only counting associated plastic strain is known, fixed by the diameter reduction. Because the R/O-model excellently maps the true strength course of test data, its plastic part is employed to estimate a value for the *plastic point* $\bar{R}_{0dc} \equiv$ ‘Onset-of-ductile-cracking’, which is of interest for plastic structural design.

This can be executed by using volume constancy applying the measured reduction of the initial radius $a = d/2$ of the tensile rod. With $Z(\bar{R}_{rup})$ taken as $Z(\bar{R}_{0dc})$ the estimation of \bar{R}_{0dc} at true ϵ_{0dc} from the Ramberg-Osgood curve is performed as shown in *Table 14-4*.

Ductile collapse or rupture \bar{R}_{rupt} , respectively, is just of theoretical interest.

Table 14-4: Derivation of an estimate of the Strength \bar{R}_{odc}

At \bar{R}^t 'Onset-of- (diffuse) necking' $d_{oon} = 3.89$ mm, at 'Onset-of-ductile cracking' $d_{odc} = 3.78$ mm.

$$\varepsilon^{pl} = 0.002 \left(\frac{\sigma}{\bar{R}_{0.2}} \right)^n, \quad \varepsilon_{rad}^{pl} = \ln\left(\frac{r}{a}\right), \quad \frac{\Delta A}{A_0} = \frac{A_0 - A}{A_0} = 1 - \frac{A}{A_0} \rightarrow \frac{A_{rupt}}{A_0} = 1 - Z = \frac{r^2}{a^2}$$

$$\varepsilon_{ax,00n}^{pl} = -2 \cdot \varepsilon_{rad}^{pl} \text{ at } \bar{R}^t \quad \text{and delivers} \quad true\bar{n} = \frac{\ln\left(\varepsilon_{ax,00n}^{pl} / 0,2\%\right)^n}{\ln\left(\bar{R}^t / \bar{R}_{p0.2}\right)}$$

With known $\varepsilon_{rad}^{pl} = \ln\left(\frac{r}{a}\right) = \ln(\sqrt{1-Z}) = \ln(\sqrt{1-0.20}) = -11.2\%$ and $\varepsilon_{ax}^{pl} = -2 \cdot \varepsilon_{rad}^{pl}$

follow for the non-corrected odc-point $\rightarrow true\varepsilon_{ax}^{pl} = 0.002 \cdot \left(\frac{\bar{R}_{odc}}{\bar{R}_{0.2}}\right)^{true\bar{n}}$

$$\Rightarrow \bar{R}_{odc} \cong \bar{R}_{0.2} \cdot \sqrt[n]{true\varepsilon_{ax}^{pl} / 0.002} = 542 \text{ MPa} \quad \text{and}$$

$$true\varepsilon_{odc} = true\varepsilon_{ax}^{el} + true\varepsilon_{ax}^{pl} = \frac{\bar{R}_{odc}}{E} + 0.002 \left(\frac{\bar{R}_{odc}}{\bar{R}_{0.2}}\right)^{true\bar{n}}$$

14.7 Beltrami's Potential Surfaces in the Elastic-plastic and as Idea for the Porous Regime

From previous investigations the author knows, that any volume change, due to the FMC 'rules', is to describe by the term I_1^2 . If a shape change occurs then the invariant J_2 is required.

Elastic-plastic transition regime:

Beltrami cites: "The deformation of a material consists of two parts, a shape and a volume change". Based on this, one can formulate for the elastic-plastic transition regime

$$\frac{(2+2\nu) \cdot 3J_2}{\bar{R}^2} \quad \text{and} \quad \frac{(1-2\nu) \cdot I_1^2}{\bar{R}^2} \rightarrow \frac{3J_2}{\bar{R}^2} + \kappa \cdot \frac{I_1^2}{\bar{R}^2} = c^{Bel} \quad \text{with} \quad \kappa = \frac{1-2\nu}{2+2\nu}$$

Into this formulation a normalizing strength is inserted: $I_1 = \bar{R}$, $J_2 = 2\bar{R} / 6 \rightarrow c^{Bel} = 1 + \kappa$ and

for the special yield potential surface ($\nu=0.5$) yields $\frac{3J_2}{\bar{R}_{02}^2} + 0 \cdot \frac{I_1^2}{\bar{R}_{02}^2} = 1 + 0$ ('Mises' cylinder).

Beltrami bridges the elastic domain with the plastic domain ($3 \cdot J_2$ is Mises part). His formulation is not a failure function but a descriptive function to predict subsequent Beltrami surfaces $\nu(\bar{R})$, which are surfaces of equal potential. This means: A pair (ν, \bar{R}) must be given for each desired ν -curve of the subsequent potential surfaces are obtained, see Fig.14-7 left. This part figure shows the change of the potential surface of the growing 'Yield' body with increasing ν in the elastic-plastic transition domain. The two center figures show the cross-section using the principal stresses and below the development of the yield body from the yellow egg ($\nu = \nu_0$) up to full yielding ($\nu = 0.5$) rendered by the 'Mises cylinder' \rightarrow Poisson's ratio ν drives the elliptic shape!

Plastic porosity affected regime: an anticipation, considering Chapter 15

Porosity causes a volume increase. This works oppositely as in the elastic-plastic transition regime, which can be described by Beltrami, too. Increasing porosity f means a decreasing

Poisson's ratio ν and a more elliptic shape. In the outer figures of *Fig.14-7* both the regimes of the changing Poisson's ratio are displayed. The right part figure, modelled by Beltrami, pre-informs (see §15) how the surface of the yield body changes its shape with decreasing ν according to the increasing porosity f .

Fig.14-7(right) displays the development of the subsequent failure surfaces whereby an increasing true stress is considered. This is relevant for the critical material location. After achieving the tensile strength a small further radial increase of the surface is obvious together with the initiation of an increasing elliptic failure surface. With increasing degradation the subsequent surfaces become more and more elliptical. This is the opposite process regarding Beltrami in the elastic-plastic transition regime. A growing f means higher true stress but less cross-section or load-carrying material in the strain-controlled 'hot spot'.

The Beltrami formulation delivers an *Idea for the ductile porous regime* and is intended to replace the 'Gurson' formulation by Cuntze's so-called 'Extended Mises' one, reading

$$\frac{3J_2}{\bar{R}_{0.2}^t} + \frac{1-2\nu}{2+2\nu} \cdot \frac{I_1^2}{\bar{R}_{0.2}^t} = c^{\text{Bel}} \Rightarrow \frac{3J_2}{\bar{R}_{0.2}^t} + c_{12} \cdot \frac{I_1^2}{\bar{R}_{0.2}^t} = c^{\text{ExtMises}} .$$

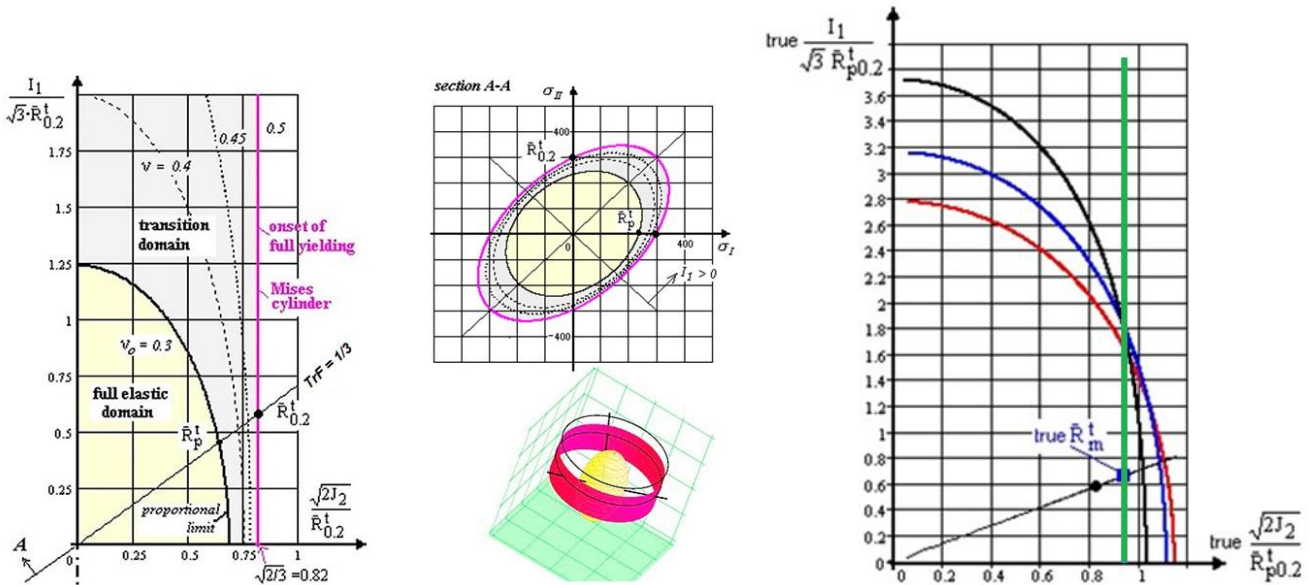


Fig.14-8: (left) Elastic-plastic transition domain, development of the Beltrami surfaces from egg shape (growing yield potential surface with $\nu_0 = 0.3$ for metals (0 for foam = sphere) $< \nu < 0.5$ ('Mises cylinder' $\rightarrow J_2 = \text{constant} = \text{incompressibility}$)) depicted in Lode-Westergaard coordinates. (center) visualization of the Beltrami potential surfaces. (right) Change of potential surfaces in the porous domain computed with the Extended Mises formulation (see [CUN22, §17]), $f = 0, 0.1, 0.2, 0.3$

Also here, the yield strength can be used for normalization. The parameters c^{Bel} , c^{ExtMises} mark the size parameter of the changing potential surface (see survey in *Table 15-4*).

In order to understand the chosen Lode-Westergaard coordinates *Fig.14-9* is provided below. The vector $\{\sigma_{\text{prin}}\} = (\sigma_I, \sigma_{II}, \sigma_{III})^T$ is a vector-addition of the principal stresses. The cone angle between all principal axes and I_1 is 54.75° .

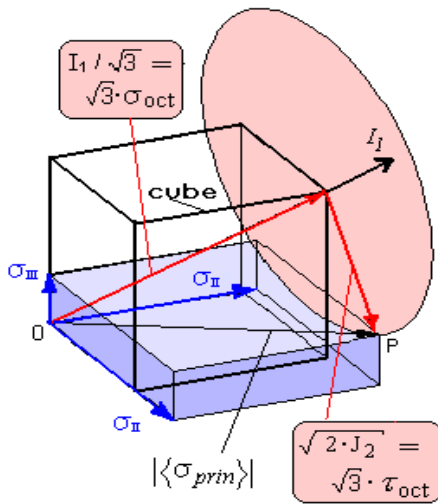


Fig.14-9:
Visualization of the used
Lode-Westergaard coordinates
by the principal stresses acting at a material
cube.

Octahedral stresses:

$$\sigma_{oct} = I_1 / 3 \quad \text{with } I_1 = \sigma_I + \sigma_{II} + \sigma_{III}$$

$$\sigma_{eq}^{Mises} = \sqrt{3 \cdot J_2} = f(\tau), \text{ with}$$

$$6 \cdot J_2 = (\sigma_I - \sigma_{II})^2 + (\sigma_{II} - \sigma_{III})^2 + (\sigma_{III} - \sigma_I)^2$$

$$\tau_{oct} = \sqrt{6 J_2} / 3 -$$

To make more familiar with potential surfaces Fig.14-10 presents two potential surfaces dedicated to different *Effs*, for fracture *Eff* = 100% and for a loading that generates *Eff* = 50 %.

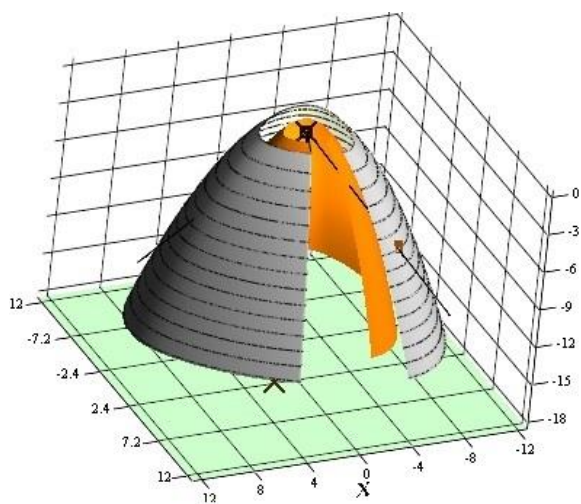


Fig.14-10: Two potential surfaces. *Eff* is the measure for the distinct potential surface with *Eff*=1=100% the fracture surface. The potential surfaces are *Eff*^{SF}=50% and *Eff*^{SF}=100%, fracture.

Indicated are the failure stress points
 $\bar{R}^t = 4$ MPa, $\bar{R}^{tt} = 3$ MPa, $\bar{R}^c = 40$ MPa, $\bar{R}^{cc} = 49$ MPa
and the principle stress axes.

'Normal Concrete', 3D test data available

$$Eff^{SF} = c^{SF} \cdot \frac{\sqrt{4J_2 \cdot \Theta^{SF} - I_1^2 / 3} + I_1}{2 \cdot \bar{R}^c}$$

LL:

- * The shape of the potential surfaces in the plastic porosity regime changes oppositely to the shape in the elastic-plastic regime. Both the surface shapes one can dedicate to the change of Poisson's ratio ν
- * In structural analysis the stresses are most-often determined in the elastic-plastic regime. This is performed very accurately, sometimes over-precise. However in this domain the Poisson's ratio changes significantly, which should be considered.

15 A measurable parameters-based ‘Extended-Mises’ Model instead of a ‘Gurson’ Model?

Aim: De-complication of highly non-linear plastic analyses, generation of a simplified model

15.1 Introduction simplified model to perform Design Verification in a Ductile Metal’s high Porous Regime

There is stress- and strain-controlled behavior. Strain-controlled locations in a structure will not break, when the stress level reaches tensile strength R^t . A fuel-outlet hole in the upper tank of the Ariane 5 central stage is such a strain-controlled case where the vicinity of the ‘overstrained’ critical material location takes over the reduced loading capability, no direct fracture is to face.

Such a (seldom) task caused MAN-Technologie to let perform an analysis together with IWM Freiburg applying a multi-parameter ‘Gurson’ yield model. Its model parameters cannot be measured directly, but are usually determined by a FE analysis which best models the deformation of the test specimen. An example for such a multi-parameter set, determined for the aluminum alloy AA2219 and using the tensile rod test specimen, is given in the table below [IWM Freiburg]:

f_0	f_n	f_c	f_F	q_1	q_2	ϵ_n	s_n
0.00	0.05	0.04	0.15	1.5	1.0	0.20	0.01

The applied ‘Gurson’-model (such a model is a model of the *Continuum (micro-)Damage Mechanics theory in the ductile materials regime*) of the IWM was a refined one. Refinement means that more parameters are to determine than for a simpler ‘Gurson’ model. Therefore, the optimal model parameter set of a ‘Gurson’ model depends on the mesh fineness and has to be inversely determined by an excellent simulation of the test specimen’s behavior, see [Fig.15-1 left](#) for the tensioned rod

(Gurson A L: *Continuum Theory of Ductile Rupture by Void Nucleation and Growth. Part 1: Yield criteria and flow rules for porous ductile media*. J. Eng. Mater. Techn.99 (1977), 2-15)

Using ‘Gurson’ model results, the responsible design engineer must ask: *What about the scatter of the parameters which are to insert in an analysis?* Without knowledge of the scatter there is no design verification possible. Might it be not better to apply a simpler model with 2 or 3 parameters at dispense of the little gain of the last load carrying portion after coalescence at ‘Onset-of-Ductile Cracking’ marked by the corresponding strength value R_{odc} ? This is the ‘technically relevant point’, where the coalescence of voids begins. Only a reduced procedure with directly measurable model parameters has the chance to capture the statistical Design Verification requirements.

In the context above the question comes up: *“How much Gurson material modelling is necessary to achieve a reliable prediction of the local design-deciding ductile fracture level of the structure?”* This failure mode ‘ductile fracture’ is defined here to be met at ‘onset-of-ductile cracking’ and it shall correspond to Design Ultimate Load. Such an application is a seldom but effortful case, where the deformation-controlled strength value $R_{odc} > R^t$ is used to *save the final design* which is not anymore possible via the load-controlled strength value R^t .

A simpler model is required. For its derivation, the various micromechanical mechanisms during ductile fracture are of basic interest:

- * Void nucleation at so-called second phase particles by debonding
- * Void growth, controlled by stress Triaxiality Factor TrF and growing plastic strain ϵ_{eq}^{pl} , and
- * Coalescence of voids by internal shear stress-driven rod necking with final ductile rupture.

Two challenging parts tasks are faced: (1) Creation of a model simpler than a multiple-parameter ‘Gurson’ model, and (2) to capture the porosity f in the equivalent σ - ε -curve, to be provided, whereby f is an additional but measurable model parameter transferring the ‘Mises’ model to the ‘Extended Mises’ model.

For the evaluation of the usual rod test results, the widely used correction formula of P.W. Bridgman is employed. *Fig.15-1(left)* presents the dependency of the rod’s diameter reduction on the load F and further shows simulation curve and test curve. The measurement of the diameter reduction is mandatory beyond the ‘End of uniform elongation’ at the tensile strength point $\bar{R}^t = \max F / A$, depicting the ‘Onset-of-diffuse necking $_{oon}$ ’ and experiencing full plasticity. Beyond \bar{R}^t only true values represent the reality. Mind: $F(\Delta d)$ is not completely of the same shape like $true\sigma(true\varepsilon)$.

In the load-controlled regime axial strain measurements are performed whereas in the transversal, plastic strain-controlled necking regime diameter reductions are to execute. In the *Fig.15-1(right)* attention is drawn to the various stress-strain curves used and associated strengths. Displayed are the mean technical and mean true strengths together with the associated Design Allowables.

If materials do **not fail** when the tensile strength is reached, then this is accompanied by the fact that $\max F$ does not essentially change over a certain range of the strain because hardening still works until a slight kink will occur due to void coalescence and destruction of piled-up dislocations. Degradation wins over hardening at the ‘Onset of ductile cracking’ strength point R_{odc} . R_{odc} and marks the coalescence-linked kink and is defined here as the critical strength.

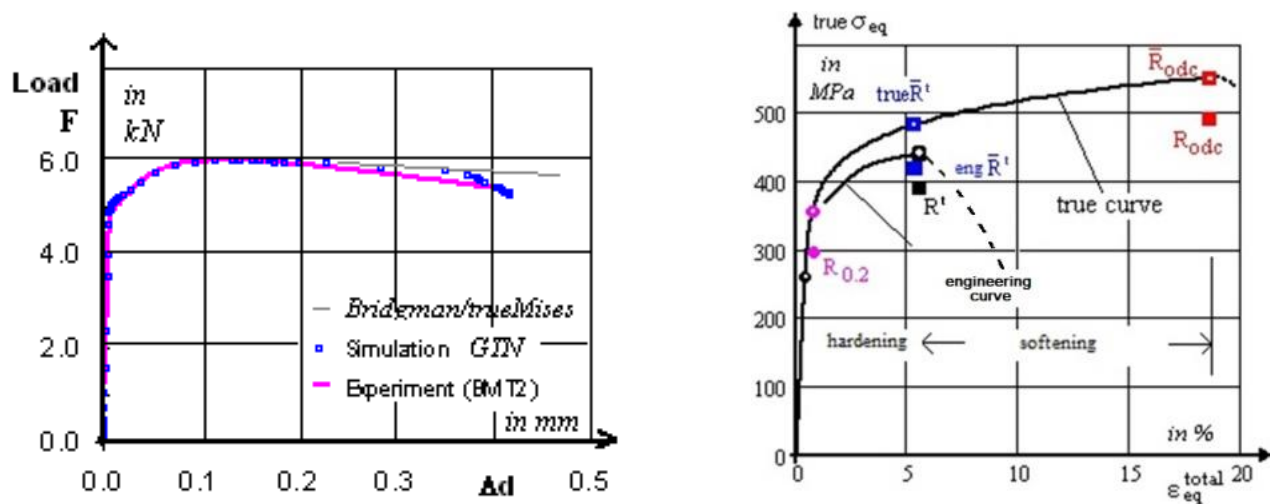


Fig.15-1: (left) Dependency of diameter reduction Δd on the applied load F . Comparison of global simulation and test results (IWM Freiburg, Dr. Sun). (right) Ramberg-Osgood-mapped true and engineering stress-strain curves of AA2219A bar over R indicates a mean value, no bar over R indicates a ‘design allowable’

15.2 Bridgman-3D Correction of the true σ - ε -Curve, employing ‘Mises’

Equivalent stress: $true\sigma_{ax} \rightarrow true\sigma_{eq}$

The validity of the uniaxial stress-strain curve measured in the smooth tensile rod test is terminated at the load-controlled strength point $\max\sigma_{true} = \bar{R}^t = \max F / A$, which corresponds to the maximum load F and to the actual minimum cross section of the neck. However, beyond \bar{R}^t (‘End-of-uniform-elongation’) begins the ‘Onset-of-diffuse necking $_{oon}$ ’ regime point and the 1D-stress

situation in the tensile rod becomes a 3D one and an equivalent stress σ_{eq}^{Mises} has to be considered in order to capture spatial stress tasks.

Under tensioning, in the plastic regime the lateral contraction of the material at the center of the neck is impeded by neighboring material leading to a 3D-stress state. Hence, a simple extrapolation of the F/A (σ - ε)-curve beyond \bar{R}^t cannot provide a physically accurate curve, because the necking-generated 3D-residual stress state σ_{hyd} is to consider in the evaluation of the tensile rod test results in order to obtain a real σ_{eq} . The three stresses within σ_{eq} reach their maximum values at the center of the rod's cross-section with approximately equal values $\sigma_{radial} = \sigma_{hoop}$, except close to the surface, as depicted in *Fig.15-2(left)* below. The values of σ_{radial} , σ_{hoop} raise with σ_{ax} and the created necking radius ρ as well. The former F/A -quantified yield capacity becomes continuously reduced with increasing necking. Hence, the true stress-strain F/A curve is to correct to obtain a realistic equivalent stress. Assuming a constant σ over the rod's cross-section *Fig.15-2(right)* illustrates the variety of TrF -beams making clear that values higher than $2/3$ (bi-axial stressing) are practically not possible. Assuming constancy is not anymore the case for a plastic rod neck, where the failure decisive location is the center of the cross-section with also there facing $maxTrF$. Notched test specimens are applied to capture higher multi-axial stress states, $TrF = 1$ limits.

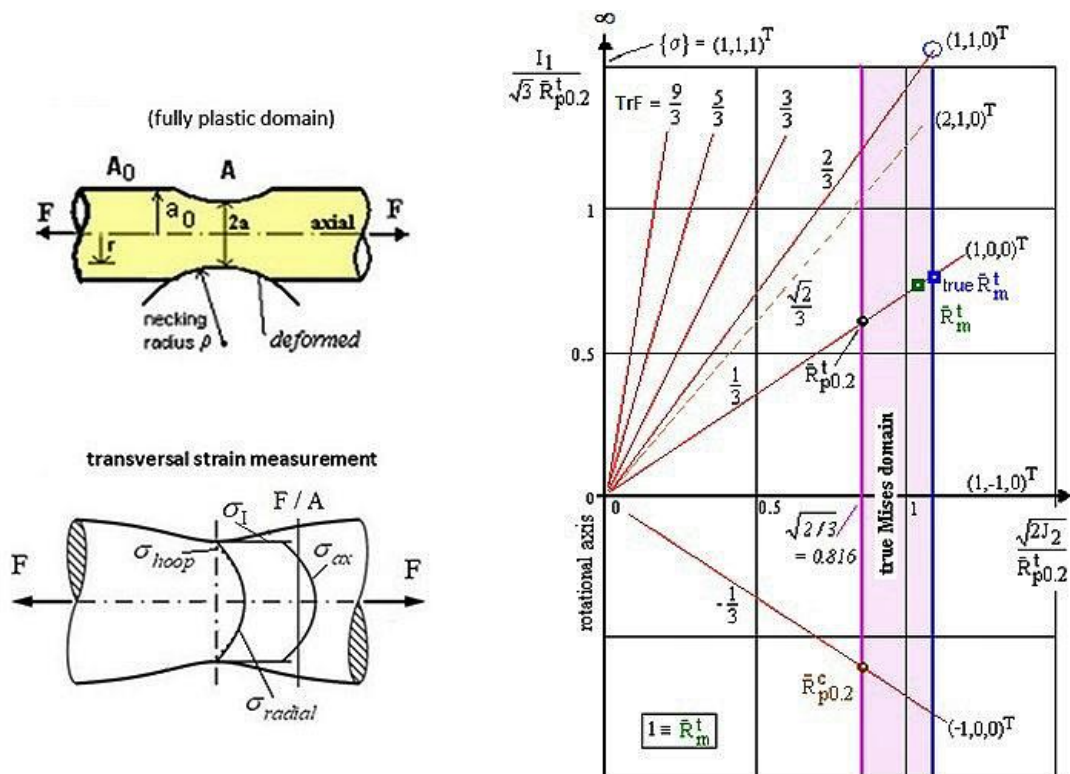


Fig.15-2: (left) Stresses and transversal (radial) strain measurement of the necked round tensile rod.

F :=force, A := minimum actual cross section of the neck. F :=Force F_{ax} , A_0 := original cross-section.

$\bar{R}^t = \max F / A_0$, $\varepsilon \leq \bar{A}_{gl}$ (permanent strain linked to load-controlled fracture at \bar{R}^t). Necking radius is ρ .

(right) Schematic visualization of the Triaxiality Factor TrF , responsible for failure in the rod center

$$\{\sigma\} = \{\sigma_I, \sigma_{II}, \sigma_{III}\}^T, TrF\{\sigma_I, \sigma_{II} = \sigma_I, 0\}^T = 2/3.$$

Fig. 15-3 shows the void volume fraction in the necking region at failure. The highest values are reached in the center of the specimen (Element 20) as expected. From the central region micro-damage spreads out over the whole cross section.

Basic task now will be the necessary transfer from the uniaxial true σ_{ax} (true ϵ_{ax}) \rightarrow tri-axial true σ_{eq} (true ϵ_{eq}) in the diffuse necking regime.

Bridgman provided a correction means how to adjust true σ_{ax} , but had to make some essential assumptions:

- (1) The cross section of the necked region remains angular (like the 'Mises' cylinder, assuming a rotationally symmetric yield body).
- (2) The inner axial contour of the neck can be approximated by the arc of a circle with the radius ρ .
- (3) 'Mises' can be applied (effect of growing voids is therefore not considered).

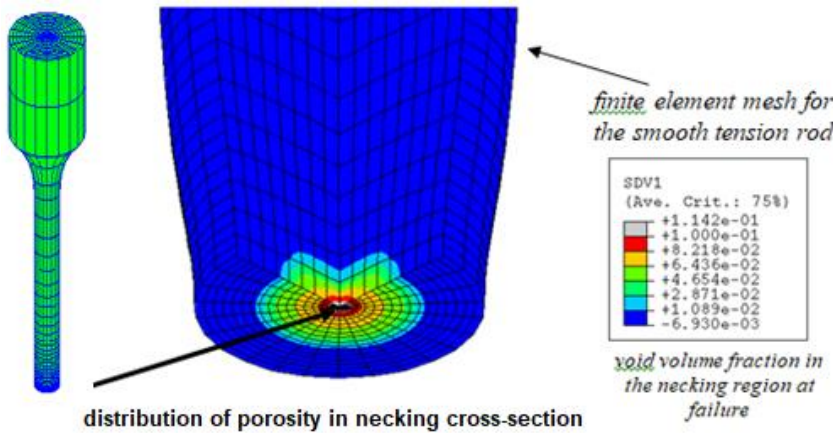


Fig.15.3: Tensile rod with porosity distribution in the 'Hot spot' center of the rod.). Finite element mesh of the rod. Void volume fraction f in the necking region at failure [Sun97, IWM7] stresses in MPa, strains in %. Material source, AA2219 variant, T2: $\rho_{initial} = \infty$, $2a = 4mm$, Elasticity properties are $E = 70000MPa$, $\nu = 0.3$, $t = 6 mm$ plate. Sample size $n = 179$, $A5 = 7.4 \%$, $Z = 20 \%$

Due to the diffuse necking', an axial load increase-caused internal hydrostatic tensile stress state σ_{hyd} is generated, representing a deformation-dependent residual stress state. Its radial distribution can be Mises-based estimated - under the axial loading $\{\sigma\} = (\sigma_I, \sigma_{II}, \sigma_{III})^T = (F/A, 0, 0)^T$ -

after Bridgman by $\sigma_{hyd}(r) \approx \sigma_I \cdot \ln\left(1 + \frac{a^2 - r^2}{2 \cdot a\rho}\right)$ with $\sigma_I < \frac{F}{A} = \frac{F}{\pi \cdot a^2}$, Fig.15-2

with $F :=$ load, $a :=$ radius of actual cross section of neck, $\rho :=$ radius of neck curvature and F/A an integral quantity capturing the external loading F . The full set of relevant relations then reads:

$$\sigma_{ax}^t(r) = \sigma_I + \sigma_{hyd}(r) \quad \text{and} \quad \sigma_{radial}(r) \approx \sigma_{hoop}(r) = \sigma_{hyd}(r) \quad \text{and as equivalent stress follows}$$

for a single stress $\rightarrow \sigma_{eq}^{Mises} = \sqrt{3 \cdot J_2} = \sqrt{\frac{1}{2} \cdot \sqrt{[(\sigma_I)^2 + (0)^2 + (-\sigma_I)^2]}} = \sigma_I$ and also

for a superimposed $\sigma_{hyd} \rightarrow \sigma_{eq}^{Mises} = \sqrt{3 \cdot J_2} = \sqrt{\frac{1}{2} \cdot \sqrt{[(\sigma_I - \sigma_{hyd})^2 + (\sigma_{hyd} - \sigma_{hyd})^2 + (\sigma_{hyd} - \sigma_I)^2]}} = \sigma_I$

$$I_1 = \max \sigma_{ax}^t + \max \sigma_{radial} + \max \sigma_{hoop} = \sqrt{3 \cdot J_2} + 3 \cdot \sigma_{hyd}, \quad \sqrt{3 \cdot J_2} = \sigma_I \quad (\leftarrow \text{no } \sigma_{hyd} \text{ effect}).$$

$$TrF(r) = \text{true} \sigma_{mean} / \text{true} \sigma_{eq}^{Mises} = (I_1 / 3) / \sqrt{3 J_2} = [\sqrt{2} / 3] \cdot (I_1 / \sqrt{3}) / \sqrt{2 J_2} = \frac{1}{3} + \frac{\sigma_{hyd}}{\sigma_I}.$$

Decisive for failure in the rod is the Triaxiality Factor TrF , which increases with the true axial loading. Its maximum is in the center, the 'hot spot' at $r = 0$. In this micro-damage critical cup-cone center the 3D-state of stresses reads

$$\max \sigma_{hyd} (r=0) = \sigma_I \cdot \ln \left(1 + \frac{a}{2 \cdot \rho} \right), \quad \max \sigma_{ax}^t (r=0) = \sigma_I + \max \sigma_{hyd}$$

with the stress state in the rod's center $\{\sigma\} = (\sigma_I + \max \sigma_{hyd}, \max \sigma_{hyd}, \max \sigma_{hyd})^T$.

In the necessary adjusting process of the F/A-curve in the diffuse necking regime (Phase 3) the first step is to integrate the axial stress, which varies over the radius. From load balance the following relations are yielded in *Table 15-1*.

The last unknown is the neck radius ρ . It could be computed during testing by measuring the shape change of the neck via a real-time Digital Image Correlation (DIC) 3D full-field measurement optical technique of the surface strains and an associated surface geometry model.

Table 15-1: Bridgman-Derivation of the cross-section quantities of the tensioned rod

$\begin{aligned} \frac{F}{A} &= 2 \cdot \int_0^a \sigma_{ax}^t \cdot \pi \cdot r \cdot dr / (\pi \cdot a^2) \\ &= 2 \cdot \int_0^a (\sigma_I + \sigma_I(r)) \cdot \pi \cdot r \cdot dr / (\pi \cdot a^2) \\ &= 2 \cdot \int_0^a \left(\sigma_I + \sigma_I \cdot \ln \left(1 + \frac{a^2 - r^2}{2 \cdot a \cdot \rho} \right) \right) \cdot \frac{\pi \cdot r \cdot dr}{\pi \cdot a^2} \end{aligned}$	
<p>integrated follows $\frac{F}{A} = \sigma_I \cdot \left(1 + \frac{2\rho}{a} \right) \cdot \ln \left(1 + \frac{a}{2\rho} \right)$ with $\sigma_{eq}^{Mises} = \sqrt{3 \cdot J_2} = \sigma_I$</p> <p>$\sigma_I = \sqrt{3 \cdot J_2} = \sigma_{eq}^{MisBri} = \frac{F}{A} / \left(1 + 2 \cdot \rho/a \right) \cdot \ln \left(1 + a/2 \cdot \rho \right)$, valid $> \bar{R}^t$ or $A < A_{oon}$, an equation, in which the ratio a/ρ is not known.</p> <p>If no test result is available, then Lorrek-Hill's approach for rupture is applied at \bar{R}_{rod} :</p> <p>maximum $\frac{a}{\rho} = \sqrt{\ln \left(\frac{A_0}{A_{rupt}} \right) - \ln \left(\frac{A_0}{A_{oon}} \right)}$, $\frac{A_{rupt}}{A_0} = 1 - Z$ with a given cross section reduction Z in % at maximum necking at \bar{R}_{rupt} and A_{oon} the cross section at $\bar{R}^t \equiv \bar{R}_m^t$, being 'Onset-of-(diffuse) necking'.</p> <p>$\frac{a}{\rho} = c_1 + c_2 + \text{true} \mathcal{E}_{ax} R_{odc}^2 + c_3 \cdot \text{true} \mathcal{E}_{ax} R_{odc}^3$.</p>	

Equivalent strain: $\text{true} \mathcal{E}_{ax} \rightarrow \text{true} \mathcal{E}_{eq}$

For the Mises equivalent strain is valid in the plastic domain (elastic part is negligible):

$$\varepsilon_{eq}^{Mises} = \frac{\sqrt{2}}{3} \cdot \sqrt{(\varepsilon_I - \varepsilon_{II})^2 + (\varepsilon_{II} - \varepsilon_{III})^2 + (\varepsilon_{III} - \varepsilon_I)^2} = \frac{\sqrt{2}}{3} \cdot \sqrt{(\varepsilon_I^{pl} - \varepsilon_{II}^{pl})^2 + (\varepsilon_{II}^{pl} - \varepsilon_{III}^{pl})^2 + (\varepsilon_{III}^{pl} - \varepsilon_I^{pl})^2}$$

considers plastic volume constancy (incompressibility) $\Sigma \varepsilon_i^{pl} = 0$ during plastic deformation it becomes

$\varepsilon_I^{pl} / 2 = -\varepsilon_{rad}^{pl} = -\varepsilon_{tan}^{pl}$ and $\varepsilon_{rad}^{pl} = \ln(r/a) = \varepsilon_{tan}^{pl} \Rightarrow \varepsilon_I^{pl} = -2 \cdot \ln(r/a)$ and it reads

$$\text{true} \mathcal{E}_{eq}^{Mises} = \frac{\sqrt{2}}{3} \cdot \sqrt{((\varepsilon_I^{pl} + \varepsilon_{rad}^{pl}) - \varepsilon_{rad}^{pl})^2 + 0 + (\varepsilon_{rad}^{pl} - (\varepsilon_I^{pl} + \varepsilon_{rad}^{pl}))^2} = \frac{\sqrt{2}}{3} \cdot \sqrt{2 \varepsilon_I^{pl2}} = \frac{2}{3} \cdot \varepsilon_I^{pl}$$

LL:

- * *Bridgman correction = approach, which considers the varying stress over the rod's cross-section regarding that the center is the critical line*
- * *Lorrek-Hill = approach, which formulates a final value for the change of the curvature radius under loading. The increasing curvature triggers the increasing hydrostatic stress and this is to map*
- * *Measured ratio F/A = stress capacity smeared over the cross-section = load ability-quantity, which represents an effective (smeared) value, which decays with increasing axial strain*
- * $\sigma_1 \equiv \sqrt{3J_2}$ = constant basic stress quantity of the Bridgman approach, see Table 15-1
- * *The applicability of axial measurement ends with 'End-of-uniform elongation' at \bar{R}*
- * *Bridgman model application is limited to about 30% cross-section reduction, due to not considering the coalescence of the voids*
- * *The Bridgman-correction is applied by using the 'Mises' yield function and not a 'Gurson'-type void growth-capturing (porosity f) yield function. This led the author 20 years ago to propose his so-called 'Extended Mises' yield condition at the end of a joint Research program MAN with IWF-Freiburg.*

Idea:

The replacement of a 'Mises'-based Bridgman correction by a porosity-considering one should lead to a more realistic stress-strain curve and should offer the advantage to escape in the analysis from the high number of non-measurable 'Gurson' model parameters except from f . In order to consider the void growth, the author proposes to replace the Bridgman-corrected Mises-model by the mentioned '**Gurson' model-linked Extended Mises-model**'.

15.3 Porosity-improved Bridgman 3D-Correction of true σ - ε -Curve employing 'Extended Mises'

Porosity means volume change due to void coalescence. Such a volume change can be transferred to a decaying Poisson's ratio as it is known from Beltrami. The author experienced, that the 'Gurson'-analyses base on a 'Mises'-linked equivalent stress-equivalent strain curve. This should be improved when considering the porosity f . The author's hypothesis about 2002 reads:

- * Formulation of an egg-shaped yield model, termed Extended Mises, with
- * Simplification to 1 measurable 'Gurson' parameter f , only
- * Improvement of this simpler model idea by applying a porosity-capturing equivalent $\sigma - \varepsilon$ curve
- * Taking a simple 'Gurson' yield model to obtain via a 'comparison of coefficients' a relation to the porosity f in the simple 'Gurson' -model from Gurson-Tvergaard-Needleman, index ^{GTN}
- * Probable 120°-material symmetry in the high porosity regime is not documented and therefore not considered. It can be captured by replacing $\frac{3J_2}{R^2}$ through $\frac{3J_2}{R^2} \cdot \Theta$ (see Chapter 11).

LL:

- * *The 'Mises' cylinder is a simplification (remember: §11, 120°-symmetry, $\Theta = 1$)*
- * *Increasing porosity also means decreasing Poisson's value ν and an increasing elliptic shape*

From knowledge in Chapter 14 is known: Values for the increasing porosity f are strain-controlled detectable. The effect of a probably initially not pore-free material is captured in the initial property values.

14.1 Measurement of rod failure stresses and estimation of the vertex of the failure body

Even for a porous plastic failure body its vertex should be known. A vertex represents the equi-triaxial tensile strength capacity of a load-controlled strength situation, remind Fig.15-2. Because

the vertex stress state $\{\sigma\} = (\text{true}\bar{R}^{III}, \text{true}\bar{R}^{III}, \text{true}\bar{R}^{III})$ with $TrF = \infty$ practically cannot be measured as best substitute a 3D-stress state - closest possible to the vertex - must be employed. Realistic is a stress state $(\text{true}\sigma_{ax} + \sigma_{hyd}, \sigma_{hyd}, \sigma_{hyd})$ by investigating the center of an un-notched tension rod test specimen, being the ‘hot spot’ in this test specimen.

In such un-notched rods a neck radius builds up and increases with further increasing axial tensile stress. Due to the diameter reduction a hydrostatic stress state is generated and can be determined from the zero volume strain regime faced in the minimum neck cross-section. Hereby, difference due to rolling of the sheet material and how the test specimen is cut out are neglected and full isotropy assumed.

From the test rig loading comes the subsequently effective stress ‘true σ_{ax} ’, whereas the remaining neck cross-section experiences in the center the multi-axial stress state $(\text{true}\sigma_{ax} + \sigma_{hyd}, \sigma_{hyd}, \sigma_{hyd})$, estimated by the Bridgman model. In order to better understand the stress situation in the rod center the effect of increasing σ_{hyd} is of interest, depicted below.

It is to conclude from mechanics, that a hydrostatic stress does not change Mises’s representative invariant J_2 for shape deformation of the solid. However, σ_{hyd} affects the tri-axiality value TrF which might be interpreted to cause some quasi-embrittlement of the material:

$$I_1 = (\sigma_I + \sigma_{II} + \sigma_{III}) = f(\sigma), \quad 6J_2 = (\sigma_I - \sigma_{II})^2 + (\sigma_{II} - \sigma_{III})^2 + (\sigma_{III} - \sigma_I)^2 = f(\tau)$$

$$(\text{true}\sigma_{ax} + \sigma_{hyd}, \sigma_{hyd}, \sigma_{hyd}), \quad \sigma_{ax}^I(r) = \sigma_I + \sigma_{hyd}(r)$$

$$\sigma_{eq}^{Mises} = \sqrt{3J_2} = \sqrt{3} \cdot \sqrt{(\sigma_1^M - \sigma_h - \sigma_h)^2 + 0 + (\sigma_h - \sigma_1^M - \sigma_h)^2} \rightarrow \sigma_{eq}^{Mises} = \sigma_1^{Mises}$$

$$TrF = \sigma_{mean} / \sigma_{eq}^{Mises} = (I_1 / 3) / \sqrt{3J_2} = [\sqrt{2} / 3] \cdot (I_1 / \sqrt{3}) / \sqrt{2J_2}$$

$$I_1 = (\text{true}\sigma_{ax} + 3\sigma_{hyd}) = f(\sigma), \quad 6J_2 = (\sigma_I - \sigma_{II})^2 + (0)^2 + (\sigma_{III} - \sigma_I)^2 = f(\tau)$$

$$\text{uni-axial } \sigma_{ax}, \text{ multi-axial } (\sigma_{ax} + \sigma_{hyd}, \sigma_{hyd}, \sigma_{hyd}) \text{ in the rod's minimum neck section} \Rightarrow \sigma_{eq}^{Mises}$$

Again: The use of notched rods is principally also possible considering that the original notch radius ρ increases. Thereby the critical rod surface stress concentration reduces a little and the originally surface-located critical material location moves to the center.

Fig.15-9(left) shall display different stress states and the associated points on the respective TrF -beams. In the subpicture down left the indicated 2D stress-states and up further the 3D stress states all collected in the table right down.

Of interest for the designing engineer is that the spatially formulated SFC $F^{NF} = 1$ dents the failure body at the pressure vessel situation $\{\sigma\} = (2,1,0) \rightarrow TrF = \sqrt{2} / 3$, *Fig.15-2* and *15-9*. In the 2D principal stress plane F^{NF} is a straight line and in the 3D failure body a hyperbolic curve!

Fig.15-9(right) shall make the non-linear development of TrF clear and further make familiar with the design failure surfaces in the very ductile regime. The figure schematically shows that the strain-controlled failure surface is outside and thereby larger than the load-controlled one. with points indicating distinct stress-states as

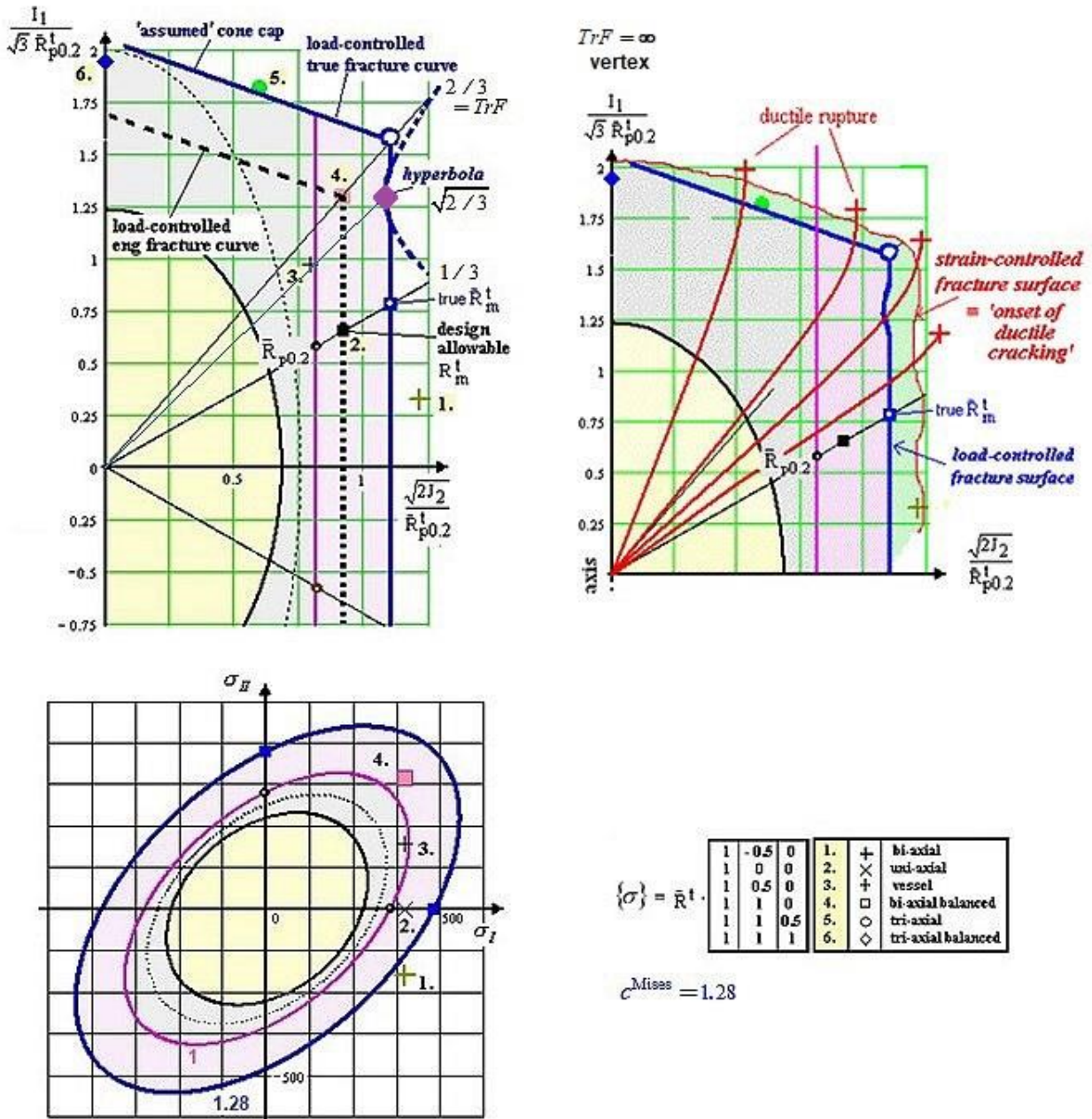


Fig. 15-9: Visualization of the effect of the TrF-beams and the related strengths, illustration of some stress state points and failure zones. 2D-potential surfaces on the inclined cross-section of the rotationally-symmetric failure body

15.4 Proposal of the Two Parameter 'Extended Mises' Yield function in the porosity domain

Extended Mises yield potential function

Originally, Gurson proposed for a metal, containing well distributed voids, a yield condition-based solution for a single spherical void. The model was modified later by Tvergaard and Needleman, including the porosity f and the increasing Flow stress σ_f of the 'matrix' material: The porous body, called bulk material (*smearred material*), consists of the matrix material and the voids or pores. The voids are nucleated in tension, only. The dense matrix phase follows the HMH ('Mises') model, and f represents the mean void volume fraction or porosity (*average value of a porous matrix*) as the so-called internal damage variable. For $f = 0$, fully dense material, the model

reduces to that of von Mises, whereas a ultimate value f_{ult} implies that the material is ultimately voided that it has lost its stress carrying capacity due to local ductile rupture. Here, f_{ult} shall be replaced by the smaller $f_{odc} = f_{crit}$. Values for the increasing porosity f are strain-controlled detectable and therefore, the ratio is fixed. *Table 15-2* describes the procedure how a relationship between the subsequent ‘Gurson’ type yield model and the ‘Extended Mises’ was developed. A further equation is needed to determine the size parameter, such as with c^{Mises} of the ‘Mises cylinder’.

Table 15-2: ‘Comparison of Coefficients’ of the models ‘Gurson’ ↔ ‘Extended Mises’ with σ_F as increasing true Flow stress as running stress variable

$$F^{GTN} = \frac{3J_2}{\sigma_F^2} + 2 \cdot f \cdot q_1 \cdot \cosh\left(\frac{I_1 \cdot q_2}{2 \cdot \sigma_F}\right) + q_3 \cdot f^2 = 1 \text{ ductile micro-damage failure function}$$

simplified to $\frac{3J_2}{\sigma_F^2} + 2 \cdot f \cdot \cosh\left(\frac{I_1 \cdot q_2}{2 \cdot \sigma_F}\right) + f^2 = 1$ appropriate for idea demonstration, $q_3 = q_3 = 1$

If the cosh-function is replaced by the first two terms of the associated Taylor row [Cun98, Cun01]
 $\cosh x = \pm (1 + x^2 / 2 + \dots) \rightarrow \cosh(I_1 \cdot q_2 / 2 \cdot \sigma_F) = \pm (1 + (I_1^2 \cdot q_2^2 / 8 \cdot \sigma_F^2) + \dots)$.

The negative sign is to chose because porosity reduces strength capacity

$$\frac{3J_2}{\sigma_F^2} - 2 \cdot f \cdot \left(1 + \frac{I_1^2 \cdot q_2^2}{8 \cdot \sigma_F^2}\right) + f^2 = 1 \Rightarrow \frac{3J_2}{\sigma_F^2} - 1 \cdot f \cdot \left(\frac{I_1^2 \cdot q_2^2}{4 \cdot \sigma_F^2}\right) + 2f - f^2 = 1.$$

With $f^2 \ll f$ can be derived

$$\frac{3J_2}{\sigma_F^2} - f \cdot \frac{q_2^2}{4} \cdot \frac{I_1^2}{\sigma_F^2} - 2f = 1 \text{ with } q_2 = 1.5 \text{ as guess for the plastic damage flow function}$$

$$\frac{3J_2}{\sigma_F^2} - f^* \cdot \frac{I_1^2}{\sigma_F^2} - 2f = 1 \text{ with the elliptic shape parameter } f^*$$

$$\kappa = \frac{1 - 2\nu}{2 + 2\nu} \equiv f \cdot \frac{q_2^2}{4} = f^* \rightarrow \nu = (4 - f^*) / (8 + 2f^*).$$

\Rightarrow Failure state, normalized again with the shear strength, to insert is $\sigma = \bar{R}_{odc}$

$$F = \frac{3J_2}{\bar{R}_{0.2}^2} + f_{ult}^* \cdot \frac{I_1^2}{\bar{R}_{0.2}^2} + 2f_{ult} = 1 = Eff = 100\% \text{ material stressing effort,}$$

$F = 100\%$ = potential surface, which may be a fracture surface or a yield surface.

From ‘Comparison of Coefficients’ finally is obtained

$$\text{ExtendedMises } F = \frac{3J_2}{\bar{R}_{0.2}^2} + c_{12} \cdot \frac{I_1^2}{\bar{R}_{0.2}^2} = c^{ExtMis}, \text{ generally}$$

Analogous to ‘Mises’ $Eff^{Mises} = \sigma_{eq}^{Mises} / \bar{R}_{0.2} = \sqrt{3J_2} / \bar{R}_{0.2} \Rightarrow Eff^{ExtMises} = \sigma_{eq}^{ExtMises} / \bar{R}_{0.2}$

follows $\sigma_{eq}^{ExtMises} = \sqrt{\frac{3J_2 - f^* \cdot I_1^2}{1 + 2f}}$.

Void Porosity-linked reduction of Poisson’s ratio $0.5 > \nu$

Porosity means volume change due to void coalescence and volume change may be transferred to a decaying Poisson’s ratio (remind Beltrami). From the ExtM-model can be deduced geometrically taking $f^* = f \cdot q_2^2$ and $\nu = (4 - f^*) / (8 + 2 \cdot f^*)$.

Fig. 15-10 points out how the Poisson ratio is linked to the true strains (left), schematically to the true equivalent stress (center), and to the porosity f^* .

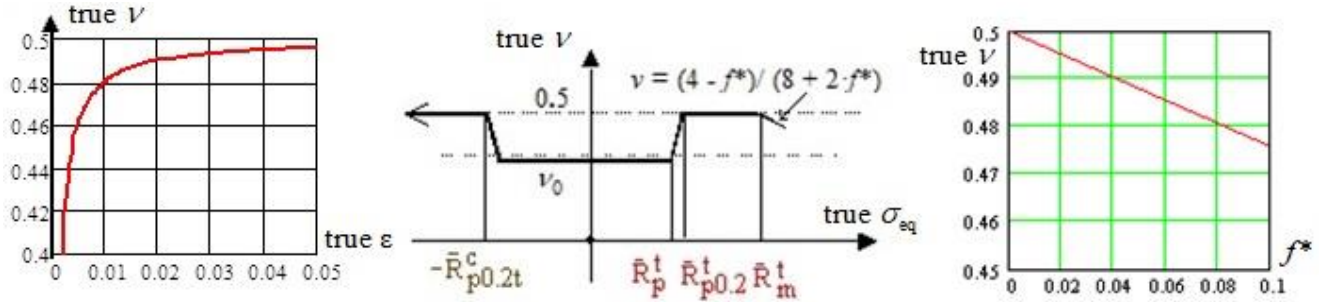


Fig. 15-10: Dependence of ν on the different parameters, the various regimes

Here, $f_{ult}(\bar{R}_{odc}) < f_{rup}$ is employed as that critical porosity which was dedicated by the author to ‘Onset of ductile cracking’, in order to ‘remain on the safe side’. The evolution function of f is assumed to follow an exponential course with practically $f = 0$ at the tensile strength point up to the defined ultimate value f_{ult} located at \bar{R}_{odc} .

15.3 Visualization of ‘Gurson’-model versus ‘Extended Mises’-model

Failure conditions enable the designer to assess multi-axial states of stress $\{\sigma\}$ by an equivalent stress σ_{eq} and to map multi-axial stress-strain behavior $\sigma_{eq}(\epsilon_{eq})$ via a measured, smeared stress F/A . For $f = 0$, fully dense material, the model reduces to that of HMH, whereas a maximum value f_{ult} implies that the material is ultimately voided that it loses its stress carrying capacity due to local ductile rupture.

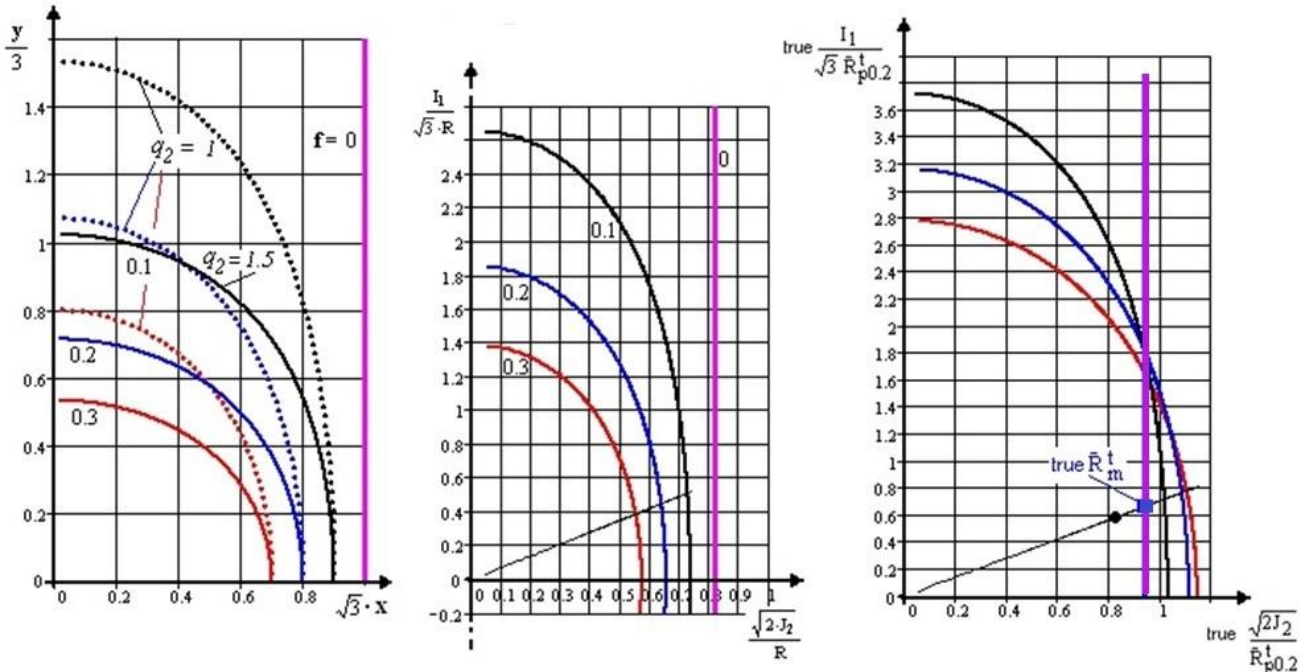


Fig. 15-11: Schematic comparison of the Gurson model (dots) and Extended Mises model Potential surfaces.

(left) Display of curve parameter porosity f influence, using the ‘Gurson’ coordinates $x = (\sqrt{J_2} / \sigma_F)$, $y =$

(I_1 / σ_F) , $\sigma_F = \bar{R}_{p0.2}^t$; (center) Display of the Gurson yield model in Lode-Haigh-Westergaard parameters $\bar{R}_{p0.2}^t =$ normalisation strength); (right) Ppotential surfaces of the ExtMises-model with four increasing true

(graphs made about 2001)AA2219, ($q_2=1.5$, $q_{2ExtM}=1.13$) $true \bar{R}^t, \bar{R}_{odc}$.

The conventional visualization – as a parameter investigation - of the Gurson model is presented in Fig.15-11(left) with f being the porosity parameter of the curves and q_2 a Gurson parameter from the comparison. A growing f means higher true stress but less cross-section or load-carrying material in the strain-controlled ‘hot spot’. This is displayed in the figure by the change of the cylinder shape versus an egg shape. Another visualization, usually practiced in structural mechanics, is given by using the Lode-Haigh-Westergaard parameters. This leads to a change in the shape, Fig.15-11 (center). For $f = 0$ the Mises cylinder is obtained.

Fig.15-11(right) depicts the various strength values such as $true\bar{R}^t, \bar{R}_{odc}$ as increasing true strength opoints to be inserted into the Extended Mises function size parameter, finally visualized as flow potential surfaces for four strength-linked porosity levels.

The parameter comparison with ‘Gurson’ let to take a reduced value $q_2 = 1.13$, however, missing test data the author sticks to 1.5. In this context, the respective ExtendedMises parameter C_{12} can be determined, decoupled from the ‘Gurson’ Comparison of Coefficients, if having a reliable test data set available.

The author’s full idea consisted of the two parts: Above ExtMises model plus porosity-improved Bridgman evaluation, which will be depicted in the Table 15-3. The table displays all relations in order to establish the ‘searched’ equivalent stress $\sigma_{eq}^{ExtMises}$.

Reminder from Chapter 11: to capture '120°-rotational symmetry' would require to replace J_2 by $J_2 \cdot \Theta$.

Table 15-3: Replacement of the Mises-based Bridgman curve $\sigma_{eq}(\epsilon_{eq})$ by an ExtMises one

<p>Table 25 - 1: $\sigma_{ax}^t(r) = \sigma_I + \sigma_{hyd}(r)$ and from Bridgman $\sigma_{hyd} \approx \sigma_I \cdot \ln\left(1 + \frac{a^2 - r^2}{2 \cdot a\rho}\right)$</p> <p>$\sigma_{eq}^{MisBri} = \sqrt{3 \cdot J_2} = \sigma_I = \frac{F}{A} / (1 + 2 \cdot \rho / a) \cdot \ln(1 + 0.5 \cdot a / \rho)$, valid $> \bar{R}^t < ?$,</p> <p>$I_1 = \sigma_I + 3\sigma_{hyd} = \sigma_I \cdot (1 + 3 \cdot \ln(1 + 0.5 \cdot a / \rho))$ for the critical central 'fiber' at $r = 0$</p> <p>considering Bridgman (above) and the notch-curvature change by Lorrek-Hill's approach,</p> <p>giving a maximum value for the unknown $\rightarrow \max \frac{a}{\rho} = \sqrt{\ln\left(\frac{1}{1-Z}\right) - \ln\left(\frac{A_0}{A_{oon}}\right)}$,</p> <p>inserting $\sqrt{3 \cdot J_2} = \sigma_I$ and $\frac{F}{A} = true\sigma_{ax}$ the equivalent stress reads:</p> <p>$\sigma_{eq}^{ExtMises} = \sqrt{\frac{3J_2 - f^* \cdot I_1^2}{1 + 2f}} = \sigma_I \sqrt{\frac{1 - f^* \cdot (1 + 3 \cdot \ln(1 + 0.5 \cdot a / \rho))^2}{1 + 2f}}$</p> <p>valid $\bar{R}^t < \bar{R}_{odc}$, (shape parameter) $f \cdot \frac{q_2^2}{4} \equiv f^*$, set $q_2 \cong 1.5 \rightarrow 1.13$.</p> <p>Porosity parameter f and curvature parameter a/ρ increase from about 0 to the maximum at \bar{R}_{odc}.</p>
--

In order to obtain a realistic equivalent stress curve it is physically mandatory to consider the increase of porosity f and the increase of the notch curvature by applying a / ρ .

15.3 Visualization of the Bridgman–corrected true curve with consideration of porosity

Mapping of the changing notch curvature: Data and determination procedure by Mathcad

$$\frac{a}{\rho} = \sqrt{\ln\left(\frac{A_0}{A_{rupt}}\right) - \ln\left(\frac{A_0}{A_{oon}}\right)} = 1.096 \text{ from } \frac{A_{rupt}}{A_0} = 1 - Z = 1 - 0.20 = 0.80,$$

$$\frac{A_0}{A_{rupt}} = \frac{1}{0.80} = 1.25, \quad \frac{A_0}{A_{oon}} = \left(\frac{4.0}{3.89}\right)^2 = 1.057 \rightarrow \max \frac{a}{\rho} = 0.409 \text{ at } R_{rup}.$$

Applying Lorrek-Hill's value Bridgman's approach delivers $\max\left(1 + \frac{2\rho}{a}\right) \cdot \ln\left(1 + \frac{a}{2\rho}\right) = 1.096$.

Then, for the previously proposed formulation the curve parameters can be computed:

$$\text{stressing} \quad \frac{a}{\rho} = a\rho = c_1 + c_2 + \text{true}\varepsilon_{ax} R_{odc}^2 + c_3 \cdot \text{true}\varepsilon_{ax} R_{odc}^3.$$

Vorgabe $ap = 1.096 \quad \text{true}\varepsilon_{ax} R_{02} = 0.0071 \quad \text{true}\varepsilon_{ax} R_t = 0.055 \quad \text{true}\varepsilon_{ax} R_{odc} = 0.231$

$c_1 := 1 \quad c_2 := 100 \quad c_3 := 1$

$$1 = c_1 + c_2 \cdot \text{true}\varepsilon_{ax} R_{02}^2 + c_3 \cdot \text{true}\varepsilon_{ax} R_{02}^3 \quad 1.00005 = c_1 + c_2 \cdot \text{true}\varepsilon_{ax} R_t^2 + c_3 \cdot \text{true}\varepsilon_{ax} R_t^3$$

$$ap = c_1 + c_2 \cdot \text{true}\varepsilon_{ax} R_{odc}^2 + c_3 \cdot \text{true}\varepsilon_{ax} R_{odc}^3$$

$Ap := \text{Suchen}(c_1, c_2, c_3)$

$$Ap = \begin{pmatrix} 1 \\ -0.548 \\ 10.148 \end{pmatrix} \quad \text{true}\varepsilon_{ax} R_{02} := Ap_0 \quad c_1 = 1 \quad \text{true}\varepsilon_{ax} R_t := Ap_1 \quad c_2 = -0.5476 \quad \text{true}\varepsilon_{ax} R_{odc} := Ap_2 \quad c_3 = 10.1478$$

$$Ap_j := c_1 + c_2 \cdot (\text{true}\varepsilon_{ax})^2 + c_3 \cdot (\text{true}\varepsilon_{ax})^3$$

Mapping of the changing porosity f : Data set used and determination by Mathcad

The set points of the curve are the porosity values at the tensile strength point R^t and at R_{odc} .

Vorgabe $e_1 := 0 \quad e_2 := 1$

$$0.0002 = \left(e_1 \cdot \exp\left(\frac{\text{true}\varepsilon_{ax} R_t}{\text{true}\varepsilon_{ax} R_{odc}} - 1\right) - 1 \right)^{e_2} \quad f_{odc} = (e_1 \cdot \exp(1 - 1))^{e_2}$$

$Af := \text{Suchen}(e_1, e_2)$

$$Af = \begin{pmatrix} 0.6292 \\ 6.9469 \end{pmatrix} \quad e_1 := Af_0 \quad e_1 = 0.6292 \quad e_2 := Af_1 \quad e_2 = 6.947$$

$$f_{exp_j} := \left(e_1 \cdot \exp\left(\frac{\text{true}\varepsilon_{ax_j}}{\text{true}\varepsilon_{ax} R_{odc}} - 1\right) - 1 \right)^{e_2}$$

Fig.15-12 displays the author's design verification idea (about 2000). The influence of the porosity practically starts at R_{odc} .

15.4 Specific Potential Surfaces being Strength Failure Criteria

Brittle 'porous' materials may still fracture in the elastic-plastic transition domain. For this fact, Ismar and Mahrenholtz [Ism82] developed a Beltrami-based SFC model which describes the failure behavior of a material between the proportional limit and the 'onset of yielding'.

In *Table 15-4* the SFC-formulations in all regimes shall be comparatively displayed. This includes potential surface descriptions and associate strength failure criteria SFCs.

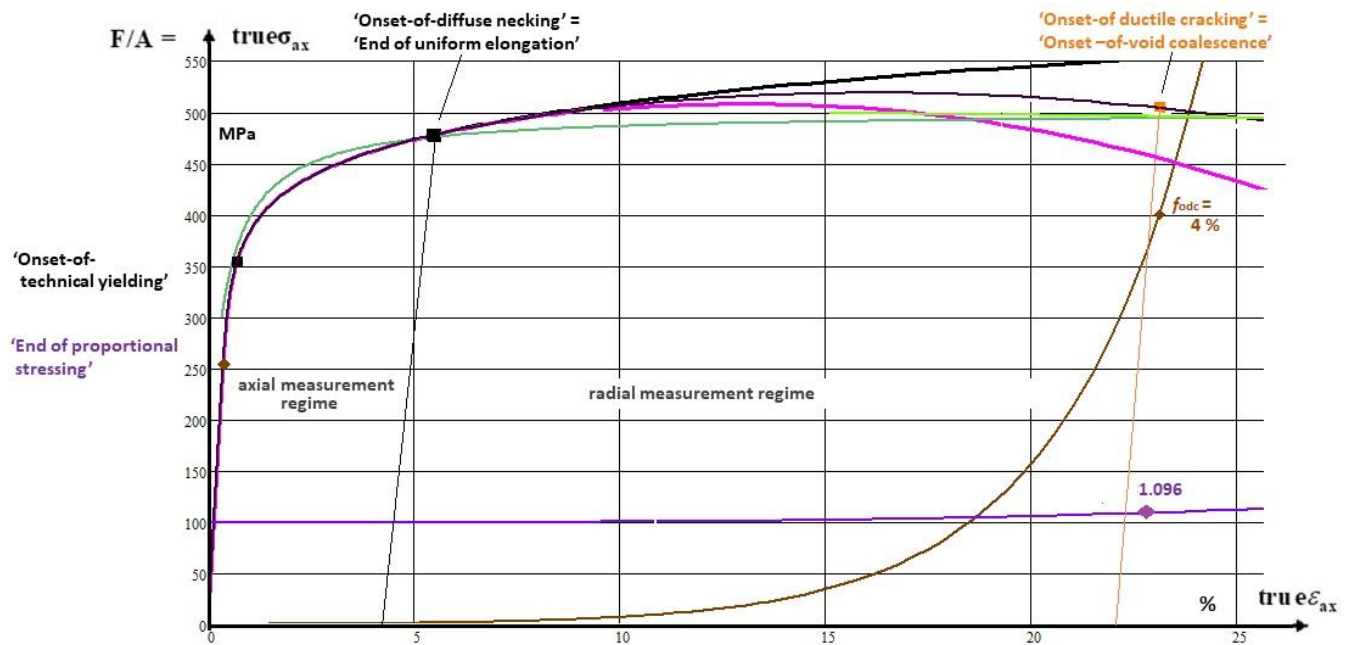


Fig. 15-12, AA2219, base material T2, 6 mm thick: Visualization of the *equivalent stress curve* $\sigma_{eq}^{ExtMises}$;
Ramberg-Osgood-mapped measured cross-section smeared axial stress F/A ;
Increase of plastic porosity f with $f_{odc} = 4\%$ at R_{odc} ;
Increase of the notch curvature a / ρ with $a / \rho = 0.409$ at R_{ult} (replacing the higher R_{odc}) ;
Increase of ν in the elastic-plastic transition domain approaching 0.5 and barely visible the decrease in the porous domain

LL:

- ✓ Whereas with the elasticity formulation of Beltrami the Poisson ratio ν is growing this is opposite with the formulation of a porosity-linked plastic model due to the increasing porosity
 - ✓ The hypotheses of Beltrami, Mises, Gurson describe an increase or decrease of surfaces of constant potential. The shape of the surface theoretically begins with $\nu = 0$ (sphere with foams) growing up from $0 < \nu$ to $\nu = 0.5$ via the growing Mises cylinder keeping $\nu = 0.5$ and ending with an ellipsoid, which shrinks into a spherical direction represented by $0.5 > \nu$.
 - ✓ For two domain limits a clear value for the varying Poisson ratio is given:

$$\text{proportional limit } \sigma \leq \bar{R}_{prop}^t \Rightarrow \nu = \nu_0 \quad \text{and} \quad \text{yield limit } \sigma = \bar{R}_{p0.2}^t \Rightarrow \nu = 0.5$$
 - ✓ Designing requires to use limit state formulations, termed failure criteria (SFCs). These are fracture failure criteria for brittle materials namely for 'Onset-of-fracture' and yield failure criteria for ductile materials. In practice, for ductile materials these failures are 'Onset-of-yielding' and - for the author - 'Onset-of-void coagulation = Onset of ductile Cracking' in the case where strain-softening applies
 - ✓ A Strength Failure Criterion represents a defined Design Limit State and is therefore a special critical Potential Surface F .
- **The novel Extended Mises model just requires the determination of one more parameter, the porosity value f . All model parameters are measurable quantities.**
- **With the novel porosity-capturing σ - ϵ curve, being a ductile porosity-improved Bridgman correction, a simplified plastic analysis procedure could be achieved.**
- **For engineering reasons $true \bar{R}^t \Rightarrow \bar{R}_{odc}$ will represent the load carrying capacity to be considered.**

Table 15-4, Isotropic materials: Determination of model parameters, single mode view.

* Modelling Functions F describing a subsequent potential surface		
elastic-plastic Beltrami	plastic Hencky-'Mises'-Huber	plastic porous 'Gurson' type
$\bar{R}_{prop}^t < \sigma_{Bel} < \bar{R}_{0.2}^t$	$\bar{R}_{0.2}^t < \sigma_{Mis} < \bar{R}_m^t$	$\bar{R}_m^t < \sigma_{eq} < \bar{R}_{odc}^t$
\leftrightarrow		\leftrightarrow
<i>stress - controlled</i>		<i>strain - controlled</i>
σ := running variable of the subsequent potential surfaces		
$\bar{R}_{prop}^t / \bar{R}_{0.2}^t < c^{Bel} < 1$	\leftrightarrow	$1 < c^{Mis} < \bar{R}_m^t / \bar{R}_{0.2}^t$
ellipsoid	\rightarrow cylinder	\rightarrow ellipsoid
$I_1 = (\sigma_I + \sigma_{II} + \sigma_{III}) = f(\sigma)$, $6J_2 = (\sigma_I - \sigma_{II})^2 + (\sigma_{II} - \sigma_{III})^2 + (\sigma_{III} - \sigma_I)^2 = f(\tau)$		
$\frac{3J_2}{\bar{R}_{0.2}^t} + \kappa \cdot \frac{I_1^2}{\bar{R}_{0.2}^t} = c^{Bel} \leftrightarrow F^{Mis} = \frac{3J_2}{\bar{R}_{0.2}^t} = c^{Mis}$, $\kappa = \frac{1-2\nu}{2+2\nu}$		
Insertion of a (measurable) normalizing strength, yield strength point with $\nu = 0.5 \rightarrow \kappa = 0$		
$F^{Bel} = \frac{3\bar{R}_{0.2}^t / 3}{\bar{R}_{0.2}^t} + \kappa \cdot \frac{\bar{R}_{0.2}^t}{\bar{R}_{0.2}^t} = c^{Bel*} \rightarrow c^{Bel} = 1 + \kappa = 1$, and κ an elliptic shape parameter		
.....		
* Strength FailureCriteria (SFC), $\bar{R} \rightarrow R$, (with $\Theta = 1$ for full rotational symmetry)		
R := strength design allowable, marking a special potential surface \equiv design limit state		
elastic, very brittle	ductile	very ductile
$Eff = \frac{\sigma_1}{\bar{R}_m^t} = 1$ *	\leftrightarrow	$Eff = \frac{3J_2}{\bar{R}_m^t} = 1 \leftrightarrow Eff = \frac{3J_2}{\bar{R}_{odc}^t} + c_{12} \cdot \frac{I_1^2}{\bar{R}_{odc}^t} - 2f_{odc} = 100\%$

For similarity reasons: for the 2 modes Normal Fracture NF , Shear Fracture SF (brittle)		
and after inserting $\sigma = R \cdot Eff$ and dissolving for Eff follows		
$I_1 > 0$: $F^{NF} = 0.5 \cdot \frac{\sqrt{4J_2 - I_1^2 / 3} + I_1}{2 \cdot \bar{R}^t} = 1$; $Eff^{NF} = 0.5 \cdot \frac{\sqrt{4J_2 - I_1^2 / 3} + I_1}{2 \cdot \bar{R}^t}$		
$I_1 < 0$: $F^{SF} = c_1^{SF} \cdot \frac{3J_2}{\bar{R}^{c^2}} + c_2^{SF} \cdot \frac{I_1}{\bar{R}^c} = 1$; $Eff^{SF} = \frac{c_2^{SF} \cdot I_1 + \sqrt{(c_2^{SF} \cdot I_1)^2 + 12 \cdot c_1^{SF} \cdot 3J_2}}{2 \cdot \bar{R}^c} = \frac{\sigma_{eq}^{SF}}{\bar{R}^c}$		
$c_1^{SF} = 1 + c_2^{SF}$ with direct consideration of the Poisson ratio $c_2^{SF} = (1 + 3 \cdot \mu) / (1 - 3 \cdot \mu)$		
Last unknown to be searched is the elliptic shape linked parameters such as c_1^{SF} by insertion of a bi-axially compressive failure stress or a fracture angle $\mu = \cos(2 \cdot \theta_{fp}^c \cdot \pi / 180)$.		

Notes:

* Regarding fracture failure NF: This failure is better captured by the author's F^{NF} , which allows a 3D-illustration instead of applying the *normal stress hypothesis* with its edges for each principal stress. For the non-linear analysis usually Co-axiality, Prandtl-Reuss equations and an Associated Flow Rule is employed in order to predict strain rate $\dot{\epsilon}_{ij}$ and the Lagrange multiplication (proportionality) factor λ .

16 Note on Continuum (micro-)Damage Mechanics (CDM)

Aim: Primarily checking CDM application whether it is mature for a reliable Static Design Verification.

CDM is applied for ductile and brittle materials. The loading may be static and cyclic, the latter requires fatigue investigation. Regarding stress-strain curves, CDM principally captures the load-controlled hardening part and the deformation-controlled softening part. Softening part examples are the still mentioned embedded UD layer (*Fig.16-1*) and the ductile metal tensile rod described in the last Chapter by a porosity-capturing ‘Gurson’ model. Results of isotropic analyses employing the softening curve branch can be used to better design notches, openings in pressure vessels (fuel tank task in Ariane 5 upper stage) etc.

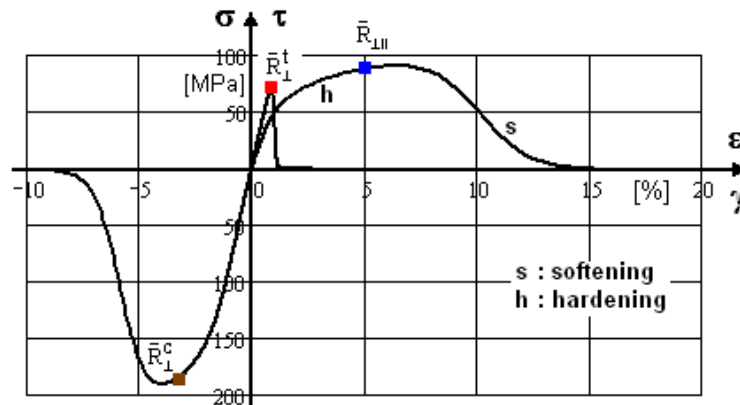


Fig.16-1: Full stress-strain curve with load-controlled hardening and deformation-controlled softening of the layer (ply) embedded in a laminate

CDM is pretty linked to multi-scale modelling, which will be looked at in the next Chapter. All materials are generally composites. Applying CDM one goes down to the constituents of a composite to metallic grains or to fiber and matrix for instance. Moving down on the scales it is helpful to use the physical formulations gained on the macro-scale such as Mises yielding with ductile metals in the tension and compression loading domain and Mohr-coulomb friction behavior of brittle materials in the compression domain. Shear stress loading is composed of a tensile stress with a compressive stress. This activates two failure modes, which leads to normal fracture in the case of brittle materials. These physical effects stay valid at the lower scale and are to consider *adjusted*.

LL: It is always to check, whether a Mises yield criterion can be applied to quantify micro-damage portions or a fracture criterion in the case of very brittle behavior, i.e. Fiber Reinforced Plastics FRP.

16.1 Static Behavior

Micro-damage formulations:

CDM is basically used to capture the evolution of the micro-damage state from micro-damage $D = 0$ up to ‘Onset-of-Failure’ at $maxD$, which is for brittle materials at the end of hardening or at achieving the strength R .

In CDM, the formulation of the describing constitutive equation is based on one of the following two approaches (*Here the stress-strain curve is meant*):

- (1) The strain equivalence principle approach or
- (2) The stress equivalence principle approach. *From engineering side, the latter is preferred because 3D stress states and residual stresses have to be considered in*

design dimensioning. The constitutive relationships are formulated in the effective undamaged configuration $\sigma_{eff} = \sigma / (1 - D)$ with a stress-strain relation linked by the stiffness elasticity matrix $[C]$, which reduces due to growing micro-damage. Fig.16-2 exemplarily depicts the relationship for a 2D-loaded transversely-isotropic UD material.

$$\{\sigma\} = [C] \cdot \{\varepsilon\} \rightarrow \{\varepsilon\} = [S] \cdot \{\sigma\} \quad \text{as practical test-linked formulation}$$

$$S_{eff} = \begin{bmatrix} \frac{1}{E_1 \cdot (1 - D_{11})} & \frac{-\nu_{21}}{E_1} & 0 \\ \frac{-\nu_{12}}{E_2} & \frac{1}{E_2 \cdot (1 - D_{22})} & 0 \\ \text{(symm)} & 0 & \frac{1}{G_{12} \cdot (1 - D_{66})} \end{bmatrix} \quad \text{with } D = \begin{bmatrix} D_{11} & D_{21} & 0 \\ D_{21} & D_{22} & 0 \\ \text{(symm)} & 0 & D_{66} \end{bmatrix}$$

usually not considering the off-diagonal D_{21} .

Fig.16-2, 2D-example UD material: Compliance matrix $[S]$ and micro-damage matrix $[D]$.
By inversion of the effective compliance matrix S_{eff} the decaying stiffness matrix C_{eff} is obtained.

The D_{ij} represent the accumulation of the micro-damage process portions and are theoretically terminated by $\max D$ at the strength point in the case of brittle materials and at the rupture point for very ductile isotropic materials. These portions may occur during a monotonically increasing static loading. For brittle materials micro-damage starts at the 'elastic' limit being a level where Eff has still reached a value, see Fig.16-3. Unfortunately, $\max D$ in static CDM cannot become 100% due to its usual modelling basis. The center figure outlines how a stress-man views the 'Onset of micro-damage' of a slightly brittle material. In the elastic domain $< R_{prop} \equiv R_{E(lastic)}$ there is no D-contribution. The blue 'flow curve' then will contribute.

The right figure (from Abaqus) surprisingly outlines that micro-damage first begins with void nucleation and void coagulation rising the Question: Does really not any micro-damage happens below R^t .

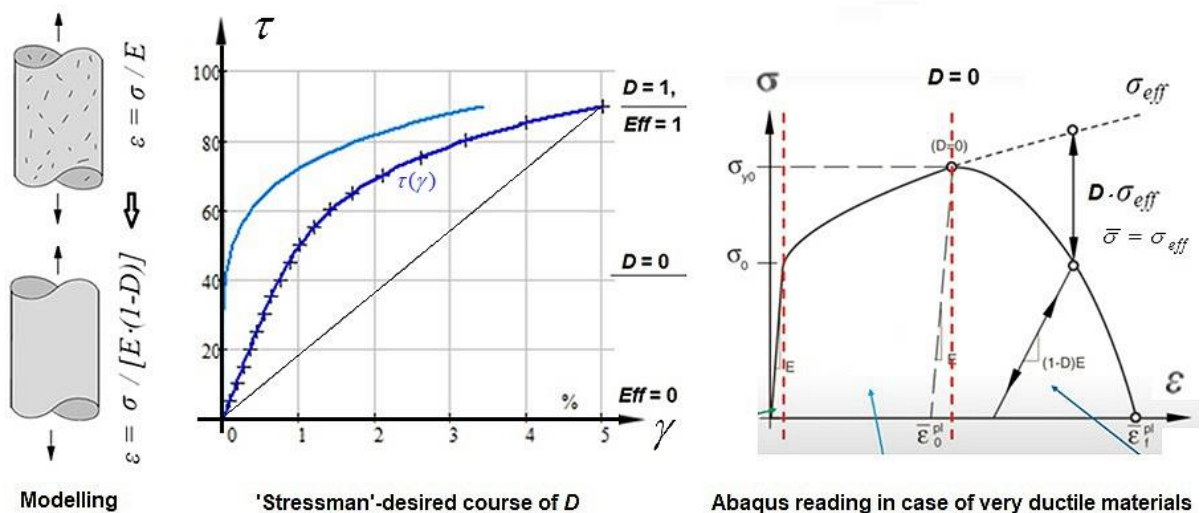


Fig.16-3: The various 'Onset-of-Failure' envelopes: (left) Smearing of the micro-damaged material, (center) shear of a slightly brittle material, (right) Ductile material (Ansys FEA code)

Remind, please: Micro-Damage-free (*in German schädigungsfrei, nicht schadensfrei*) and crack (= macro-damage, *in German Schaden*)-free does not mean free of flaws.

LL:

* CDM is generally always good for understanding static & cyclic material behavior

* Confusing is faced regarding 'Onset of counting micro-damage', in static case once $< R'$ but also $> R'$

Material behavior-determined slip and failure angles:

The number of slip systems in ductile metals is usually high, and those that are active possess an orientation near to the planes with maximum shear stress. Under uniaxial loading the planes of micro-cracks are always inclined approximately 45° to the direction of the applied tensile stress, see (*Fig.16-4*). In single crystals, the lattice structure is spatially oriented in such a way that a sliding plane is obtained at an angle of 45° . In poly-crystalline metals with randomly distributed lattice sub-structures this will change a little.

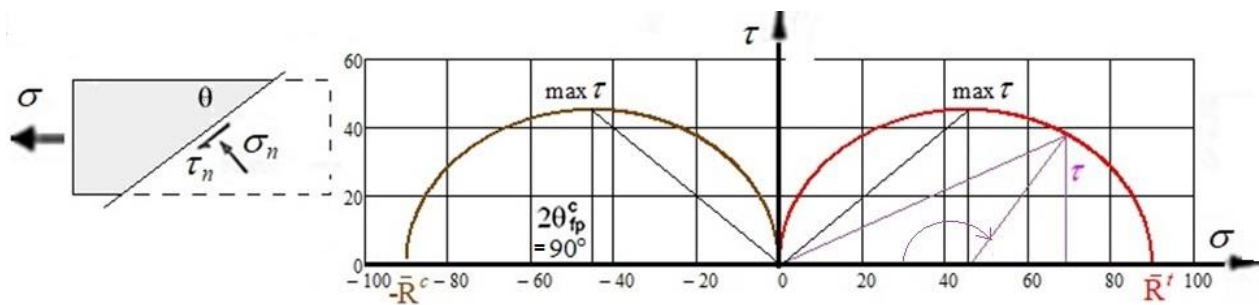


Fig. 16-4, very ductile metal material: Mohr stress circle for a compressive and a tensile uniaxial external stress of a ductile material

$$\tau_n = \sigma \cdot \cos(\alpha) \cdot \sin(\alpha) \text{ with } \alpha \text{ the angle to } \sigma \text{ direction, } 2 \cdot \max \tau = \sigma \text{ for } \alpha = 45^\circ$$

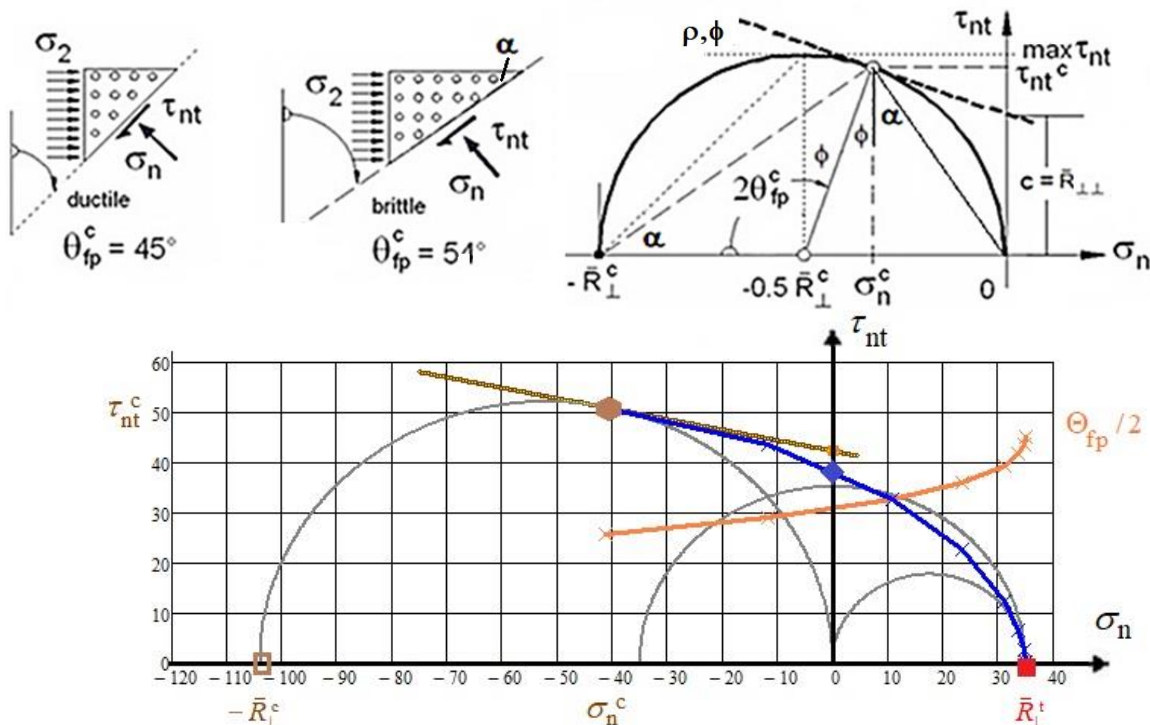


Fig.16-5, brittle UD-material: Joint display of the UD failure curve in Mohr stresses, indicating *angle increase* Θ_{fp}° when approaching \bar{R}_\perp^t . Shear fracture plane angle in the touch point 51° and *linear* Mohr-as well as a more realistic *curved* Coulomb friction curve. Touch point is defined by $(\sigma_n^c, \tau_{nt}^c)$, linked to \bar{R}_\perp^c .

Known from brittle material behavior under compression is: *The failure angle depends on the friction value μ* . After the formula, derived in [Cun23c], the computation of the failure angle with the Mohr-Coulomb model delivers exemplarily for a material friction value $\mu = 0$ (= *fully ductile*) the expected value of 45° and for a friction value $\mu = 0.2$ the angle 51° , see Fig.16-5. The author presents in this figure that the angle changes from the 51° at the compression strength point \bar{R}_\perp^c up to 90° at the tensile strength point \bar{R}_\perp^t .

16.2 Cyclic Behavior of Ductile Metals applying Micro-scale Material Modelling

Once micro-cracks have nucleated due to strain accumulation from cyclic slip, they grow in the early stage typically in the order of the material's grain size (text from M. Mlikota - S. Schmauder: *Thanks to Siegfried*). In the course of further cyclic loading, micro-cracks - formed along these slip bands - will grow and link together. In metals and alloys they grow predominantly along the crystallographic planes because they are highly affected by microstructural barriers such as grain boundaries or other micro-structural features. The coalescence of trans-granular micro-cracks, namely, if two micro-cracks meet each other at the same grain boundary, is performed in the numerical simulation of the crack initiation after Tanaka-Mura. It occurs if the average stress in between their tips surpasses the elastic limit Re of the material's new micro-crack, created on this grain boundary line, uniting the two trans-granular micro-cracks into a single one (*example pure iron $Re = 260\text{ MPa}$*).

Already nucleated crack segments tend to extend along the whole grain, causing local stress relaxation as well as concentrations at their tips and by that amplifying the likelihood for new crack formation in the vicinity. In the course, micro-cracks form along the slip bands, grow and join. The change of the crack plane from the crystallographic plane to a non-crystallographic plane perpendicular to the external stress axis is called the transition from Stage I (*crystallographic growth*) to Stage II (*non-crystallographic growth*) or transition from the micro-crack initiation to a micro-crack growth stage resulting in a short crack, as depicted in Fig.16-6.

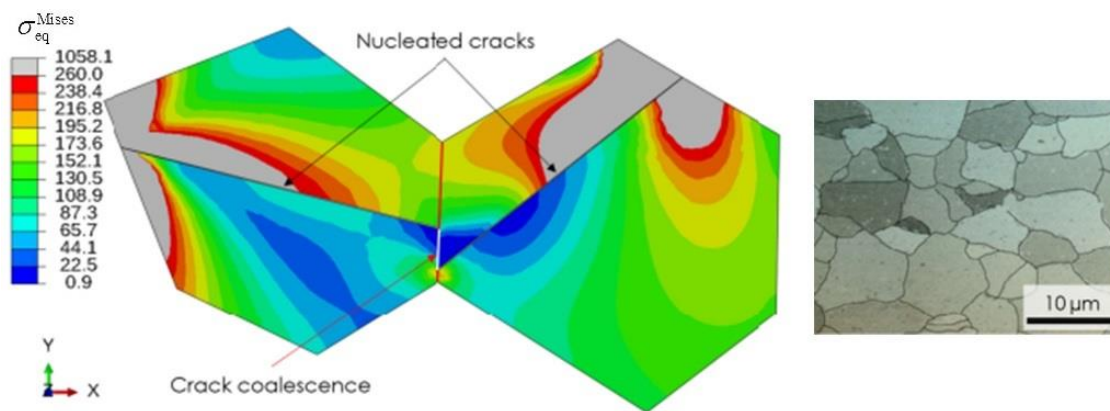


Fig.16-6: Simulation of AA micro-crack coalescence (Lorenzino, P., Navarro, A. & Krupp, U. (2013), 'Naked eye observations of microstructurally short fatigue cracks', *Int. J. of Fatigue* 56(0), 8-16.

However, the dominant short crack does not always continue propagating. Namely, in the case of a lower stress level, the short crack may stop growing. Such a situation is typically known as run-out, which indicates that at very low stress levels an infinite life may be obtained. Run-out below the endurance limit means crack-retardation, Fig.16-7. In the long-crack regime the fatigue crack

growth rate da/dn can be characterized by the stress intensity factor range ΔK as a dominant driving parameter.

The CDM-driven Region I in the figure below is here of interest, but should be illustrated as part of the full crack failure picture: A typical fatigue crack growth rate curve da/dn (ΔK) for the long crack is illustrated in Fig.16-7, too. If in a double logarithmic scale the long crack propagation rate follows a straight line in region II, in sufficient distance from the threshold ΔK_{th} .

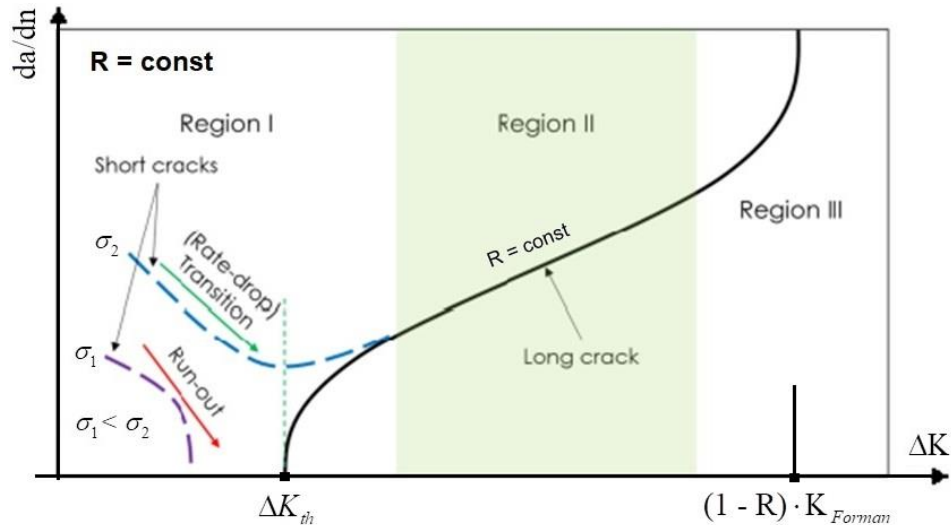


Fig.16-7: Fatigue growth rates of micro-cracks (short) and long cracks in dependence of Δ stress intensity factor. Schematic representation of the loading level- dependent transition from region I into region II. (Newman, J.; Phillips, E. & Swain, M. (1999), 'Fatigue-life prediction methodology using small-crack theory', Int. Journal of Fatigue 21(2), 109-119)

The long crack growth rate domain in Region II can be well described for most engineering alloys by the so-called Paris law:

$$\text{Paris: } da / dn = C_{Paris} \cdot \Delta K^{n_{Paris}} \quad , \quad \text{Forman: } da / dn = \frac{C_{Forman} \cdot \Delta K^{n_{Forman}}}{(1-R) \cdot K_{Forman} - \Delta K} \quad [\text{HSB 63205 - 01}]$$

In the figure and the formulas above da/dn is the crack growth increment per cycle, $\Delta K = \max K - \min K$ is the range of stress intensity factor, and C (intercept with the y-axis) and n (slope) are material curve parameters that are deduced by fitting the course of experimental data. K_{Ic} is the so-called fracture toughness.

LL:

- * There is a hope, that in future for metals a basis will provided, that the estimation of an endurance limit will be possible.
- * A grain is usually polycrystalline with crystal planes in various spatial orientations. Hence, a metallic 'composite' material can be only termed homogeneous and isotropic if these orientations are randomly distributed in order to become quasi-homogeneous. By the way, this is the same for an isotropic short fiber-reinforced polymeric material, otherwise, the so-called orientation tensor has to take care of the non-isotropy.

16.3 Note on Application of Continuum (micro)-Damage Mechanics (CDM) in Static Strength

Note on Stress effort Eff versus micro-damage development D :

For the designer of interest is how the material's stiffness decreases with increasing stress effort or load, respectively. Design allowable R and average strength \bar{R} lead to different stress efforts in

design verification and in modelling of material damaging (50% value = highest expectance probability), see Fig.16-8. The enlarging effect of the design FoS j on the value of Eff , when reaching failure, is considered in the design verification curve (dashed line) depicted below. The more reserve is, indicated by a positive Margin of Safety MoS , the lower Eff is. This has an effect on the actual strain in the non-linear analysis case. It becomes smaller and the strain is less plastic, which is of interest for the validity limit of an elastic analysis.

In the case of 3D modal SFCs (FMC for instance) the common microdamage-caused degradation is considered by an interaction equation that reflects the micro-damage influence of all acting stress states and associated modes. The single mode efforts are interact via the interaction exponent m experience-based being about $m = 2.6$.

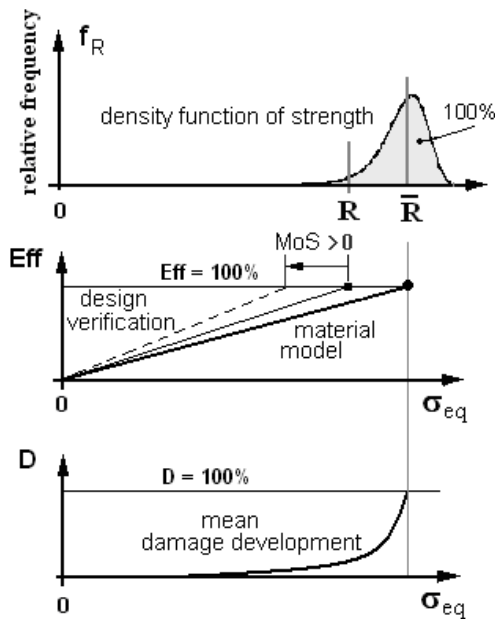


Fig.16-8:
Visualization of the development of stress effort, strength value, equivalent strength, and
Micro-damage understanding of a 'stressman'.

$$MoS = RF - 1$$

'Stressman's' Assessment of CDM applications:

During his engineering life CDM was often propagated to make in future a Design Verification possible. In literature, i.e. [Jai20], Continuum (micro-)Damage Mechanics (CDM) models are also used to determine a RF . However, this intention faces some obstacles.

Analogous to the standard procedure then statistically-based micro-damage model parameters are required and a total maximum value D is to define according to $D < D_{admissible} < 100\%$ at failure and this must be statistically based. Defining such a D -value is a challenge for the application of (micro-)Damage Models in the DV for serial production certification. This challenge is novel and higher than providing the classical strength design allowables R necessary for computing Eff .

Further, in known standard procedures Eff runs $0 < Eff < 100\%$, whereas D begins at a distinct Eff -value but should principally also end at 100%, see [CUN22, §15.3]. Here, a very essential question comes up: "How does the designer assess a stress level that is below the 'Onset-of-micro-damage'?" In this context another question arises: "How are to consider low stresses in Low Cycle Fatigue?"

Stiffness decay CDM model parameters are difficult to apply.

The provision of a CDM-failure body would be mandatory for obtaining DV. Hence, up to now CDM seems not to meet the authority-demanded DV-requirements regarding the statistically

reduced design strength R and regarding the relationship $\sigma \sim R \cdot Eff$, which is valid in the linear elastic and in the non-linear regime.

LL:

- * The 'stress-man' will not understand that at maximum load, which is at the strength point, the sum of micro-damage does not approach 100%.
- * The author could not sort out a consistent procedure that might be used in design verification. A clear derivation of the maximum micro-damage values seems to be missing.
- * How is the interaction of the damage portions in 3D-CDM solved?
- * Stiffness decay CDM model parameters are difficult to apply
- * Looking at 'well analyzing', which requires well-mapping of the stress-strain behavior in the hardening domain, one should always remember the scatter of the measured curves.

Engineer's question, regarding above:

Is it possible to provide the engineer with similar information when using micro-damage quantities D_i ?

Note:

Fig.16.-9 left shows the scatter and distributions of some strength and strain quantities. *Fig.16.-9 right up* demonstrates that a compression test can – due to barreling - just give a value for the yield strength $R_{0.2}^c$. This requires the determination of the increased hoop diameter, when aiming at realistic $R_{0.2}$ - and E-values for tensile and compression. The figure also informs that for a static test specimen of a product the directions are marked by the subscripts L, LT and ST and that these are used for the description of sheet-type test specimens. These specimens are machined in the rolling direction (letter L), transversal direction (T) and thickness direction (S). In the case of thick structural parts smooth tension bar test specimens are cut out, in the case of thin plates flat test specimens are investigated, which better represent 2D-structural shapes. (Above convention mentally leads over from the not fully isotropic materials to the transversely-isotropic ones). This is similarly performed for the radial and axial direction of a cylindrical test specimen.

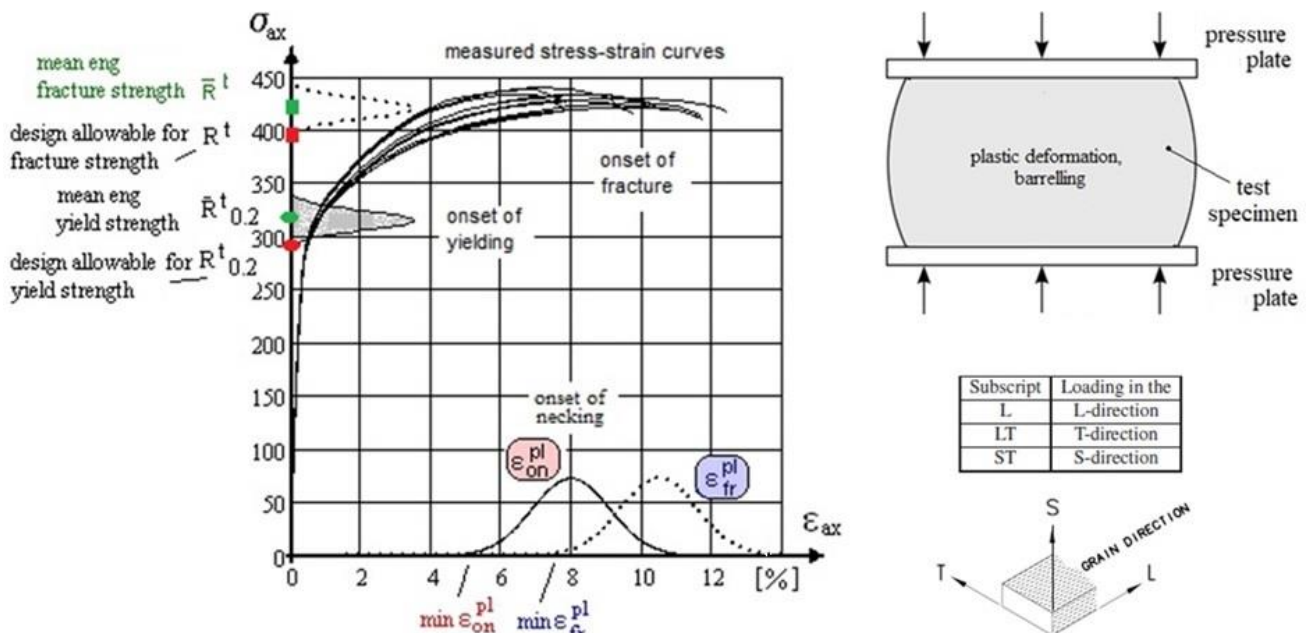


Fig.16-9: AA2219 engineering quantities and curves, deformation of a compressed ductile test specimen. (right down) Marking of sheet-type test specimens

Eventually *Fig.16.10* shall show the shape of the tensile rod test specimen and a picture of the porous fracture surface of the ductile material.

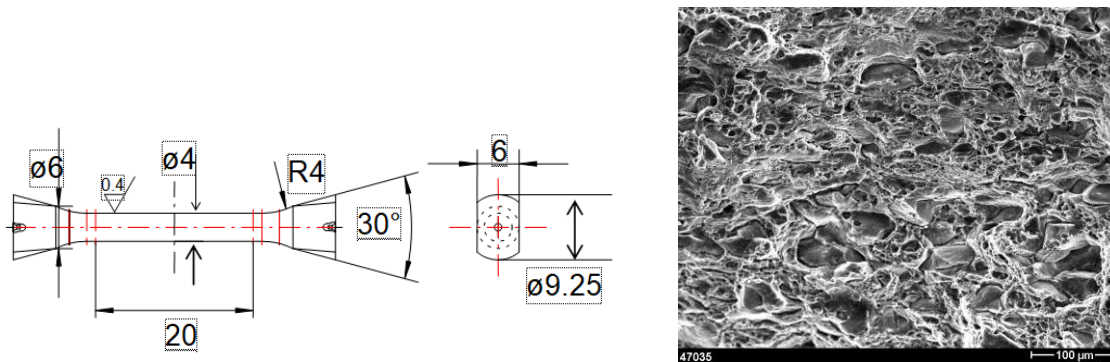


Fig.16-10: (left) Geometry of the tensile rod; (right) Voids on the fracture surface [IWM]

LL:

- * Before executing any analysis with a distinct code the designer has to check whether the actual stress-strain curve fits to the shape of the implemented curve
- * For the best possible estimation of the component behavior, the average stress-strain curve $\bar{\sigma}\bar{\epsilon}$ must be taken
- * The average stress-strain curve $\bar{\sigma}\bar{\epsilon}$ does not inescapably run through the means of yield $(\bar{\sigma} - \bar{\epsilon})_{\text{yield}}$ and of fracture $(\bar{\sigma} - \bar{\epsilon})_{\text{fr}}$.

17 Multi-scale Structural modelling with Material Modelling and its Analyzing

Aim: Making aware of limits applying validated macro-scale formulations at lower scales.

17.1 Structural Analyses over the Scales

Structural modelling with associate analyses is performed at many scales, see *Fig.17-1*, from the macro-scale up to the Burj Khalifa building size.

Thereby, the challenging task is the input of the right material properties: Which values are to insert when analyzing at the lower scale? What about the stress-strain curve, which for instance for the anisotropic UD material remains always bound to the macro-scale?

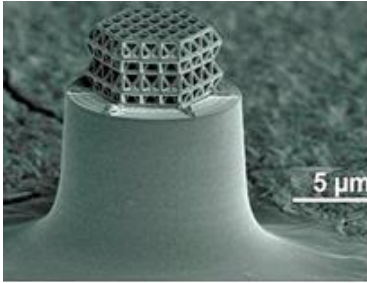


Fig.17-1: Size variety of structures.

(left) Truss structure, created by J. Bauer and O. Kraft with laser lithography. Glass-like carbon nano-framework $R^c = 3000$ MPa. Advanced Materials, Progress Report, 'Nanolattices: An Emerging Class of Mechanical Metamaterials'. Jens Bauer, Lucas R. Meza, Tobias A. Schaedler, Ruth Schwaiger, Xiaoyu Zheng, Lorenzo Valdevit. 2017, Wiley Online Library



Burj Khalifa, 828 m

All this requires investigating the applicability of the usual macro-scale formulations especially concerning strength and fracture mechanics. For the assessment of a stress state, when viewing Design Verification (DV), it is to know the 'Onset-of-micro-damage' and the later following 'Onset-of-micro-cracking'.

Multi-scale modelling is executed for static and cyclic problems. In the cyclic case, there are three key 'points' that separate the regions in *Fig.17-2*:

- Ultimate strength R_m^t : Stress level required to fail with one cycle, $n = 1$
- Onset of Yield, R_e : Stress value at onset of plastic behavior with being $R_e < R_{0.2}$
- Endurance limit $S_{e(\text{ndurance})}$: Stress corresponding to the horizontal asymptote of the SN-curve.

The course of the cyclic failure test data, termed SN-curve, is again mapped by the 4-parameter Weibull formula $R = \text{constant} : \sigma_{\max}(R, N) = c_1 + (c_2 - c_1) / \exp(\log N / c_3)^{c_4}$.

As the average SN-curve cannot be applied in fatigue life DV, a statistically reduced curve is to determine as design curve. This design curve defines a full $D_{\text{design}} = 100\%$ -SN-curve from the tensile strength as original point and ending in the running-out defining an endurance limit stress.

LL:

* DV demands for a statistically reduced SN-curve

* It is always necessary to check whether the material at the lower level behaves in such a way that physically-based macro-mechanical formulations can be used.

* The material data input should satisfy physical model demands, which includes measurable parameters.

17-2 SN-curve with Relationship Material Stressing Effort $Eff \leftrightarrow$ Micro-damage D

There are practically two possibilities to present SN curves:

- (1) Ductile: Applying the stress amplitude $\sigma_a(R, N)$, also termed alternating stress

(2) Brittle: Applying the upper stress $\sigma_{max}(R,N)$

The maximum stress is physically simpler to understand by the ‘stress-man’ than the amplitude, according to smooth transfer from the static to the cyclic behavior, *Fig.17-2*. Namely, a decaying SN curve is interpretable like a decaying ‘static’ strength after a micro-damage process with n cycles.

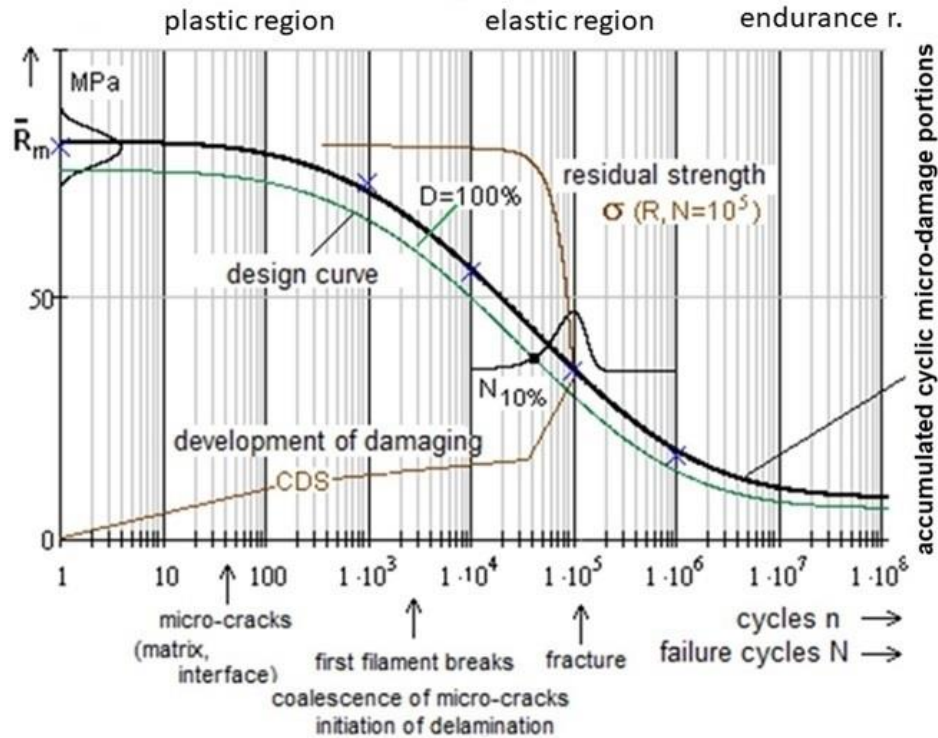


Fig.17-2, Design Verification: Fatigue average curve and design curve $R = 0.1$. $D = D_{design}$ for a survival probability P with a confidence level C . CDS is ‘characteristic damage state’ of a lamina

[Hiatt, J. (2016), ‘What is a SN-Curve?’, Technical report, Siemens PLM Community). $N_f = N_{initial} + N_{crackgrowth}$. Run-out below the endurance limit means crack-retardation]

Thereby, the static material stressing effort Eff (Werkstoffanstrengung, $N_f = 1$) is replaced by the accumulated cyclic micro-damage sum $D(N)$. Applied here is the classical 4-parameter Weibull curve with one parameter still fixed as strength point origin, because for brittle materials the strength value $\bar{R}^t = \sigma_{max}$ ($n = N = 1$) is preferably used as origin in the tension domain and anchor point of the SN curve and in the compression domain $-\bar{R}^c = \sigma_{min}$ ($n = N = 1$). In detail, *Fig.17-3* visualizes the transfer from the static load-driven increase of the material stressing effort ($n = N = 1$) $Eff = 100\%$ (expectance value 50%) at the strength point to the cycle-driven micro-damage sum $D_{mapping} = 100\%$ (expectance value 50%) of the SN curve. The evolution of Eff is not linked to the accumulation of the micro-damage. At onset-of-micro-cracking Eff is still > 0 .

If static failure $\rightarrow \max \sigma = \bar{R}_{static}$ at $Eff = 1$ and if cyclic failure $\max \sigma = \bar{R}_{cyclic}$, at $D = 1$.

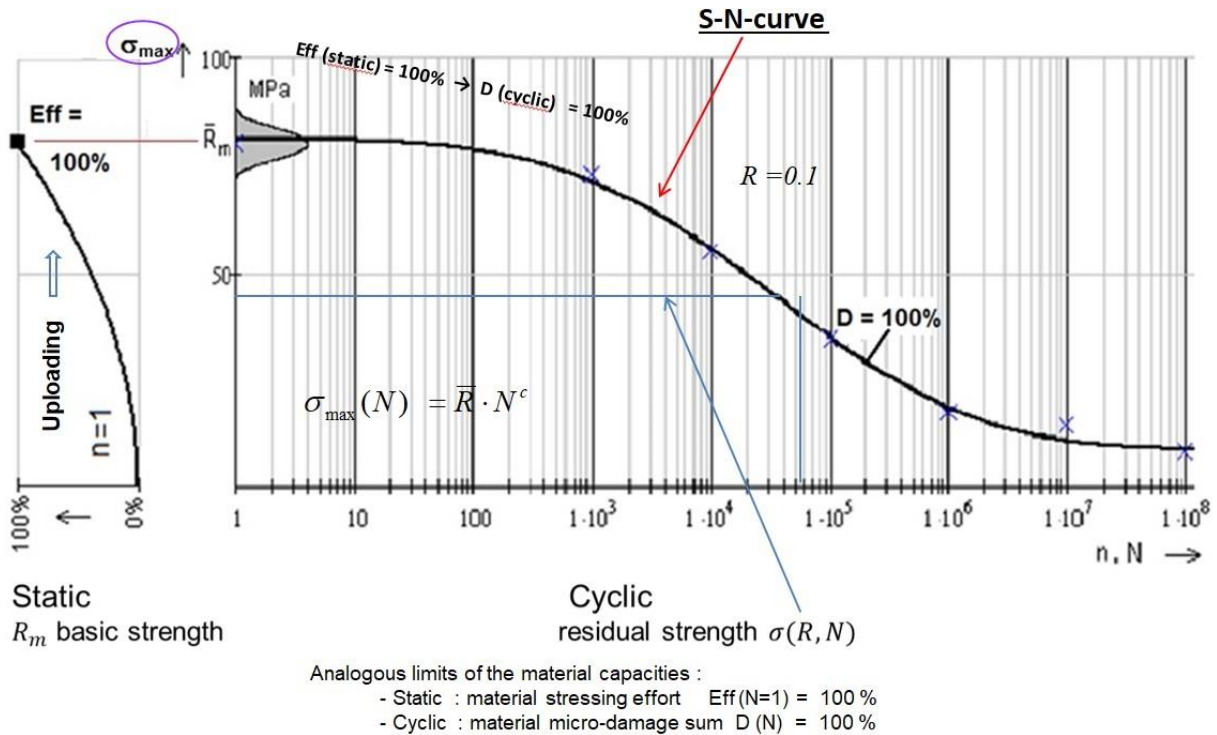


Fig.17-3, Mapping: Eff versus D. Mapping deals with averages \equiv 50% expectance value

17.3 Multi-scale Material Modelling regarding Infinite Life (endurance limit) of Metals

Infinite life or, in other words, the endurance limit is an ever-lasting topic of highest interest in structural design and concerns all materials.

Nowadays, valuable investigations on the micro-mechanics level seem to bring a significant progress for isotropic metals by using CDM.

Mlikota and Schmauder found that the so-called critical resolved shear stress CRSS is the relevant fatigue-responsible quantity, (Fig.17-4), regarding the behavior of ductile metals in the micro-scale regime. Multi-scale Material modelling (MMM), based on enough computer power will probably allow in future 'Computational material mechanics' from < micro-scale models (Molecular Dynamics-treated and test results-supported from statically and cyclically loaded 10 μm thick pillars for instance) via micro-scale to bridge with the necessary properties (hopefully statistically based) to the classical macro-scale models in structural design.

Multiscale materials modelling (MMM) could grow and become a significant tool for understanding complex material micro-damage processes for many homogeneous isotropic materials

The conclusions of Mlikota are:

- The CRSS is the resistance for the dislocations to move through the crystal. It is governed by the present strengthening mechanisms in the crystal. The CRSS is - according to critical stress strength - a micro-shear strength.
- The fatigue crack growth modeling procedure in the High Cycle Fatigue regime should include the following steps: Micro-crack nucleation within a grain \rightarrow Coalescence of already existing flaws and/or arrest at grain boundaries \rightarrow Short crack or Stage I growth \rightarrow Transition from Stage I to Long crack or Stage II growth

- The discovered relation between endurance limit and the CRSS allows the virtual selection of those types of materials, which are more fatigue resistant! The physically-based MMM approach represents a breakthrough in the field of fatigue research
- The higher the CRSS magnitude of the metal of interest, the higher the loading stress level σ will be necessary to accomplish the transition from infinite to finite life
- The multiscale fatigue simulation approach is capable of properly taking into account the mean stress $\sigma_m = \max \sigma \cdot (1+R) / 2$ with the stress ratio $R = \min \sigma / \max \sigma$ and capturing the stress concentration factor K_b , which are influencing factors when designing structural components.
- Experimental tests demonstrate, that there is a drop in resistance to fatigue fracture with the increase of the grain size.

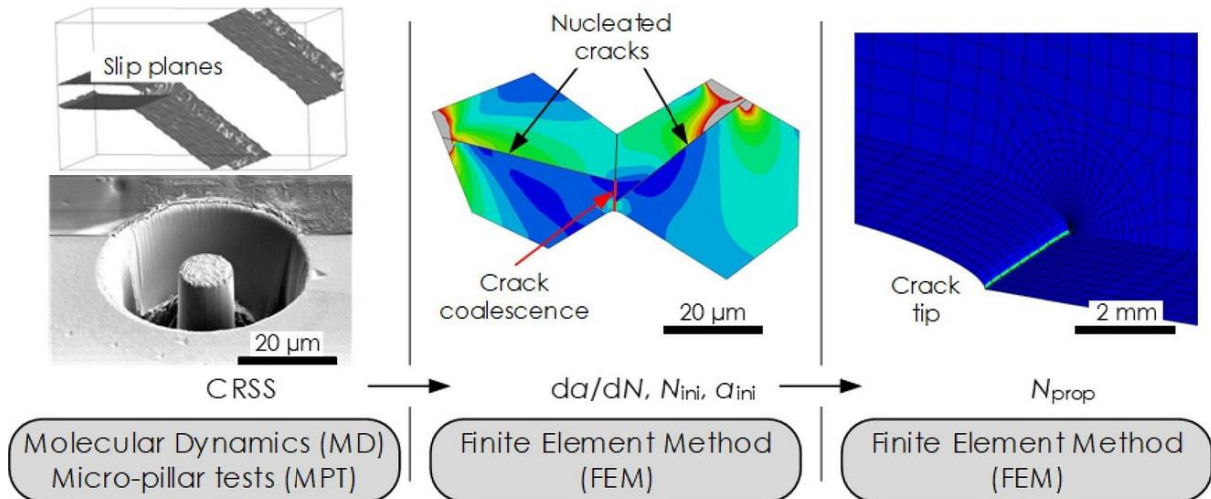


Fig.17-4: Full modelling approach. CRSS critical resolved shear stress, da/dn crack growth rate, N_{in} number of stress cycles until *short-crack* initiation, a_{ini} initiation short-crack length, N_{pro} number of stress cycles until short-crack propagation.

[Mlikota M. & Schmauder S. (2018), 'On the critical resolved shear stress and its importance in the fatigue performance of steels and other metals with different crystallographic structures', Metals 8(11), 883]

LL:

- * *There is a hope for some ductile materials in future to estimate the endurance limits of various metallic materials in the Ultra HCF regime just by knowing their CRSS values ! Available CDM models seem to be neither to be clear-defined nor classified to be used for Design Verification (DV). A DV-procedure is searched*
- * *A grain is usually polycrystalline with crystal planes in various spatial orientations. Hence, a metallic material can be only termed homogeneous and isotropic if these orientations are randomly distributed in order to become quasi-homogeneous. (By the way, this is the same for an isotropic short fiber-reinforced polymeric material. Otherwise, the so-called orientation tensor has to take care of the non-isotropy).*
- * *For the analysis the Mises SFC was employed in order to localize the peaks of shear banding of the investigated steel material*

$$\sigma_{eq}^{Mises} = \sqrt{3 \cdot J_2} \quad \text{with} \quad 6J_2 = (\sigma_I - \sigma_{II})^2 + (\sigma_{II} - \sigma_{III})^2 + (\sigma_{III} - \sigma_I)^2 = f(\tau), \tau_{oct} = \sqrt{J_2 / 3}$$
- * *Clearly to be defined is the quantification of the D-portions for ductile and brittle behavior with a maximum value of total D = 100%:*
 - *static case: the achieved micro-damage value at a distinct (equivalent) stress level*
 - *cyclic case: the cycle-associated micro-damage portions with its derivation formula.*

17.3 Multi-scale Material Modelling and ‘Meso’–Modelling of the Example UD material

Fig.17-5 gives a look at the present multi-scale modelling performed with Fiber-Reinforced-Polymers (FRP). Two scales are linked together, the micro-scale with the macro-scale by a meso-model. What is meso? Meso is no scale, per definitionem!

- * Micro-scale > μm , macro-scale > mm .
- * The author experienced in a BMFT R&D discussion (1999) round on three MaTech Competence centers of institutes working from polymer-scale to the structural macro-scale - after one day - that the term meso-scale is used in polymer mechanics by the research colleagues at the nano-level which is a level of one thousand smaller than the solid mechanics people use it.
- * A further classification is available for porous materials, according to pore size: ‘microporous’ pores < 2 nm, ‘mesoporous’ pores between 2 nm and 50 nm, ‘macro-porous’ pores > 50 nm. [*International Union of Pure and Applied Chemistry*].

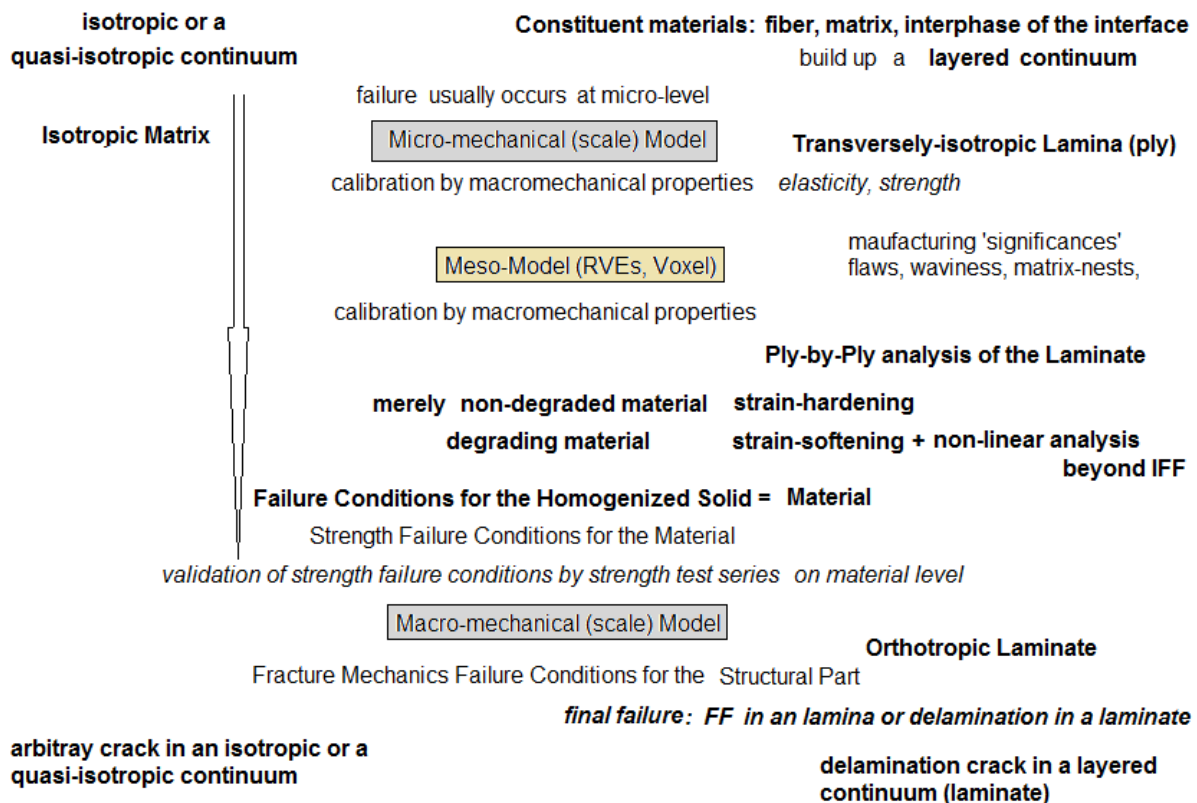


Fig.17-5: Multi-scale modelling, example FRP, brittle, 2 scales. RVE: Representative Volume Element, Voxel: volumetric pixel

LL: The term meso is a task-linked chosen size level. Apply the term meso-model, not meso-scale, and define it. In structural engineering meso is used at about 0.1 mm.

17.5 Note on Micro-mechanical Formulas (mixture rules) for Example UD lamina (ply)

Aim: Guideline how to use micro-mechanical models and properties, giving some warning.

Mixture rules are employed in many technical disciplines. Exemplarily, here just at the so-called micro-mechanical formulas of UD-materials will be looked at.

Creep investigations and pressure-related effects on the matrix and in consequence on the UD material of composite materials i.e. usually require a micro-mechanical input. For an example the non-creeping constituent fiber is to separate from the creeping/relaxing constituent matrix. In order to capture these features the use of ‘micro-mechanical mixture rules’ in structural engineering is common practice. It requires properties of the constituents and the so-called mixture rule, how these constituent properties are linked, to be able to predict properties of the envisaged (‘smeared’) material on the macro-scale.

Not all micro-mechanical properties applied can be measured. A solution will be obtained by setting up above mixture rules and calibrate them via macro-mechanical test results on the lamina macro-level. This makes an inverse parameter-identification necessary.

Hence, the application of a micro-mechanical formula underlies the constraint that the given micro-mechanical properties can be only used together with the formulas they are based on. Otherwise the results might be pretty wrong. For example within the WWFE, Test Case 1, the organizer QinetiQ just provided micro-mechanical material properties but not the associated micro-mechanical formula. Therefore, the author had to apply micro-mechanical UD formulas from [VDI 2014, sheet 3] and found a discrepancy of a factor 2 for the data to be predicted! This is not acceptable for the WWFE-task model validation.

LL: Micro-mechanical properties can be used only together with the formulas they have been determined with! ⇐ Warning

18 Some Lessons Learned from Testing and from Evaluation of Test Results

Aim: Forwarding lessons learned.

In structural design one basically faces 3 types of testing:

- Structural Testing (destructive, non-destructive)
 - Materials Testing (destructive, non-destructive) and
 - Non-Destructive Testing of structure and material (NDT, NDI, NDE).
- Other tasks here are: Failure detection, localization, size + shape, Failure assessment (risk-based).

All structural tests to be performed aim to uncover a deficiency: Workmanship, design mistake, oversight of a failure mode, tightness, shock resistance etc.

Fig.18-1 presents the test strategy of the MIL handbook 17, a forerunner guideline for the development of composite structures which are more challenging than developing isotropic structures.

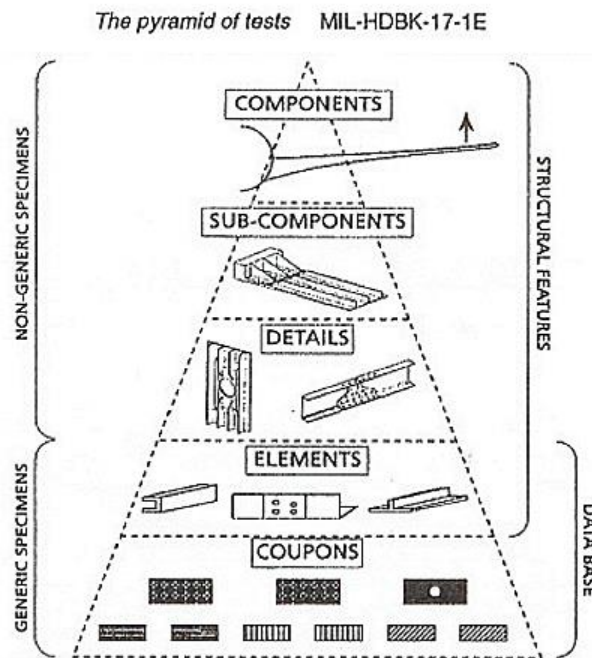


Fig18-1: Test strategy of MIL-HDBK 17 (original edition about 1970). MIL-HDBK-17/1F (VOL. 1 OF 5), DEPARTMENT OF DEFENSE HANDBOOK: COMPOSITE MATERIALS HANDBOOK - POLYMER MATRIX COMPOSITES GUIDELINES FOR CHARACTERIZATION

In this Chapter some personal experience is depicted, beginning with structural testing.

18.1 Structural Testing primarily based on the Ariane launcher development

At first, a Test Agreement is to provide. It consists of test rig, test specification, test specimen and test data evaluation method and the Test Procedure. Therefore, one can only speak about 'exact test results in the frame of the obtained test quality'.

Fig.18-2 presents the so-called sub-structuring (affecting shares between the participating partners) an example for violated mechanics. MAN was not permitted to include the neighboring structural part despite of the fact that it was also a MAN contract part. We could not implement the FE model of this neighboring part in order to optimally represent the real boundary stiffness

conditions in the model of the ‘studied structural part’. This caused a wrong behavior of the ‘studied structure’ and was a real mess regarding the evaluation of the test results.

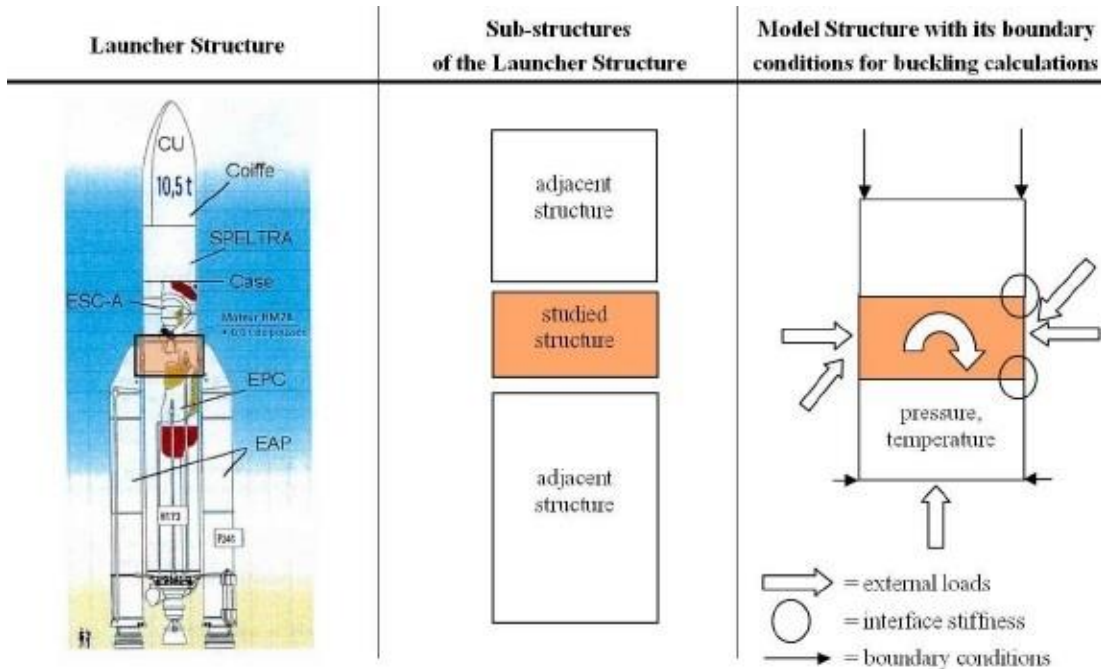


Fig.18-2: Sub-structuring of the Ariane 5 launcher, Front Skirt test

LL

- * Test article analysis is mandatory to interpret the test results and simulation-based improve the design.. Only well-understood experiments can verify the design assumptions made!
- * Splitting of a large structure (Ariane experience) is dangerous: The first buckling mode can appear on an adjacent structure and not on the studied one
- * Mandatory for a realistic qualification of a sub-structure is a realistic set of cross-section loadings and pressure loading with an accurate structural designing of the interface stiffness of the adjacent structural parts. If the interface is too stiff in the test assembly this will attract loading and lead to a non- realistic failure site (experience from Ariane 5 tests)
- * Not all critical locations of a structural component can be tested, because an ‘over-testing’ of some parts may happen to be. ‘Verification By-Analysis-Only’ is to be considered if the structure is too big or if the test model shall e.g. be applied later as flight model
- * Put strain gauges there where a clear stress situation is in order to avoid useless discussions about the interpretation. Check locally by strain measurements and then rely globally on FEA-test result comparison
- * Specific design requirements drive testing
- * Requiring different so-called system margins MoS_{sys} (suffered nonsense in a Ariane Technical Specification) for the various structural parts, then not all critical locations can be tested without overloading other integrated parts. Components of such a structural assembly cannot be verified by a qualification test, because system margins cannot be used locally like a ‘fitting factor’. They should have been considered directly in the Ariane 5 as a usual design FoS, applying $j_{sys} = (MoS_{sys} + 1) \cdot j$. Otherwise, the design process is obscured and is prevented from applying the most economic measure in order to take risk out of the structure
- * Requirement to put a design FoS j on a design temperature violates physics and structure behavior
- * So-called test correction factors are applied to adjust the design verifications by accurately evaluated structural test results linked to the test article analysis results.

18.2 Material Testing primarily based on the World-Wide-Failure-Exercises-I and -II

The author succeeded with test-validation of 3D-strength criteria models for isotropic concrete, transversely-isotropic UD-material, orthotropic ceramic (fabrics) with visualization of the derived 3D failure surfaces if reliable test data sets were given.

This was only partly given in the *the World-Wide-Failure-Exercises-I, concerning 2D-mapping, and -II, concerning 3D-mapping of UD materials*. The author's WWFE-I and -II contributions had to be based on an intensive assessment of provided test results. In this sub-chapter the Lessons Learned during the examination of several WWFE-Test Cases (TC) will be collected.

Validation of the lamina-material SFCs models can be only achieved by 2D- together with 3D-lamina test results. Since SFC-model validation is focused just lamina-TCs are now investigated in detail. The normal user is just interested to well map his course of failure test data by a UD-SFC and not on the laminate analysis tools.

The laminate test cases serve for the verification of the laminate design. There the full WWFE failure theory is required. This makes a comparison between the contributions very challenging because different FE codes were applied by the contributing competing institutes. These better tools further had to be equally compared to the retired author's tools. He could just use his handmade non-linear CLT-code upgraded by experience and using his sensibleness for the problem and the delivered input.

LL, more general ones

** Measurement data is the result of a Test Agreement (norm or standard), that serves the desire to make a comparability of different test procedure results possible. Hence, there are no exact property values. Material properties are the result of the material model applied inclusively mapping process.*

** Stresses, strength, strains, elasticity properties cannot be directly measured*

** Check of assumptions is necessary before designing (example: WWFE on UD-material). Pore-free material, specimen surfaces polished, well-sealed, fiber volume is constant, tube specimens show no warping and do not bulge, perfect bonding, no layer waviness, edge effects do not exist*

** Sometimes one must live with a substitute test situation in order to get some approximate properties (Example: UD-Tension/Compression-Torsion test device → Arcan test device)*

** Before thinking about test data evaluation the associated underlying micro-damage processes must be sorted out in order to get a better understanding of failure*

** Test specimens shall be manufactured like the structure ('as-built')*

** Comparisons between theoretical predictions and test data help to identify the major discrepancies, limitations, and areas which require further theoretical and experimental work. There is always a lot to be done and following Moslik Saadi "All is difficult prior to becoming simple"! This begins with the provision of appropriate test specimens for the various material families being extreme ductile or brittle and ends with appropriate test procedures and an appropriate test data evaluation*

** Considering FE-results: We must more and more 3D-design! However the situation of properties, especially for composites is: „3D-property data test sets are seldom sufficiently available“.*

Of high interest for future scientists and engineers might be the following assessment results of the provided properties during the author's many WWFE-designated years. They are results which stem from a very careful and effortful test data evaluation of about one man year. Otherwise, a successful WWFE-contribution could not have been made possible.

Thereby, some essential TestCase-examples for lamina-input shortcomings were found:

* WWFE-I, TC1: the provided strengths have been changed from Part A to B and two test points are doubtful regarding own test results (*Reason is known: non-accurate raw test data evaluation of the test engineer at DLR Stuttgart. Organizers did not question the test data but required mapping of the false ones!*).

* WWFE-I TC2: the author informed the organizers that apples and oranges have been put here together in a diagram. One cannot fill into the same diagram 90°-wound tube test specimen data together with 0°-wound tube data. The 0°-stresses have to be transformed in the 2D-plane due to the fact that shearing under torsion loading turns the fiber direction (see *Fig.17-3*) and the lamina coordinate system CoS is not anymore identical with the structure coordinate system of the tube. In order to also use these test data the author exemplarily transformed magenta-colored **two fracture test points** by the occurring twisting angle γ using a non-linear CLT-analysis. Then he could achieve a good mapping showing, that the two transformed fracture points accurately lie in the lamina CoS on the 90°-curve.

* WWFE-II, TC3: the same mistake happened again! However, here the much more complicated 3D-stress situation was to face, so that the 3D-transformation of the 0°-data set could be simply performed.

* WWFE-II, TC2 an average stress-strain curve should have been provided because otherwise no realistic treatment is possible. Therefore the Part A results could be only inaccurate. From the Part B information the author could derive an average curve and then all 3 TC test data courses could be mapped and the mutual check points in the fully connected TC2-TC3-TC4 matched. Incomprehensively, there was no response of the organizers to the author's idea, which made 3 TCs to successful test cases.

* Viewing the final papers of the WWFE-organizers "A comparison of the predictive capabilities of current failure theories for composite (UD-composed) laminates, judged against experimental evidence" and "Maturity of 3D failure criteria for fiber-reinforced composites, comparison between theories and experiments", there is not any doubt to find concerning the quality of the only available, provided test data sets.

One third of the provided TC test data was at least questionable till not applicable for model validation.

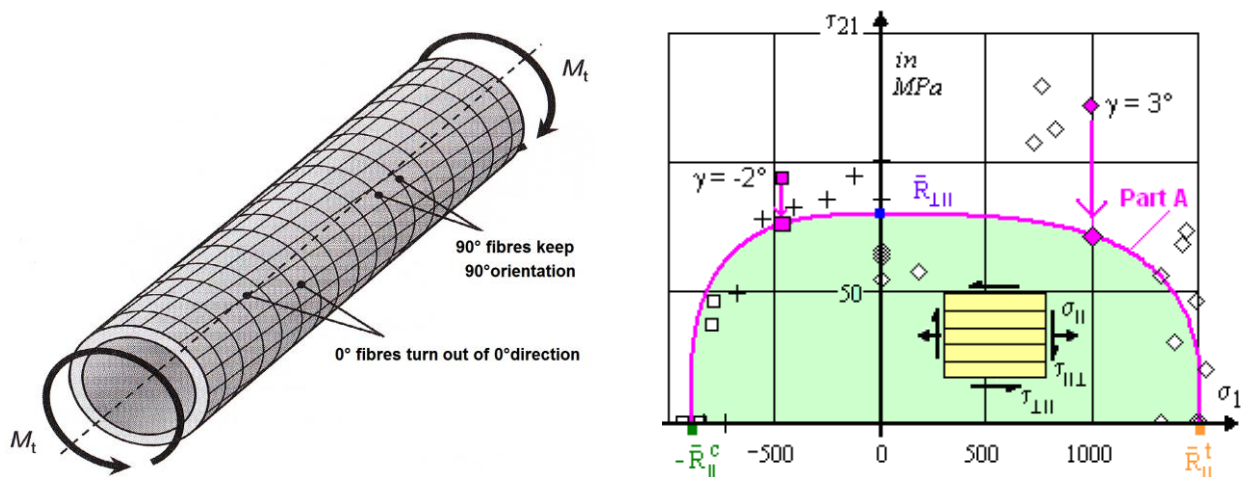


Fig.18-3, $\tau_{21}^{fr}(\sigma_2)$ basic cross-section of the fracture failure body: (right) WWFE-I, TC2, UD lamina, CFRP, T300/BSL914C Ep ; (left) Tube test specimen picture: [Courtesy IKV Aachen] The normal user is just interested to well map his course of failure test data by a SFC

* Test results can be far away from the reality like an inaccurate theoretical model.

* Theory creates a model of the reality, one experiment shows one realization of the reality.

19 Determination of 2D ‘Omni principal FPF strain failure envelopes and Reserve Factor

Aim: Replacing the ply-by-ply analysis of multiple-ply laminates by a much simpler method

Steve Tsai’s idea was to by-pass the effortful ply-by-ply analysis of multiple-ply laminates by using a so-called ‘Omni-(principal FPF strain) failure envelope’. This envelope surrounds an intact Non-FPF area whereby FirstPlyFailure (FPF) includes Fiber Failure FF and Inter-Fiber-Failure IFF. Such an ‘Omni failure envelope’ is to determine for each composite material, applying a FPF-Strength Failure Criterion (SFC), and will capture all possible laminate stacks. The used SCF significantly determines the shape of the envelope, see Fig.19-1. Dimensioning is performed by showing that the design loading-caused principal strains are lying within the Non-FPF area. The idea can serve as a very helpful Pre-design tool.

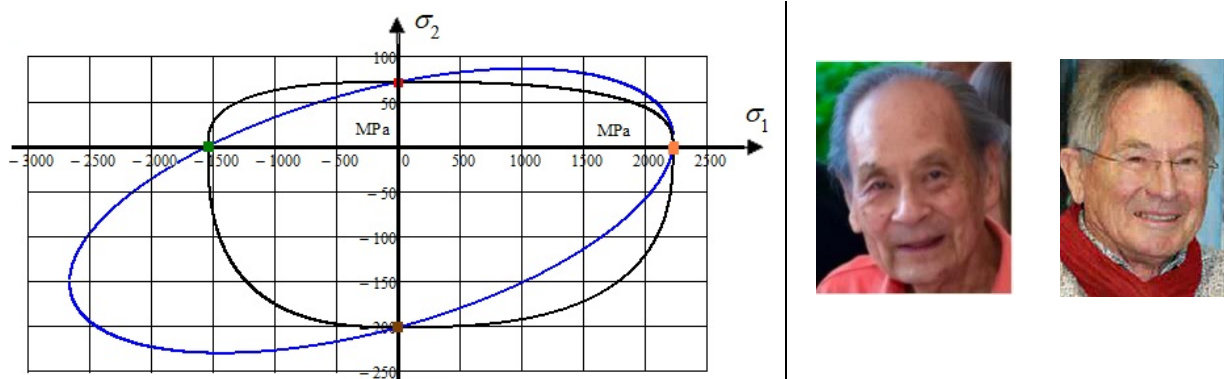


Fig.19-1: Cross-section $\sigma_2(\sigma_1)$ of the failure body, Tsai-Wu versus Cuntze

19.1 Tsai’s indirect Determination of the 2D ‘Omni envelope’

Fig.19-2 displays different ‘butterflies’ (name, how the author Cuntze termed the bundle of i FPF-curves), derived using the SFCs of Tsai-Wu and Cuntze). These numerical results of the FPF-linked principal strain curves clearly depict the significant effect of the chosen SFC, see above figure. The different lateral properties determine the shape (wing edge) of the obtained symmetric ‘butterfly’ with its single, grey-marked principal strain curves provided by E. Kappel.

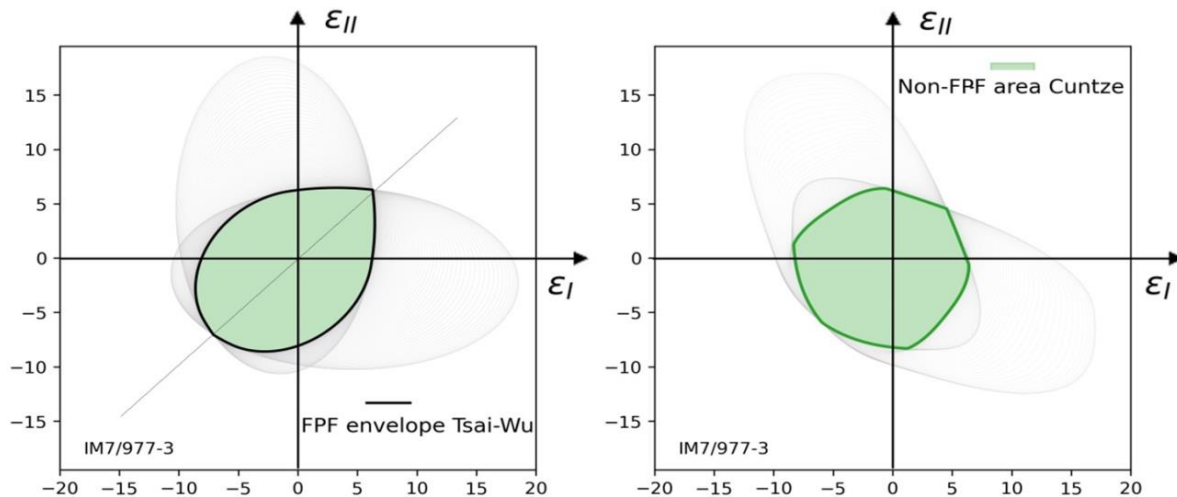


Fig.19-2, bundle of all FPF envelopes = ‘butterflies’: All ply FPF-envelopes enclosing a non-FPF failure area; $0^\circ < \alpha < 90^\circ$ (91 ply angles). Principal strain in %, suffix FPF is skipped. CFRP IM7/977-3. In all pictures: (left) Tsai-Wu with $\mu_{\perp} = 0$, $F_{12} = -0.5$ and (right) Cuntze with $\mu_{\perp} = 0.2$, $m = 2.7$

19.2 Cuntze's Determination of the 2D 'Omni Envelope'

The derivation of such an 'Omni failure envelope' is pretty effortful and no direct formulation could be found in the past. Recently, this bottleneck could be by-passed by an idea of the author, who examined various horizontal cross-sections $\tau_{21} = \text{constant}$ of the UD-FPF failure body, Fig.19-3 below. He found that $\tau_{21}=0$ delivers the smallest non-FPF area. Pre-Dimensioning can now be performed by showing that the design loading-caused principal strains are located within the Non-FPF area. A simpler pre-design of arbitrary laminates is possible.

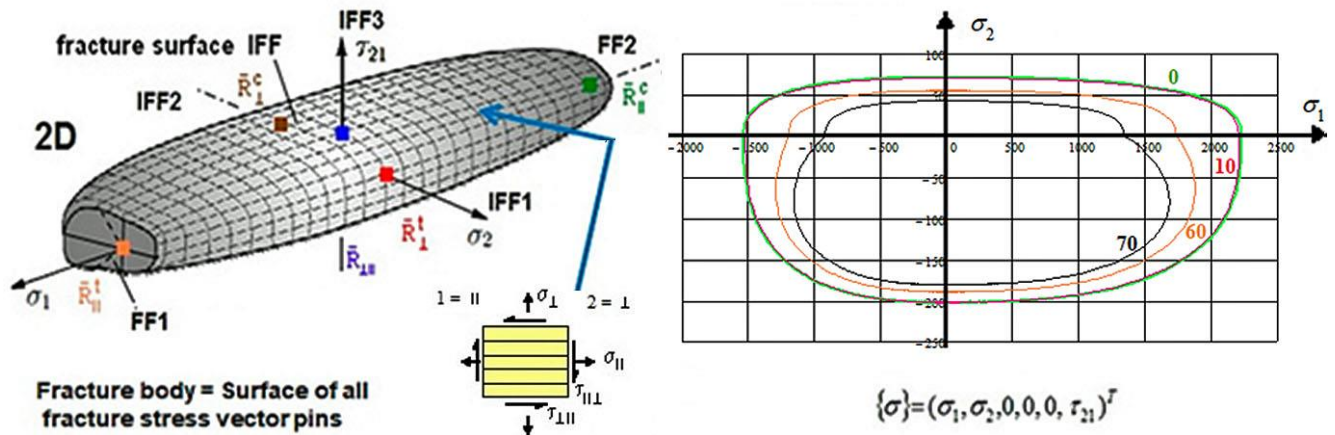


Fig.19-3: (left) 3D UD Failure body. (right) FPF-envelopes for 3 planes $\tau_{21} = \text{const}$. CFRP IM7/977-3

Fig.19-4 (left) presents the resulting Omni principal strain FPF curves $\varepsilon_{II}(\varepsilon_I)$ with a not unambiguously solution $\varepsilon_{II}(\varepsilon_I)$ for each parameter level $\tau_{21} = \text{const}$. \rightarrow The failure curve $\sigma_2(\sigma_1, \tau_{21} = 0)$ describes the 'Omni envelope'

Originally, the 'second' solution-linked additional outer curve parts were excluded in the graph and the right figure eventually shows the 'cleaned-up' envelope, representing the limit $Eff = 100\%$ enveloping the Non-FPF area. The cleaned-up graph is identical to the Non-FPF area obtained by the Tsai 'butterfly'-determination procedure.

Domains of the envelope can be dedicated to the locally faced failure mode types FF and IFF.

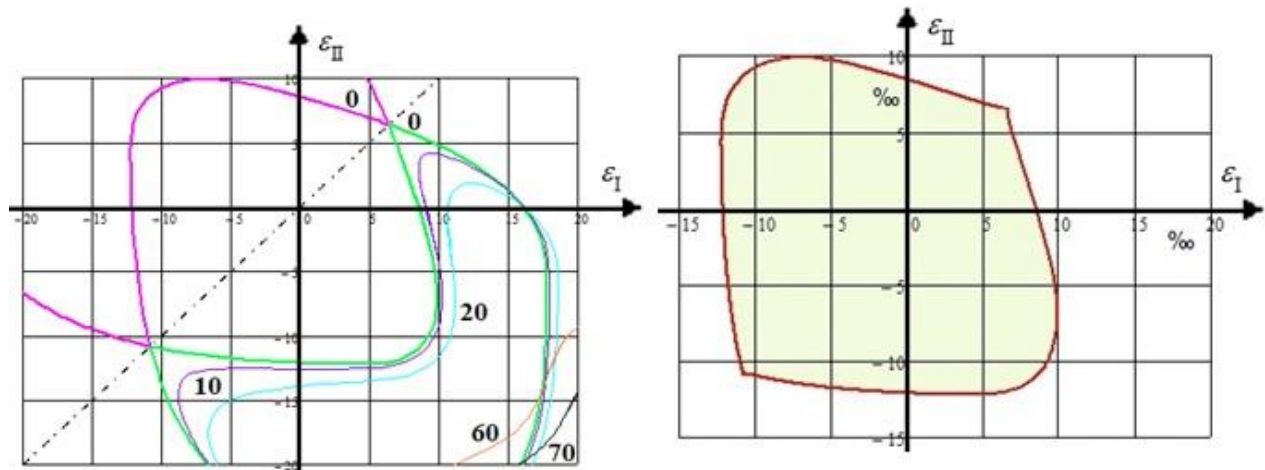


Fig.19-4: Mirrored envelope of the Non-FPF area (Cuntze procedure), CFRP IM7/977-3

In a novel investigation, detailed in *Table 19-1*, Cuntze could give a complete look of the different envelopes in *Fig.19-4 (left)*. Depicted are the ‘butterfly’ wings (outside) and internally the green shadowed Non-FPF area. For optical comparison reasons E. Kappel ‘traditionally’ provided the ‘butterfly’ procedure plots for *Fig.19-4 (right)* and *Fig.19-5*.

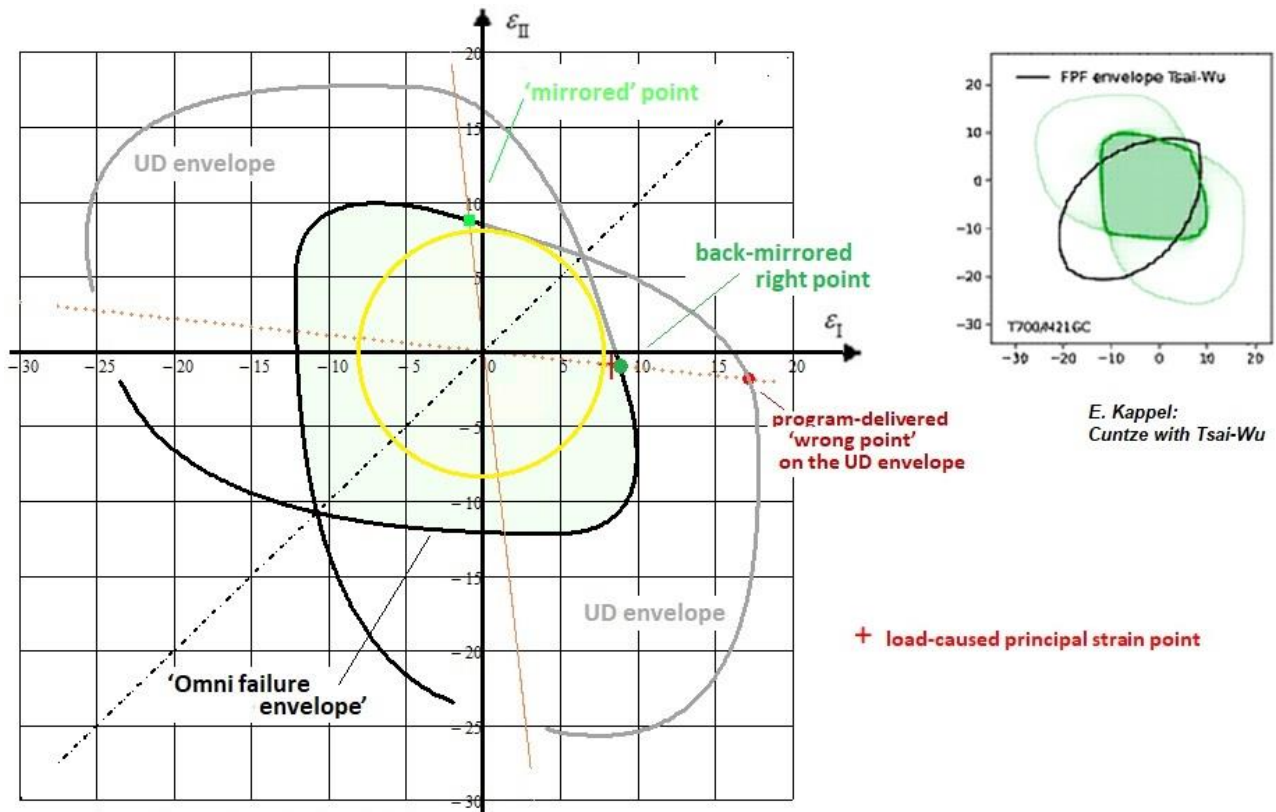


Fig.19-5: (left) Various envelopes of the Non-FPF area (Cuntze procedure following Principal Strain Procedure Cuntze in Table 19-1)..(right) ‘Butterfly’ and Non-FPF area applying the SFCs of Tsai-Wu and Cuntze

19.3 Pre-design Example using the ‘Omni Non-FPF area’ and Determination of Reserve Factor

Of highest interest is the reserve factor which must be smaller for a simplified design method than obtained by the classical ‘Ply-by-ply procedure’, thus remaining on the Safe Side.

Laminate Design Verification is traditionally performed by above ‘ply-by-ply’ analysis, assessing the obtained ply (lamina) stresses $\{\sigma\}$ in the critical location of the most critical plies. Now, a simpler more global assessment is possible (*Table 19-2*) by using the in-plane principal strains of the laminate, strains which represent the loading. Such principal strains are a standard output of modern FE software. They are mathematical and not material symmetry-linked quantities.

Table19-2: Procedure of checking a probably critical design stress state

A Non-FPF area within an ‘Omni failure envelope’ is given for the chosen laminate material

- FEA delivers the maximum state of the 3 strains of the laminate stack
- Transformation into the 2 principal strains as coordinates of the Non-FPF area
- Check, whether the strain point $(\epsilon_I, \epsilon_{II})$ lies within the envelope or Non-FPF area
- Determine material reserve factor $f_{RF} = \text{vector length ratio of failure strain/design strain}$.

Remember, please: The execution of the Design Check runs under the Presumption
“Linear Analysis, proportional stressing $\sigma \sim \varepsilon$ is permitted”.

Table 19-1: Procedures, how to obtain the material reserve factor f_{RF}

SFC Cuntze: Failure Function $F(\{\sigma\}, \{\bar{R}\}, \mu \text{ directly}) = 1$

$$Eff_{FPF} = [(Eff^{//\sigma})^m + (Eff^{//\tau})^m + (Eff^{\perp\sigma})^m + (Eff^{\perp\tau})^m + (0)^m]^{m^{-1}} = 1, \quad m = 2.7$$

Input

$$\{\sigma\} = (\sigma_1, \sigma_2, \sigma_3, \tau_{23}, \tau_{31}, \tau_{21})^T \rightarrow (\sigma_1 = 900, \sigma_2 = 20, 0, 0, 0, \tau_{21} = 25)^T \text{ MPa,}$$

$$\{\bar{R}\} = (\bar{R}'_{//}, \bar{R}^c_{//}, \bar{R}'_{\perp}, \bar{R}^c_{\perp}, \bar{R}_{\perp//})^T \rightarrow (2230, 537, 71, 202, 78)^T \text{ MPa, } \mu_{\perp//} = 0.2.$$

$\{\sigma\}$ -loading-caused ply strains and loading-representing principal strains

$$\varepsilon_1 = s_{11} \cdot \sigma_1 + s_{21} \cdot \sigma_2, \quad \varepsilon_2 = s_{21} \cdot \sigma_1 + s_{22} \cdot \sigma_2, \quad \gamma_{21} = s_{66} \cdot \tau_{21}$$

$$\varepsilon_I = 0.5 \cdot \left[(\varepsilon_1 + \varepsilon_2) + \sqrt{(\varepsilon_1 - \varepsilon_2)^2 + \gamma_{21}^2} \right], \quad \varepsilon_{II} = 0.5 \cdot \left[(\varepsilon_1 + \varepsilon_2) - \sqrt{(\varepsilon_1 - \varepsilon_2)^2 + \gamma_{21}^2} \right]$$

$$\varepsilon_I = 0.0083 \equiv UD\varepsilon I, \quad \varepsilon_{II} = f_{\varepsilon} \cdot \varepsilon_I = 0.0009, \quad f_{\varepsilon} = \varepsilon_{II} / \varepsilon_I = -0.109.$$

*Stress Procedure Cuntze: Lamina task, solved by ply-by-ply failure analysis

$$Eff^m = [(Eff^{//\sigma})^m + (Eff^{//\tau})^m + (Eff^{\perp\sigma})^m + (Eff^{\perp\tau})^m + (Eff^{\perp//})^m] \text{ with the mode portions inserted,}$$

$$Eff = \left[\left(\frac{(\sigma_1 + |\sigma_1|)}{2 \cdot \bar{R}'_{//}} \right)^m + \left(\frac{(-\sigma_1 + |\sigma_1|)}{2 \cdot \bar{R}^c_{//}} \right)^m + \left(\frac{(\sigma_2 + |\sigma_2|)}{2 \cdot \bar{R}'_{\perp}} \right)^m + \left(\frac{(-\sigma_2 + |\sigma_2|)}{2 \cdot \bar{R}^c_{\perp}} \right)^m + \left(\frac{|\tau_{21}|}{\bar{R}_{\perp//} + 0.5 \cdot \mu_{\perp//} \cdot (-\sigma_2 + |\sigma_2|)} \right)^m \right]^{1/m}$$

$$\rightarrow Eff = 0.513 \Rightarrow \text{material reserve factor } f_{RF} = 1 / Eff = 1.95.$$

*Principal Strain Procedure Cuntze: classical laminate task, solved by a laminate failure analysis; $\tau_{12} = 0$

Due to $\varepsilon_1 = \varepsilon_I, \varepsilon_2 = \varepsilon_{II}$ for the 2 failure determining stresses follows, $\gamma_{21} = 0$

$$\sigma_1 = (s_{21} \cdot \varepsilon_2 - s_{22} \cdot \varepsilon_1) / (s_{21}^2 - s_{11} \cdot s_{22}) \quad \text{and} \quad \sigma_2 = (\varepsilon_2 - s_{21} \cdot \sigma_1) / s_{22} \text{ which is to insert into}$$

the FPF-criterion-based 'Omni principal strain failure envelope' formula

$$\left(\frac{(\sigma_1 + |\sigma_1|)}{2\bar{R}'_{//}} \right)^m + \left(\frac{(-\sigma_1 + |\sigma_1|)}{2\bar{R}^c_{//}} \right)^m + \left(\frac{(\sigma_2 + |\sigma_2|)}{2\bar{R}'_{\perp}} \right)^m + \left(\frac{(-\sigma_2 + |\sigma_2|)}{2\bar{R}^c_{\perp}} \right)^m + (0)^m = 1 = 100\% .$$

With the chosen SFC the \rightarrow Non-FPF area $\varepsilon(\sigma_{FPF})$ is to derive .

On the strain beam $f_{\varepsilon} = \frac{\varepsilon_{II}}{\varepsilon_I} = \frac{\varepsilon_{II,FPF}}{\varepsilon_{I,FPF}}$ it will be finally obtained

$$f_{RF} = \sqrt{(\varepsilon_{I,FPF}^2 + \varepsilon_{II,FPF}^2)} / \sqrt{(\varepsilon_I^2 + \varepsilon_{II}^2)} = \varepsilon_{I,FPF} / \varepsilon_I = 1.06 .$$

Cuntze’s direct determination of the ‘Omni failure envelope’ enables to determine the reserve factor straightforward instead of using the *Non-FPF smaller* internal circle in Fig.19-5, how it was usually performed up to now, see [Cun 24].

However, there was a computational problem: Mathcad unfortunately delivers a principal failure strain value ε_{FPF} outside of the Non-FPF area as result of its solution process. The other solution seems to be received if a shear strength is involved. This **wrong** point value can be localized on the

UD 'butterfly wing' edge in Fig 19-4 which enabled to successfully use the symmetry of the envelope as it is executed in Fig-19-6.

Now, Design Verification can be performed as described below:

$$f_{\bar{\epsilon}} = \frac{\epsilon_{II}}{\epsilon_I} \quad f_{\bar{\epsilon}} = -0.109 \quad UD\epsilon_I = 0.0083$$

Vorgabe $\epsilon_{IFPF} := 0.01 \quad \sigma_1 := 100 \quad \sigma_2 := 10$

$$\boxed{\epsilon_{IFPF} = s_{11} \cdot \sigma_1 + s_{21} \cdot \sigma_2} \quad \boxed{f_{\bar{\epsilon}} \cdot \epsilon_{IFPF} = s_{21} \cdot \sigma_1 + s_{22} \cdot \sigma_2}$$

$$\left(\frac{\sigma_1 + |\sigma_1|}{2R_{1t}} \right)^{mint} + \left(\frac{\sigma_2 + |\sigma_2|}{2R_{2t}} \right)^{mint} + \left(\frac{-\sigma_1 + |\sigma_1|}{2R_{1c}} \right)^{mint} + \left(\frac{-\sigma_2 + |\sigma_2|}{2R_{2c}} \right)^{mint} = 1$$

$A\epsilon := \text{Suchen}(\epsilon_{IFPF}, \sigma_1, \sigma_2) \quad \epsilon_{IFPF} := A\epsilon_0 \quad \epsilon_{IFPF} = 0.01712$

$$f_{\bar{\epsilon}} = -0.109 \quad f_{RF\bar{\epsilon}} := \frac{\epsilon_{IFPF}}{UD\epsilon_I} \quad \boxed{f_{RF\bar{\epsilon}} = 2.07}$$

This result of the Mathcad program leads to a value which belongs to another solution brunch (see the figure). Using the plot's symmetry the real value can be found after the replacement of $f_{\bar{\epsilon}}$ by $f_{\bar{\epsilon}r} = 1/f_{\bar{\epsilon}}$

$$f_{\bar{\epsilon}r} := \frac{1}{f_{\bar{\epsilon}}} \quad f_{\bar{\epsilon}r} = -9.214 \quad f_{RF\bar{\epsilon}r} := \frac{\epsilon_{IFPFr}}{UD\epsilon_I} \quad \boxed{f_{RF\bar{\epsilon}r} = 1.06}$$

$$< \boxed{f_{RF\sigma} = 1.95}$$

Fig.19-6 Successful computation of f_{RF} after utilizing the plot's symmetry (code Mathcad 15). $\epsilon_I \equiv UD\epsilon_I$

Note, once again please:

Tsai's 'Omni principal strain envelope' principally surrounds a Non-FPF or even a Non-LPF area.

- *FPF is required if the design requirement asks to fulfill a First-Ply-Failure in the critical locations of the plies of the laminate. It is more or less a linear method.
- *LPF, if to apply, is required to fulfill a Last-Ply-Failure limit. However, this usually involves a non-linear analysis up to the ultimate failure load of the structural part.

In order to cope with the reserve factor definition these shall be sketched again below:

About 'linear' FPF: stress-defined $f_{RF} = \frac{\text{Strength Design Allowable } R}{\text{Stress at } j \cdot \text{Design Limit Load}} > 1$

Non-linear LPF: load-defined $RF_{ult} = \frac{\text{non-linearly determined ultimate failure load at } Eff = 100\%}{j_{ult} \cdot \text{Design Limit Load}}$

LL:

* The investigation of various cross-sections $\tau_{21}=\text{constant}$ proved, that $\tau_{21}=0$ delivers the smallest Non-FPF area, thus making a simpler pre-design of arbitrary laminates possible

* **Basic result:**

The principal strain approach delivers the required smaller reserve factor compared to the conventional ply-by-ply stress-based procedure. The approach is 'On the safe side' !

20 Note on Fiber Micro-Fragments and Dusts of CFRP/CFRConcrete

Matter of my heart:

Supporting the application of sustainable carbon concrete with low-risk PAN-CFs in Production and Recycling

Facts: CFs usually are produced using the precursors Polyacrylonitrile (PAN) and Pitch. Pan-based CFs can be classified into the types: intermediate-modulus (IM), high-modulus (HM) and ultrahigh-modulus (UHM). Machined Pitch CFs generated many toxic split-up fiber fragments, UHM-CFs seem to show some and the lower modulus Standard PAN none. These facts ask for an investigation of the UHM-CF with the objective to finally sort out that the use of the less 'risky' Standard PAN CF cause no threat. Inhaled particles with its size, geometric shape and contaminants adhering to the surface are relevant for a health effect. Of course, targeted workplace prescriptions always have to counteract the occurrence of excessive stress on the lungs from inhaling too large amounts.

Respirable bio-persistent particles accumulate in the alveoli of the lungs. These so-called 'WHO fibres' pierce the macrophages in the lungs and can migrate into the abdomen and pleural tissues and cause cancer.

CF application in Construction

As structural engineer, who has founded and led two working groups in the carbon concrete sector for 10 years: *"It is my deep wish to use more fatigue-resistant [VDI2014] PAN-CF in the construction industry in order to save concrete, which has a negative CO₂ footprint due to the clinker production required for this."*

The next figure displays a CFRP application by a fiber grid (*mat*) as a slack reinforcement (*no pretension*) of a bridge.

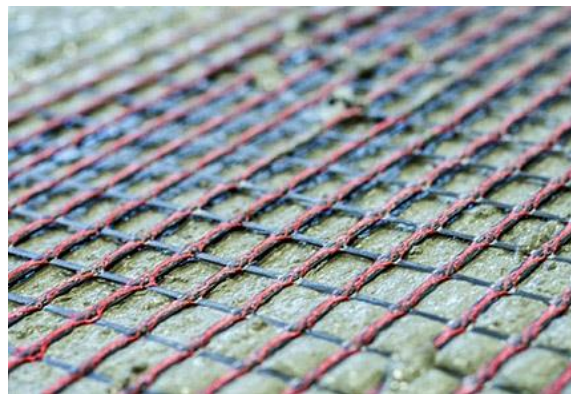


Fig.20-1: Bridge Wurschen, 2022: (left) Superstructure made exclusively of carbon concrete, shell construction. (right) Textile FRP mats in the super-structure) (Foto: Stefan Gröschel, IMB, TU Dresden)

Note: Full exploitation of the Carbon Fiber (CF) is to achieve by pre-tensioning, which will advantageously compress the usual low tensile strength of the matrices concrete and plastic. Just pre-tensioning of plates is series production.

Carbon Fiber Production

CF-properties strongly depend on the production process and above precursors which need different conditions but the essential processes are similar. A CF requires a heating and stretching treatment to get the high strength products. A thermoset treatment is first applied in the temperature range from 200 to 400 °C in air under stretching to get the stabilized fiber, followed by a

carbonization process in the temperature range from 800 to 1500 °C in oxygen-free condition to remove impurities and to improve the crystallinity of carbon. To further improve the performance of CFs, a graphitization process is required to graphitize carbonized fibers with temperature up to 3000 °C. During these processes, stretching is required to get preferred orientated carbon crystals, because the crystal alignment makes the fiber incredibly strong and stiff. The graphitization process leads to differences between PAN and Pitch and within the PAN-CFs. This will be later of interest.

The very expensive Pitch CF is mainly used in spacecraft and antennas. The market is dominated by the PAN-CF. With regard to possible toxic fragments, PAN-CF is therefore of interest, especially the 'highly' graphitized UHM-PANCF such as Torayca's M60J, which comes next to the Pitch-CF considering the tensile modulus (stiffness). CF tensile modulus and fracture toughness naturally depend on the fabrication regarding precursor, on carbonization and graphitization. Furthermore, Pitch-CFs are more layer-like in their crystal structure in contrast to the more granular PAN-CF. This probably further explains the higher tensile modulus compared to the PAN-CF. Knowing the different crystal structure is therefore important for explaining the splintering process, originator of possible toxic fragments.

'WHO-Fiber' criticality

WHO criterion for respirable fibers: 'WHO-Fiber' \equiv tiny filament fragment with a diameter \emptyset of less than 3 μm , a length L of greater than 5 μm and a length-to-diameter ratio of $L/\emptyset > 3:1$. (*Naming Fiber: So it's not about long CFs, which of course never meet the WHO criterion. Asbestos fiber, for example, is just a fiber-like looking fragment*).

Too many dust-related particles, smaller than the WHO 'fiber' size, can also cause a hazard. Particulate matter of PM2.5 size can penetrate into the alveoli, and ultrafine particles with a diameter of less than 0.1 μm can even penetrate into the lung tissue. The figure below summarizes the topics faced when considering the criticality.

The macrophage lifespan of a few weeks is one of the decisive factors for the success of disposal or 'cleaning'. 'WHO-fiber'-pierced macrophages usually die.

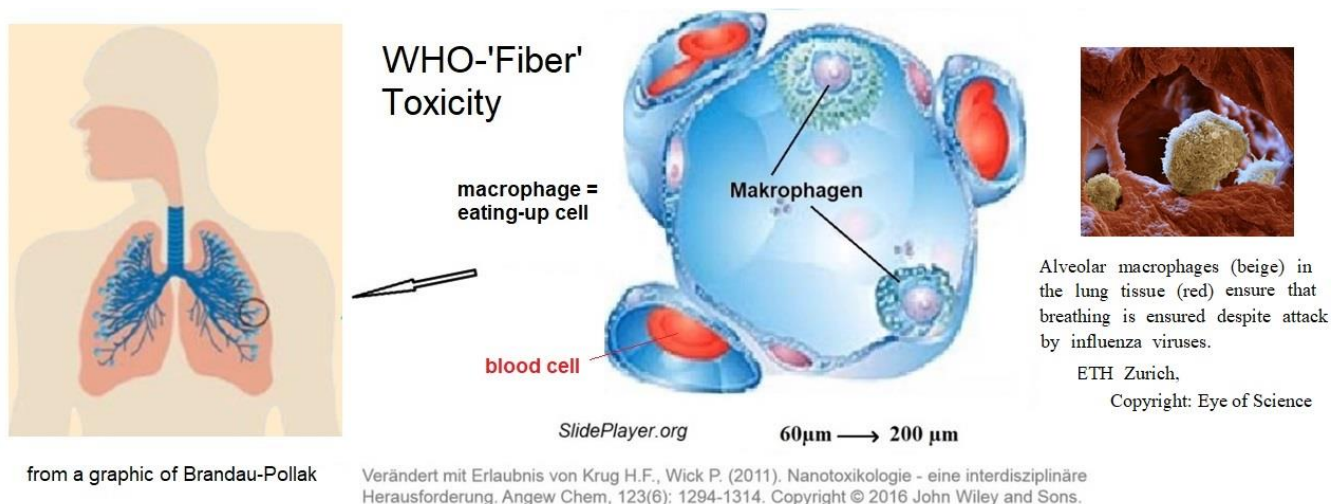


Fig.20-2: Effect of WHO- 'Fibers'

A distinction must be made between long fibers, micro-fragments of fibers such as the 'WHO-fiber' size, as well as the micro-fragments of composites, i.e. fiber-reinforced polymers FRP or fiber-reinforced concrete FRC. In addition to the fiber, the matrix with the interphase material in the

fiber-matrix interface must be considered, too. A threat can arise from inhaling too large amounts of dust and 'WHO-fibers'.

Criticality-relevant variables are the both: geometry and bio-resistance:

Geometry: Critical are the already defined 'WHO-'fiber', as well as dusts and fiber fragments with $\varnothing < 3\mu\text{m}$, which penetrate directly into the alveoli and the lung tissue. Since the 'WHO-fiber' size is smaller than the diameter of common CFs, the fiber fragment must experience a reduction of the diameter. This can happen by splintering or by burning. CF is not toxic per se!

Bio-persistence: High bio-persistence causes high toxicity, a low bio-solubility in living organisms already speaks as an indication of possible carcinogenicity. Fragments with short residence times that are quickly dissolved or removed are less risky.

Only if a sufficiently high amount of CF-'WHO-'fibers' is produced and inhaled there is a potential for danger, whereby the following applies:

$$\text{Risk} = \text{hazard potential (severity)} \cdot \text{probability of occurrence.}$$

The hazard potential is the exposure to CF-WHO (size) particles combined with toxicity. The duration of the exposure in terms of quantity and the possible frequency of occurrence of the event per unit of time are therefore decisive.

Generation and Counting of WHO 'fibers'

A quantity for the risk assessment delivers the counting of the fragments which are generated in machining processes. Question: *Which machining processes seems to be the worst for the generation of 'WHO-fiber' shaped CF particles, faced in production and recycling?*

Some answer is given in the BMBF research project *CarboBreak* (headed by the BAuA. This Federal Institute for Occupational Safety and Health conducts research for a safe, healthy and humane working environment): Investigation of the release behaviour of respirable fragments made of pure fibres and fibre composites (consisting of CF, sizing, matrix etc) under mechanical stress. Basically here, rovings were subjected to an extreme mechanical stress in a so-called ball vibrating mill (an assumed 'worst case' machining process), the resulting CF fragments were evaluated with regard to their morphology and then the WHO 'fibers' counted, namely the 'WHO-Fiber' Quantity / Unit Volume. The CF portion is considered to be the critical part of the full composite.

One significant finding is the different splintering process between PAN (left) and Pitch CF (right).

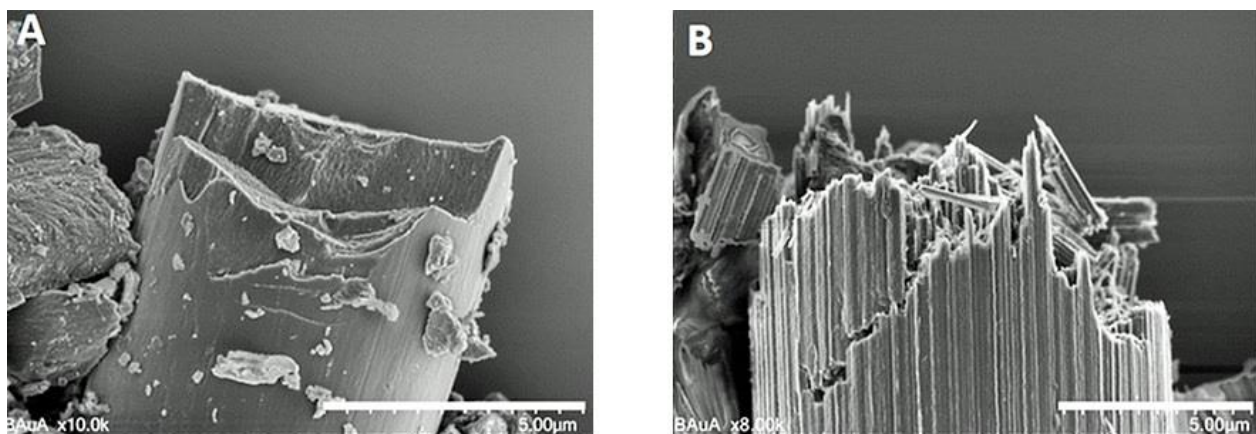


Fig. 20-3:(left) PAN-based, (right) Pitch-based. (Courtesy BAuA, Berlin)

The pitch fibers are obviously more dangerous because they do extremely splinter. Since the UHM-CF comes closest to the pitch fiber in terms of stiffness of all PAN-CFs, the PAN-UHM represents the more critical PAN side in terms of risk of splintering.

→ a CF-parameter is being sought that could be a parameter for explaining the fiber splintering hazard.

Model-Idea for such a Parameter characterizing the splintering

The sought-after, splinter hazard-descriptive parameter could be fracture toughness. This property is likely to show some difference in relatively similarly stiff (Young's modulus) brittle materials. Test proposal is a micro-fracture mechanics investigation of a laser-notched single fiber to determine the different brittleness based on the fracture toughness values of K_{Ic} to be measured. In fracture mechanics, fracture toughness describes the resistance of a material to unstable crack progression. An ultra-high graphitized UHM PAN CF such as Torayca's M60J is to be basically investigated, because it is to place at the transition to the critical Pitch-Fiber.

Believe: *Different fracture toughness values indicate different risk of splintering.*

*The proposed test specimens, together with the difficult notching of a single CF by a laser beam, have already been realized in Kaiserslautern by the institutes IVW with PZKL!

*The search for a fracture mechanics model that allows us to estimate the fracture toughness of a CF is essential for the qualitative differentiation of the envisaged fibers. A formula will provide a not realistic 'exact', but a quantified relationship which is fully sufficient.

The searched characteristic for the tensioned notched test specimen is the so-called critical stress intensity factor (SIF) K_{Icr} (= fracture toughness), at which the unstable crack progression begins. Its formula reads $K_{Icr} = \sigma_{fracture} \cdot \sqrt{\pi \cdot a_{cr}} \cdot Y$ with the so-called geometry factor Y taking the fact into account that the SIF value is theoretically independent of the dimensions of the test specimen only for infinitely large plates. Therefore, the corresponding function Y must be sought for the intended test specimen 'Notched Single Fiber'. This was made possible by the author-available manual "*NASGRO Reference Manual Version 9.01 Final; December 2018. Fracture Mechanics and Fatigue Crack Growth Analysis Software*".

The application of this model requires assumptions:

- CF is a very brittle material
- The crack instability, expressed by the formula, can be applied at the μm -level for these brittle materials!
- The cross-section, cut by the laser beam, is just a circle section but can be transferred to the elliptical shape of a typical crack
- The 'model for a full cylinder' given as SC07 in the NASGRO document is applicable. Experience has shown that the impact is small, the model can be used also in the μm range
- The crack depth a is given by the laser notch depth.
- Diameter $D = \varnothing = 0.007 \text{ mm}$, UHM 60J.
- The applied stress $\sigma_{fracture}$ at the fiber ends = breaking tensile force F / area A
- The cross-section cut by the laser beam can be transferred to the elliptical shape of a typical SC07 crack. The difference in surface area is neglected because it is the same for all tested fibers. In the SC07 associated Table C15: For $R/t = 0$, i.e. a solid cylinder with $R = 0$ ($t = \text{wall thickness} = R$), approximately to be expected $a/t = 0.3$, gives $c/t = 0.35$ and thus $Y = 1.6$.

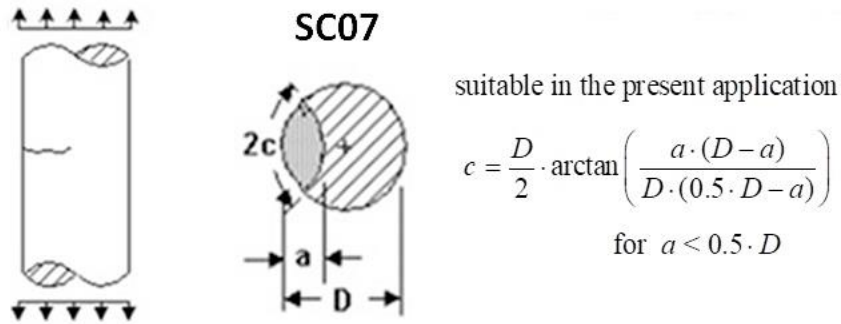


Table C15: CC07 (one crack) - SIF Correction Factors by BEM Analysis (FRANC3D)

Fig. 20-4: Thumbnail crack in a solid cylinder. Surface crack case SC07
 Manual NASGRO Reference Manual Version 9.01 Final; December 2018.
 Fracture Mechanics and Fatigue Crack Growth Analysis Software

The author's great wish, driven as a GROWIAN wind turbine co-responsible (*about 1980*), in view of further future fear-spreading media coverage of a wind turbine breakage with blades made of standard CFs, i.e. not UHM-CFs:

Submission of an official recommendation by BAuA together with Composites United (CU) on working with CFRP in general and on PAN-CF carbon reinforced concrete, including adapted recycling safety requirements.

LL:

** The test idea could be fully realized, which is a seldom experienced luck when testing.*

21 A novel Determination of the Residual Strength R_{res} , non-cracked, Fatigue Phase 2

Aim: Derivation of a procedure to determine and rendering the residual strength value R_{res}

21.1 General for a Proof of Structural Integrity in Projects

Residual strength R_{res} is the fracture stress after pre-damage and re-loading. Not only in mechanical engineering design but also in civil engineering residual strength values are required such as in soil mechanics or for UD-hangers of a railway bridge at Stuttgart, below a hanger.



*Stuttgart Stadtbahn bridge.
World's first network arch railway bridge
(127 m) that hangs entirely on tension
elements made of carbon fiber-reinforced
plastic (CFRP). The 72 hangers are
produced by Carbo-Link AG*

or for tension rods of cranes. The value is of basic interest, because – due to authority demands - Design Ultimate Load is to sustain even after a distinct fatigue life. The residual strength task is one task to demonstrate structural integrity.

This subject is linked to cyclically micro-damaged structural components (*Phase 2 of fatigue life, strength tools applied*) and macro-damaged ones (*Phase 3 of fatigue life, fracture mechanics problem, damage tolerance mechanics tools applied*), as displayed in [Fig.21-1](#). The cyclic loading may range from constant amplitude-loading up to spectrum-loading and has to capture proportional and non-proportional loading scenarios.

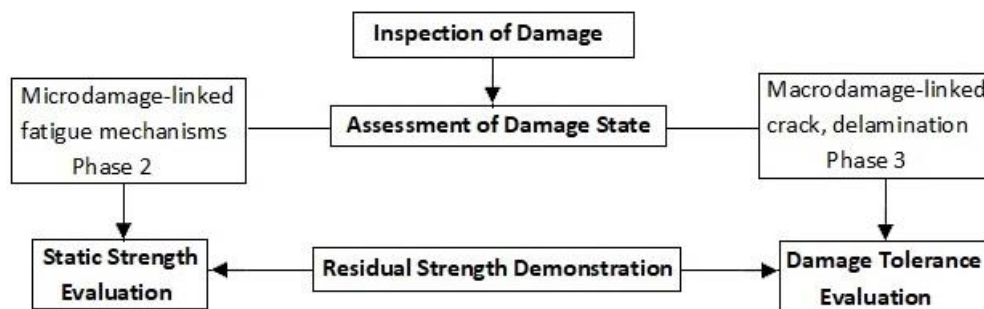


Fig.21-1: Ways of residual strength determination

Especially this task comes up in cases such as: A multiple site damage phenomenon is faced with aerospace components such as fabrication-induced flaw clouds (fatigue strength problem, Ariane 5 Booster wall) or real short-crack ‘clouds’ from e.g. multiple rivet holes in stringer-stiffened panels of aging aircraft components (fracture mechanics problem). Here, the focus is on the Phase 2 residual strength R_{res} . (R_{res} should not be confused with *residual stress* σ_{res}).

In some projects a number for the residual strength at a certain operation cycle value is required. This is well known from impact cases of laminated panels. There, a compression-after-impact (CAI) test is to execute after the impact event because the impact may result in a barely visible external damage and it may generate a dramatic reduction of compressive strength due to separation of layers resulting in a large bending stiffness loss. Regarding the crack-linked Phase 3 residual strength problems the reader is referred to literature on fracture mechanics.

Residual strength tests are long-lasting and expensive. Therefore, procedures are searched that help to reduce the test effort if enough physical knowledge is available.

First step is to map the relevant SN-curve (Wöhlerkurve) by taking the widely used 4-parameter Weibull function

$$\text{stress ratio } R = \sigma_{\min} / \sigma_{\max} = \text{constant} : \sigma_{\max}(R, N) = c1 + (c2 - c1) / \exp(\log N / c3)^{c4}.$$

(stress ratio \rightarrow straight letter R, strength \rightarrow bias letter R). The SN-curve describes the relation between the cyclic loading and the number of cycles to failure N . On the horizontal axis in *Fig.21-2* the number of cycles to failure is given on logarithmic scale. On the vertical axis (*either linear or logarithmic*) the stress amplitude $\sigma_{\text{amplitude}}$ of the cycle is often given. (*sometimes the maximum stress σ_{\max}*) The provided mean SN-curves, $R = \text{constant}$, base on the fatigue test measurement types ‘pearl-chain testing’ or ‘horizontal load level testing’. Fatigue curves are given for un-notched test specimens ($K_t = 1$) and for notched ones, the loading can be uniaxial or multi-axial. Considering residual strengths, measurements on the vertical axis at $n = \text{constant}$ are required.

In design verification very often as fractile (quantile) numbers, representing the failure probability p_f , 5% or 10% are taken in order to capture some uncertainty compared to the average of 50%. For the loading side the design FoS j , in construction γ , capture the uncertainty of the loading. The residual strength design verification has to meet DUL. Following HSB 62200-01 the determination of the static residual strength for single load paths must be made with statistically significant A-values; for possible multiple load path structural parts B-values may be used.

Moving to the required statistical properties some notions are to depict. Capturing the uncertainty of the resistance quantities, the following is performed: Denoting P the survival probability and C the confidence level applied, when estimating a basic population value from test samples, partly enriched by some knowledge of the basic population. Regarding C a one-sided tolerance level it reads:

Static \rightarrow Statistical reduction of average strength from (P= 50%, C= 50%) to e.g. (B-value: P = 90%, C = **95%**).

Cyclic \rightarrow Statistical reduction of average SN curve from (P=50%, C= 50%) to e.g. (P= 90%, C= **50%**).

All this is executed to keep a generally accepted survival reliability of about $\mathfrak{R} = 1 - p_f > 1 - 10^{-7}$.

21.2 Classical way to determine Rres,

Determination via the interpretation “*The course of the residual strength is the difference of the static strength and the maximum strength $\sigma_{\max}(N)$ of an SN curve R*”, see *Fig.21-2*. This leads to

the formulation $R_{res} = \sigma_{\max}(N) + [R^f - \sigma_{\max}(N)] \cdot \rho(n)$ with $\rho(n) = 1 - (n/N)^p \equiv 1 - D^p$,

where the exponent p describes the decay of the residual strength capacity and D the micro-damage quantity, (see Hahne C: *Zur Festigkeitsbewertung von Strukturbauteilen aus Kohlenstofffaser-Kunststoff-Verbunden unter PKW-Betriebslasten*. Shaker Verlag, Dissertation 2015, TU-Darmstadt). *Fig.21-2* depicts for $R = 0.1$ the mean (average) 50% SN-curve and the 90% SN-curve. The residual strength curve R_{res} is given for the point (10^5 cycles, $\sigma = 34$ MPa **rhomboid**). The stress σ belongs to a so-called ‘one stage test’ or constant amplitude test. Regarding the residual strength value at the 90% SN-curve the question arises: “*Where does the necessary statistical basis for a reduced SN-curve come from, if not sufficient test series on vertical and horizontal levels were run*”? Due to missing test data a test

data-based work case cannot be presented. Therefore, the author tried to figure out a procedure which gives an understanding of the subject.

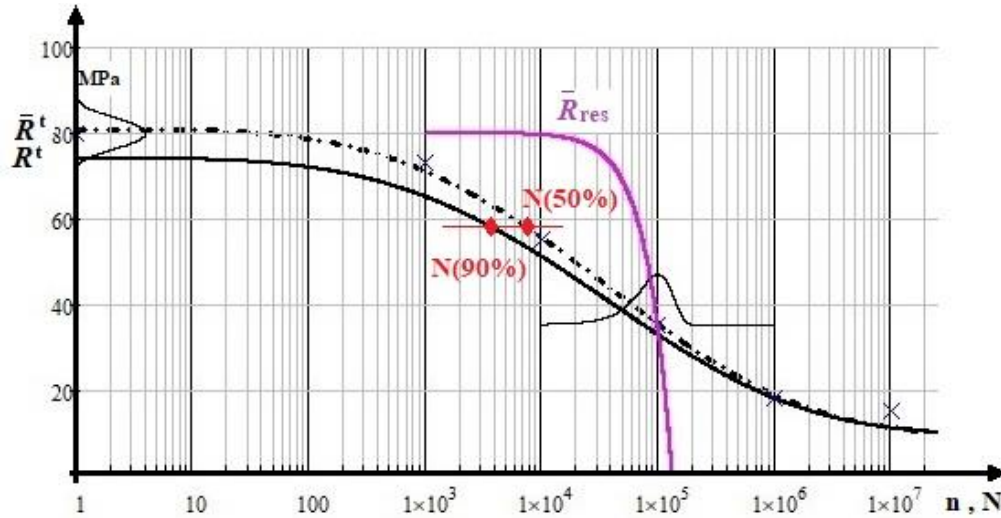


Fig.21-2, Schematic example, uniaxial loading: $R= 0.1$. \bar{R}_{res} is mean tensile residual strength

21.3 Idea Cuntze, probabilistic way to determine a 90% value by the convolution integral

A possibility to determine a 90%-value is given by the application of the so-called convolution integral, using density distributions of R_{res} and of N with just a little hope to find the distribution measured, Fig.21-3. The output of the mathematical expression convolution integral represents the probability of failure p_f . The numerical analysis is based here on the assumption: ‘The density distributions on x- (f_N) and y-axis (f_{Res}) are approximately basic populations and of Normal Distribution-type’ f_{ND} (for the density distributions also a logarithmic, a Weibull density function or a truncated function could be employed). The convolution integral, solved by Mathcad 15, reads

$$(1 - p_f) = \mathfrak{R} = p_{\bar{u}} = \int_{-\infty}^{\infty} \left(\int_{R_{res}} f_{Res}(R) \cdot dR \cdot f_N(N) \right) dN = 90\% \text{ fractile for ND density distributions}$$

$$\text{with } f_{ND}(x) = \frac{1}{\sigma \cdot \sqrt{2 \cdot \pi}} \cdot \exp \left[-\frac{1}{2} \left(\frac{x - \mu}{\sigma} \right)^2 \right] \text{ for abscissa } N \text{ and ordinate } R^t .$$

Data base of the numerical probabilistic example (statistical: μ = mean, σ = standard deviation) is:

- * Static strength distribution $\mu = 80$ MPa, $\sigma = 3.2$ MPa
- * R_{res} distribution in computation point, y-axis, $\mu = 43.5$ MPa, $\sigma = 2.9$ MPa
- * Cycle distribution in computation point, x-axis, $\mu = 3431$ cycles, $\sigma = 446$ cycles and the Coordinates of the chosen computation point * (38 MPa, $n = 2000$ cycles in Fig.21-3).

The presented application outlines a limit of the Mathcad 15 code application. Mathcad has no computation problem with the computation of the required so-called convolution integral. However, when visualizing the probability hill in Fig.21-4, it is not able to manage the ‘big data’ problem and runs into endless loops. Therefore the author had to sort out a work case with reduced stress and cycle regimes. The original SN data set was for fiber fracture (FF) of CFRP considering the hanger. This reduction to a relatively simple numerical example does not matter because the procedure is of interest and will explain the posed task.

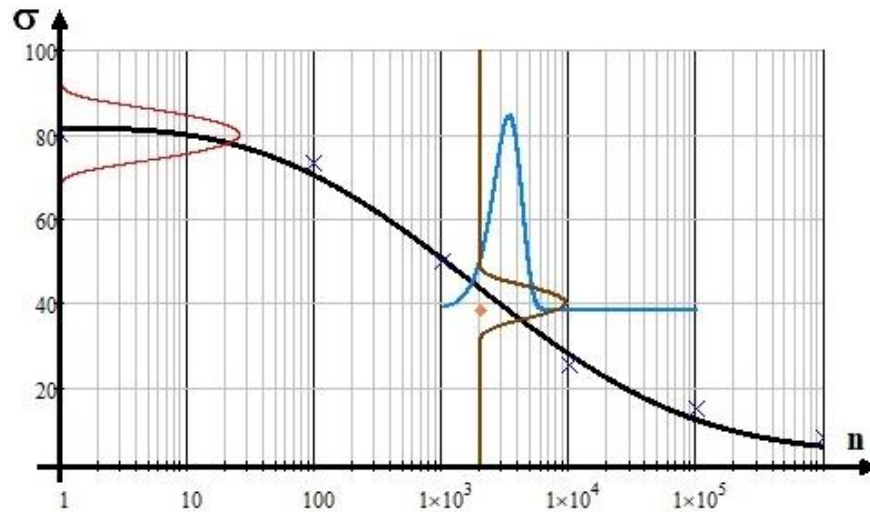


Fig.21-3, Simplified Mathcad calculable example: Assumed distributions of residual strength and cycles linked to R_{res} (38 MPa, 2000 cycles). SN-curve, $R = 0.1$: $c1 = 20$ MPa, $c2 = 80$ MPa, $c3 = 3.77$, $c4 = 2.92$

Fig.21-3 depicts the SN-curve, the chosen computation point, static strength distribution with an assumed residual strength distribution and cycle distribution, all through the computation point *. It is a semi-logarithmic graph. As it is a brittle example material, the use of σ_{max} (involves R^t as origin!) as ordinate is of advantage for the ‘strength-oriented’ design engineer compared to using a stress amplitude σ_a .

The probabilistic treatment delivers the ‘joint’ probability hill of both the distribution functions in Fig.21-4, right figure. The hill’s average center coordinates are 43.5 MPa, 3430 cycles. The figure further depicts the density distributions of the residual strength $R_{res}(\sigma)$ and of the fracture cycle $N(n)$. In the right part figure, the residual strength distribution is not clearly visible due to additional Mathcad-drawn beams running out from the origin, which are to neglect. The task seems to be an overloading of the Mathcad code which could not anymore handle the numerically effortful task for too large cycle numbers. The left figure shows the projection of the probability hill with lines of equal probability belonging to the chosen computation point *. Below, the computation parameter input set is depicted:.

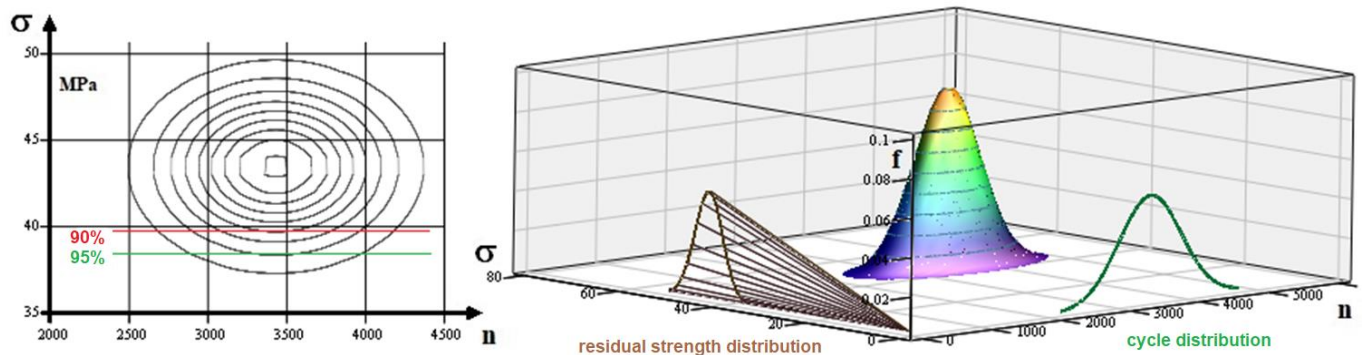


Fig.21-4: (right) Cyclic distributions and assumed residual strength distribution with survival probability hill applying the convolution integral. (left) Projection of lines of equal probability with two chosen residual strength cut-offs, M is the hill designation

Design Safety considering the scatter of the design parameters is tackled as follows:

The scatter of loading is considered in the residual strength design verification because DUL with its design safety factor j_{ult} has to be verified. The scatter of the residual strength R_{res} and of the

fracture cycle N is captured by a joint probability calculation indicated below. This procedure is effortful, however of high fidelity if test data is available.

Under above assumptions an estimation of a required 90%-linked residual (tensile) strength value can be determined according to the formula below representing the probability hill volume truncated by R_{res}

$$\begin{aligned}
 &\mu_{NR} = 3431 \quad \sigma_{NR} = 446 \quad \mu_{\sigma R} = 43.5 \quad \sigma_{\sigma R} = 2.9 \quad n := 2000..6000 \quad \sigma := 0..80 \\
 &x_n := \text{dnorm}(n, \mu_{NR}, \sigma_{NR}) \quad y_\sigma := \text{dnorm}(\sigma, \mu_{\sigma R}, \sigma_{\sigma R}) \quad F(x, y) := x \cdot y \quad M_{n, \sigma} := F(x_n, y_\sigma) \cdot 750 \\
 &p_{\ddot{u}} := \int_{\sigma_{res}}^{Rt + \sigma Rt} \int_{2500}^{5500} \frac{1}{\sigma_{\sigma R} \cdot \sqrt{2\pi}} \cdot e^{-\frac{1}{2} \cdot \left(\frac{y - \mu_{\sigma R}}{\sigma_{\sigma R}}\right)^2} \cdot \left[\frac{1}{\sigma_{NR} \cdot \sqrt{2\pi}} \cdot e^{-\frac{1}{2} \cdot \left(\frac{x - \mu_{NR}}{\sigma_{NR}}\right)^2} \right] dx dy
 \end{aligned}$$

The computation delivers for the point ($\sigma_{res} \equiv R_{res} = 38.0$ MPa, 2000 cycles) the value $p_{\ddot{u}} = P = 95\% = \mathfrak{R}$.

Setting the value 39.5 MPa, the demanded survival probability $p_{\ddot{u}} = 90\% = (1 - p_f)$ is obtained for R_{res} .

21.4 Residual Strength R_{res} , pre-cracked, Fatigue phase 3, Fracture Mechanics (for completion)

To estimate the residual strength of a pre-cracked structural part or the critical length of an initial macro-crack is essential regarding the questions: (1) Is the crack-length at the end of static loading critical? (2) Is the crack-length at the end of cyclic loading critical for further static loading, considering a SN-curve? Here, the certification of cracked components in aircraft structures requires a damage tolerance assessment.

LL:

- *The proposed procedure clearly shows how to statistically understand a residual strength value*
- *It could be proven that the proposed model leads to an acceptable value for the residual strength of fatigued, non-cracked structural parts.*

22 Technical Terms, Glossar

Aim: Bridging mutual understanding between engineering disciplines

22.1 Indexing and Material Notations

Indexing is a chaos in the disciplines: It seems to be that the author could find (*some years ago for the planned novel ESA –Material Handbook*) a physically clear indexing system for the 3 material family models isotropic, transversely-isotropic UD and orthotropic materials (fabrics etc.). This indexing captures all material properties and allows a switching between.

The author’s Glossar on ‘Technical Terms’ (Springer) hopefully shall be a contribution to a better mutual understanding of 'constructive' engineers from the building industry and engineers from mechanical engineering and further, of engineers from the textile, manufacturing and material discipline as well in order to better manage the more and more interdisciplinary future project tasks.

Notes on designations: As a consequence to isotropic materials (European standardization) the letter R has to be used for strength. US notations for UD material with letters X (*direction 1, ||*) and Y (*direction 2, ⊥*) confuse with the structural axes’ descriptions X and Y . $R_m :=$ ‘resistance maximale’ (French) = tensile fracture strength (superscript t is usually skipped because in mechanical engineering design runs in the tensile domain, which is opposite to civil engineering, where fiber reinforcement is coming up viewing carbon concrete). See further [*Cun23c, Glossar*].

In the following Table, on basis of investigations of the VDI-2014 Working Group and on investigations for above Materials Handbook, Cuntze proposed internationally not confusing terms for strengths and physical properties. These self-explaining symbolic designations read for UD-materials:

Property type	UD quantities	‘generic’ number
fracture strength properties + friction properties	$\{R\} = (R_{ }^t, R_{ }^c, R_{\perp}^t, R_{\perp}^c, R_{\perp })^T,$ $\mu_{\perp }, \mu_{\perp\perp}$	5 2
elasticity properties	$\{E\} = (E_{ }, E_{\perp}, G_{ \perp}, \nu_{\perp }, \nu_{\perp\perp})$	5
hygrothermal properties	$\{\alpha\} = \text{CTE } (\alpha_{ }^T, \alpha_{\perp}^T); \text{CME } (\alpha_{ }^M, \alpha_{\perp}^M)$	2 ; 2

It seems again to be necessary to cite for the different disciplines two long-time used terms in the composite domain:

Material composite (Werkstoffverbund): structural-mechanically a composed ‘construction of different materials.

Note: A not smearable ‘conglomerate’ is usually the Fiber-grid-Reinforced-Concrete.

Composite material (Verbundwerkstoff): combination of constituent materials, different in composition.

For the strength properties it is to discriminate in the English language:

Yield stress (unfortunately termed yield strength, despite of the fact that it is not set as a strength property for Design Verification): material property corresponding to the point at which the material begins to deform plastically (in German Streckgrenze R_e), is end of proportionality σ_{prop}

Proof stress: point at which the material exhibits 0.2% of plastic deformation, known as stress at 0.2% strain- offset and set as yield strength property $R_{p0.2}$. (in German Fließgrenze or 0.2% -Dehngrenze).

Table 22-1: Notations of material properties

9	general orthotropic	R_1^r	R_2^r	R_3^r	R_1^c	R_2^c	R_3^c	R_{12}	R_{23}	R_{13}
5	UD, \cong non-crimp fabrics	$R_{ }^r$ NF	R_{\perp}^r NF	R_{\perp}^r NF	$R_{ }^c$ SF	R_{\perp}^c SF	R_{\perp}^c SF	$R_{ \perp}$ SF	$R_{\perp\perp}$ NF	$R_{ \perp}$ SF
6	fabrics	R_W^r	R_F^r	R_3^r	R_W^c	R_F^c	R_3^c	R_{WF}	R_{F3}	R_{W3}
9	fabrics general	R_W^r	R_F^r	R_3^r	R_W^c	R_F^c	R_3^c	R_{WF}	R_{F3}	R_{W3}
5	mat	R_{1M}^r	R_{2M}^r	R_{3M}^r	R_M^c	R_{1M}^c	R_{2M}^c	R_M^r	R_M^r	R_M^r
2	ductile isotropic	R_m SF	R_m SF	R_m SF	deformation-limited			R_m^r	R_m^r	R_m^r
	brittle	R_m NF	R_m NF	R_m NF	R_m^c SF	R_m^c SF	R_m^c SF	R_m^r NF	R_m^r NF	R_m^r NF

9	general orthotr.	E_1	E_2	E_3	G_{12}	G_{23}	G_{13}	ν_{12}	ν_{23}	ν_{13}	comments
5	UD, \cong non-crimp fabrics	$E_{ }$	E_{\perp}	E_{\perp}	$G_{ \perp}$	$G_{\perp\perp}$	$G_{ \perp}$	$\nu_{ \perp}$	$\nu_{\perp\perp}$	$\nu_{ \perp}$	$G_{\perp\perp} = E_{\perp} / (2 + 2\nu_{\perp\perp})$ $\nu_{\perp\perp} = \nu_{ \perp} E_{\perp} / E_{ }$ 3 is perpendicular to quasi-isotropic 2-3-plane
6	fabrics	E_W	E_F	E_3	G_{WF}	G_{W3}	G_{W3}	ν_{WF}	ν_{W3}	ν_{W3}	Warp = Fill
9	fabrics general	E_W	E_F	E_3	G_{WF}	G_{W3}	G_{F3}	ν_{WF}	ν_{F3}	ν_{W3}	Warp \neq Fill
5	mat	E_M	E_M	E_3	G_M	G_{M3}	G_{M3}	ν_M	ν_{M3}	ν_{M3}	$G_M = E_M / (2 + 2\nu_M)$ 1 is perpendicular to quasi-isotropic mat plane
2	isotropic	E	E	E	G	G	G	ν	ν	ν	$G = E / (2 + 2\nu)$

9	general orthotropic	α_{T1}	α_{T2}	α_{T3}	α_{M1}	α_{M2}	α_{M3}
5	UD \cong non-crimp fabrics	$\alpha_{r }$	$\alpha_{T\perp}$	$\alpha_{T\perp}$	$\alpha_{M }$	$\alpha_{M\perp}$	$\alpha_{M\perp}$
6	fabrics	α_{TW}	α_{TF}	α_{T3}	α_{MW}	α_{MF}	α_{M3}
9	fabrics general	α_W	α_F	α_F	α_{MW}	α_{MF}	α_{M3}
5	mat	α_{TM}	α_{TM}	α_{TB}	α_{MM}	α_{MM}	α_{MB}
2	isotropic for comparison	α_T	α_T	α_T	α_M	α_M	α_M

Table of structural properties

Strength properties: NF:= Normal Fracture, SF:= Shear Fracture, R:= strength, σ, τ := indicate the fracture responsible normal or shear stress acting on the fracture 'plane'.

Hygro-thermal properties: T:= Thermal, M:= Moisture and Mat. λ, c : not listed.

Elasticity properties: E:=Young's modulus, ν :=Poisson's ratio, G:=shear modulus. ||:= parallel to the fiber, \perp := transversal to the fiber direction; W:= Weft, F:= Fill, M:= Mat. $\nu_{||\perp}$:= (here!) larger Poisson's ratio.

1:= lamina fiber direction, 2:= lamina transverse fiber direction across the width or the plane, 3:= through-thickness direction; x, y := principal in-plane laminate directions, z := thickness direction (interlaminar)

Notes:

- (1) The constituents retain their identities in the composite; that is, they do not dissolve or otherwise merge completely into each other although they act in concert. Composite materials provide improved characteristics not obtainable by any of the original constituents acting alone.
- (2) Normally the constituents can be physically identified, and there is an interface between them.
- (3) Composites include fibrous materials, fabrics, laminated (layers of materials), and combinations of any of them.
- (4) Composite materials can be metallic, non-metallic or a hybrid combination thereof. Carbon concrete is one example.
- (5) Approximately homogenizable to a smeared material are short fiber-reinforced FRC, SMC, UD-ply = UD-lamella. The lamella is smearable and therefore it can be modelled as a ‘composite material’.
- (6) Layered materials and foam materials are also forms of composite materials.
- (7) Cement-based mortar is a ‘smearable’ composite material (the construction organization RILEM has a problem here, because they do not discriminate ‘material composite’ from ‘composite material’).

22.2 Upcoming construction standards in Germany with comments

Standards in Germany are finalized, see Fig.22-1:

- polymer matrix: BÜV 10 update
- mineral matrix: novel DAfStb-Richtlinie “Betonbauteile mit nicht-metallischer Bewehrung“.

BÜV-Empfehlung

Überarbeitung 2019

Tragende Kunststoffbauteile im Bauwesen [TKB]

- Entwurf, Bemessung und Konstruktion -
Stand 08 / 2010

Zwanzig20 - Verbundvorhaben Carbon Concrete Composite C³
V1.2: Nachweis- und Prüfkonzepte für Normen und Zulassungen

C3 V1.2 PG3
DAfStb D 109

C3 V1.2 PG1/2
DAfStb D 161

Arbeitspapier Bewehrung

Carbonbewehrung; Sorten, Eigenschaften, Kennzeichnung, Prüfkonzepte

Schlussfassung V1 2 (16.07.2019)

Ansprechpartner:

DAfStb
FTA Albstadt
Glasoiden GmbH Oschatz
ILK TU Dresden
IMB TU Dresden
ITM TU Dresden

Warnhinweis:

Dieses Dokument stellt keine DIN-Norm oder Richtlinie dar.

Es handelt sich um ein Arbeitsdokument, welches im Rahmen des Projekts C3 V1.2 als möglicher Vorschlag für eine Richtlinie erarbeitet wurde und im Rahmen des Projekts C3 L9 weiterentwickelt wird.

DEUTSCHER AUSSCHUSS FÜR STAHLBETON

D 36 DAfStb UA
Nichtmetallische Bewehrung

DAfStb-Richtlinie

Betonbauteile mit nichtmetallischer Bewehrung

Entwurf 19. August 2019
Cyan – Änderungen und Ergänzungen gegenüber D 39

Teil 1: Bemessung und Konstruktion
Teil 2: Bewehrungsprodukte
Teil 3: Hinweise zur Ausführung
Teil 4: Prüfverfahren

Notifiziert gemäß der Richtlinie (EU) 2015/1535 des Europäischen Parlaments und des Rates vom 9. September 2015 über ein Informationsverfahren auf dem Gebiet der technischen Vorschriften und der Vorschriften für die Dienste der Informationsgesellschaft (kodifizierter Text) (ABl. L 241/1 vom 17.09.2015).

Bezüglich der in dieser Richtlinie genannten Normen, anderen Unterlagen und technischen Anforderungen, die sich auf Produkte oder Prüfverfahren beziehen, gilt, dass auch Produkte bzw. Prüfverfahren angewandt werden dürfen, die Normen oder sonstigen Bestimmungen und/oder technischen Vorschriften anderer Mitgliedstaaten der Europäischen Union oder der Türkei oder einem EFTA-Staat, der Vertragspartei des EWR-Abkommens ist, entsprechen, sofern das geforderte Schutzniveau in Bezug auf Sicherheit, Gesundheit und Gebrauchstauglichkeit gleichermaßen dauerhaft erreicht wird.

Herausgeber:
Deutscher Ausschuss für Stahlbeton e. V. – DAfStb
Budapester Straße 31
D-10787 Berlin
Telefon: 030 2693-1320
info@dafstb.de

Der Deutsche Ausschuss für Stahlbeton (DAfStb) beansprucht alle Rechte, auch das der Übersetzung in fremde Sprachen. Ohne ausdrückliche Genehmigung des DAfStb ist es nicht gestattet, diese Veröffentlichung oder Teile daraus auf fotomechanischem Wege oder auf andere Art zu vervielfältigen.

Guideline work ahead! In Germany

Verkauf durch den Beuth Verlag GmbH, Berlin, Vertriebsnummer 05300X

Other standard works on fiber-reinforced materials are :
wind energy GL re-work, Deutsche Bundesbahn

Comments of the author after a careful investigation of the two standard proposals, about 2020:

The DAfStb guideline “Concrete components with non-metallic reinforcement” is intended for fiber-reinforced components with concrete matrix.

- *For engineers it is confusing not to clearly say which fiber material group the guideline is for. The fiber type CF, GF sets the limits of application.
- *Originally for the *open* fiber grid the name lamella for a *dense* non-crimp fabric was used. The lamella however was still intensively used in construction repair of corroding steel-concrete ceilings (see Fig.22-2)
- *The suffix _{nm} could be replaced by the indices of the polymer matrix world, namely for the pure fiber_f and the cured fiber strand _{||}.
- *Why sticking further to the old German-originated letter *f* (strength). Still at the GruSiBau-time (*about 1985, development of the excellent partial safety factor concept*) the author used the international letter *R* for the resistance entity strength in construction. Using the letter *R* – internationally and partly nationally still started - makes life of engineers over the technical fences simpler, internationally at least.

The BÜV-recommendation for load-carrying composite parts in construction is intended for fiber-reinforced components with polymer matrix.

- *Above two upcoming standards are not harmonized regarding the designations amongst themselves and w.r.t. terms half a century internationally used in timber construction and also with polymer matrices. This is all the sadder for the author, because he edited the VDI 2014, sheet 3 guideline - initiated by civil engineers !- but not used in construction. The European Codes hopefully will improve this unfortunate situation.

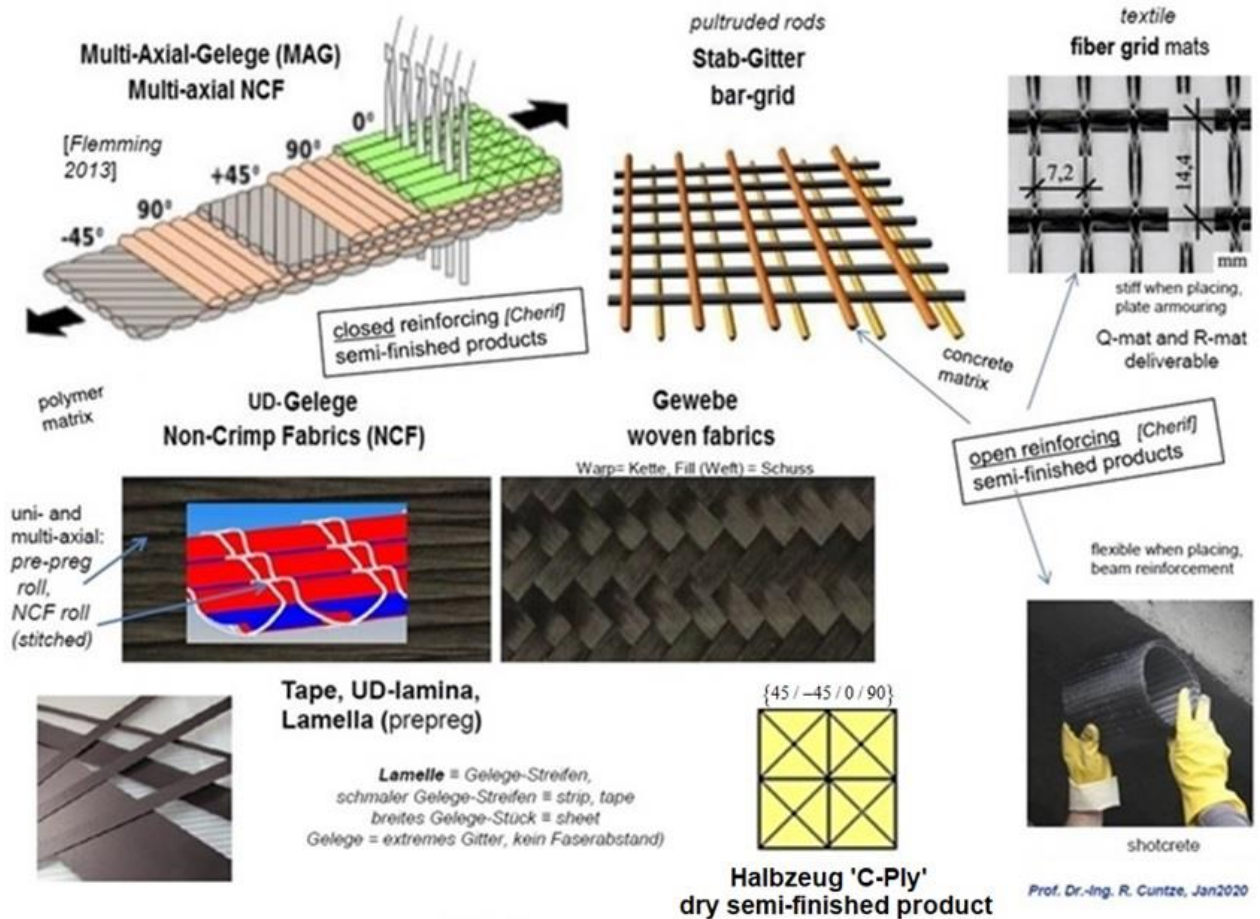


Fig.22-2: Basic fiber-reinforcing products in Engineering

Fig.22-3 presents a proposal for an ordering scheme.

isotropic	Normal-Concrete	Concrete matrix	water + cement (CEM I, CEM III) + aggregate (sand, gravel) + possibly additives, such as super-plasticiser, retarder				max. grain > 4 mm ¹⁾	Fiber Reinforced Concrete GFRC CFRC PPFRC PBOFRC	FCM
	Fine ¹⁾ Concrete						max. grain < 4 mm		
anisotropic	CRC ³⁾ or CC GFC or GC	FRP Reinforcement Form	grid-type reinforcing structures						F(R)C
			Fiber-Concrete-Composite FCC						
			UDRC		Textile-Reinforced Concrete TRC				
			rope bar	rebar grid	R-, Q-grid	embroidered sandwich	non-woven (randomly oriented, oriented)	short fiber long fiber	
CFRP GFRP AFP BsFRP	FRP	1D	2D Reinforcement Alignment		2D	2D – 3D	2D – 3D	for matrix improvement	
		semi-finished products for reinforcements (endless fiber, long fiber)							
isotropic	Thermosets Thermoplastics	Polymer matrix	UD ply lamella strips		NCF lamella sheet	fabric	non-woven (randomly oriented, oriented)	SMC, BMC	FP
			Fiber-Polymer-Composite FPC						
			closed reinforcing structures						
			Resin Systems: thermosets, thermoplastics, with catalysts etc.						

Fig.22-3: Ordering scheme proposal for Fiber-Composite Materials FCM, construction-linked

such as *Fiber-Reinforced Polymer FRP, Fiber-Reinforced Concrete FRC, CFRC:= CarbonFiber-Reinforced Concrete, Bi-Directionally Reinforced Concrete BDRC, UHP-(short)Fiber-Reinforced Concrete, UHPFRC*. Green coloured are still fixed notions.
Matrix types of the Reinforcements *FRPm = Fiber-Reinforced Polymer matrix, Fiber-Reinforced-Mineral matrix FRMm*. International subscripts *f = filament, m = matrix; superscripts t = tension, c = compression*

LL: *Harmonization of denotations remains an urgent on-going task .*

Production of optimal structural components firstly requires an optimum design including all connections / joints and possible materials.
Then the locally best materials are to determine and to sort out - regarding production - to ensure the required optimum component properties considering sustainability.



*Surprising picture, Sambia 2011:
Learning from Crocodile and hippo??*

Desire of the author: “It were good for both the disciplines, mechanical and civil engineering, to act side-by-side - such as croco and hippo document

23 Miscellaneous

In this chapter some results of the author's works are collected, which have been discussed in his various working groups.

23.1 Construction.-linked Additive Fabrication AF

Classification of fabrication processes: Subtractive processes (waste), Formative processes and Additive processes (automatically digitized fabrication now) [VDI 2403]. *The term manufacture is not accurate: Manus and facere → means made by hand.*

1. In subtractive processes, the geometry to be created is created by defining the removal of individual volume regions. Typical representatives of this group of manufacturing processes are machining processes such as turning, drilling or milling. (timber construction etc.)
2. Formative processes refer to the production of geometries by forming in compliance with volume constancy. Formative manufacturing processes are deep drawing, forging or primary forming.
3. Additive fabrication processes create a geometry by joining together volume elements (so-called "voxels"), such as the standard processes concreting, bracketing, plastering a wall etc.

The engineer's desire is to obtain accurate process names in the additive fabrication point 3, the term 3D-print does not give a clear process information. Therefore some basic definitions

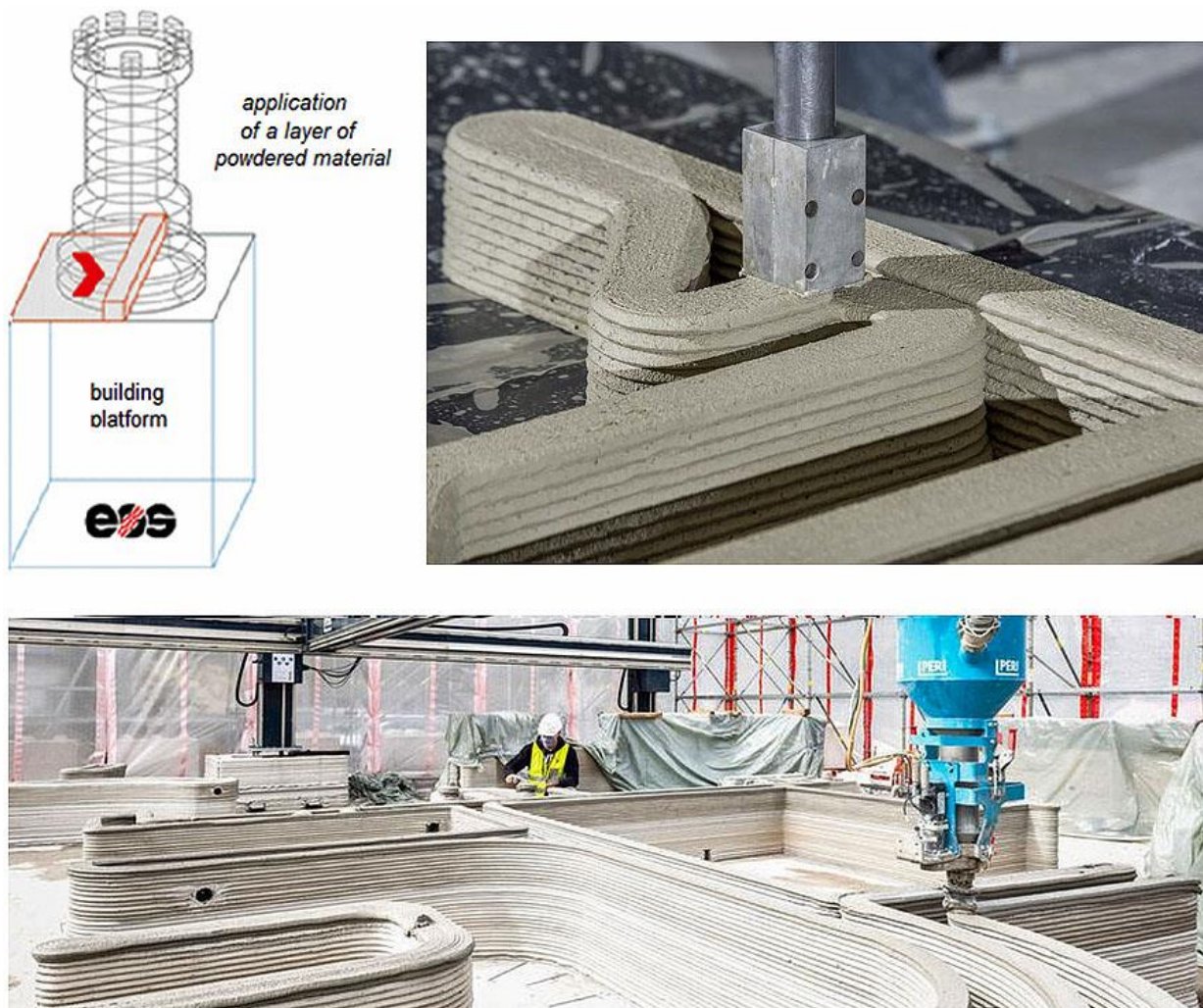


Fig.23-1: Particle-bed technique (up left), Mortar strand depositing (up, right); (below) Peri GmbH 2021, building a two-story house in Beckum

are provided for construction. The two basic digitized additive fabrication processes in construction are to term:

(3a) **Powder bed process:** *true original 3D horizontal slice printing in construction*

Total cross-section including the 'openings' is produced in a powder bed layering process. Layer thickness is usually $\ll 1$ mm. (*for formwork production, usually*). Technique Selective Laser Sintering, does pretty well correspond with the printing definition 'Procedure, to apply something by pressure like printing a book'.

(3b) **Extruded mortar-strand deposit process:** *no 3D printing*

Total cross-section including 'openings' is produced in a 'path tracking operation'. Layer thickness is several mm, depending on the strand thickness. Technique Extruded mortar strand deposit.

LL:

- * *Any material that can be glued, welded or melted can be used in AF. For industrial purposes, metals, plastics, sand and ceramics are common materials, but the process is to adapt*
- * *The extrusion process is for walls and other compressed load-bearing building structures!. That's why there is no fully '3D-printed house' existing.*
- * *Cost-effective conventional ceiling slabs are still required*
- * *Any material that can be glued, welded or melted can be used in AF. For industrial purposes, metals, plastics, sand and ceramics are common materials, but the process is to adapt.*

23.2 Buckling analysis versus Strength analysis

This chapter provides introductory information about buckling of columns (beams), plates, panels and shells. It shortly addresses just essential features in stability analysis (*speaking stability is more positive than buckling*).

This chapter is just dealing with static stability problems. It covers a very basic background in order to guide the practicing designer to better understand the manuals of commercial analysis software.

The following contents basically stems from the creation of the ESA Buckling Handbook, ECSS-E-HB-32-24A (Cuntze was first convenor and founder of the team as well as a co-author of the later prepared HSB 40100-04] from R. Cuntze and J. Broede. Noteworthy: In the HSB, section 40000, for a wide spectrum of columns, rods, rings and deep beams design sheets are found. The same is given in the chapter plates where the available design sheets on anisotropic plates provided by J. Broede and colleagues are outstanding sheets.

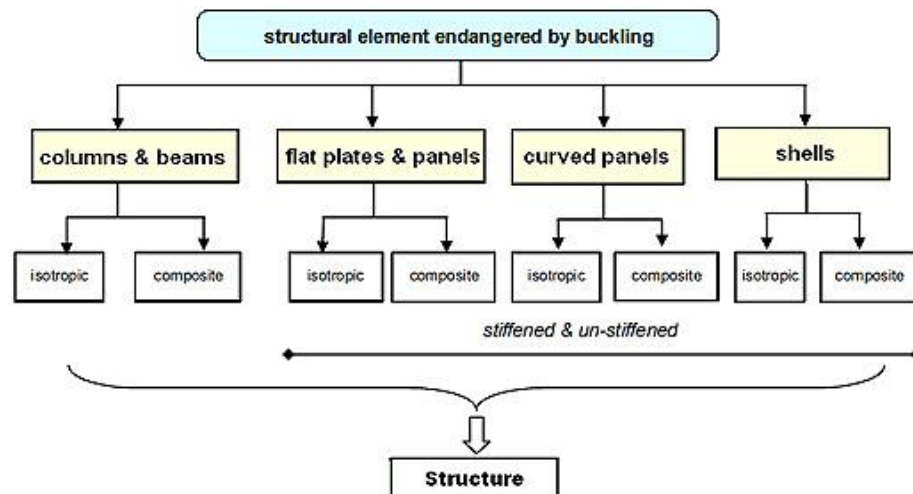


Fig.23-2: Breakdown of buckling of endangered structural elements [Cuntze, ECSS]

Different levels of analysis complexity are treated in the literature above. Going in steps from the lower level of complexity to the higher level of complexity (which will be denoted as a “hierarchical approach”) the structural analyst is able to carry out and finally to successfully interpret analyses at the highest level of complexity, typically finite element computations (see [CUN22]).

In structural design the following subjects must be demonstrated: *Material Strength*, applying SFCs, strength criteria, and *Structural Strength*, applying buckling resistance conditions. *Fig.23-3* compiles these subjects.

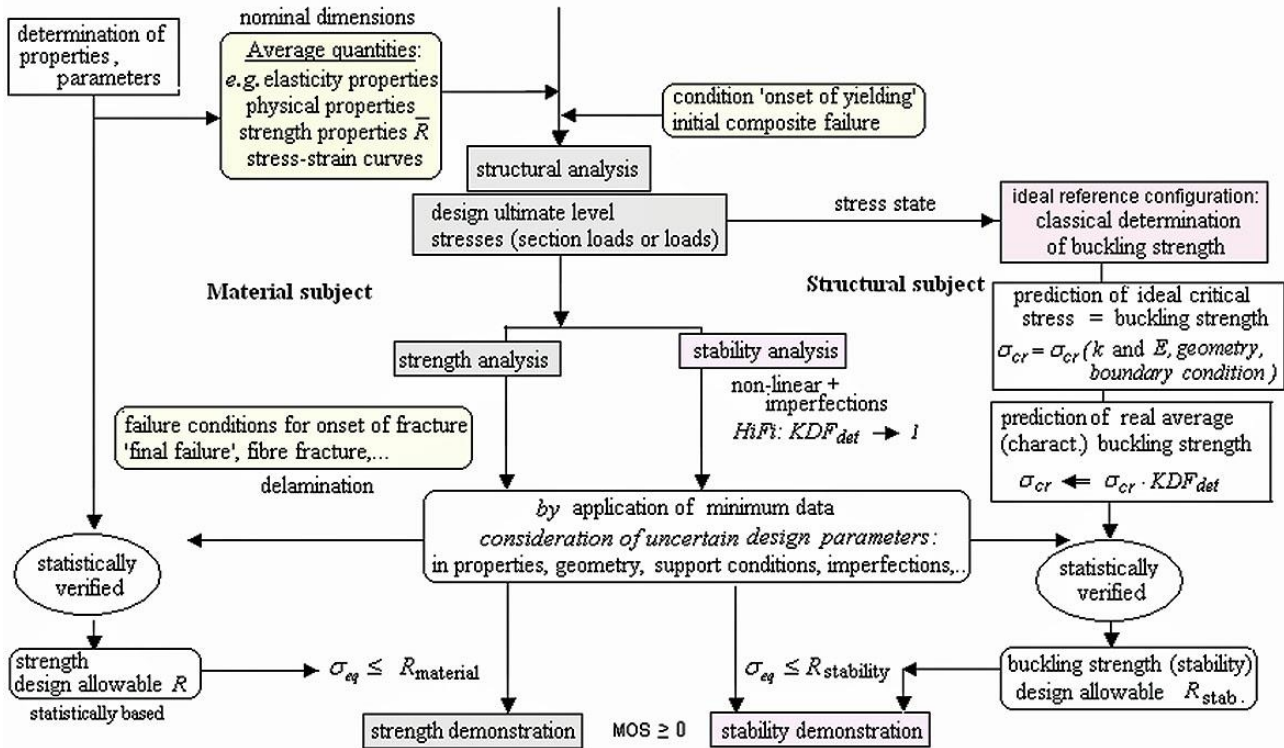


Fig. 23-3: Visualization of the (actually) required deterministic input demands.

KDF usually corrects difference of calculation model to experiment (50% expectance value), k : =buckling factor (from handbook tables), MoS : =Margin of Safety

Using such an engineering procedure the engineer is able to analyze the stability of (large) structures composed of structural elements, also referred to in literature as structural components or structural items. The term structural element includes typical elements such as columns and beams, plates, panels, and shells. In practice these structural elements often contain structural details, e.g. shells containing openings or reinforcements. The associated “basic” structural elements, the elements without structural details are denoted in the ECSS as “Typical Structural Elements”. Non-axial symmetric shells and truss systems are not addressed in the book.

22.3 Some Final Notes from Personal Experience

- ✓ Mechanics remains one very essential basis when developing light-weight structural components and Artificial Intelligence (AI) with its algorithms is a helpful supporting tool
- ✓ Only System Engineering with experienced engineers using mechanics and the necessary other disciplines - together with AI - enables to produce qualified products
- ✓ **At the end someone has to sign that the developed structure will work and by that will take over responsibility. This experienced person is the absolutely necessary ‘plausibility checker’ for the obtained analysis and test results including generic AI-supported results.**

- ✓ Bridge disciplines and materials by showing up similarities to simplify engineering life!
- ✓ In the present multi-physics applications product development is the work of several experienced engineers. Otherwise one does not deliver qualified ‘Multiple function structural products’.
- ✓ In the case of bending of FRPlastic- and FRConcrete-parts carbon fibers can be only exploited using pre-tensioning and thereby compressing the tension-sensitive matrices Plastic or Concrete
- ✓ Viewing SFCs, one must be careful with conclusions reported in literature (unpleasant personal experience): SFC model *modifications* - created by another author - are used under the name of the originator and then poorly rated, however, the modification was not reported!
- ✓ Experienced engineers know: “Check your test together with test data evaluation. Check your analysis including assumptions.”
- ✓ There is a rationale to take a distinct $\sigma - \varepsilon$ curve: From risk analyses and decision theory the best prediction will be achieved by applying the mean(\square, ε)-curve = 50% probability !
- ✓ Certification by Analysis, only: Here, simulation can optimize the output of the usually only permitted minimum number of physical tests, and enabling to better manage risk and improve prediction.

22.4 Annex, see [CUN22]

If one might be interested one can find information on the following subjects in the compilation

- Influence of low Cross-sectional Shear Rigidity and Rotatory Inertia on the Critical Speeds of Shafts with Uniformly Distributed Mass (1984 for centrifuges)
- The Influence of Cross-sectional Shear Flexibility and Rotatory Inertia on the Natural Frequencies of Beams with Uniformly Distributed Mass (1983)
- Natural Frequencies of a Cracked Beam for Production Quality-testing of Rotor blades
- Design of the Metallic Energy storage Flywheel for the floating crane ship Swartow (1982)
- Design of Fiber-reinforced Gas-Ultra-Centrifuges, GUZ (1971-1986)
- A New concept of a Composite Flywheel due to novel fiber-reinforced materials (1988)
- Increasing the Limit of Usability of CFRP Tubes by Built-in-Stresses (1993)
- Structural Reliability, Factors of Safety and Design Values, §12
- Some Winding Theory of Filament Wound Pressure Vessels, §20.

The annual books piled up over the decades.

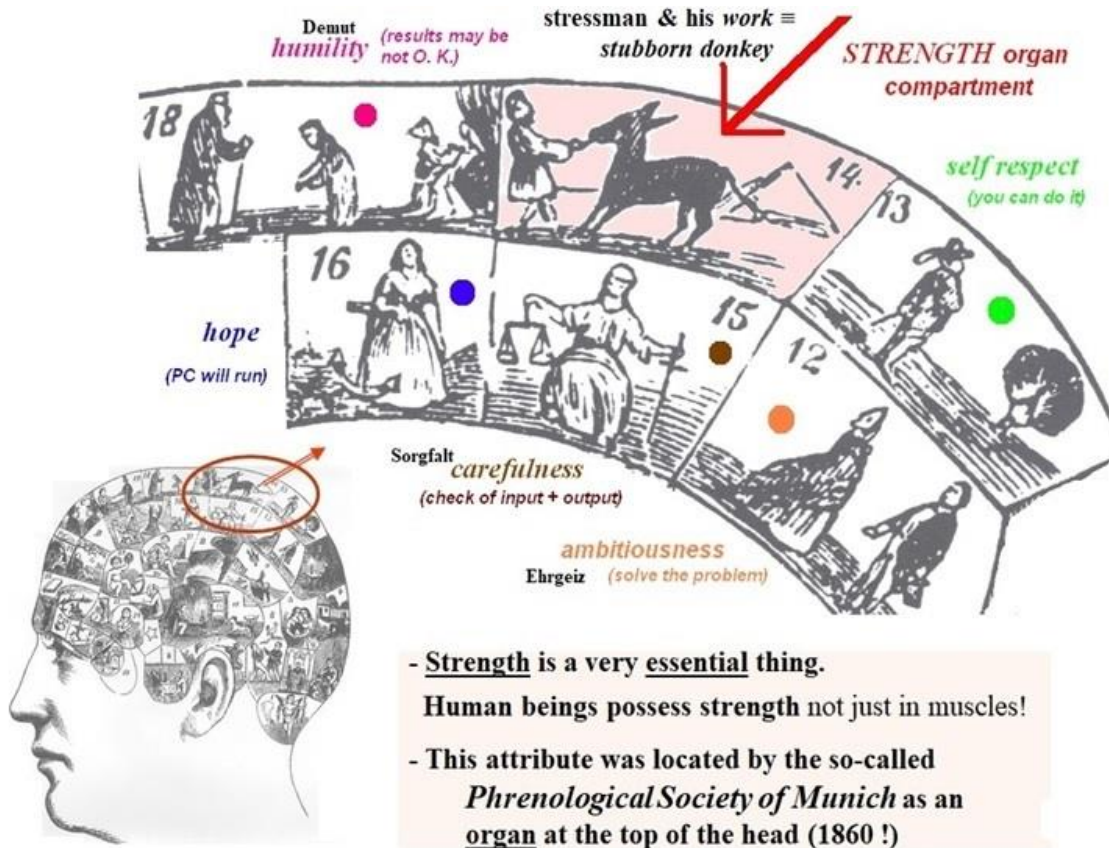


Annual booklets
with their
technical project-records
from
1970 up to 2023

Two typical Bavarian peculiarities addressing Strength and Composites

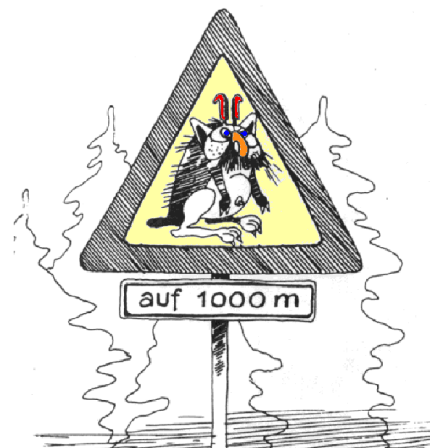
How much do you think this 'organ' is weighing?

About 15 g → extreme lightweight !



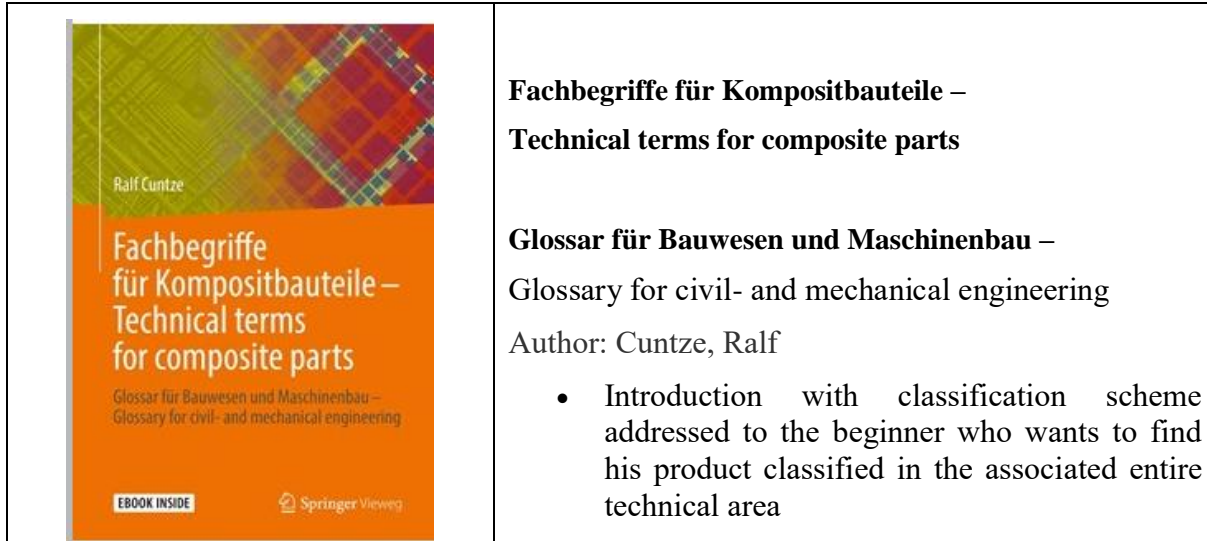
(For southern Germans: This has nothing to do with the beloved soccer club 1860 Munich, but it might stimulate more club success in future.)

The Wolperdinger,
the most famous
Bavarian Composite



Fiber-reinforced Composites in the various technical disciplines were a basic topic in the author's work. Being also civil engineer, the author tries to more inform about composite applications in construction.

22.5 Contributions to Handbooks, Guidelines etc.



SHORT COURSE
DEVELOPMENT OF FIBRE REINFORCED PLASTIC
COMPONENTS

Pretoria

16th to 18th April 1986

repeated 1989


Presented by : Dr R G Cuntze

Course Organizer : P A Coetzer



➤ *Design sheet contributor 1972-2015*

➤ *Co-reworker and Co-translator of the 'Airbus' structural handbook into English (2004)*

HSB HANDBUCH STRUKTUR BERECHNUNG	General description	Issue E Year 2018	
<p style="text-align: center;">Luftfahrt-Technisches Handbuch (LTH)</p> <p style="text-align: center;">HSB</p> <p style="text-align: center;">HANDBUCH STRUKTUR BERECHNUNG</p> <p style="text-align: center;">Fundamentals and Methods for Aeronautical Design and Analyses</p> <p style="text-align: center;">issued by</p> <div style="text-align: center;"><p>INDUSTRIE- AUSSCHUSS- STRUKTUR- BERECHNUNGSUNTERLAGEN</p></div>		Page 1 of 21	
		Prepared: Dr. M. Schagerl	Checked: Dr. M. Magin

22.11.2018 12:05 page 1 of 2
Overlay WS-VH8B001uk Source File: ~\www\id\brocknar\www\glary\BROCKNAR\1-lyr-1-5.kx

©Industrie Ausschuss Struktur Berechnungsunterlagen (IASB). All rights reserved. Confirmed and proprietary document

Digitally signed by Michael Magin
Date: 2020.10.20 00:13:05 CEST

VEREIN DEUTSCHER INGENIEURE	Entwicklung von Bauteilen aus Faser-Kunststoff-Verbund Berechnungen Development of FRP components (fibre reinforced plastics) Analysis	VDI 2014 Blatt 3 / Part 3 Ausg. deutsch/englisch Issue German/English
--	---	---

Frühere Ausgabe: 04.97 Entwurf, deutsch
Former edition: 04.97 Draft, in German only

Zu beziehen durch / Available at Beuth Verlag GmbH, 10772 Berlin - Alle Rechte vorbehalten / All rights reserved © Verein Deutscher Ingenieure e.V., Düsseldorf 2006

Die deutsche Version dieser Richtlinie ist verbindlich.

No guarantee can be given with respect to the English translation. The German version of this guideline shall be taken as authoritative.

Inhalt	Seite	Contents	Page
Vorbemerkung	3	Preliminary note	3
1 Anwendungsbereich	3	1 Scope	3
2 Abkürzungen, Begriffe, Symbole, Indizierung	4	2 Abbreviations, terminology, symbols, superscripts and subscripts	4
3 Berechnungsablauf	12	3 Analytical procedure	12
3.1 Allgemeines	12	3.1 General comments	12
3.2 Auslegungsphilosophie	14	3.2 Design philosophy	14
3.3 Berechnungsprogramme	15	3.3 Computer programs	15
4 Modellierung der Schicht	16	4 Modelling the lamina	16
4.1 Allgemeines	16	4.1 General comments	16
4.2 Eben beanspruchte Schicht	18	4.2 Two-dimensionally loaded lamina	18
4.2.1 UD-Schicht (faserparalleles KOS)	18	4.2.1 UD lamina (parallel-to-fibre COS)	18
4.2.2 G-Schicht und M-Schicht	20	4.2.2 WF lamina and M lamina	20
4.2.3 Drehung der UD-Schicht in das Laminat-KOS	21	4.2.3 Rotation of the UD lamina into the laminate	21
4.2.4 Berücksichtigung der Schubspannungen aus Querkraft bei UD-Schichten	22	4.2.4 Inclusion of shear stresses from transverse forces in case of UD laminae	22
4.3 Räumlich beanspruchte Schichten	23	4.3 Laminae subject to three-dimensional loading	23
4.3.1 Mechanische Beanspruchung (faserparalleles KOS)	23	4.3.1 Mechanical loading (parallel-to-fibre COS)	23
4.3.2 Mechanische Beanspruchung einer UD-Schicht (gedrehtes KOS)	25	4.3.2 Mechanical loading of a UD lamina (rotated COS)	25
4.4 Einfluss von Beanspruchungsarten/-dauer	26	4.4 Influence of loading type and duration	26
4.4.1 Kurzzeitbeanspruchung	26	4.4.1 Short-term load	26
4.4.2 Ruhende Langzeitbeanspruchung	26	4.4.2 Long-term static load	26
4.4.3 Schwingbeanspruchung	30	4.4.3 Cyclic load	30
4.4.4 Stoßbeanspruchung	31	4.4.4 Impact load	31
4.5 Festigkeitskriterien	31	4.5 Strength criteria	31
4.5.1 Allgemeines	32	4.5.1 General comments	32
4.5.2 Bruchbedingungen für UD-Schichten	36	4.5.2 Fracture conditions for UD lamina	36
4.5.3 G-Schicht	44	4.5.3 WF lamina	44
4.5.4 M-Schicht	45	4.5.4 M lamina	45
4.5.5 Einzusetzende Festigkeitswerte	46	4.5.5 Strength values to be used	46
4.6 Anwendung von Berechnungsprogrammen	46	4.6 Application of calculation programs	46
4.6.1 UD-Schicht	46	4.6.1 UD lamina	46
4.6.2 G-Schicht	48	4.6.2 WF lamina	48

VDI-Gesellschaft Kunststofftechnik

VDI-Handbuch Kunststofftechnik
VDI-Handbuch Konstruktion

Vervielfältigung – auch für innerbetriebliche Zwecke – nicht gestattet / Reproduction – even for internal use – not permitted



Space engineering

Buckling of structures

ECSS Secretariat
ESA-ESTEC
Requirements & Standards Division
Noordwijk, The Netherlands

This Handbook has been authored and agreed upon by:

J. Arboez, TU Delft
C. Bisagni, Politecnico di Milano
A. Calvi, ESA-ESTEC (Convenor)
E. Carrera, Politecnico di Torino
R. Cuntze, formerly MAN-Technologie
R. Degenhardt, DLR Braunschweig and PFH Göttingen
N. Gualtieri, Thales Alenia Space
H. Haller, Intales
N. Impollonia, Università di Catania
M. Jacquesson, CNES
E. Jansen, TU Delft
H.R. Meyer-Piening, ETH Zuerich
H. Oery, RWTH Aachen
A. Rittweger, Astrium EADS
R. Rolfes, Leibniz Universitaet Hannover
G. Schullerer, MT Aerospace
G. Turzo, CNES
T. Weller, Technion, Haifa
J. Wijker, Dutch Space

The valuable contributions of the following persons are acknowledged:

C. Huehne, DLR Braunschweig; D. Petry, Astrium EADS;
H. G. Reimerdes, RWTH Aachen; K. Rohwer, DLR Braunschweig;
R. Zimmermann, DLR Braunschweig.

The ECSS-E-HB-32-24 has been prepared by merging the volunteer contributions of the authors. Comments concerning the technical content of this handbook will be welcomed by the European Cooperation for Space Standardization, Noordwijk, the Netherlands, www.ecss.nl.

➤ Author was organizer of above Working Group (WG), convenor and contributor

-
- Member of DVM-WG "Characteristic Value Determination and Application of Fracture Mechanics". Headed by *K.-H. Schwalbe (1980)*
 - Member of the Probability Working group of *G. Schueller (1986)*
 - Founder and organizer of 4 Working Groups at Composites United e.V.
 - Engineering, aerospace, mechanical engineering
 - Composites Fatigue, aerospace, mechanical engineering
 - Design Dimensioning and Design Verification, civil engineering
 - Automated fabrication in construction including serial production including '3D-Printing', civil engineering.)

VEREIN DEUTSCHER INGENIEURE	Entwicklung von Bauteilen aus Faser-Kunststoff-Verbund Zuverlässigkeit und Sicherheit	VDI 2014 Blatt 4 (4. Entwurf) Zusammengestellt R. Cuntze, MAN
Development of FRP components (fibre reinforced plastics) Reliability and Safety		<i>Einsprüche bis ??,??,1995 an Verein Deutscher Ingenieure VDI-Gesellschaft Kunststofftechnik Postfach 10 11 39 40002 Düsseldorf</i>
Inhalt	Seite	
Vorbemerkung		6. Bestimmung von Kennwerten
1. Anwendungsbereich, Nutzen		6.1 Definition und Verwendung von Dimensionierungskennwerten
2. Abkürzungen, Begriffe, Symbole		6.2 Ermittlung der statistischen Parameter aus Meßdaten.....
3. Nachweis		6.3 Ermittlung Charakteristischer Werte
3.1 Allgemeines zu Rechnerischem und Experimentellem Nachweis		7. Produktsicherung
3.2 Mechanische Modellierung (Grenzzustände)		7.1 RAMS-orientierte Entwicklung.....
3.3 Experimenteller Nachweis.....		7.2 Qualitätssicherungskonzept und Integritätskontrolle mit Prüfmethoden.....
4. Traditionelles Sicherheitskonzept (TSK)		7.3 Versuche zur Erzielung der Strukturzuverlässigkeit des FKV-Bauteils
4.1 Allgemeines, charakteristische Werte		Literatur
4.2 Unsichere Eingangsgrößen beim Rechnerischen Nachweis		Anhang 1 Schätzverfahren, Statistische Tests, Updating Verfahren, Bayes.....
4.3 Sicherheitsfaktoren (Auslegung) und Sicherheitsmargen (rechn. und experim. Nachweis)		
4.4 Kritik am TSK.....		
5. Probabilistisches Sicherheitskonzept (PSK)		
5.1 Allgemeines		
5.2 Einwirkungsgrößen, Widerstandsgrößen und stochastische Konstruktionsparameter.....		
5.3 Teilsicherheitsfaktoren (semiprobabilistische Vorgehensweise)		
5.4 Stochastische Modellierung und Logische Modellierung des Versagenssystems		
5.5 Berechnung von Versagenswahrscheinlichkeit oder Zuverlässigkeit.....		
Vorbemerkung		
Die Richtlinie enthält Empfehlungen für das Entwickeln von Bauteilen aus Faser-Kunststoff-Verbunden (FKV), die aus einzelnen faserverstärkten Schichten bestehen, bei denen Fasern in einer Kunststoff-Matrix eingebettet sind. Die Bauteilentwicklung wird dargestellt, wobei die Berechnungen eingehender behandelt werden. Die Richtlinie will durch Systematisieren und Vereinheitlichen der Bauteildimensionierung auch die Zulassungsverfahren und die		Qualitätssicherung erleichtern. Sie ist in vier Teile gegliedert: • Blatt 1 Grundlagen • Blatt 2 Konzeption und Gestaltung..... • Blatt 3 Berechnung..... • Blatt 4 Zuverlässigkeit und Sicherheit.
		Beispielsammlung: s. VDI Report??
VDI-Gesellschaft Kunststofftechnik		
VDI-Handbuch Kunststofftechnik		

CC Bau-Forum

“Carbonbeton-Anwendungen in der Praxis - auf der Baustelle und im Fertigteilwerk“

Transformation von praktischem Anwendungswissen.
Zielgruppe: Hersteller, Sanierer, Vertreter der Betonbranche
am 25. Februar, Donnerstag, als Podium integriert bei den
Ulmer Betontagen vom 23. - 26.02.2021

25 min Vortrag + 5 min Diskussion. Folien: deutsch oder englisch. Vortrag: falls möglich möglich deutsch

08:30	Kaffeepause – Networking
09:00	Einführende Worte <i>Prof. Dr.-Ing. habil. Ralf Cuntze, CU Bau, Augsburg. Composites United e.V. CUeV (formerly CCeV)</i>
09:15	Digitale Entwicklung – von der Faser zum textilen Gelege. <i>Roy Thyroff, rothycon – Roy Thyroff Consulting, Naila</i>
09:30	Carbonbeton: Zwischen Theorie & Praxis. <i>Dipl.-Ing. Oliver Heppes, GOLDBECK Bauelemente Bielefeld SE</i>
12:10	Größer, stärker, wirtschaftlicher - Carbonbewehrungen in neuen Dimensionen. <i>Dipl.-Ing. Stephan Gießler, Solidian, Albstadt</i>
12:40	Mittagspause und Besuch der Ausstellung
14:00	Tragwerksplanung des C³-Ergebnishauses „CUBE“ – Bemessung, Nachweisführung und Zulassung im Einzelfall. <i>Dipl.-Ing. Hendrik Ritter, Assmann Beraten und Bauen, Dresden</i>
14:30	Modulare Brückenbauwerke aus Carbonbeton <i>M.Sc. Sven Bosbach, Lehrstuhl und Institut für Massivbau, RWTH Aachen</i>
15:00	Bauen mit CPC-Carbonbetonplatten, einer komplett neuen Bauweise in Beton – Verfahren, Konstruieren, Bemessen. <i>Prof. Joseph Kurath, ZHAW Winterthur, Schweiz</i>
15:30	Stadtbahnbrücke Stuttgart: CFK-Zugglieder finden Akzeptanz. <i>Prof. Dr. Urs Meier, EMPA, Dübendorf, Schweiz</i>
16:00	Ausgewählte Ingenieurbauwerke - nachträgliche Bauteilverstärkung mit Carbon-Faser-Kunststoffen „CFK“ (geklebte Lamellen). <i>Dr.-Ing. Horst Peters, HPTL Carbon GmbH, Ditzingen</i>

Ihr *Ralf Cuntze* und der weitere Vorstand des Netzwerks CU Bau

Weitere Termine 2020 / 2021 des Netzwerks CU Bau:

- 19.11. 2020: CU Thementag „Richtlinien, bauaufsichtliche Zulassungen und Bauartgenehmigungen für die potenziellen Anwender Architekten, Tragwerksplaner und Bauherm“. Zoom-Konferenz
- 17.03.2021: Thementag aller Arbeitsgruppen des Netzwerks CU BAU mit TU Chemnitz. Zoom-Konferenz?
- 30.03.2021: 4. Thementag der AG „Automatisierte Fertigung im Bauwesen inkl. Serielles Bauen“. Zoom-Konferenz?

Das Netzwerk CU Bau, besteht aus 4 Arbeitsgruppen: Bemessung und Nachweis (Prof. Ralf Cuntze), Faserverbundarmierter Beton (Dr. Ingeborg Gaitzsch), Faserverstärkte Kunststoffe (Prof. Jens Ridzewski), Automatisierte Fertigung im Bauwesen inkl. Serielles Bauen (Cuntze)



Former affiliations:

40 years German Society of Aeronautical Engineers

30 years Chaine de Rotisseurs

10 years L'Ordre des Coteaux de Champagne



My last large presentation:

*Static 3D-Strength Failure Criteria for the
Structural Material Families
Isotropic, Transversely–isotropic UD-
Lamina and Orthotropic Fabrics.
And? Achievement of a Novel, Simpler
Structural Mechanics Building,
on basis of Cuntze's successfully Test
Data-linked Failure-Mode-Concept (FMC)*

*DGM-Fachausschuss Hybride Werkstoffe,
21.2. 2024*

IASB 1972-2024

24 References since 2000

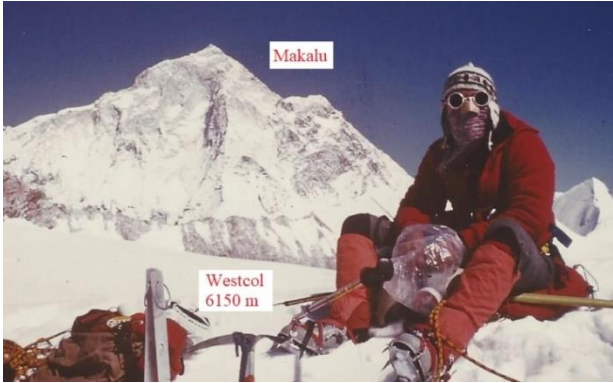
- [Cun00] Progressive failure of 3D-stressed laminates: Multiple nonlinearity treated by the Failure Mode Concept. Recent Developments in Durability Analysis of Composite Structures. Balkema, ISBN 90 5809 103 1
- [Cun01] *Assessment of Load- and Strain-controlled States of Stress in 'Hot Spots' – on the way to an Industrial Approach for 'Gurson Materials'*. Europ. Conf. on Launcher Technology Strascourg , De1.11-14, 2001
- [Cun03] Cuntze R and Memhard D: *Evaluation of the Tension Rod Test for Ductile Material Behavior*. European Conference on Spacecraft Structures, Materials & Mechanical Testing CNES, DLR; ESA, ISU: Toulouse, 11-13 December, 2002. Conference Proceedings
- [Cun06] *Failure Conditions for Isotropic Materials, Unidirectional Composites, Woven Fabrics - their Visualization and Links*. <https://www.ndt.net › cdc2006 › papers › cuntze, PDF>
- [Cun13] *Comparison between Experimental and Theoretical Results using Cuntze's Failure Mode Concept model for Composites under Tri-axial Loadings – Part B of the WWFE-II*. Journal of Composite Materials”, Vol.47 (2013), 893-924
- [Cun12] *The Predictive Capability of Failure Mode Concept-based Strength Criteria for Multidirectional Laminates*. Part B, Composites Science and Technology 63 (2004), 487-516
- [Cun17] *Fracture Failure Bodies of Porous Concrete (foam-like), Normal Concrete, Ultra-High-Performance-Concrete and of the Lamella - generated on basis of Cuntze's Failure-Mode-Concept (FMC)*. NWC2017, June 11-14, NAFEMS, Stockholm *
- [Cun19] *Technical terms for composite components in civil engineering and mechanical engineering*. Fachbegriffe mit Erklärung und Definition. In: Fachbegriffe für Kompositbauteile – Technical terms for composite parts. 171 pages, Springer Vieweg, Wiesbaden (2019). Pre-print *
- [CUN22] *Life-Work Cuntze - a compilation*. 2022/2023. *The Failure-Mode-Concept FMC, a physical and theoretical Material Symmetry-driven basis to generate Strength Criteria, that gave a reason to look after a 'more closed' Strength Mechanics Building, and in addition Very Much on Structural Materials, Techniques and Design including work-life experiences of the author in many engineering fields*. (about 850 pages), downloadable from <https://www.carbon-connected.de/Group/Prof.Ralf.Cuntze>
- [Cun23a] *Design of Composites using Failure-Mode-Concept-based tools— from Failure Model Validation to Design Verification*. Mechanics of Composite Materials, Vol. 59, No. 2, May, 2023, pp. 263-282*
- [Cun23b] *Minimum Test Effort-based Derivation of Constant-Fatigue-Life curves - displayed for the brittle UD composite materials*. Springer, Advanced Structured Materials, Vol.199, 107–146, draft *
- [Cun23c] *Comparative Characterization of Four Significant UD Strength Failure Criteria (SFC) with focusing a direct use of Friction Values, use of 'Strength' and 'Proportional Loading'*. 54 pages*
- [Cun23d] *Gedanken eines faseranwendungserfahrenen Ingenieurs zum Umgang mit Faser-Mikrobruchstücken und Feinstäuben bei Herstellung und Recycling faserverstärkter Bauteile*. Composites United construction (CU Bau) *
- [Cun23a] *Design of Composites using Failure-Mode-Concept-based tools— from Failure Model Validation to Design Verification*. Mechanics of Composite Materials, Vol. 59, No. 2, May, 2023, pp. 263-282*
- [Cun24b] Ceramic Strength Models for Monolithic (isotropic), Transversely-isotropic UD and Fabric Materials*
- [Cun24c] Cuntze R and Kappel E: *Benefits, applying Tsai's Ideas 'Trace', 'Double-Double' and 'Omni Failure Envelope' to Multiply UD-ply composed Laminates?* 60 pages *
- [HSB 02000-01] Cuntze R: *Essential topics in the determination of a reliable reserve factor*. 2012, 20 pages
HSB = (luftfahrttechnisches) Handbuch für Strukturberechnung (*German aerospace handbook*). Edited by the industrial committee (*working group!*) IASB = IndustrieAusschuss für StrukturBerechnung

“Theory is the Quintessence of all Practical Experience” (A. Föppl)

”Quid quid agis, prudenter agas, et respice finem” (a slogan of my school class)
Whatever you do, do it wisely and remember where it leads. (from *Gesta Romanorum*)

I hope that I followed this saying

25 Hobbies: Globetrotter, Hiking, photography, house & garden with alpine-cyclamen breeding





The caiman mother Maria observes limit the “No trespassing (No pase!)”. That was very good for the personal health of my friend Eddi (he unfortunately fell in front of her snout while running away). We learn: Structural engineers should always observe the limits set by the structural specifications. (2013)



Eastern 2012
7.28 o'clock

There was the
East-West
Main Road
of Bhutan
until 30 min
before arrival

*It is very seldom good to be late!
If we had been half of an hour earlier, after schedule, I would probably lie down in the ravine.
In this context my construction engineer plea is:
“Use the mentioned new fantastic build possibilities, whenever reasonable.
It is not beneficial to wait and to become too late!”*



1980, inauguration of ‘my’ climbing garden



In the Alps and at home



(left) **Ralf & Maria.**

(right) The relative *narrowness* of a **ROTEL** sleeping cabin, 80cm x 80cm x 210cm) helped the author to explore the *wide* world of nature and his good basic engineering education helped him to widely explore the *wide* world of engineering



Mountain luggage



Ras Dashen, East Africa, 4550 m



(left) Hiking in the Alps. (right) West Col 6150m



Pinatubo, Renatured after about 15 years, nature repairs



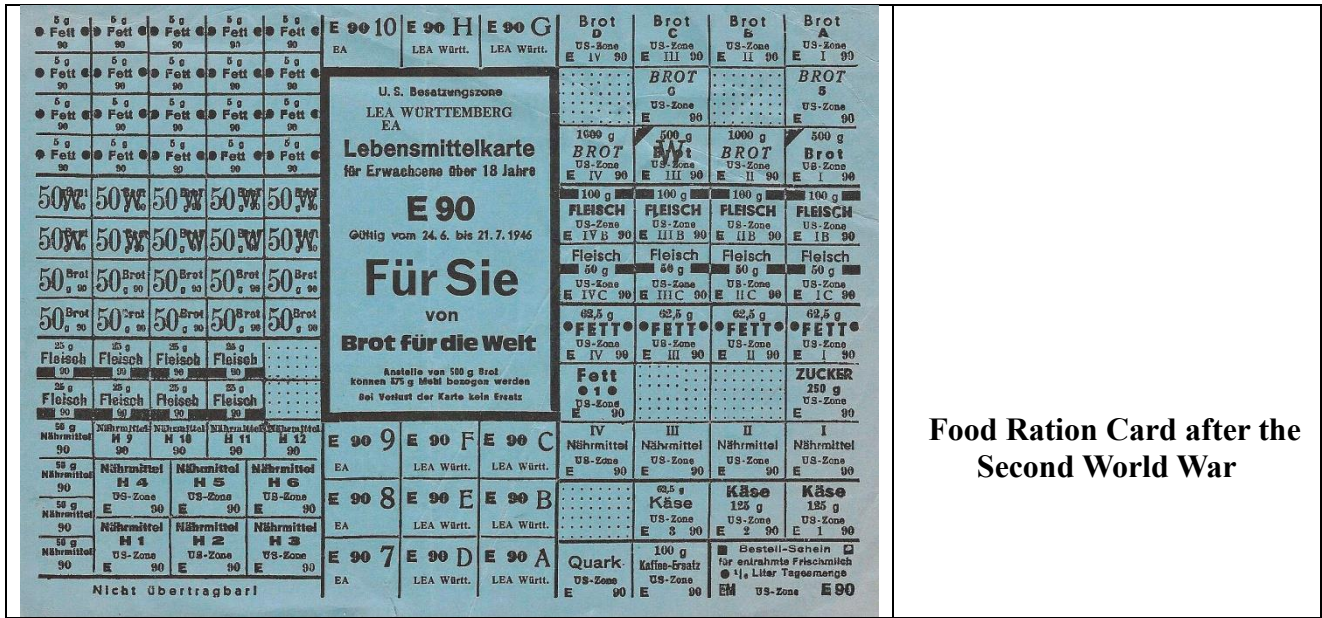
Venezuela
Me and the guide

Venezuela

**“Challenging
tasks
strengthen!”**



Leopard, hyacinth, elephant



Food Ration Card after the Second World War



Wig maker in Eastern Iran



Columbia

Friend or lazy beneficiary

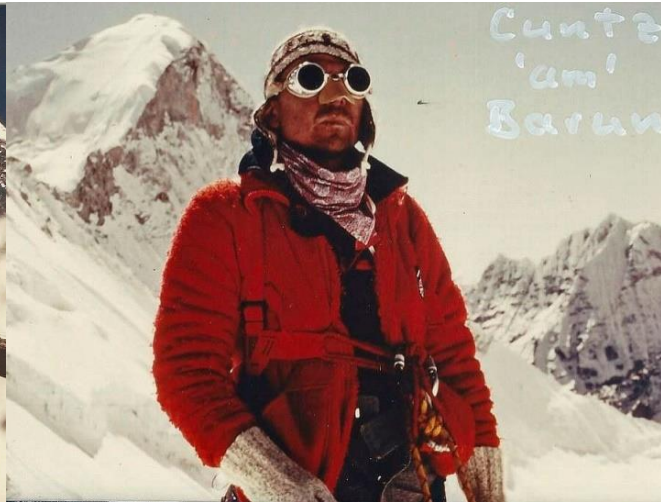
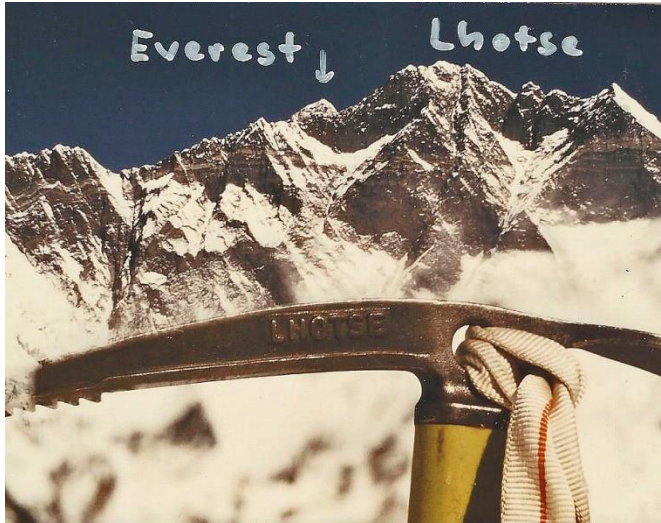


Cut out of the mountain rock, Aethiopia



Lilibela





Cuntze at the Baruntze



Kikuyu ladies



Feeding an Oran-Utan



North-Corea Border, room of Space peace treaty with the USA



Yemen, Sanaa



Deamavend Iran, 1975



Fitz Roy hiking, Patagonia, 1987



Largest moth in the world



Smallest ape, Makaki



Ladakh (West Tibet) 1980



Crossing the Atlantic



Kamtchatka, 2001



Chinese family on the Great Wall, 2000



Yemen



Namibia